FINAL REPORT

SURFACE WAVE MEASUREMENTS

CALIFORNIA STRONG MOTION INSTRUMENTATION PROGRAM STATIONS
RIVERSIDE COUNTY, CALIFORNIA

GEO*Vision* Project No. 16192

Prepared for

State of California
Department of Conservation
California Geological Survey
Strong Motion Instrumentation Program
801 K Street
Sacramento, CA 94612

Prepared by

GEO*Vision* Geophysical Services, Inc.
1124 Olympic Drive
Corona, California 92881

Report 16192-01 Rev 2

September 15, 2016

TABLE OF CONTENTS

APPENDICES

APPENDIX A DATA REPORTS

LIST OF TABLES

LIST OF FIGURES

1 INTRODUCTION

In-situ seismic measurements using active and passive (ambient noise) surface wave techniques were performed at twelve (12) California Strong Motion Instrumentation Program (CSMIP) stations in Riverside County, California from May 24th to July 6th, 2016. The purpose of this investigation was to provide a shear (S) wave velocity profile to a minimum depth of 40 meters (m) and an estimate of the average S-wave velocity of the upper 30 m (V_{S30}) for each CSMIP site. The active surface wave technique utilized during this investigation consisted of the multi-channel analysis of surface waves (MASW) method. The passive surface wave techniques utilized consisted of the single station horizontal/vertical spectral ratio (HVSR), array microtremor, and refraction microtremor methods. The location and description of the CSIMP stations characterized during this investigation are summarized in Figure 1 and Table 1.

V_{S30} is used in the NEHRP provisions and the Uniform Building Code (UBC) to separate sites into classes for earthquake engineering design (BSSC, 1994). The average shear wave velocity of the upper 100 ft (V_{S100ft}) is used in the International Building Code (IBC) for site classification. These site classes are as follows:

Class A – hard rock – $V_{S30} > 1500$ m/s (UBC) or $V_{S100ft} > 5{,}000$ ft/s (IBC)
Class B – rock – $760 < V_{S30} \leq 1500$ m/s (UBC) or $2{,}500 < V_{S100ft} \leq 5{,}000$ ft/s (IBC)
Class C – very dense soil and soft rock – $360 < V_{S30} \leq 760$ m/s (UBC)
or $1{,}200 < V_{S100ft} \leq 2{,}500$ ft/s (IBC)
Class D – stiff soil – $180 < V_{S30} \leq 360$ m/s (UBC) or $600 < V_{S100ft} \leq 1{,}200$ ft/s (IBC)
Class E – soft soil – $V_{S30} < 180$ m/s (UBC) or $V_{S100ft} < 600$ ft/s (IBC)
Class F – soils requiring site-specific evaluation

At many sites, active surface wave techniques with the utilization of portable energy sources, such as hammers and weight drops, are sufficient to obtain a S-wave velocity model to a depth of 30 m. At sites with high ambient noise levels and/or very soft soils, these energy sources may not be sufficient to image to 30 m and a larger energy source, such as a bulldozer, is necessary. Alternatively, passive surface wave techniques, such as the array microtremor technique or the refraction microtremor method of Louie (2001), can be used to extend the depth of investigation at sites that have adequate ambient noise conditions. It should be noted that two-dimensional passive surface wave arrays (e.g. triangular, circular or L-shaped arrays) will provide better accuracy than linear arrays.

This report contains the results of the active and passive surface wave measurements conducted at 12 CSMIP station sites. An overview of the surface wave methods is given in Section 2. Field and data reduction/modeling procedures are discussed in Sections 3 and 4, respectively. Results are presented in Section 5. References and our professional certification are presented in Sections 6 and 7, respectively.

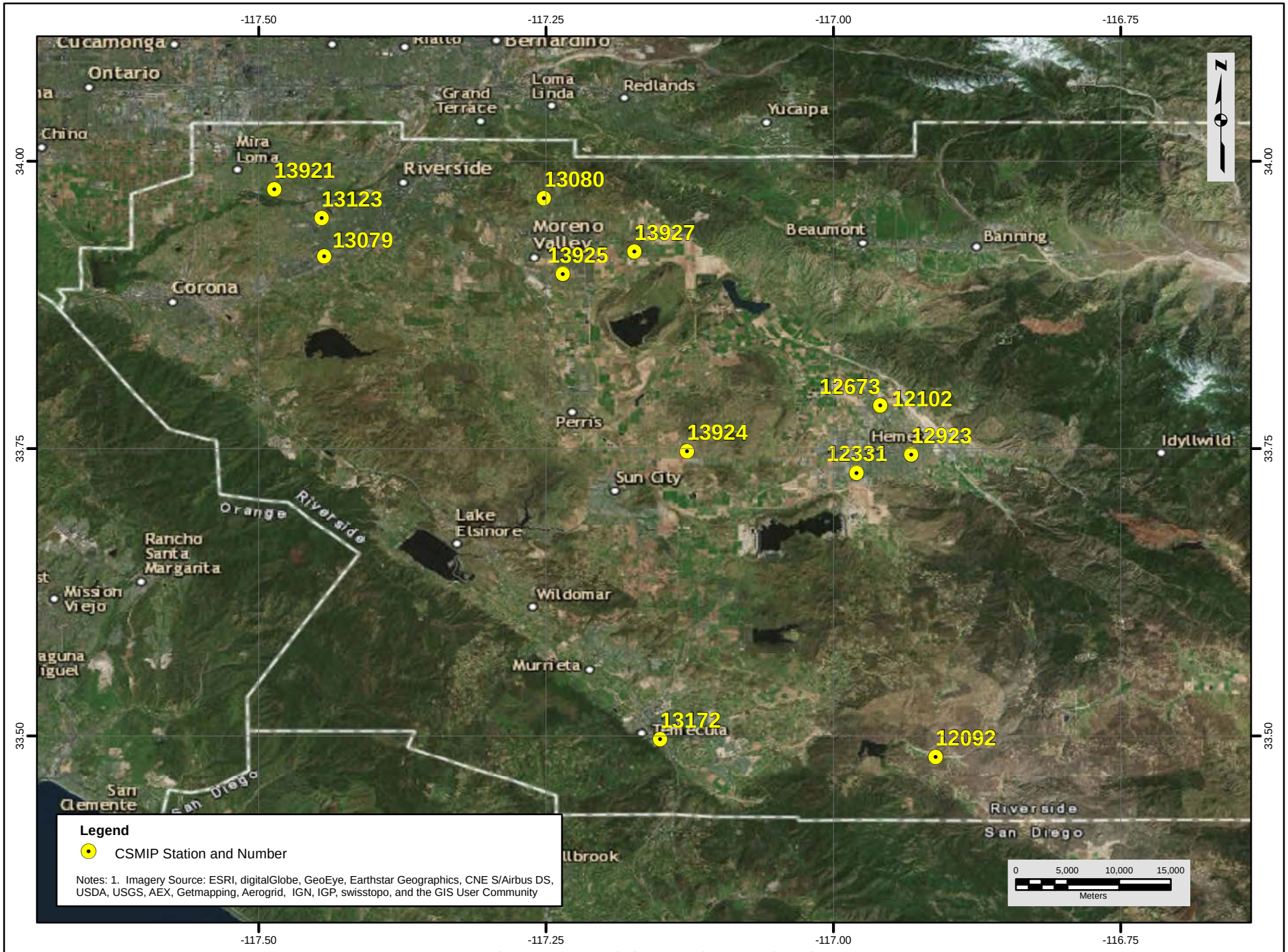

FIGURE 1 - CSMIP STATIONS

Table 1 CSMIP Stations

Station No.	Station Name	Latitude	Longitude	Location	Address
12092	Radec - Sage & Cottonwood School Rds	33.4818	-116.9114	Cottonwood Fire Station	44222 Sage Rd., Aguanga, CA 92536
12102	San Jacinto - CDF Fire Station 25	33.7869	-116.9592	San Jacinto Fire Station	132 S. San Jacinto Ave., San Jacinto, CA 92583
12331	Hemet - Stetson Ave Fire Station	33.7289	-116.9797	Hemet City Fire Station #2	895 Stetson Ave., Hemet, CA
12673[1]	San Jacinto - CDF Fire Station	33.7873	-116.9592	San Jacinto Fire Station	132 S. San Jacinto Ave., San Jacinto, CA 92583
12923	Hemet - Acacia & Stanford	33.7448	-116.9322	Little Lake Fire Station	25954 Stanford St., Hemet CA
13079	Riverside - Hwy 91 & Van Buren	33.9174	-117.443	Riverside City Fire Station #2	9449 Andrew St., Arlington, CA 92503
13080	Moreno Valley - Sunnymead & Village	33.9677	-117.2519	Sunnymead Ranch Fire Station	10511 Village Rd., Moreno Valley, CA 92557
13123	Riverside - Airport	33.9506	-117.4453	Riverside Airport	6905 Airport Dr., Riverside, CA 92504
13172	Temecula - 6th & Mercedes	33.4971	-117.1507	Temecula Fire Station	28330 Mercedes St., Temecula, CA 92590
13921	Riverside - Limonite & Downey	33.9753	-117.4865	Pedley Fire Station	9270 Limonite Ave., Riverside, CA 92509
13924	Homeland - Hwy 74 & Sultanas	33.7475	-117.1274	Homeland Fire Station	25730 Sultanas Rd., Homeland, CA 92548
13925	Moreno Valley - Indian & Kennedy	33.9019	-117.2355	Kennedy Park Fire Station	15111 Indian Ave., Moreno Valley, CA 92551
13927	Moreno Valley - Alessandro & Moreno Bch	33.9212	-117.1731	Moreno Fire Station	28020 Bay Ave., Moreno Valley, CA 92555

1. Located at same fire station as CE.12102

2 OVERVIEW OF SURFACE WAVE METHODS

Both active and passive (ambient noise) surface wave techniques were utilized during this investigation. Active surface wave techniques include the spectral analysis of surface waves (SASW) and multi-channel array surface wave (MASW) methods. Passive surface wave techniques include the HVSR technique and the array and refraction microtremor methods.

The basis of surface wave methods is the dispersive characteristic of Rayleigh and Love waves when propagating in a layered medium. The Rayleigh wave phase velocity (V_R) depends primarily on the material properties (V_S, mass density, and Poisson's ratio or compression wave velocity) over a depth of approximately one wavelength. The Love wave phase velocity (V_L) depends primarily on V_S and mass density. Rayleigh and Love wave propagation are also affected by damping or seismic quality factor (Q). Rayleigh wave techniques are utilized to measure vertically polarized S-waves (S_V-wave); whereas, Love wave techniques are utilized to measure horizontally polarized S-waves (S_H-wave).

Surface waves of different wavelengths (λ) or frequencies (f) sample different depths (Figure 2). As a result of variance in the shear stiffness of the distinct layers, waves with different wavelengths propagate at different phase velocities; hence, dispersion. A surface wave dispersion curve is the variation of V_R or V_L with λ or f (Figure 2).

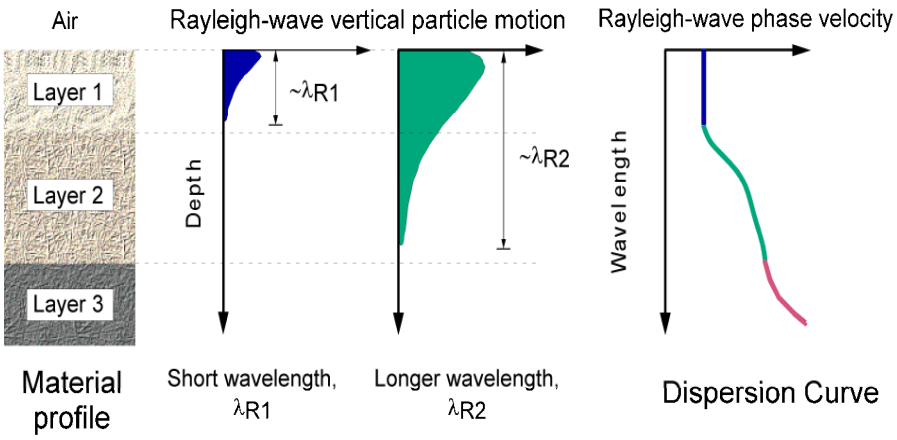

Figure 2 Relationship between the wavelength of surface waves and investigation depth

The SASW and MASW methods are in-situ seismic methods for determining shear wave velocity (V_S) profiles (Stokoe et al., 1994; Stokoe et al., 1989; Park et al., 1999a and 1999b, Foti, 2000). Surface wave techniques are non-invasive and non-destructive, with all testing performed on the ground surface at strain levels in the soil in the elastic range (< 0.001%). SASW testing consists of collecting surface wave phase data in the field, generating the dispersion curve, and then using iterative forward or inverse modeling to calculate the shear wave velocity profile. MASW testing consists of collecting multi-channel seismic data in the field, applying a wavefield transform to obtain the dispersion curve, and data modeling to obtain the V_S profile.

A detailed description of the SASW field procedure is given in Joh, 1996. A typical SASW setup is shown in Figure 3. A vertical dynamic load is used to generate horizontally-propagating Rayleigh waves and a horizontal force is used to generate Love waves. The ground motions are monitored by two, or more, vertical (Rayleigh wave) or horizontal (Love wave) receivers and recorded by the data acquisition system capable of performing both time and frequency-domain calculations. Theoretical, as well as practical considerations, such as signal attenuation, necessitate the use of several receiver spacings to generate the dispersion curve over the wavelength range required to evaluate the stiffness profile. To identify and/or minimize phase shifts due to differences in receiver coupling and subsurface variability, the source location is reversed. To develop a V_S model to a 30 meter depth using Rayleigh wave methods, energy sources typically include: small hammers (rock hammer or 3 lb hammer) for short receiver intervals; 10 to 20 lb sledgehammers for intermediate separations, and accelerated weight drops (AWD) or an electromechanical shaker for larger spacings. More energetic sources, such as bulldozers or seismic vibrators (Vibroseis™), can be used to characterize velocity structure to depths of 100 m or more. Energy sources for shallow imaging using Love waves include a hammer and horizontal traction plank, portable hammer impact aluminum source, and inclined or horizontal accelerated weight drop systems. Energy sources for deeper imaging using Love waves include horizontal seismic vibrators. Generally, high frequency (short wavelength) surface waves are recorded across receiver pairs spaced at short intervals, whereas low frequency (long wavelength) surface waves require greater spacing between receivers. Dispersion data averaged across greater distances are often smoother because effects of localized heterogeneities are averaged.

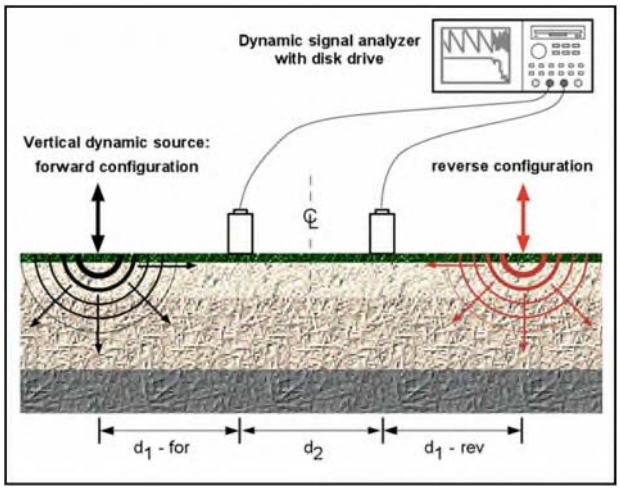

Figure 3 Typical SASW setup

After the time-domain motions from the two receivers are converted to frequency-domain records using the Fast Fourier Transform, the cross power spectrum and coherence are calculated. The phase of the cross power spectrum represents the phase differences between the two receivers as the wave train propagates past them. It ranges from $-\pi$ to π in a wrapped form and must be unwrapped through an interactive process called masking. Phase jumps are specified, near-field data (wavelengths longer than two times the distance from the source to first receiver) and low-coherence data are removed. The experimental dispersion curve is calculated from the unwrapped phase angle and the distance between receivers by:

$$V_{R/L} = f * d_2/(\Delta\phi/2\pi)$$

where V_R = Rayleigh wave phase velocity
V_L = Love wave phase velocity
f = frequency
d_2 = distance between receivers
$\Delta\phi$ = the phase difference in radians

Figure 4 demonstrates phase unwrapping of the cross power spectrum during SASW data reduction.

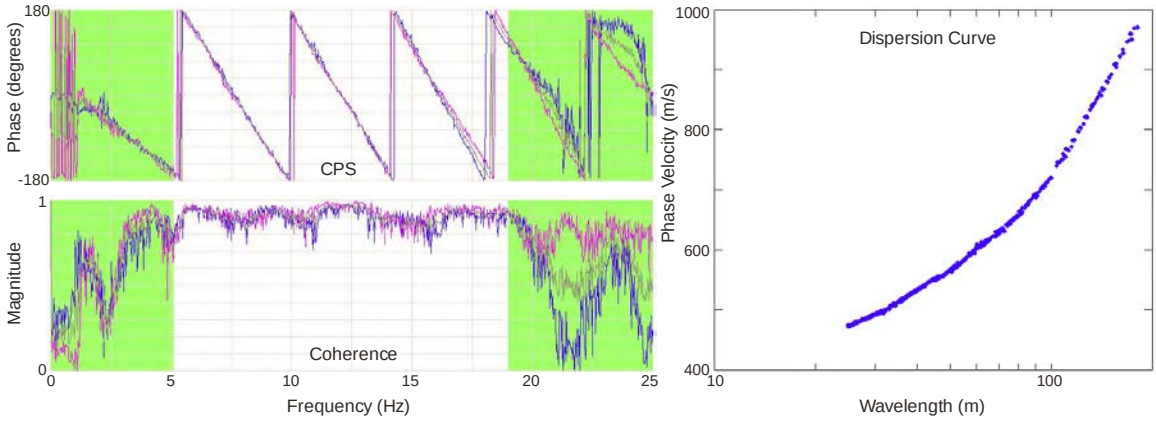

Figure 4 Masking of wrapped phase spectrum and resulting dispersion curve

A detailed description of the MASW method is given by Park, 1999a and 1999b. Ground motions are recorded by 24, or more, geophones typically spaced 1 to 3 m apart along a linear array and connected to a seismograph. Energy sources are the same as those outlined above for SASW testing. When applying the MASW technique to develop a one-dimensional (1-D) V_S model, the surface-wave data, preferably, are acquired using multiple-source offsets at both ends of the array. The most commonly applied MASW technique is the Rayleigh-wave based MASW method, which we refer to as MAS_RW to distinguish from Love-wave based MASW (MAS_LW). MAS_RW and MAS_LW acquisition can easily be combined with P- and S-wave seismic refraction acquisition, respectively. MAS_RW data are generally recorded using a vertical source and vertical geophone, but may also be recorded using a horizontal geophone with radial (in-line) orientation. MAS_LW data are recorded using transversely orientated horizontal source and transverse horizontal geophone.

A wavefield transform is applied to the time-history data to convert the seismic record from time-offset space to frequency-phase velocity space in which the surface-wave dispersion curve can be easily identified. Common wave-field transforms include: the frequency-wavenumber (f-k) transform, slant-stack transform (τ-p), frequency domain beamformer, and phase-shift transform. Occasionally, SASW analysis procedures are used to extract surface wave dispersion data, from fixed receiver pairs, at smaller wavelengths than can be recovered by wavefield transformation. Construction of a dispersion curve, over the wide frequency/wavelength range necessary to develop a robust V_S model while also limiting the maximum wavelength based on an established near-field criteria (e.g. Yoon and Rix, 2009; Li and Rosenblad, 2011), generally

requires multiple source offsets. Although, the vast majority of MASW surveys record Rayleigh waves, it has been shown that Love wave techniques can be more effective in some environments, particularly shallow rock sites and sites with a highly attenuative, low velocity surface layer (Xia, et al., 2012; **GEO***Vision*, 2012; Yong, et al., 2013; Martin, et al., 2014). Figure 5 provides an example of frequency-velocity (f-v) transforms of MAS_RW and MAS_LW data from site CE.13929 (Yong, et al., 2013) where the fundamental mode Love wave was much more easily interpreted.

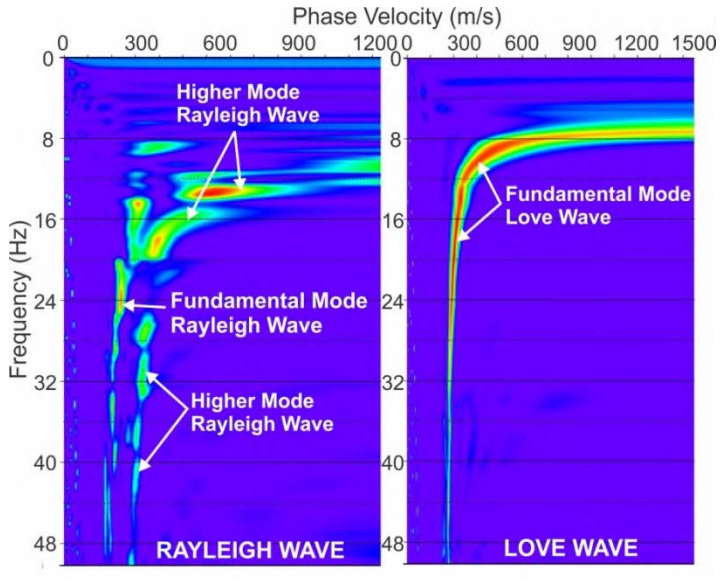

Figure 5 Comparison of Rayleigh and Love wave f-v transforms

Rayleigh wave techniques, however, are generally more effective at sites where velocity gradually increases with depth because larger energy sources are readily available for generation of Rayleigh waves. Rayleigh wave techniques are generally more applicable to sites with high velocity layers and/or velocity inversions because the presence of such structures is more apparent in the Rayleigh wave dispersion curves than in Love wave dispersion curves. Rayleigh wave techniques are preferable at sites with a high velocity surface layer because Love waves do not theoretically exist in such environments. Occasionally, the horizontal radial component of a Rayleigh wave may yield higher quality dispersion data than the vertical component because different modes of propagation may have more energy in one component than the other. Recording both the vertical and horizontal components of the Rayleigh wave is particularly useful at sites with complex modes of propagation or when attempting to recover multiple Rayleigh wave modes for multi-mode modeling as demonstrated in Dal Moro, et al, 2015. Figure 6 provides example f-v transforms of vertical and horizontal radial component Rayleigh wave data from site CE.13924 where the horizontal component data yields a better defined dispersion curve at low frequencies than the vertical component data. Joint inversion of Rayleigh and Love wave data may yield more accurate V_S models and also offer a means to investigate anisotropy, where S_V- and S_H-wave velocity are not equal, as shown in Dal Moro and Ferigo, 2011.

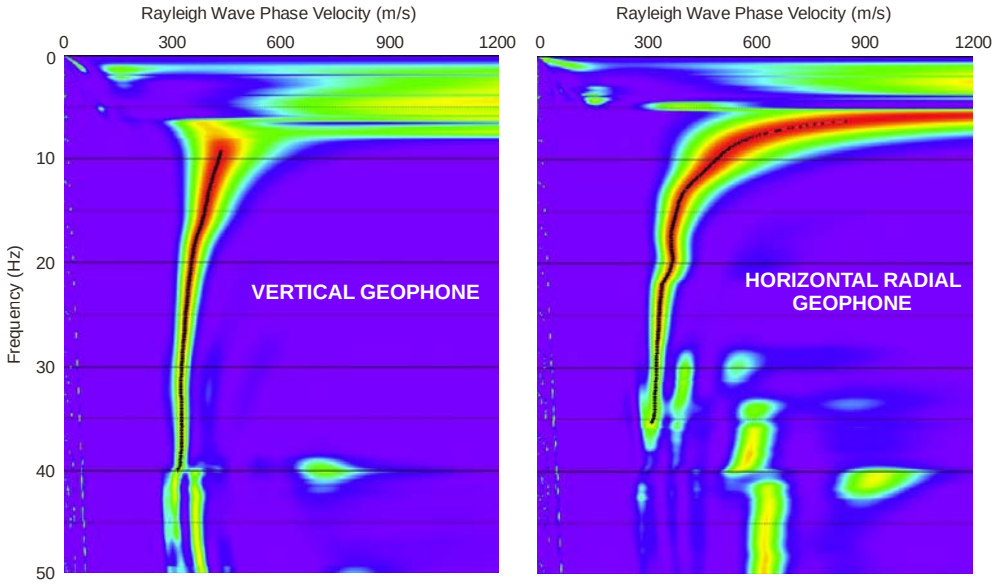

Figure 6 Comparison of f-v transforms between vertical and radial horizontal component Rayleigh wave seismic data at seismic station CE.13924

A detailed discussion of the array microtremor method can be found in Okada, 2003. This technique uses 4, or more, receivers aligned in a 2-dimensional array. Triangle, circle, semi-circle, and "L" shaped arrays are commonly used, although any 2-dimensional arrangement of receivers can be used. For investigation of the upper 100 m, receivers typically consist of 1 to 4.5 Hz geophones. The nested triangle array, which consists of several embedded equilateral triangles, is often used as it provides accurate dispersion curves with a relatively small number of geophones. With this array, the outer side of the triangle should be equal to or greater than the desired depth of investigation. The "L" array is useful at sites located at the corner of perpendicular intersecting streets. Typically 20, or more, 30-second noise records are acquired for analysis. The surface wave dispersion curve is typically estimated from array microtremor data using various f-k methods such as beam-forming (Lacoss, et al., 1969), and maximum-likelihood (Capon, 1969), and the spatial-autocorrelation (SPAC) method, which was originally based on work by Aki, 1957. The SPAC method has since been extended and modified (Ling and Okada, 1993 and Ohori *et al*., 2002) to permit the use of noncircular arrays, and is now collectively referred to as extended spatial autocorrelation (ESPAC or ESAC). Further modifications to the SPAC method permit the use of irregular or random arrays (Bettig *et al*., 2001). Although it is common to apply SPAC methods to obtain a surface wave dispersion curve for modeling, other approaches involve direct modeling of the coherency data, also referred to as SPAC coefficients (Asten, 2006 and Asten, *et al*., 2015).

The refraction microtremor technique (ReMi™), a detailed description of which can be found in Louie (2001), differs from the more established array microtremor technique in that it uses a linear receiver array rather than a two dimensional array. Unlike the SASW method, which uses an active energy source (i.e. hammer), the microtremor technique records background noise emanating from ocean wave activity, wind noise, traffic, industrial activity, construction, etc. Refraction microtremor field procedures typically consist of laying out a linear array of at least 24 4.5 Hz geophones and recording 20, or more, 30 second noise records. These noise records are reduced using the software package SeisOpt® ReMi™ v2.0 by Optim™ Software and Data

Services. This package is used to generate and combine the slowness (p) – frequency (f) transform of the noise records. The surface wave dispersion curve is picked at the lower envelope of the surface wave energy identified in the p-f spectrum. It should be noted that other data reduction techniques such as seismic interferometry and ESAC can also be used to extract surface wave dispersion curves from linear array, passive surface wave data.

The horizontal-to-vertical spectral ratio (HVSR) technique was first introduced by Nogoshi and Igarashi (1971) and popularized by Nakamura (1989). This technique utilizes single-station recordings of ambient vibrations (microtremor or noise) made with a three-component seismometer. In this method, the ratio of the Fourier amplitude spectra of the horizontal and vertical components is calculated to determine the frequency of the maximum HVSR response (HVSR peak frequency), commonly accepted as an approximation of the fundamental frequency (f_0) of the sediment column overlying bedrock. The HVSR peak frequency associated with bedrock is a function of the bedrock depth and S-wave velocity of the sediments overlying bedrock. The theoretical HVSR response can be calculated for an S-wave velocity model using modeling schemes based on surface wave ellipticity, vertically propagating body waves, or diffuse wavefields containing body and surface waves. The HVSR frequency peak can also be estimated using the quarter-wavelength approximation:

$$f_0 = \frac{\overline{V}_S}{4z}$$

where f_0 is the site fundamental frequency and $\overline{V}_S$ is the average shear-wave velocity of the soil column overlying bedrock at depth z.

The active and passive surface wave techniques complement one another as outlined below:

- SASW/MASW techniques image the shallow velocity structure which cannot be imaged by the microtremor technique and are needed for an accurate V_S model and V_{S30}/V_{S100ft} estimate.
- Microtremor techniques often perform well in noisy environments where SASW/MASW depth investigation may be limited.
- In a high noise environment, the microtremor technique will extend the depth of investigation of SASW/MASW soundings.

The dispersion curves generated from the active and passive surface wave soundings are generally combined and modeled using iterative forward and inverse modeling routines. The final model profile is assumed to represent actual site conditions. Several options exist for the Rayleigh wave forward solution: a formulation that takes into account only fundamental-mode Rayleigh wave motion; one that includes all stress waves and incorporates receiver geometry in an SASW test named the 3-D solution (Roesset et al., 1991); one that computes an effective mode for an MASW test but assumes a plane Rayleigh wave and no body wave effects, and a multi-mode solution that models different Rayleigh wave modes. Both fundamental mode and multi-mode forward solutions are available for modeling of Love wave data.

The theoretical model used to interpret the dispersion curve assumes horizontally layered, laterally invariant, homogeneous-isotropic material. Although these conditions are seldom strictly met at a site, the results of active and/or passive surface wave testing provide a good

"global" estimate of the material properties along the array. The results may be more representative of the site than a borehole "point" estimate.

It may not always be possible to develop a coherent, fundamental mode dispersion curve over sufficient frequency range for modeling due to dominant higher modes with the higher modes not clearly identifiable for multi-mode modeling. It may, however, be possible to identify the Rayleigh wave phase velocity of the fundamental mode at 40 m wavelength (V_{R40}) in which case V_{S30} can at least be estimated using the Brown et al., 2000 relationship:

$$V_{S30} = 1.045 V_{R40}$$

This relationship was established based on statistical analysis of a large number of surface wave data sets from sites with control by velocities measured in nearby boreholes and has been further evaluated by Martin and Diehl, 2004, and Albarello and Gargani, 2010.

As with all surface geophysical methods, inversion of surface wave dispersion data does not yield a unique V_S model and there are multiple possible solutions that may equally well fit the experimental data. Based on our experience at other sites, the shear wave velocity models (V_S and layer thicknesses) determined by surface wave testing are within 20% of the velocities and layer thicknesses that would be determined by other seismic methods (Brown, 1998). The average velocity of the upper 30 m or 100 ft, however, is much more accurate, often to better than 5%, because it is not sensitive to the layering in the model. V_{S30} does not appear to suffer from the non-uniqueness inherent in V_S models derived from surface wave dispersion curves (Martin et al., 2006, Comina et al., 2011). Therefore, V_{S30} is more accurately estimated from inversion of surface wave dispersion data than the resulting V_S models.

3 FIELD PROCEDURES

3.1 Site Preparation and Survey Control

Active and passive surface wave sounding and HVSR measurement locations were established by **GEO***Vision* personnel after review of site conditions and accessibility. When possible, a 70.5 m long MASW array was established at each site, although there was only sufficient space for a 47 m long array at two sites (CE.13080 and CE.13172). The primary passive surface wave array established at each site consisted of a nested triangle or L-shaped array. Passive linear arrays were also established at sites where triangle arrays were utilized for the purpose of comparing the performance of 2-D and linear microtremor arrays. An HVSR measurement location was established in relatively close proximity to the seismic station. At sites where field observations and geologic maps indicated that bedrock could be present in the upper 30 m, additional HVSR measurement locations were established in the vicinity of the surface wave testing arrays to demonstrate that bedrock depth was not highly variable across the site. The locations of the surface wave and HVSR measurement locations were generally surveyed using a Magellan Professional MobileMapper™ CX GPS system and are summarized in the data reports presented for each site in Appendix A. A summary of the geophysical techniques utilized at each site is presented as Table 2.

Table 2 Surface Wave Techniques Utilized at each CSMIP Station

Station No.	Active Surface Wave			Passive Surface Wave			
	MAS_RW (vertical geophone)	**MAS_RW (horizontal radial geophone)**	**MAS_LW**	**Nested Triangle Array**	**L-shaped Array[1]**	**Linear Array**	**HVSR**
12092	✓			✓		✓	✓
12102 & 12673	✓				✓		✓
12331	✓				✓		✓
12923	✓				✓		✓
13079	✓			✓		✓	✓
13080	✓			✓		✓	✓
13123	✓	✓	✓	✓		✓	✓
13172	✓				✓		✓
13921	✓			✓	✓		✓
13924	✓	✓	✓		✓		✓
13925	✓			✓		✓	✓
13927	✓			✓	✓		✓

1. Two linear arrays also extracted from data set.

3.2 MASW Survey

A typical MASW field layout is shown in Figure 7. The seismic data acquisition system consisted of two 24-channel Geometrics Geode signal enhancement seismographs combined to form a 48-channel system and a laptop computer running Geometrics Seismodule Controller Software (Figure 8). Other seismic equipment utilized during this investigation consisted of: Geospace 4.5 Hz vertical and horizontal geophones, seismic cables, hammer switches, and multiple energy sources including a 240-lb accelerated weight drop (AWD), 4 lb hammer, 12 and 20 lb sledgehammers, an aluminum plate, horizontal traction plank, and hammer-impact aluminum shear wave seismic source (Figure 9).

Figure 7 Typical MASW field layout

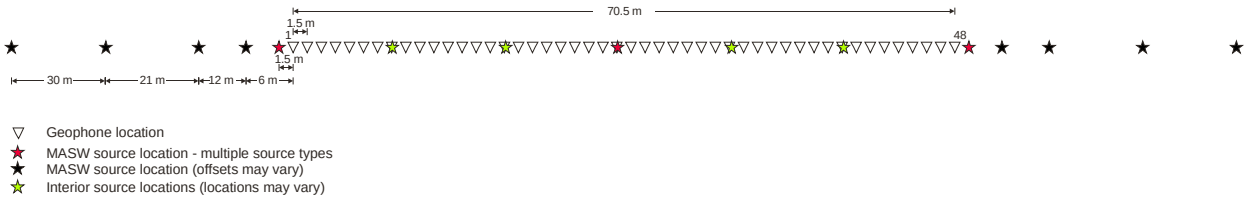

Figure 8 Geometrics Geode seismograph

MAS_RW data were acquired along a linear array of 48 vertical geophones spaced 1.5 m apart for an array length of 70.5 m; except for sites CE.13080 and CE.13172 where there was only sufficient space for a 1 m geophone spacing. For the 70.5 m arrays, source locations were generally located 1.5, 6, 12, 21, and 30 m from the end geophone locations where space permitted. For the 47 m long arrays, source locations were generally located 1, 5, 10 and 20 m from the end geophone locations where space permitted. Additional, interior source locations were located at an 8 geophone interval. The 4 lb hammer and 12 lb sledgehammer were used for the 1 or 1.5 m offset source locations and the center source location (geophone 24). The 12 lb hammer was also used for all other interior source locations. The AWD was used for all off-end source locations, where possible, and the 20 lb sledgehammer was used in areas inaccessible to the AWD. Data from the transient impacts (hammers) were averaged 10 times, or more, to improve the signal-to-noise ratio. At two sites (CE.13123 and CE.13924) the MAS_RW survey was repeated using a horizontal geophone with radial (in-line) orientation because the Rayleigh wave dispersion curves were not well developed at low frequencies in the vertical geophone data.

Figure 9 4 lb hammer, 12 lb sledgehammer, and 240 lb AWD used for MAS_RW acquisition

MAS_LW data were also acquired along the same array used for MAS_RW data acquisition at two sites (CE.13123 and CE.13924) because the effectiveness of the Rayleigh wave method was not clear in the field. Horizontal, transverse orientation 4.5 Hz geophones were used for Love wave acquisition. A horizontal traction plank weighted down by a vehicle or a hammer impact aluminum S-wave seismic source and 20 lb sledgehammer (Figure 10) were used as the energy source for Love wave data acquisition. Love wave seismic data were obtained by striking each end of the source to facilitate identification of S-waves and Love waves, which are expected to have reversed polarity on the two seismic records. The seismic data were typically acquired using a 0.125 ms sample rate (fine sample rate required for seismic refraction analysis) and 1 s record length (long record length required for surface wave analysis). The final seismic record at each shot point was the result of stacking 5 to 15 shots to increase the signal to noise ratio. All seismic records were stored on a laptop computer with file names and acquisition parameters documented on a field log.

Figure 10 Hammer impact aluminum source and wood traction plank used for MAS_LW acquisition

3.3 Array Microtremor Survey

The passive surface wave equipment consisted of one or two Geometrics Geode signal enhancement seismographs, Geospace 1 Hz vertical geophones, Geospace 4.5 Hz vertical geophones, and seismic cables. Array microtremor measurements were made using three types of arrays: 10 channel nested triangle array using 1 Hz geophones, 48 channel L-shaped array using 4.5 Hz geophones and 24 channel linear arrays using 4.5 Hz geophones (Figure 11). An L-shaped array yields two linear arrays that can be analyzed separately. Passive surface wave data were acquired using nested triangle arrays at sites where there was sufficient accessible open space to deploy the array. L-shaped arrays were utilized when only the perimeter of a site or the sidewalks of intersecting streets were accessible. Passive surface wave data were also acquired along linear arrays during this investigation, primarily to assess the performance of this array type relative to the preferred 2-D array geometry. Photographs of the array microtremor equipment are presented in Figure 12. Ambient noise measurements were generally recorded along each array for 30 minutes at a 2 ms sample rate (60, 30 second records). Data were stored on a laptop computer for later processing. The field geometry and associated files names were documented in field data acquisition forms.

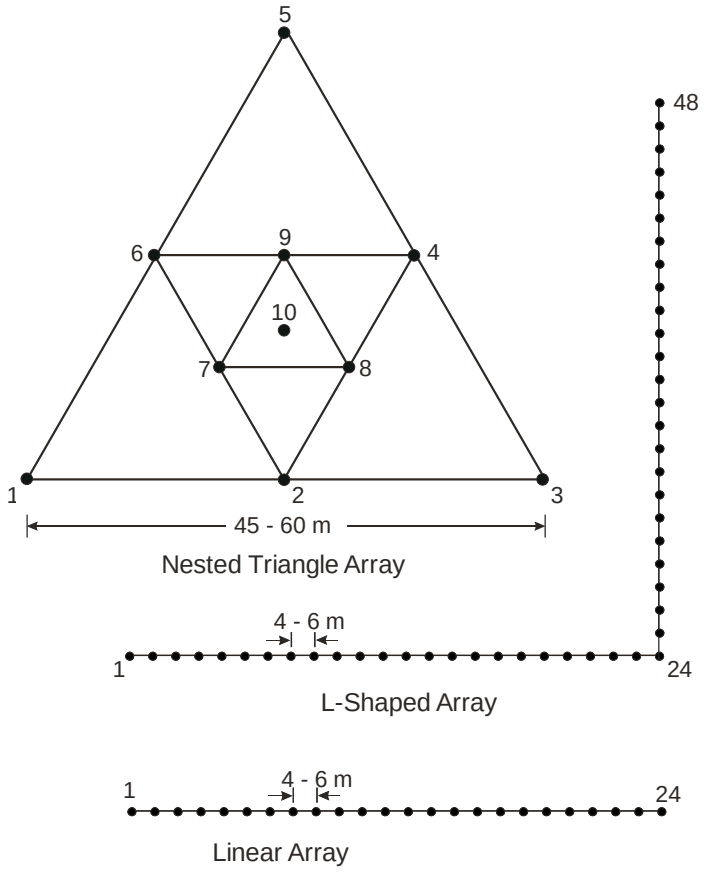

Figure 11 Array types utilized for array microtremor measurements

At sites where the primary nearby noise source was a single road (CE.12092), seismic records where vehicles were in the site vicinity or, in the case of a linear array oriented perpendicular to the road, passed the end of the array were documented in field notes. At one shallow rock site (CE.13123), there was very little vehicular traffic in the site vicinity during acquisition of passive

surface wave data along the nested triangle array. Therefore, additional array microtremor data were acquired with our field vehicle driving on the road around the perimeter of the parking lot where the array was established.

Figure 12 Nested triangle and linear arrays used for array microtremor measurements at CE.13079

3.4 HVSR Measurements

The seismic systems used to acquire HVSR data consisted of a Nanometrics Trillium Compact 120 second seismometer coupled to a Nanometrics Taurus data acquisition unit (referred to herein as Trillium) and a Micromed Tromino® ENGY (herein referred to as Tromino) as shown in Figures 13 and 14. The Trillium was coupled to the ground using an aluminum cradle with or without spikes depending upon whether the system was deployed on concrete or on soil. The Tromino was coupled to the ground using either geophone spikes adapted for measurements on soil or aluminum legs adapted for measurements on hard surfaces. The Trillium was set up at location near the seismic station with measurements made for the duration of array microtremor acquisition (> 1 hour) with ambient noise data recorded at 200 samples per second. Microtremor data were stored in the Taurus data acquisition system and downloaded as miniseed format files at the end of each field day. At sites with expected shallow bedrock (< 60 m depth), HVSR measurements were also made at two other locations near the surface wave testing arrays, using a Tromino, to demonstrate that bedrock depth was not highly variable across the site. These microtremor measurements were made for 20 to 30 minutes at each measurement location with data recorded at 128 samples per second. Recordings were stored in the instrument's internal memory, downloaded to a laptop computer, viewed in the software package (Grilla) provided by Micromed, and reformatted to an ASCII file for further analysis. It should be noted that the Trillium is expected to provide the most reliable HVSR data in deep sedimentary basins and can yield reliable results at frequencies as low as 0.1 Hz, although such measurements require a long recording interval at night. On the other hand, the Tromino is designed for rapid, short duration deployment in shallow basins and will not yield reliable results at frequencies less than about 1.5 Hz in low noise environments.

Figure 13 Nanometrics Trillium Compact seismometer used for HVSR measurements

Figure 14 Micromed Tromino® ENGR seismometer used for HVSR measurements

4 DATA REDUCTION AND MODELING

4.1 MASW Data Reduction

Prior to data reduction, seismic records were reviewed to identify relevant geologic structures that could be constrained during data modeling; the most pertinent being approximate depth to high Poisson's ratio saturated sediments identified from P-wave refraction first arrival data in MAS_RW seismic records. It is important to constrain the approximate depth to and P-wave velocity of the saturated zone when modeling Rayleigh wave dispersion data in order to develop as accurate a V_S model as possible. A similar data reduction sequence is used for both MAS_RW and MAS_LW data.

The MASW data were reduced using the software Seismic Pro Surface V8.0 developed by Geogiga using the following steps:

- Input seismic record into software.
- Enter receiver spacing, geometry, offset range used for analysis, etc.
- Apply wavefield transform to seismic record to convert the data from time – offset to frequency – phase velocity space.
- Identify and pick Rayleigh wave dispersion curve.
- Repeat for all seismic records.
- Apply near-field criteria (maximum wavelength equal 1 to 1.3 times the source to midpoint of receiver array distance for Rayleigh wave data and 1.5 times the source to midpoint of receiver array distance for Love wave data).
- Merge multiple dispersion curves extracted from the MASW data collected along each seismic spread (different source types, source locations, different receiver offset ranges, etc.).
- Convert dispersion curves to required format for modeling.
- Calculate a representative dispersion curve for the combined MASW dispersion data using a moving average polynomial curve fitting routine.

A unique data acquisition and data reduction procedure used by **GEO***Vision* for 1-D MASW soundings is the use of multiple source types and source locations during data acquisition and the extraction of multiple (>50) dispersion curves from the different source locations and limited offset range receiver gathers associated with each source location. The use of such a data acquisition and processing strategy ensures that the modeled dispersion curve covers as wide a frequency/wavelength range as possible and is representative of average conditions beneath the array.

As an example, Figure 15 presents the frequency-phase velocity images of the seismic record offset 1 m from the near geophone at site CE.13080. The image on the left is from a seismic record collected using the AWD source with all 48 channels used for analysis. The image on the right is from a seismic record collected using a 4 lb hammer source with only the near 12 channels used for analysis in order to extract higher frequency (smaller wavelength) dispersion data. The 48 channel receiver gather only recovers the fundamental mode Rayleigh wave at frequencies less than 30 Hz with the 1st higher mode Rayleigh wave dominant at higher frequencies. The receiver gather comprised of the nearest 12 geophones recovers the fundamental mode Rayleigh wave to a frequency of greater than 100 Hz.

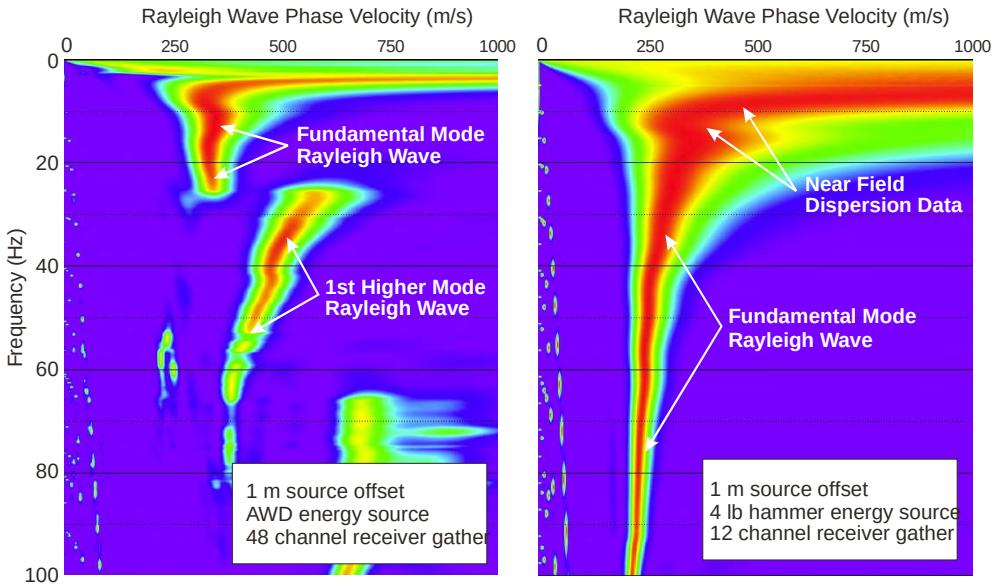

Figure 15 Comparison of Rayleigh wave f-v transforms from 48 and 12 channel receiver gathers at seismic station CE.13080.

4.2 Array Microtremor Data Reduction

Array microtremor data collected along nested triangle, L-shaped, and linear arrays were reduced using the ESAC method. Array microtremor data collected along linear arrays were also reduced using the ReMi™ method.

The processing sequence for implementation of the ESAC method in the SeisImager software package is as follows:

- Input all seismic records for a dataset into software.
- Load geometry (x and y positions) for each channel in seismic records.
- Calculate the SPAC coefficients for each seismic record and average.
- For each frequency calculate the RMS error between the SPAC coefficients and a Bessel function of the first kind and order zero over a user defined phase velocity range and velocity step.
- Plot an image of RMS error as a function for frequency (f) and phase velocity (v).
- Identify and pick the dispersion curve as the continuous trend on the f-v image with the lowest RMS error.
- Convert dispersion curves to appropriate format for modeling.
- Combine multiple passive dispersion curves, as appropriate.
- Calculate a representative dispersion curve for the passive dispersion data using a moving average polynomial curve fitting routine.

Figure 16 provides an example result from ESAC data processing (note that data are not from the current investigation). The velocity-frequency image shows the degree of fit of the Bessel function to the SPAC coefficients. The receiver offset versus coherence plot shows the best fitting Bessel function for the SPAC coefficients at 1.7 Hz, which, in this case, is at a velocity of 463 m/s.

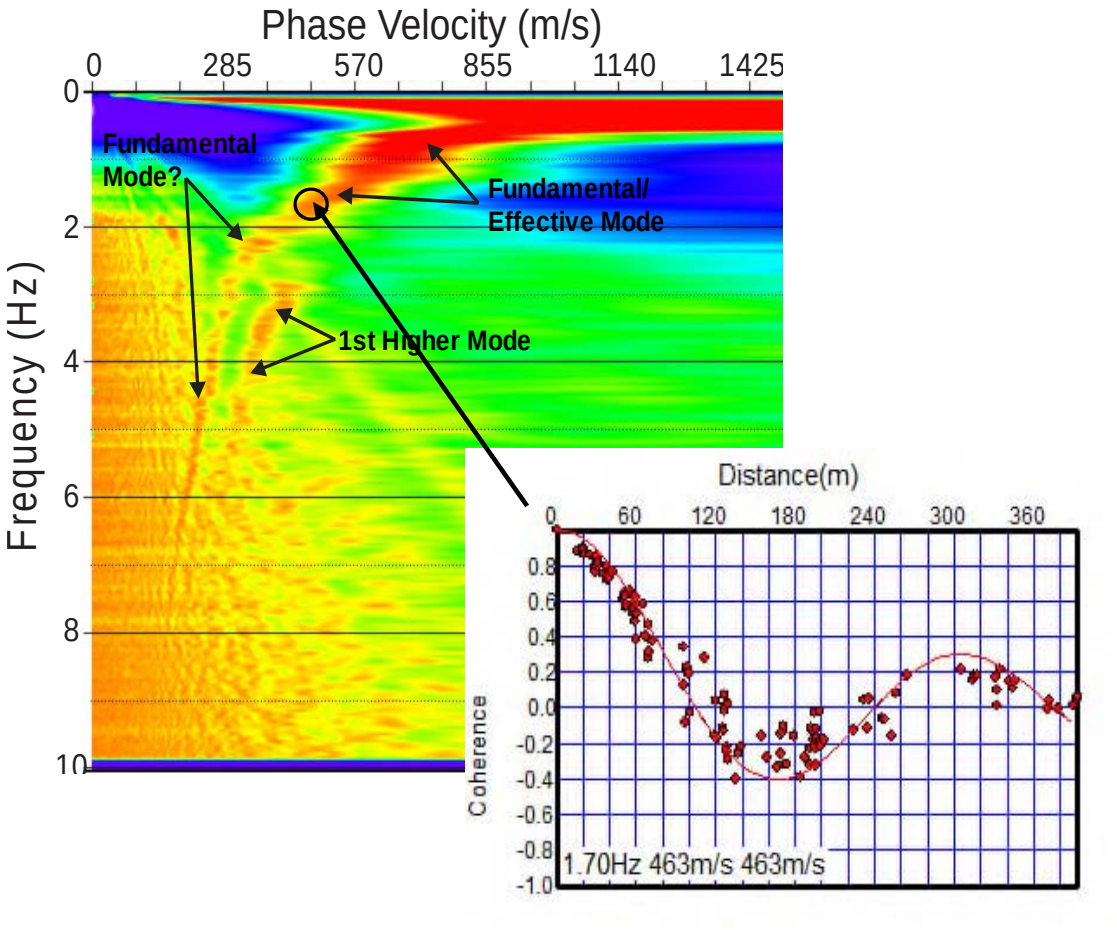

Figure 16 Example of ESAC data reduction

The linear array microtremor data were reduced using both the Optim™ Software and Data Services SeisOpt® ReMi™ v5.0 data analysis package and ESAC method described above. Data reduction steps using the ReMi™ software included the following:

- Conversion of SEG-2 format field files to SEG-Y format.
- Data preprocessing which includes trace-equalization gaining and DC offset removal.
- Inputting receiver geometry.
- Computing the velocity spectrum of each record by p-f transformation in both forward and reverse directions.
- Combining the individual p-f transforms (either all or selected) into one image.
- Picking and saving the dispersion curve.
- Conversion of the dispersion curve to appropriate format for modeling.
- Combination of dispersion curve with other passive dispersion curves as appropriate.

An example of the interpretation of linear array microtremor data collected at seismic station CE.12092 is presented as Figure 17. The ReMi™ technique requires that the dispersion curve is interpreted along the lower envelope of the surface wave energy, which is subjective. Analysis of linear array microtremor data using the ESAC technique is not subjective; however, the resulting dispersion curve is only accurate if the multi-directional noise criteria are adequately satisfied.

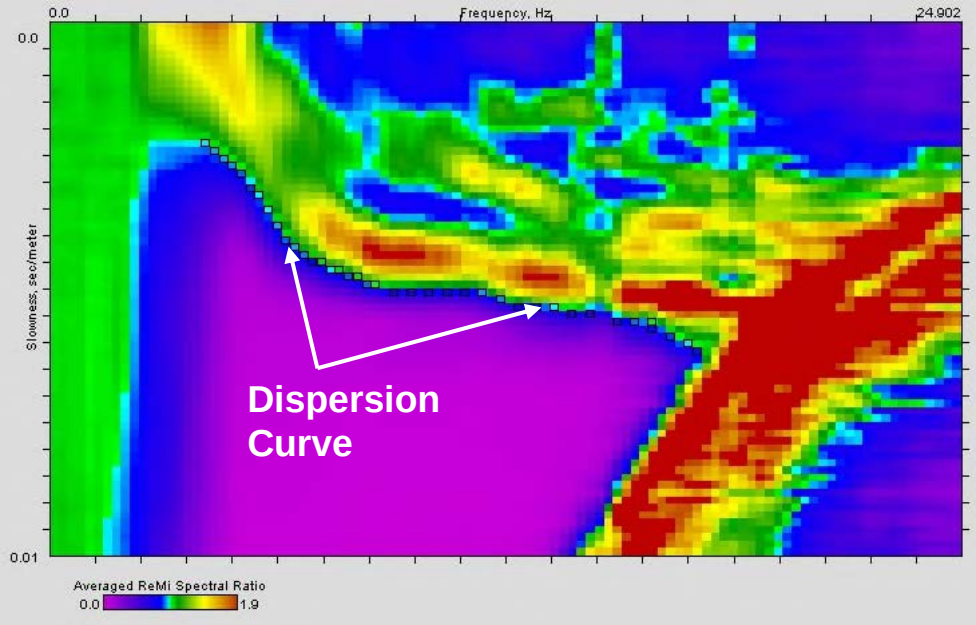

Figure 17 Example of ReMi™ processing with dispersion curve picked along lower envelope of Rayleigh wave energy

4.3 Horizontal/Vertical Spectral Ratio Measurements

HVSR data were reduced using the Geopsy Version 2.9.1 software package (http://www.geopsy.org) developed by Marc Wathelet, ISTerre, Grenoble, France with the help of many other researchers.

Microtremor data recorded by the Trillium were exported to miniseed format. Microtremor data recorded by the Tromino were exported to an ASCII file using the software package Grilla, provided with the instrument. Upon export, a 0.3-Hz low-cut filter was automatically applied to the Tromino data. Data files were then loaded into the Geopsy software package, where data file columns containing the vertical and horizontal (north and east) components and the sample rate were specified. HVSR was typically calculated over a frequency range dependent upon the observed site response and using a time window length of 30 to 200 s. Time windows were automatically picked. Fourier amplitude spectra were calculated after applying a 10% cosine taper and smoothed by the Konno and Ohmachi filter with a smoothing coefficient value of 30. The vertical amplitude spectra were divided by the root-mean-square (RMS) of the horizontal amplitude spectra to calculate the HVSR for each time window and the average HVSR. Time windows containing clear transients (nearby foot or vehicular traffic) or yielding poor quality results were then deleted and the computations repeated. The average HVSR peak frequency

and standard deviation from all time windows used for analysis is computed and presented along with the standard deviation of the HVSR amplitudes for all time windows.

Figure 18 presents example HVSR data from seismic station CE.13921. The colored lines are the HVSR for each 200 s time window used for analysis. The solid black line is the average HVSR response and the dashed lines represent the HVSR standard deviation. The vertical grey bars represent the average peak frequency of all of the time windows and the standard deviation.

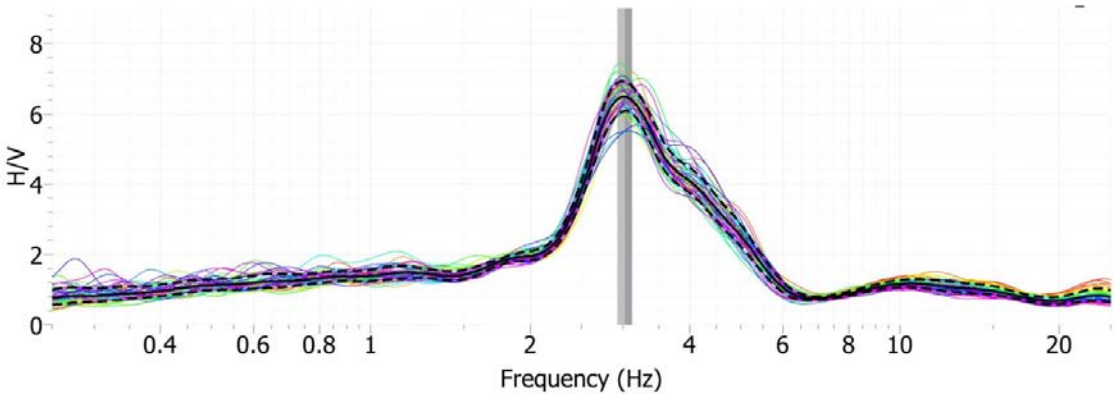

Figure 18 Example HVSR data from seismic station CE.13921

4.4 Surface Wave Modeling

The representative dispersion curves from the active and passive surface wave data at each sounding location were combined and the moving average polynomial curve fitting routine in WinSASW V3 was used to generate a composite representative dispersion curve for modeling. During this process the active surface wave data were given equal weight to the combined passive surface wave data in the overlapping wavelength range and the combined weight of any linear passive arrays used for analysis was always less than that of the 2D arrays. An equal logarithm wavelength sample rate was used for the representative dispersion curve to reflect the gradual loss in model resolution with depth. During this process the active surface wave data were given equal weight to the combined passive surface wave data in the overlapping wavelength range.

Dispersion data from linear arrays were only combined with those from 2D arrays for modeling at 6 of the 12 sites. Additionally, one linear leg of an L array generally provided more reliable dispersion curves than the other. It should be noted, however, that almost all passive surface wave dispersion curves, regardless of data reduction methodology, would have yielded acceptable estimates of V_{S30}. However, V_S models developed from combined MASW and 2D array microtremor array dispersion data are much more robust and reliable. In fact, V_S models developed from some of the linear passive surface wave data would have been very inaccurate at some sites, even though the estimates of V_{S30} would have been acceptable. The mean and standard deviation of V_{R40} were calculated from the combined and weighted dispersion data from the active and passive surface wave soundings for use in estimating the error in V_{S30}. The scatter in V_{R40} is a function of measurement and analytical errors as well as the lateral velocity

variability beneath the measurement array(s). V_{R40} can also be used to estimate V_{S30} using the Brown, et al., 2000 relationship presented previously.

The final composite representative dispersion curve for each site was loading into an inverse modeling software package to develop a V_S model. During this process an initial velocity model was generated based on general characteristics of the dispersion curve and the inverse modeling routine utilized to adjust the layer V_S until an acceptable agreement with the observed data was obtained. Layer thicknesses were adjusted and the inversion process repeated until a V_S model was developed with low RMS error between the observed and calculated dispersion curves. Finally, at sites where high velocity bedrock was encountered within the depth of investigation, multiple V_S models were developed to demonstrate model non-uniqueness, particularly in depth to and velocity of the half space (bedrock unit). Typically, the V_S model with intermediate depth to rock was selected for the purpose of site characterization unless HVSR data indicated another V_S model was more appropriate. V_{S30} was estimated from the resulting V_S models as the ratio of 30 m and the travel time of an S-wave through the 30 m soil/rock column. At sites where rock was encountered within the depth of investigation, the predicted HVSR peak based on the diffuse field assumption was computed for all V_S models using the software package *HV-Inv* Release 1.0 Beta, which is summarized in García-Jerez, et al., 2016, and compared to the observed HVSR peaks.

Rayleigh wave dispersion data were modeled using either the fundamental or effective mode solution in the WinSASW V3 and Seisimager software packages. Three sites (CE.13123, CE.13925, and CE.13927) required an effective mode solution to model a smooth transition from fundamental to 1st higher mode Rayleigh wave at low frequencies. Love wave dispersion data collected at site CE.13924 were modeled using the fundamental mode Love wave solution in the Seisimager software package. Data inputs into the modeling software include layer thickness, S-wave velocity, P-wave velocity or Poisson's ratio (Rayleigh wave only), and mass density. P-wave velocity and mass density only have a very small influence (i.e. less than 10% providing realistic parameters used) on the S-wave velocity model generated from a surface wave dispersion curve. However, realistic assumptions for P-wave velocity, which is significantly impacted by the location of the saturated zone, and mass density will significantly improve the accuracy of the S-wave velocity model.

Constant mass density values of 1.7 to 2.3 g/cm^3 were used in the V_S profiles for subsurface soils depending on P and S-wave velocity. Within the normal range encountered in geotechnical engineering, variation in mass density has a negligible (±2%) affect on the estimated V_S from surface wave dispersion data. Figure 19 demonstrates the effect of density on the resulting V_S model. V_S models are developed for a synthetic model with identical dispersion curves the only variable being constant density (i.e. no reflectivity associated with density) in one model, realistic variation in density with seismic velocity and depth in another model, and an unrealistic amount of density variation in the final model. Relative to the V_S model with realistic density variation, V_{S30} is overestimated by about 1.5% in the V_S model with constant density and underestimated by about 4.5% in the V_S model with an unrealistic amount of density variation. Based on this example, we conclude that the use of realistic density variation in the V_S models will result in an error in V_{S30} associated with density on the order of 1%.

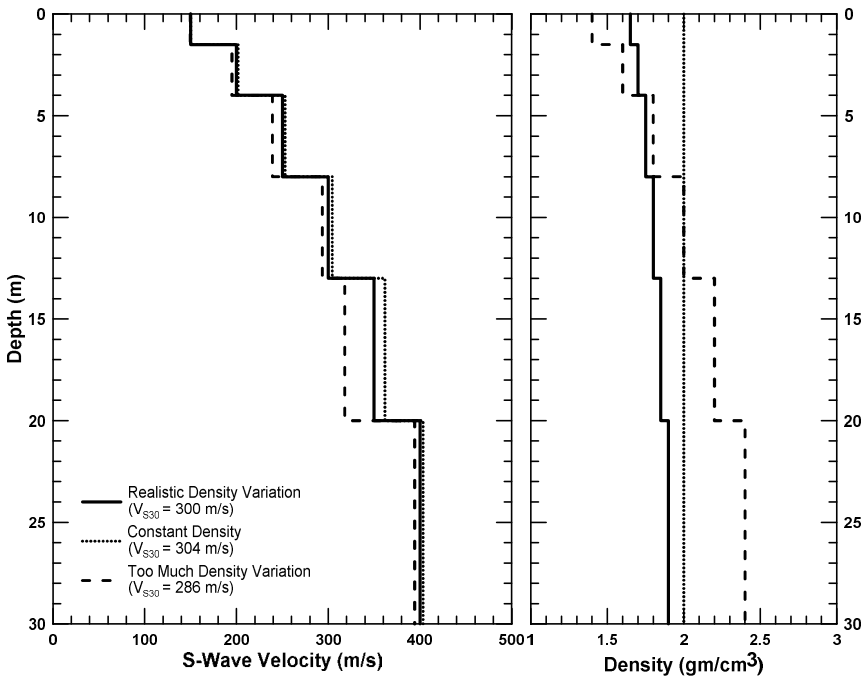

Figure 19 Influence of density on V_S models

During modeling of Rayleigh wave dispersion data, the compression wave velocity (V_P) for unsaturated sediments and weathered rock was estimated using a Poisson's ratio (v) of 0.3 and the relationship:

$$V_P = V_S\,[(2(1-v))/(1-2v)]^{0.5}$$

Poisson's ratio has a larger affect than density on the estimated V_S from Rayleigh wave dispersion data. Achenbach (1973) provides approximate relationship between Rayleigh wave velocity (V_R), V_S and v:

$$V_R = V_S\,[(0.862 + 1.14\,v)/(1+\,v)]$$

Using this relationship, it can be shown that V_S derived from V_R only varies by about 10% over possible 0 to 0.5 range for Poisson's ratio where:

$V_S = 1.16V_R$ for $v = 0$
$V_S = 1.05V_R$ for $v = 0.5$

The common range of the Poisson's ratio for unsaturated sediments and rock is about 0.25 to 0.35, although there can be exceptions. Over this range, V_S derived from modeling of Rayleigh wave dispersion data will vary by about 5%. An intermediate Poisson's ratio of 0.3 was, therefore, selected for modeling to minimize any error associated with the assumed Poisson's ratio.

To reduce errors associated with expected high Poisson's ratio of saturated sediments, seismic refraction first arrival data were reviewed in the MASRW seismic records to determine if there was any evidence of a refractor associated with the top of the saturated zone in the upper 20 to

30 m. If a saturated zone refractor was identified, interactive layer based modeling was conducted to estimate the depth to and V_P (>1,500 m/s) of the saturated sediments, which was then constrained when modeling the dispersion data. Poisson's ratio of saturated, soft sediments can be slightly less than 0.5, and gradually decrease with depth as the sediments become stiffer. It should be noted that Poisson's ratio only affects V_S models developed from Rayleigh wave dispersion data and not those developed from Love wave dispersion data.

Figure 20 demonstrates the effect of Poisson's ratio on the resulting V_S model. V_S models are developed for a synthetic model with identical dispersion curves the only variable being constant Poisson's ratio, which is allowed to vary from 0.1 to 0.495. There is a 20% variation in V_{S30} for V_S models with constant Poisson's ratio over the 0.1 to 0.495 range, but only 6% variation in V_{S30} for V_S models with Poisson's ratio over the common 0.25 to 0.35 range for unsaturated sediments and rock. Therefore, the error in V_{S30} associated with assumed Poisson's ratio may only be on the order of 3% providing the depth to and V_P of the saturated zone is constrained and a Poisson's ratio near 0.3 is used for unsaturated sediments when modeling Rayleigh wave dispersion data.

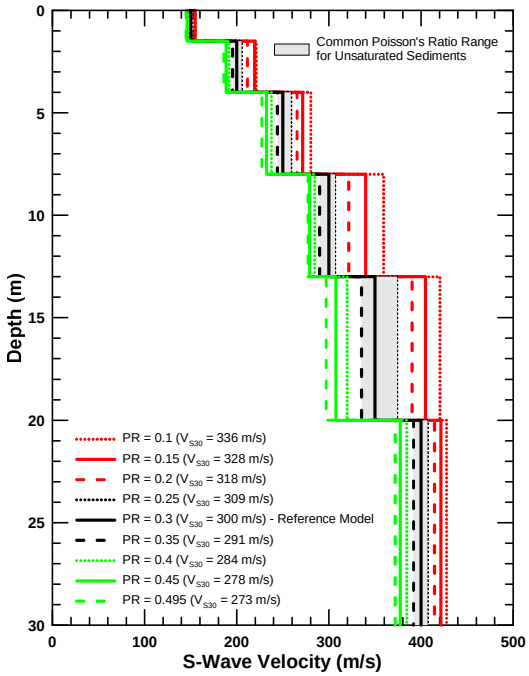

Figure 20 Influence of Poisson's ratio on V_S models derived from Rayleigh wave dispersion data

When modeling surface wave dispersion data, multiple V_S models exist that equally well fit the observed dispersion curve; referred to as non-uniqueness. Non-uniqueness has been found to have very little effect on estimated V_{S30} as shown in the example presented as Figure 21. In this example from station CE.13929, characterized as part of Yong, et al., 2013, multiple V_S models are presented with effectively identical Love wave dispersion curve yet only result in about 2% variation in V_{S30}. The variation in V_{S30} would have been greater had multiple models been generated that fit within error bars defined by the scatter in the dispersion data. However, we address this component of error using the scatter in V_{R40}.

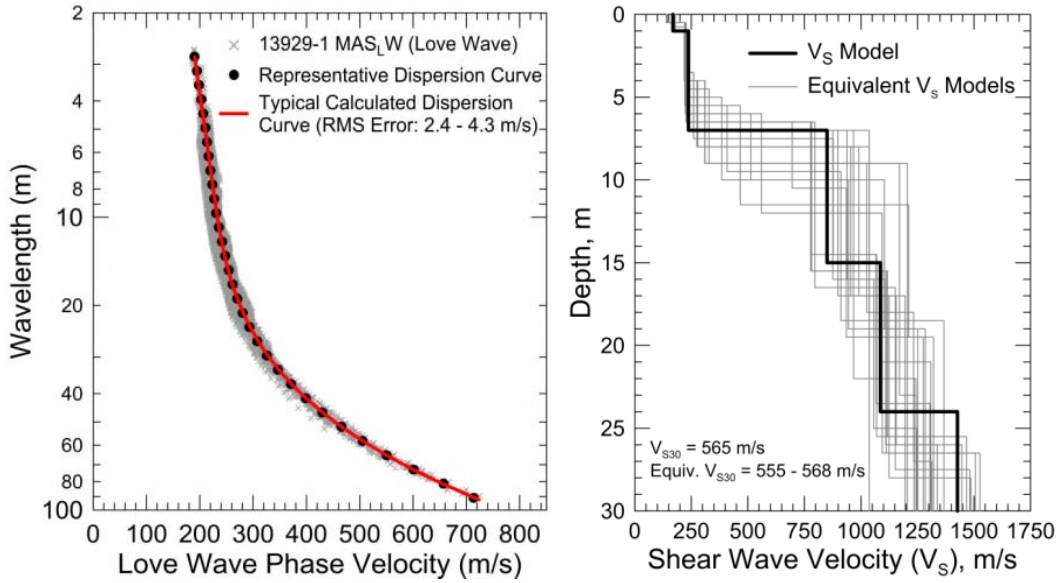

Figure 21 Influence of non-uniqueness on estimated V_{S30}

The error in V_{S30} is the combined effect of assumed density and Poisson's ratio on the resulting V_S models, the error in V_{S30} associated with non-uniqueness, and error in the dispersion curves which is accounted for using the scatter in V_{R40}. Therefore, the estimated error in V_{S30}, which includes some effects of the lateral velocity variability beneath the testing arrays, was computed as the sum of the following rounded up to the nearest 5 m/s: an estimated error of 3% from the realistic assumed layer Poisson's ratios in the model, 1% error from the realistic assumed layer densities in the model, 2% for the variation in V_{S30} associated with non-uniqueness, and the standard deviation in V_{R40} between the combined active and passive surface wave dispersion data. In general, resulting errors are slightly less than 10%. Because this error includes some component of the lateral variability beneath the testing arrays, actual error may be lower. It is of interest to note that V_{S30} estimates based on V_{R40} are within 4% of those estimated from the V_S models at all of the sites.

5 RESULTS

Data reports for each site are presented in Appendix A. These reports include the following:

- Site name and location.
- V_{S30} and estimated error.
- NEHRP Site Class.
- Geomatrix Code.
- Geologic and site conditions.
- Description of testing arrays.
- Tabulated V_S model.
- Discussion and comments.
- Site map showing the approximate location of the seismic station and testing arrays.
- Geologic map.
- Photographs of surface wave testing.
- Plots of HVSR data.
- A composite plot of all dispersion data reduced from the active and passive surface wave data along with a discussion of data sets used for site characterization.
- Plots of field, representative and calculated dispersion data and V_S models.

The V_{S30}, estimated error in V_{S30}, and NEHRP site class for the seismic stations characterized during this investigation are summarized in Table 3.

Table 3 Summary of Results

Station No.	V_{S30} (m/s)	Estimated Error (m/s)	NEHRP Site Class
12092	274	25	D
12102 & 12673	289	25	D
12331	297	25	D
12923	273	25	D
13079	305	30	D
13080	420	40	C
13123	547	55	C
13172	350	35	D/C
13921	427	35	C
13924	475	40	C
13925	380	30	C
13927	325	35	D

6 REFERENCES

Achenbach J, 1973, Wave Propagation in Elastic Solids, Elsevier, Amsterdam, Netherlands.

Aki K, 1957, Space and time spectra of stationary stochastic waves, with special reference to microtremors. *Bull. Earthq. Inst. Univ. Tokyo*, v. 35, pp. 415–457.

Albarello D and Gargani G, 2010, "Providing NEHRP soil classification from the direct interpretation of effective Rayleigh-wave dispersion curves", *Bulletin of the Seismological Society of America,* Vol. 100, No. 6, p 3284-3294.

Asten M, 2006, Site shear velocity profile interpretation from microtremor array data by direct fitting of SPAC curves, in *Proceedings of the Third Int. Symp. Effects of Surface Geol. Seismic Motion*, Vol. 2, LCPC Edition, Grenoble, France, August 30–September 01, Paper No. 99, 1069-1080.

Asten M, Stephenson WJand Hartzell, S, 2015, The use of wavenumber normalization in computing spatially averaged coherencies (krSPAC) of microtremor data from asymmetric arrays, *Proceedings 6th International Conference on Earthquake Geotechnical Engineering*, Christchurch, New Zealand, 9 p.

Bettig B, Bard PY, Scherbaum F, Riepl J, Cotton F, Cornou C and Hatzfeld D, 2001, Analysis of dense array noise measurements using the modified spatial auto-correlation method (SPAC): application to the Grenoble area, *Bollettino di Geofisica Teoricaed Applicata*, Vol 42, p 281–304.

Brown L, 1998, Comparison of V_S profiles from SASW and borehole measurements at strong motion sites in Southern California, Master's thesis, University of Texas, Austin.

Brown L, Diehl J and Nigbor R, 2000, A simplified method to measure average shear-wave velocity in the top 30 m (V_s30), *Proc. 6th International Conference on Seismic Zonation*, 1–6.

BSSC, 2003, *NEHRP recommended provisions for seismic regulations for new buildings and other structure (FEMA 450), Part I: Provisions*, Building Seismic Safety Council, Federal Emergency Management Agency, Washington D.C.

Capon J, 1969, High-resolution frequency-wavenumber spectrum analysis, *Proc. Institute of Electrical and Electronics Engineers (IEEE)*, Vol. 57, no. 8, p 1408–1418.

Comina C, Foti S, Boiero D, and Socco LV, 2011, Reliability of $V_{S,30}$ evaluation from surface-wave tests, *J. Geotech. Geoenviron. Eng.*, p 579–586.

Dal Moro G, Moura R, Moustafa A, 2015, Multi-component joint analysis of surface waves, *Journal of Applied Geophysics*, Vol. 119, p 128-138.

Dal Moro G and Ferigo F, 2011, Joint Analysis of Rayleigh- and Love-wave dispersion curves: Issues, criteria and improvements, *Journal of Applied Geophysics*, Vol. 75, p 573-589.

Ellefsen K, 2003, Seg2_edit: a program for editing and manipulating SEG-2 files, *U.S. Geol. Surv. Open-File Rept. 03-141*, 11 pp.

Foti S, 2000, Multistation Methods for Geotechnical Characterization using Surface Waves, Ph.D. Dissertation, Politecnico di Torino, Italy.

GEOVision, Inc (2012): EPRI (2004, 2006) ground-motion model (GMM) review project: Shear wave velocity measurements at seismic recording stations, http://www.epri.com/abstracts/Pages/ProductAbstract. aspx?ProductId=000000003002000719.

Imai T, Fumoto H, and Yokota K, 1976, P- and S-Wave Velocities in Subsurface Layers of Ground in Japan, Oyo Corporation Technical Note N-14.

International Committee of Building Officials, 2000 International Building Code, ICC, Hauppauge, NY, Section 1615.1.1

García-Jerez A, Piña-Flores J, Sánchez-Sesma F, Luzón, F, Perton, M, 2016, A computer code for forward computation and inversion of the H/V spectral ratio under the diffuse field assumption, Computers & Geosciences, In Press.

Joh S, 1996, Advances in interpretation and analysis techniques for spectral-analysis-of-surface-waves (SASW) measurements, Ph.D. Dissertation, University of Texas, Austin.

Joh S, 2002, WinSASW V2.0, Data Interpretation and Analysis for SASW Measurements, Department of Civil Engineering, Chung-Ang University, Anseong, Korea.

Lacoss R, Kelly E and Toksöz M, 1969, Estimation of seismic noise structure using arrays, *Geophysics*, v. 34, pp. 21-38.

Li J and Rosenblad B, 2011, Experimental study of near-field effects in multichannel array-based surface wave velocity measurements, *Near Surface Geophysics*, Vol. 9, 357-366.

Ling S and Okada H, 1993, An extended use of the spatial correlation technique for the estimation of geological structure using microtremors, *Proc. the 89th Conference Society of Exploration Geophysicists Japan (SEGJ)*, pp. 44–48 (in Japanese).

Louie J, 2001, Faster, Better: Shear-Wave Velocity to 100 Meters Depth from Refraction Microtremor Arrays, *Bulletin of the Seismological Society of America*, vol. 91, no. 2, p. 347-364.

Martin A and Diehl J, 2004, Practical experience using a simplified procedure to measure average shear-wave velocity to a depth of 30 meters (V_S30), *Proceedings of the 13th World Conference on Earthquake Engineering*, Vancouver, B.C., Canada, August 1-6, 2004, Paper No. 952.

Martin A, Shawver J and Diehl J, 2006, Combined use of Active and Passive Surface Wave Techniques for Cost Effective UBC/IBC Site Classification, *Proceedings of the 8th National Conference on Earthquake Engineering*, San Francisco, California, Paper No. 1013.

Martin A, Yong A and Salomone L, 2014, Advantages of active Love wave techniques in geophysical characterization of seismographic station sites – case studies in California and the Central and Eastern United States, Proceedings of the Tenth U.S. National Conference on Earthquake Engineering, Frontiers of Earthquake Engineering, July 21-25, Anchorage, Alaska.

Nakamura Y, 1989, A method for dynamic characteristics estimation of subsurface using microtremor on the ground surface, *Quart. Reprt Rail. Tech. Res. Inst.*, Vol. 30, no. 1, p 25–33.

Nogoshi M and Igarashi T, 1971, On the amplitude characteristics of microtremor (part 2), *J. Seismol. Soc. Japan*, Vol. 24, p 26–40 (in Japanese).

Ohori M, Nobata A, and Wakamatsu K, 2002, A comparison of ESAC and FK methods of estimating phase velocity using arbitrarily shaped microtremor arrays, *Bull. Seismol. Soc. Am.*, v. 92, no. 6, p. 2323–2332.

Okada H, 2003, The Microtremor Survey Method, *Society of Exploration Geophysics Geophysical Monograph Series*, Number 12, 135p.

Park C, Miller R and Xia J, 1999a, Multimodal analysis of high frequency surface waves, *Proceedings of the Symposium on the Application of Geophysics to Engineering and Environmental Problems '99*, 115-121.

Park C, Miller R and Xia, J, 1999b, Multichannel analysis of surface waves, *Geophysics*, Vol 64, No. 3, 800-808.

Rix G, 1988, Experimental study of factors affecting the spectral-analysis-of surface-waves method, Ph.D. Dissertation, University of Texas, Austin.

Roesset J, Chang D and Stokoe K, 1991, Comparison of 2-D and 3-D Models for Analysis of Surface Wave Tests, *Proceedings*, 5th *International Conference on Soil Dynamics and Earthquake Engineering*, Karlsruhe, Germany.

Stokoe K, Rix G and Nazarian S, 1989, In situ seismic testing with surface waves, *Proceedings, Twelfth International Conference on Soil Mechanics and Foundation Engineering, Vol. 1,* Rio de Janeiro, Brazil, pp. 330-334.

Stokoe K, Wright S, Bay J and Roesset J, 1994, Characterization of Geotechnical Sites by SASW Method, *ISSMFE Technical Committee 10 for XIII ICSMFE, Geophysical Characteristics of Sites*, A.A. Balkema Publishers/Rotterdam & Brookfield, Netherlands, pp. 146.

Xia J, Xu Y, Luo Y, Miller R, Cakir R and Zeng C, 2012, Advantages of using Multichannel analysis of Love waves (MALW) to estimate near-surface shear-wave velocity, *Surveys in Geophysics*, 841–860.

Yong A, Martin A, Stokoe K and Diehl J, 2013, ARRA-funded V_{S30} measurements using multi-technique method approach at strong-motion stations in California and Central-Eastern United States, Open-File Report 2013-1102, United States Geological Survey, http://pubs.usgs.gov/of/2013/1102/.

Yoon S and Rix G, 2009, Near-field effects on Array-based surface wave methods with active sources, *Journal of Geotechnical and Geoenvironmental Engineering*, Vol. 135, no. 3, 399-406.

7 CERTIFICATION

All geophysical data, analysis, interpretations, conclusions, and recommendations in this document have been prepared under the supervision of and reviewed by a **GEO*Vision*** California Professional Geophysicist.

Reviewed and approved by

9/15/2016

Antony Martin Date
California Professional Geophysicist, P. GP 989
GEO*Vision* Geophysical Services

* This geophysical investigation was conducted under the supervision of a California Professional Geophysicist using industry standard methods and equipment. A high degree of professionalism was maintained during all aspects of the project from the field investigation and data acquisition, through data processing interpretation and reporting. All original field data files, field notes and observations, and other pertinent information are maintained in the project files and are available for the client to review for a period of at least one year.

  A professional geophysicist's certification of interpreted geophysical conditions comprises a declaration of his/her professional judgment. It does not constitute a warranty or guarantee, expressed or implied, nor does it relieve any other party of its responsibility to abide by contract documents, applicable codes, standards, regulations or ordinances.

APPENDIX A

DATA REPORTS

Site CE.12092

Station Name: Radec - Sage & Cottonwood School Roads

Location: Cottonwood Fire Station, 44222 Sage Rd., Aguanga, CA 92536

Latitude: 33.4818 **Longitude:** -116.9114

V_{S30} (measured): 274 m/s

Estimated error in V_{S30}: ± 25 m/s

NEHRP Site Class: D

Geomatrix Code: AHC/AQC

Geologic Conditions/Observations: Site located in area mapped as Quaternary (Holocene and late Pleistocene) flood plain deposits. Outcrop of Tertiary Temecula Arkose approximately 90 m west of seismic station. Outcrop of Cretaceous tonalite approximately 325 m northwest of seismic station.

Site Conditions: Rural site with minor traffic noise from nearby roads, particularly Sage Road. Relatively flat terrain in immediate site vicinity.

Geophysical Methods Utilized: MAS_RW, array microtremor, HVSR

Geophysical Testing Arrays:

1. Array 1: 10 channel, nested triangle passive surface wave array utilizing 1 Hz geophones and a 60 m length for outer side of array.
2. Array 2: 24 channel, linear passive surface wave array utilizing 4.5 Hz vertical geophones spaced 4.5 m apart for a length of 103.5 m.
3. Array 3: 48 channel MAS_RW array utilizing 4.5 Hz vertical geophones spaced 1.5 m apart for a length of 70.5 m, forward and reverse shot locations with multiple source offsets (1.5 m at east end of array and 1.5 to 30 m at west end of array) and multiple interior source locations. Accelerated weight drop used at all source locations offset from ends of array and 4 and 12 lb hammers used at near-offset source location and interior source locations.
4. Two HVSR measurement locations; one in the vicinity of the MAS_RW and microtremor arrays and one near the seismic station.

Location of Geophysical Testing Arrays:

Location	Latitude	Longitude
Array 1 Passive, Corner of Array, Sensor Location 1	33.48207	-116.91126
Array 1 Passive, Corner of Array, Sensor Location 3	33.48261	-116.91132
Array 1 Passive, Corner of Array, Sensor Location 5	33.48229	-116.91184
Array 1 Passive, Center of Array, Sensor Location 10	33.48230	-116.91147
Array 2 Passive, West End of Array	33.48194	-116.91199
Array 2 Passive, East End of Array	33.48199	-116.91085
Array 3 MASW, West End of Array	33.48197	-116.91166
Array 3 MASW, East End of Array	33.48199	-116.91090
HVSR Location 1	33.48188	-116.91134
HVSR Location 2	33.48223	-116.91142

Notes: 1) WGS84 Coordinate System (decimal degrees)

Results:

V_S Model

Depth to Top of Layer (m)	Layer Thickness (m)	S-Wave Velocity (m/s)	Inferred P-Wave Velocity (m/s)	Assumed Poisson's Ratio	Assumed Density (g/cm^3)
0	1	221	414	0.300	1.80
1	3	198	371	0.300	1.80
4	5	210	392	0.300	1.80
9	8	223	1700	0.491	1.80
17	25	430	1750	0.468	2.00
42	>18	615	1800	0.434	2.10

Notes: 1) Depth of investigation is about 60 m.
2) Depth to groundwater anchored at 9 m depth with V_P > 1700 m/s based on review of seismic refraction first arrival data.

Observations/Discussion:

- The HVSR curves derived from single station ambient noise measurements at two locations on site are similar, validating the 1-D velocity structure assumption.
- The HVSR plots show a peak in the 2.7 to 3.1 Hz range indicative of significant impedance contrast within the expected depth of investigation of the active and passive surface wave sounding. The HVSR data collected using both the Trillium Compact and Tromino sensors at Location 1 are similar at frequencies above 1.5 Hz. The Trillium Compact yields much more reliable HVSR data at lower frequencies.

- The 2.7 to 3.1 Hz HVSR peaks are likely associated with the top of the Tertiary Temecula Arkose geologic unit based on mapped geology in the site vicinity. A lower amplitude 0.5 Hz HVSR peak is evident in the HVSR data collected at Location 1 using the Trillium Compact and could be associated with crystalline basement rocks at greater depth.
- Primary noise source near the site is Sage Road, which provided ambient noise from vehicle traffic over a 180 degree azimuth. The ambient noise seismic records where one, or more, vehicles passed the array during data recording were documented and only these seismic records were used for final data analysis.
- The ESAC technique was used to extract surface wave dispersion data from the ambient noise data collected at the nested triangle Array 1. The minimum wavelength Rayleigh wave extracted from Array 1 was 13 m. The maximum wavelength Rayleigh wave extracted from this array was set to 150 m, 2.5 times the maximum receiver separation.
- Both the ReMi™ and ESAC techniques used to extract surface wave dispersion data from the ambient noise data collected at the linear Array 2. The minimum wavelength Rayleigh wave that could be extracted from these arrays using the ESAC and ReMi™ techniques was about 10 m. The maximum wavelength Rayleigh wave that could be extracted from these arrays using the ESAC and ReMi™ techniques were about 95 and 110 m, respectively.
- All passive surface wave dispersion data are in good agreement and were used for analysis.
- Rayleigh wave dispersion data were interpreted from 17 MAS_RW seismic records collected at 12 different source locations using 4 lb hammer, 12 lb sledgehammer, and 240 lb accelerated weight drop energy sources. Using variable receiver offset ranges, over 60 dispersion curves were extracted and combined for analysis.
- To minimize near field effects, the maximum wavelength Rayleigh wave data extracted from the MAS_RW data set was set equal to the lesser of 90 m or 1.3 times the distance between the source and midpoint of the active receiver array.
- There is nominally about 25 to 35 m/s of scatter in MAS_RW dispersion data, which is likely in part related to lateral velocity variation.
- The minimum wavelength Rayleigh wave phase velocity data extracted from a 48-channel MAS_RW receiver gather was 3 to 12 m, depending on source location. Reducing data from smaller hammer sources using a limited offset range receiver gather (i.e. less active geophones) allowed for extraction of surface wave dispersion data to a minimum wavelength of about 1.7 m.
- Surface wave dispersion data from active and passive surface wave data sets are in excellent agreement over the approximate 10 to 90 m overlapping wavelength range.
- The phase velocity of a 40 m wavelength Rayleigh wave (V_{R40}) is 248 m/s from ESAC analysis of the ambient noise data collected along Array 1 and 260 and 252 m/s from the analysis of the ambient noise data collected along Array 2 using the ESAC and ReMi™ techniques, respectively. V_{R40} from the MAS_RW dispersion data ranges from 244 to 256 m/s with a mean of 252 m/s and standard deviation of 3.5 m/s. The similarity in V_{R40} of the various surface wave techniques and arrays indicates that each method would have independently yielded similar estimates of V_{S30}.
- The mean V_{R40} from the combined MAS_RW and array microtremor dispersion data is 252 m/s with a standard deviation of 4.2 m/s. During these computations the combined array

microtremor data was given equal weight to the MAS_RW data and the combined dispersion data from the passive linear arrays had equal to or lesser weight than that of the 2-D array.

- Representative dispersion curves were generated for each surface wave data set using a moving average, polynomial curve fitting routine. These individual representative dispersion curves were combined and a composite representative dispersion curve generated for the combined data set for data modeling.
- The composite representative dispersion curve was inverted using an iterative non-linear least squares inversion routine and fundamental mode Rayleigh wave assumption to derive V_S models. Realistic estimates of Poisson's ratio and density were used to make models as accurate as possible. High Poisson's ratio, saturated sediments were constrained at a depth of about 9 m with $V_P > 1{,}700$ m/s based on interactive, layer-based analysis of seismic refraction first arrival data. Poisson's ratio of the saturated sediments was allowed to gradually decrease with depth as the sediments became stiffer, a common observation in borehole V_P and V_S logs. Model layer thicknesses increased with depth to reflect the reduction in model resolution with depth.
- Several V_S models were developed with almost identical calculated dispersion curves to demonstrate the non-uniqueness inherent in the inversion of surface wave dispersion data; especially at layer boundaries where an abrupt change in seismic velocity occurs. These equivalent V_S models have an abrupt increase in velocity, likely associated with the top of the Tertiary Temecula Arkose geologic unit, between depths of about 13 and 21 m.
- The predicted HVSR peak based on the diffuse field assumption, as computed using the software package *HV-Inv* Release 1.0 Beta, is about 2.6 Hz for all of the equivalent V_S models which is similar to that observed at the site. The predicted HVSR peak for the presented V_S model based on the quarter wavelength approximation is 3.2 Hz, also similar to that observed at the site.
- The V_S model presented herein has the inferred top of the Tertiary Temecula Arkose geologic unit at an intermediate depth of 17 m, the average depth of the equivalent V_S models.
- Surface wave depth of investigation is about 60 m based on the one-half to one-third of the maximum wavelength criteria.
- V_{S30} is 274 m/s for the V_S model presented for the purpose of site characterization (NEHRP Site Class D).
- V_{S30} is between 269 and 274 m/s for the equivalent V_S models, demonstrating that non-uniqueness does not have a large impact on estimated V_{S30}.
- The estimated error in V_{S30}, which includes some effects of the lateral velocity variability beneath the testing arrays, is 25 m/s. This is computed based on the sum of the following rounded up to the nearest 5 m/s: an estimated error of 3% from the realistic assumed layer Poisson's ratios in the model, 1% error from the realistic assumed layer densities in the model, 2% for the variation in V_{S30} associated with non-uniqueness, and the 4.2 m/s standard deviation in V_{R40} between the combined active and passive surface wave dispersion data.
- Interestingly, V_{S30} estimated from V_{R40} using the Brown et al., 2000 relationship ($V_{S30} \cong 1.045V_{R40}$, assuming V_{R40} represents the fundamental mode Rayleigh wave) is 263 m/s, only 4% different than that estimated from the V_S model.

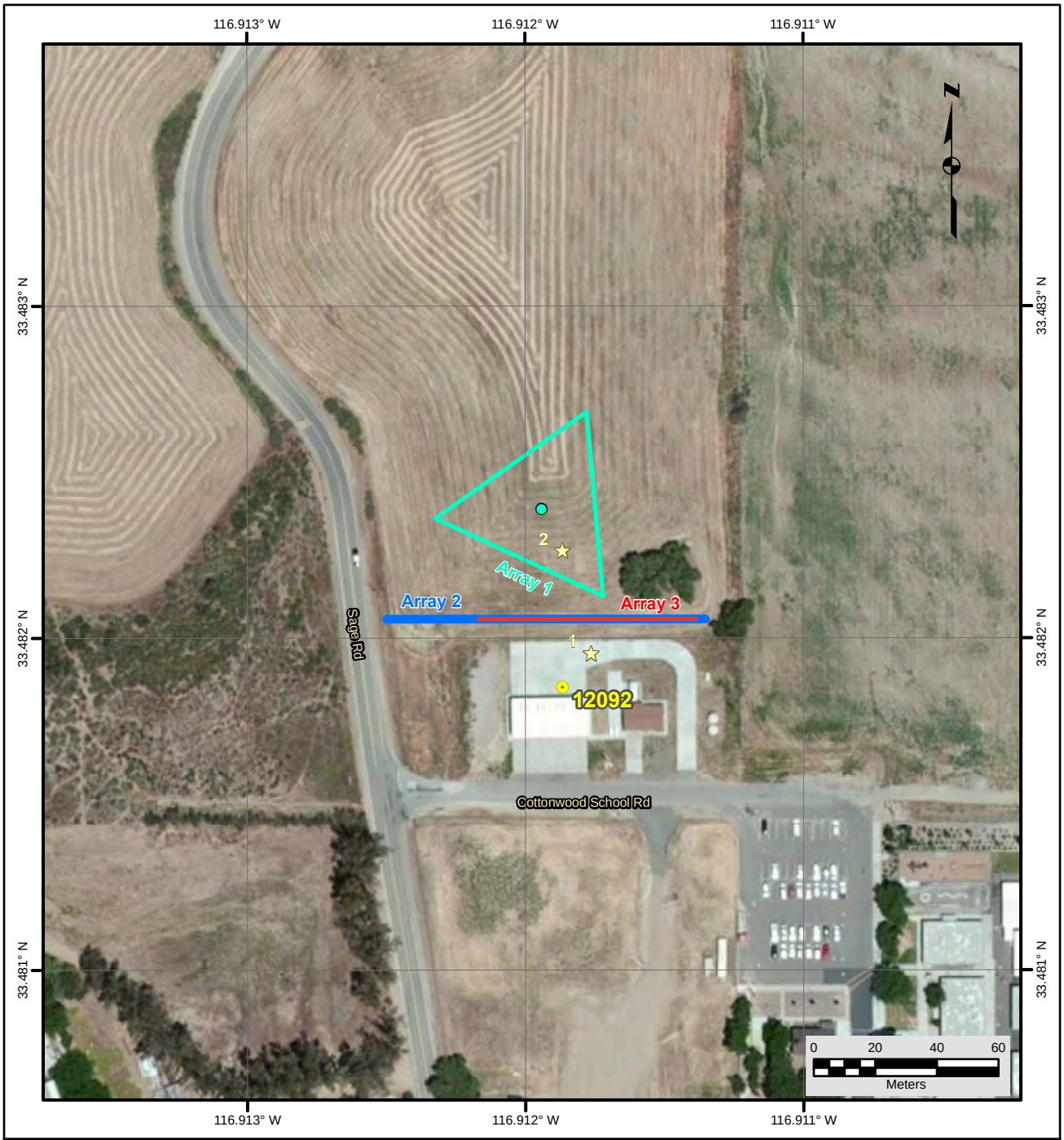

Legend

- CSMIP Station and Number
- H/V Spectral Ratio Measurement Location
- MASW Array
- Passive Surface Wave Array
- Passive Surface Wave Triangle Array

NOTES:
1. WGS 1984 COORDINATE SYSTEM
2. Image Source: Esri, DigitalGlobe, GeoEye, Earthstar Geographics, CNES/Airbus DS, USDA, USGS, AEX, Getmapping, Aerogrid, IGN, IGP, swisstopo, and the GIS User Community

File Name: 16192_12092-l

Date: 6/30/2016

GEOVision geophysical services

SITE MAP
CE•12092

CGS CALIFORNIA GEOLOGICAL SURVEY

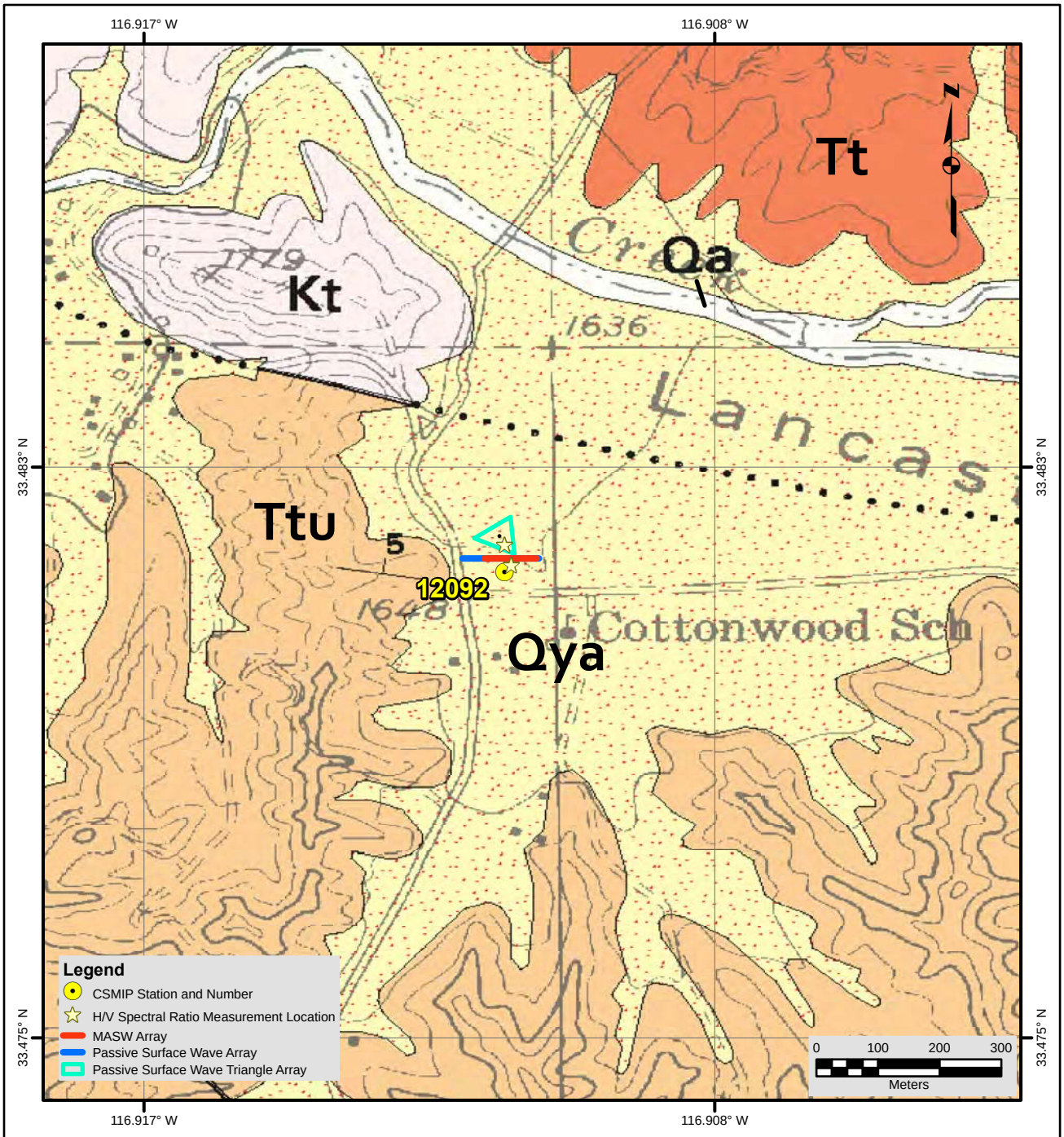

Description of Geologic Map Units

Qa = Quaternary (late Holocene) alluvial deposits.
Qya = Quaternary (Holocene and late Pleistocene) flood plain deposits.
Tt = Tertiary (early to late Pliocene) Temecula Arkose.
Ttu = Tertiary (late Pliocene) Temecula Arkose.
Kt = Cretaceous tonalite.

NOTES:
1. WGS 1984 COORDINATE SYSTEM
2. Vail Lake 7.5' Quadrangle, San Diego and Riverside Counties, California by Michael P. Kennedy (2003)

File Name: 16192_12092

Date: 7/13/2016

GEOVision geophysical services

GEOLOGIC MAP
CE•12092

CGS CALIFORNIA GEOLOGICAL SURVEY

Looking southwest towards building housing CE.12092 seismic station from center of array 12092-3

Looking east along MASW array 12092-3

Looking east along passive surface wave array 12092-2

Looking south towards building housing CE.12092 seismic station from HVSR Location 1

Looking south from center of passive surface wave array 12092-1

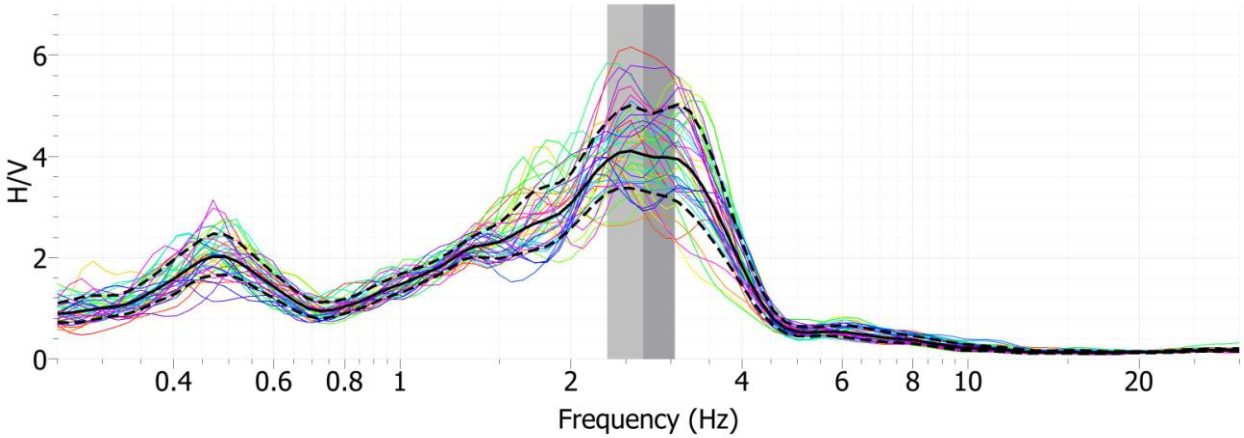

Site CE.12092, HVSR Location 1, Nanometrics Trillium Compact Sensor

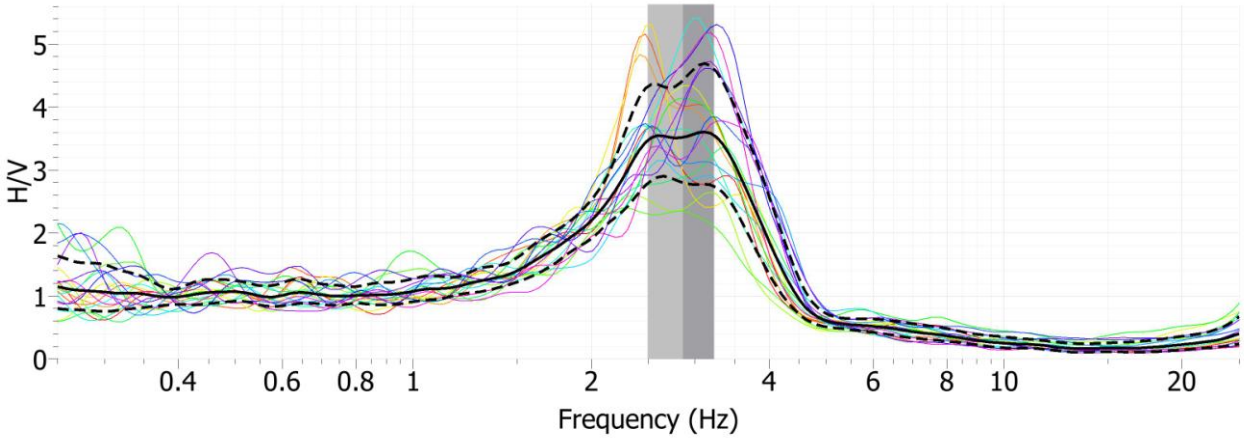

Site CE.12092, HVSR Location 1, Micromed Tromino ENGR Sensor

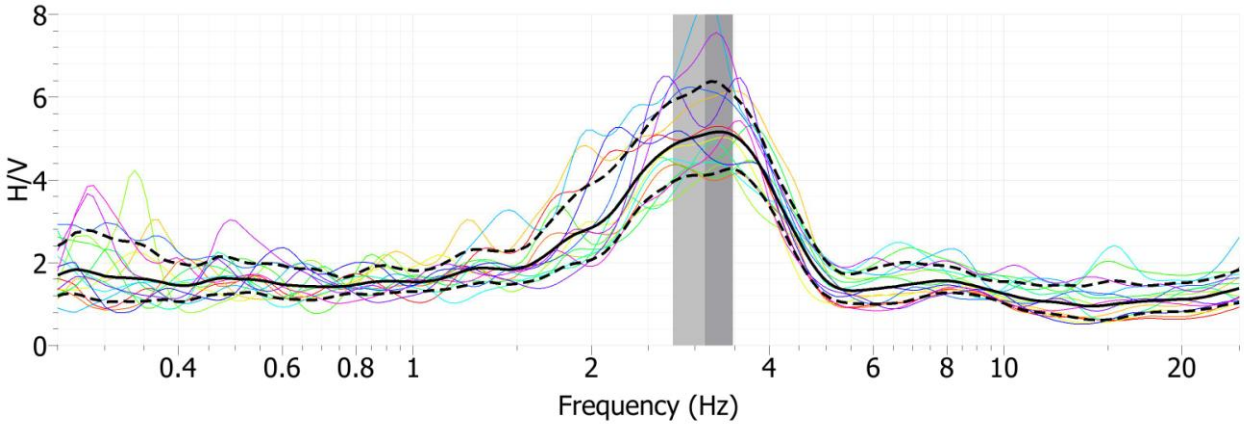

Site CE.12092, HVSR Location 2, Micromed Tromino ENGR Sensor

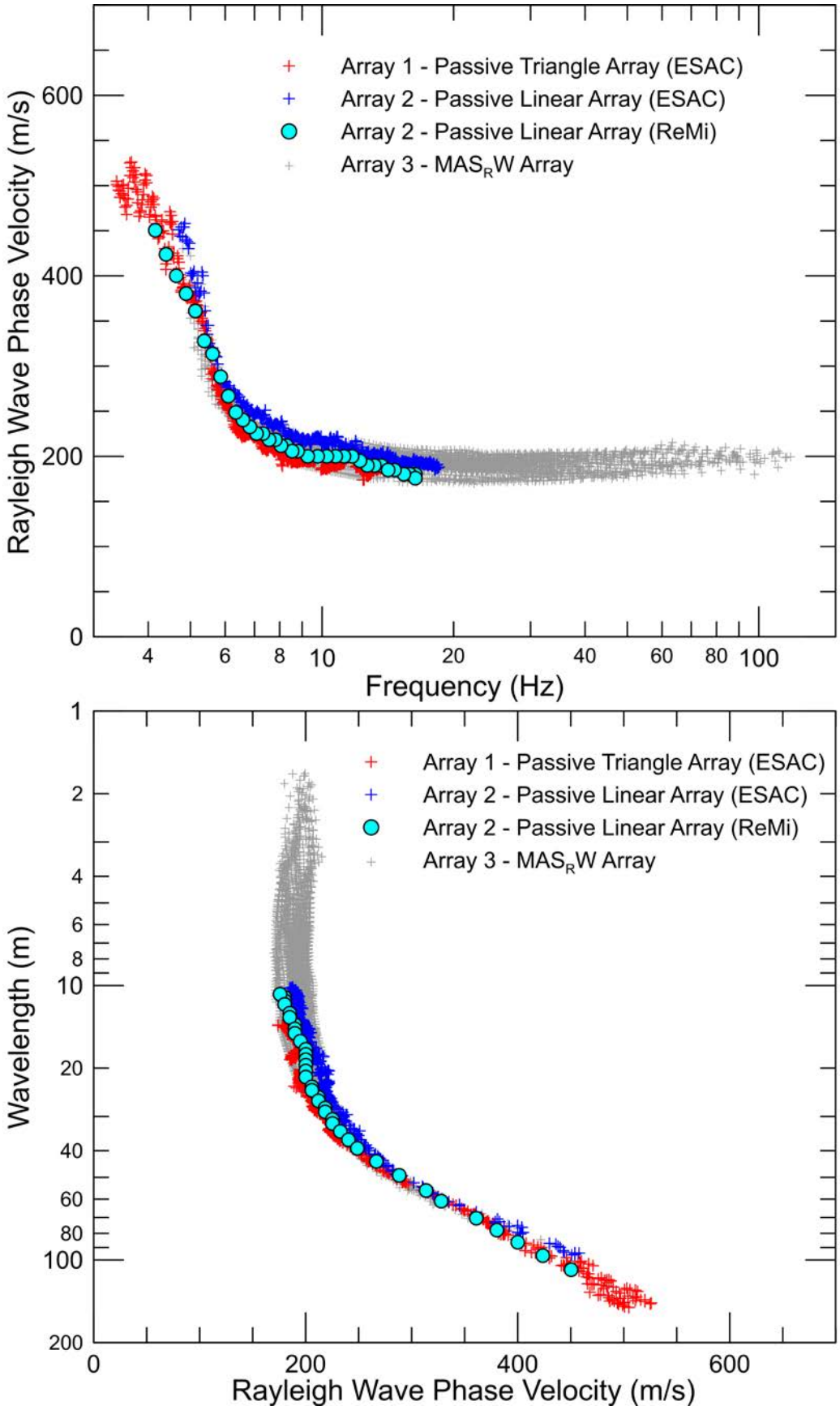

CE.12092 – Dispersion curves derived from active and passive surface wave data. Passive surface wave data from linear array reduced using both ESAC and ReMi™ techniques. All of the dispersion curves were used for site characterization.

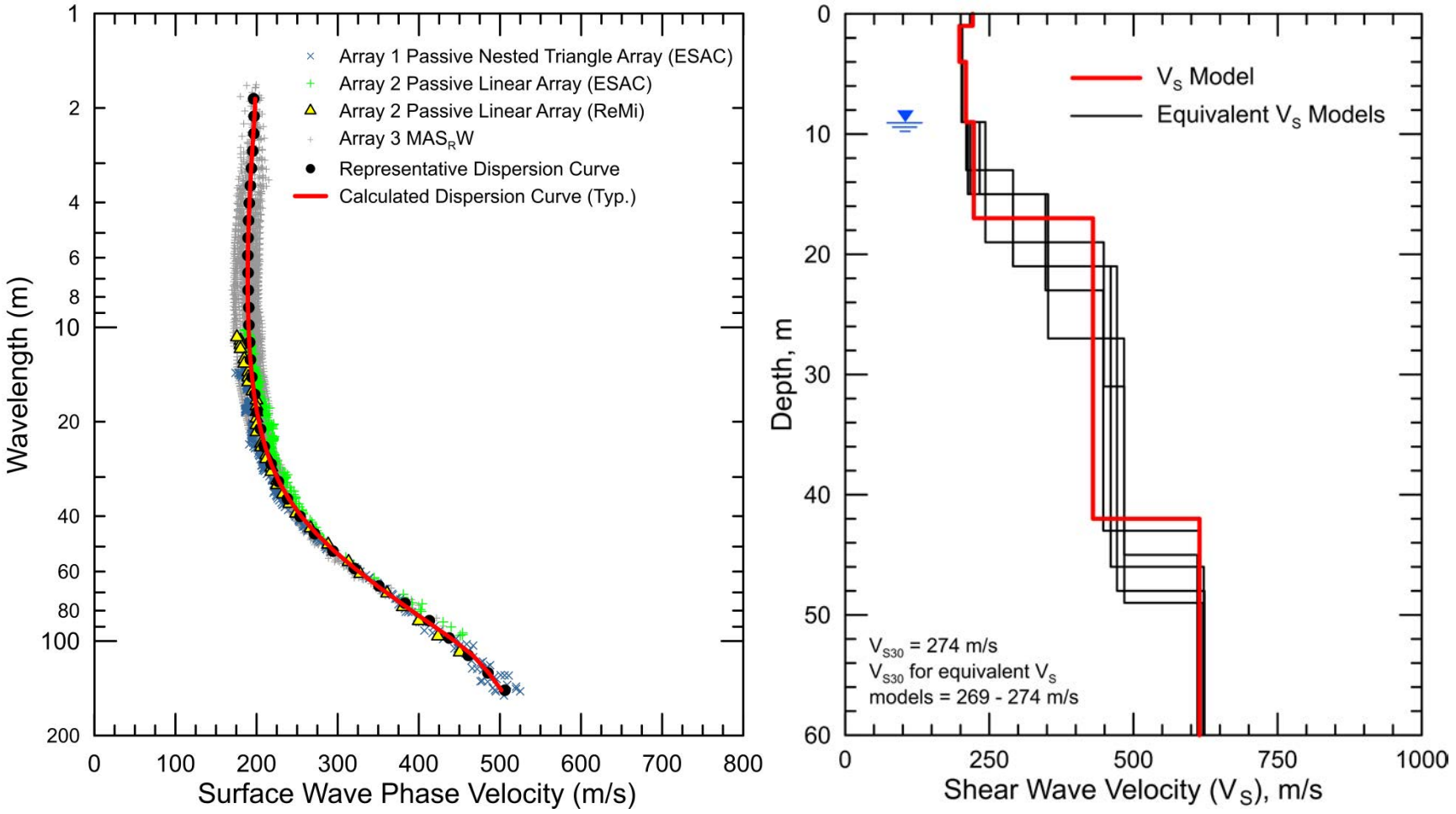

CE.12092 - Field, representative and calculated surface wave dispersion data (left) and associated V_S models (right)

Site CE.12102 & 12673

Station Name: CE.12102: San Jacinto - CDF Fire Station 25
CE.12673: San Jacinto - CDF Fire Station

Location: San Jacinto Fire Station, 132 S. San Jacinto Ave., San Jacinto, CA 92583

CE. 12102 **Latitude:** 33.7869 **Longitude:** -116.9592

CE. 12673 **Latitude:** 33.7873 **Longitude:** -116.9592

V_{S30} (measured): 289 m/s

Estimated error in V_{S30}: ± 25 m/s

NEHRP Site Class: D

Geomatrix Code: AHD (CE.12102), IHD (CE.12673)

Geologic Conditions/Observations: Site located in area mapped as Quaternary (Holocene) alluvial sand and clay.

Site Conditions: Suburban site with traffic noise from nearby roads. Relatively flat terrain in site vicinity.

Geophysical Methods Utilized: MAS_RW, array microtremor, HVSR

Geophysical Testing Arrays:

1. Array 1: 48 channel MAS_RW array utilizing 4.5 Hz vertical geophones spaced 1.5 m apart for a length of 70.5 m, forward and reverse shot locations with multiple source offsets (1.5 to 16 m at east end of array and 1.5 to 30 m at west end of array) and multiple interior source locations. Accelerated weight drop or 20 lb sledgehammer used at all source locations offset from ends of array and 4 and 12 lb hammers used at near-offset source locations and interior source locations.
2. Array 2: 48 channel "L" shaped array utilizing 4.5 Hz vertical geophones spaced 5 m apart used to acquire passive surface wave data. The W-E and S-N linear segments of array have lengths of 90 and 145 m, respectively.
3. One HVSR measurement location; in the vicinity of the MAS_RW array, microtremor array, and the seismic station.

Location of Geophysical Testing Arrays:

Location	Latitude	Longitude
Array 1 MASW, West End of Array	33.78729	-116.95990
Array 1 MASW, East End of Array	33.78730	-116.95914
Array 2 Passive, South End of Array	33.78610	-116.95899
Array 2 Passive, Northeast Corner of Array	33.78741	-116.95898
Array 2 Passive, West End of Array	33.78741	-116.95996
HVSR Location 1	33.78717	-116.95935

Notes: 1) WGS84 Coordinate System (decimal degrees)

Results:

V_S Model

Depth to Top of Layer (m)	Layer Thickness (m)	S-Wave Velocity (m/s)	Inferred P-Wave Velocity (m/s)	Assumed Poisson's Ratio	Assumed Density (g/cm^3)
0	2	183	342	0.300	1.80
2	3	250	467	0.300	1.90
5	5	272	509	0.300	1.90
10	8	289	540	0.300	1.90
18	12	344	643	0.300	1.95
30	15	382	714	0.300	1.95
45	21	462	1700	0.460	2.05
66	>14	532	1750	0.449	2.05

Notes: 1) Depth of investigation is about 80 m.
2) Bottom layer is a half space.

Observations/Discussion:

- There is no clear peak in the HVSR plot derived from the single station ambient noise measurement at one location on site; which is expected as the basement rock is expected to be very deep in the site vicinity. The HVSR plot has similar characteristics to that from seismic station CI.MSJ, located 2.5 km to the northwest.
- Noise conditions at the site (multi-directional noise sources) appeared sufficient for successful application of passive surface wave techniques.
- The ESAC technique was used to extract surface wave dispersion data from the ambient noise data collected on the L- shaped Array 2. The minimum wavelength Rayleigh wave extracted from Array 2 was 12 m. The maximum wavelength Rayleigh wave extracted from this array was 165 m.
- Both the ReMi™ and ESAC techniques used to extract surface wave dispersion data from the S-N and W-E linear legs of Array 2. The minimum wavelength Rayleigh wave that could be extracted from these arrays using the ESAC and ReMi™ techniques was about

10 m. The maximum wavelength Rayleigh wave that could be extracted from these arrays using the ESAC and ReMi™ techniques were in the 135 to 160 m range.

- Although all of the passive surface wave dispersion data are similar, there were differences between the dispersion curves derived from the linear legs of the L-array using the ESAC and ReMi™ techniques. Therefore, only the dispersion curve from the more reliable L-shaped array was used for modeling.
- Rayleigh wave dispersion data were interpreted from 18 MAS_RW seismic records collected at 13 different source locations using 4 lb hammer, 12 and 20 lb sledgehammer, and 240 lb accelerated weight drop energy sources. Using variable receiver offset ranges, over 70 dispersion curves were extracted and combined for analysis.
- To minimize near field effects and data degradation due to local traffic, the maximum wavelength Rayleigh wave data extracted from the MAS_RW data set was set equal to the lesser of 60 m or one times the distance between the source and midpoint of the active receiver array.
- There is nominally about 30 m/s of scatter in MAS_RW dispersion data, which is likely in part due to lateral velocity variation.
- The minimum wavelength Rayleigh wave phase velocity data extracted froma 48-channel MAS_RW receiver gather was 9 to 11 m, depending on source location. Reducing data from smaller hammer sources using a limited offset range receiver gather (i.e. less active geophones) allowed for extraction of surface wave dispersion data to a minimum wavelength of about 3 m.
- Surface wave dispersion data from active and passive surface wave data sets are in excellent agreement over the approximate 10 to 55 m overlapping wavelength range.
- The phase velocity of a 40 m wavelength Rayleigh wave (V_{R40}) is 277 m/s from ESAC analysis of the ambient noise data collected along L-shaped Array 2. V_{R40} is 274 and 258 m/s (6% difference) from the analysis of the ambient noise data collected along the S-N linear leg of Array 2 using the ESAC and ReMi™ techniques, respectively. V_{R40} is 270 and 264 m/s (2% difference) from the analysis of the ambient noise data collected along the W-E linear leg of Array 2 using the ESAC and ReMi™ techniques, respectively. V_{R40} from the MAS_RW dispersion data ranges from 258 to 278 m/s with a mean of 265 m/s and standard deviation of 4.6 m/s. The similarity in V_{R40} of the various surface wave techniques and arrays indicates that each method would have independently yielded similar estimates of V_{S30}.
- The mean V_{R40} from the combined MAS_RW and array microtremor dispersion data is 271 m/s with a standard deviation of 6.5 m/s. During these computations the array microtremor data was given equal weight to the MAS_RW data.
- Representative dispersion curves were generated for each surface wave data set using a moving average, polynomial curve fitting routine. These individual representative dispersion curves were combined and a composite representative dispersion curve generated for the combined data set for data modeling.
- The composite representative dispersion curve was inverted using an iterative non-linear least squares inversion routine and fundamental mode Rayleigh wave assumption to derive V_S models. Realistic estimates of Poisson's ratio and density were used to make models as accurate as possible. Review of seismic refraction first arrival data from the seismic records indicates that there is no evidence of saturated sediments in the upper 30 m. The saturated zone is assumed to be located at a depth of 45 m for data modeling.

Model layer thicknesses increased with depth to reflect the reduction in model resolution with depth.

- Only a single V_S model was developed to represent the velocity structure at the site because V_S increases gradually with depth and all V_S models with equivalent theoretical dispersion curves would show a similar velocity-depth trend.
- Surface wave depth of investigation is about 80 m based on the one-half of maximum wavelength criteria.
- V_{S30} is 289 m/s (NEHRP Site Class D).
- The average V_S of the upper 80 m (V_{S80}) is 372 m/s.
- The estimated error in V_{S30}, which includes some effects of the lateral velocity variability beneath the testing arrays, is 25 m/s. This is computed based on the sum of the following rounded up to the nearest 5 m/s: an estimated error of 3% and from the realistic assumed layer Poisson's ratios in the model, 1% error from the realistic assumed layer densities in the model, 2% for the variation in V_{S30} associated with non-uniqueness, and the 6.5 m/s standard deviation in V_{R40} between the combined active and passive surface wave dispersion data.
- Interestingly, V_{S30} estimated from V_{R40} using the Brown et al., 2000 relationship ($V_{S30} \cong 1.045V_{R40}$, assuming V_{R40} represents the fundamental mode Rayleigh wave) is 283 m/s, only 2% different than that estimated from the V_S model.

Legend

- CSMIP Station and Number
- H/V Spectral Ratio Measurement Location
- MASW Array
- Passive Surface Wave Array
- Passive Surface Wave Triangle Array

NOTES:
1. WGS 1984 COORDINATE SYSTEM
2. Image Source: Esri, DigitalGlobe, GeoEye, Earthstar Geographics, CNES/Airbus DS, USDA, USGS, AEX, Getmapping, Aerogrid, IGN, IGP, swisstopo, and the GIS User Community

File Name: 16192_12102-I

Date: 8/1/2016

GEOVision geophysical services

SITE MAP
CE•12102

CGS CALIFORNIA GEOLOGICAL SURVEY

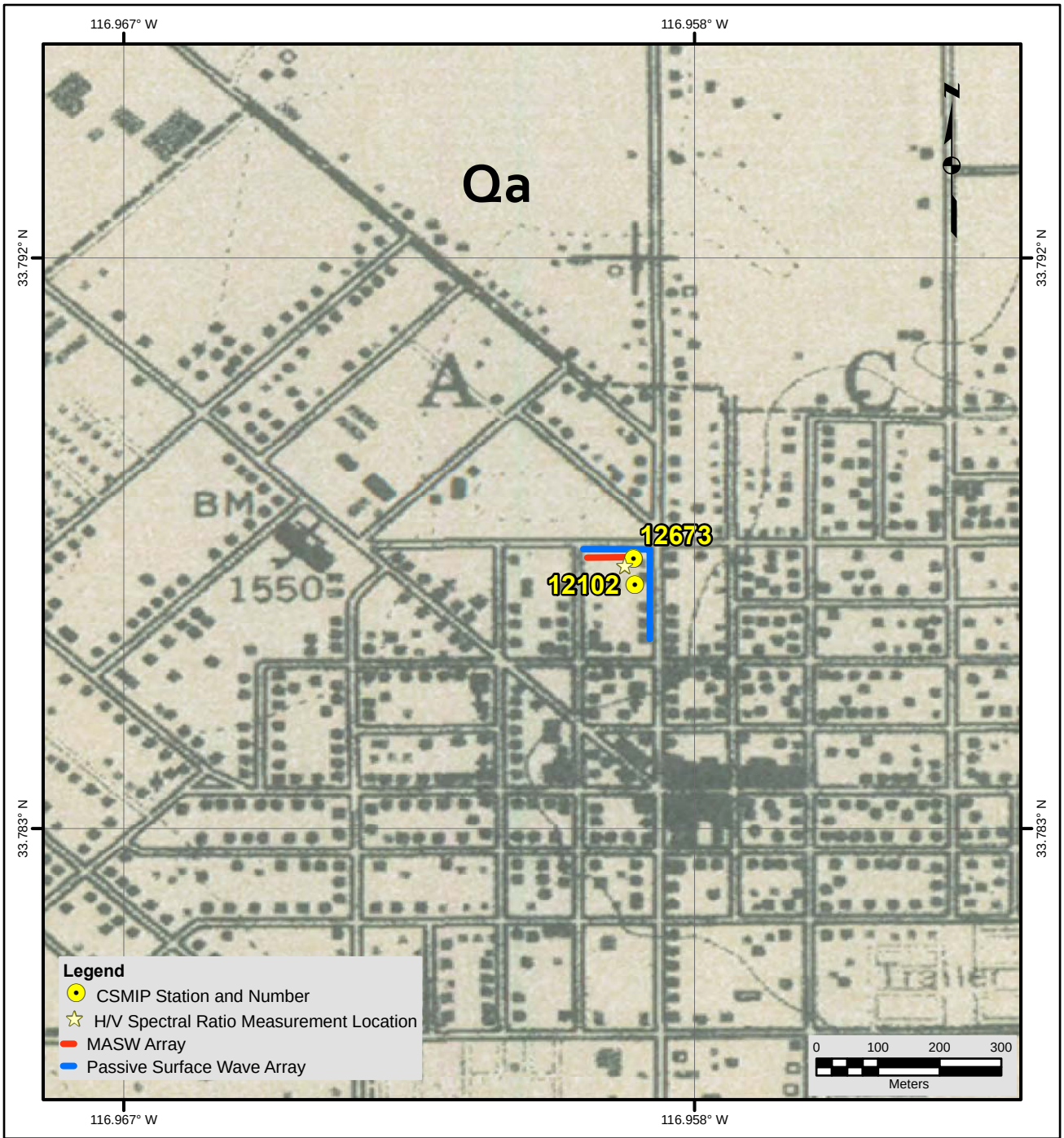

Description of Geologic Map Units

Qa = Quaternary (Holocene) alluvial sand and clay.

NOTES:
1. WGS 1984 COORDINATE SYSTEM
2. Geologic Map of the San Jacinto Quadrangle, Riverside County, California by Thomas W. Dibblee, Jr., 2003

File Name: 16192_12102

Date: 8/1/2016

GEOVision geophysical services

GEOLOGIC MAP
CE•12102

CGS CALIFORNIA GEOLOGICAL SURVEY

Looking south from array 12102-1 towards enclosure housing CE.12673 seismic station and fire station housing CE.12102 seismic station

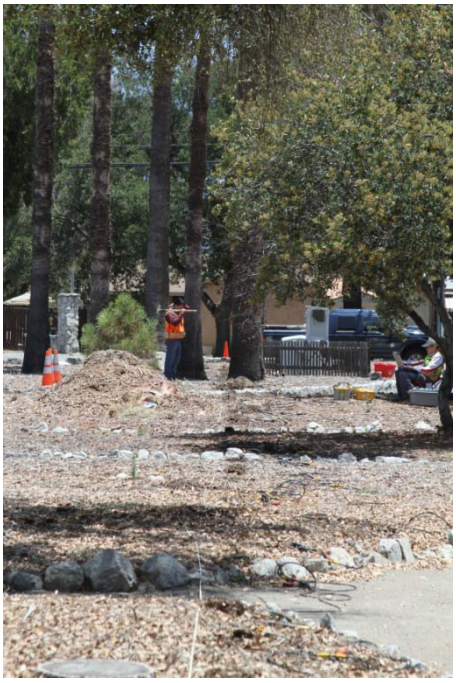

Looking east along MASW array 12102-1

Looking southwest towards fire station from the corner of passive surface wave array 12102-2

Looking southeast towards fire station from HVSR Location 1

Data acquisition along MASW array 12102-1

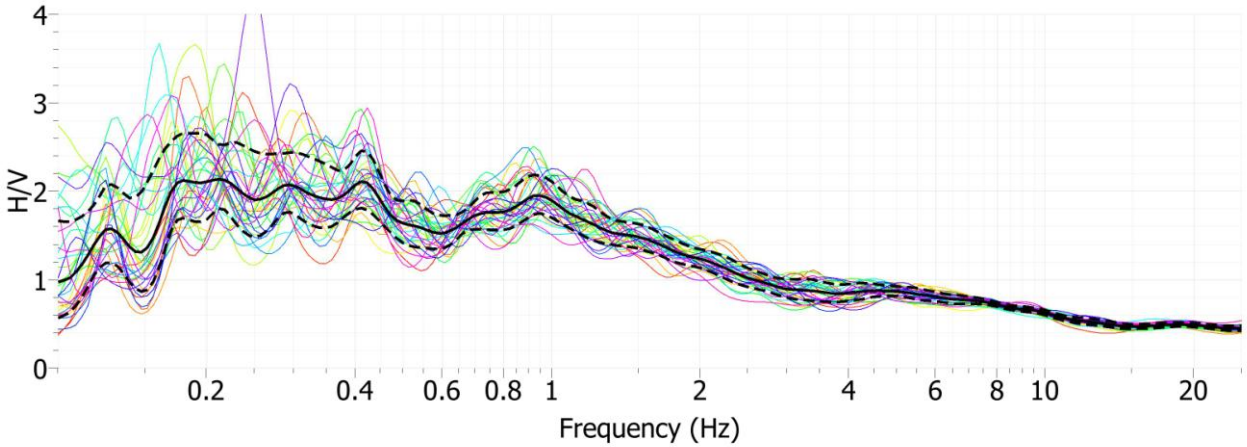

Site CE.12102, HVSR Location 1, Nanometrics Trillium Compact Sensor

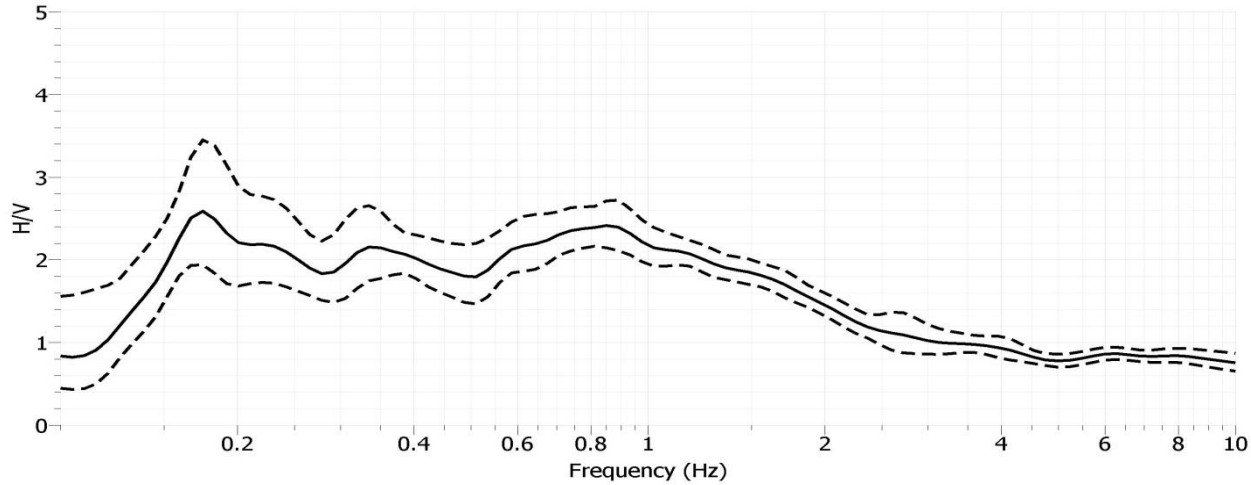

Site CI.MSJ, HVSR Location Near Seismic Station, Nanometrics Trillium Compact Sensor

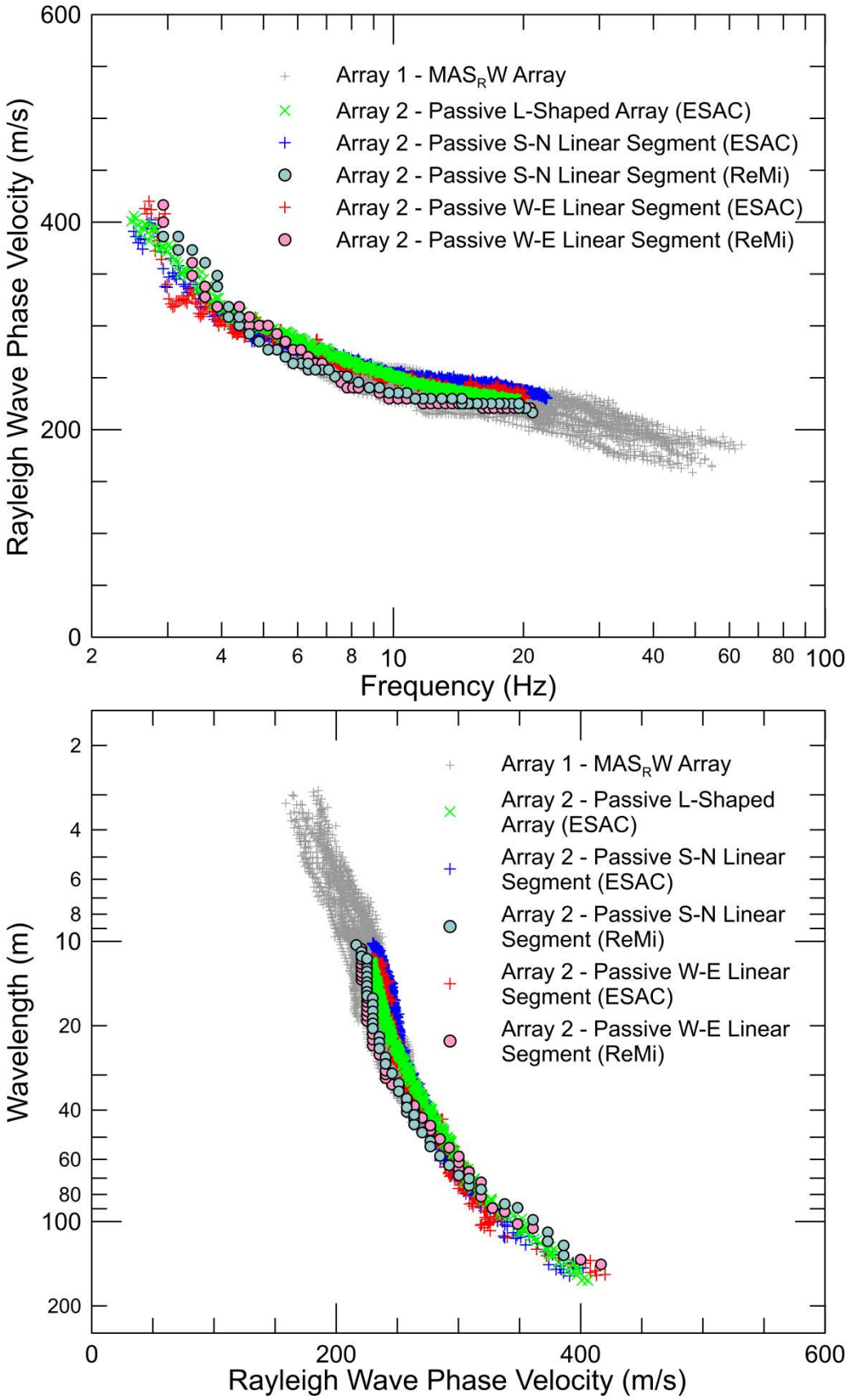

CE.12102 – Dispersion curves derived from active and passive surface wave data. Although all of the dispersion curves from the passive surface wave arrays are similar, the ESAC and ReMi™ analysis of the linear arrays have significant differences at low frequency. Only the passive surface wave data from the more reliable L-shaped array were used for modeling.

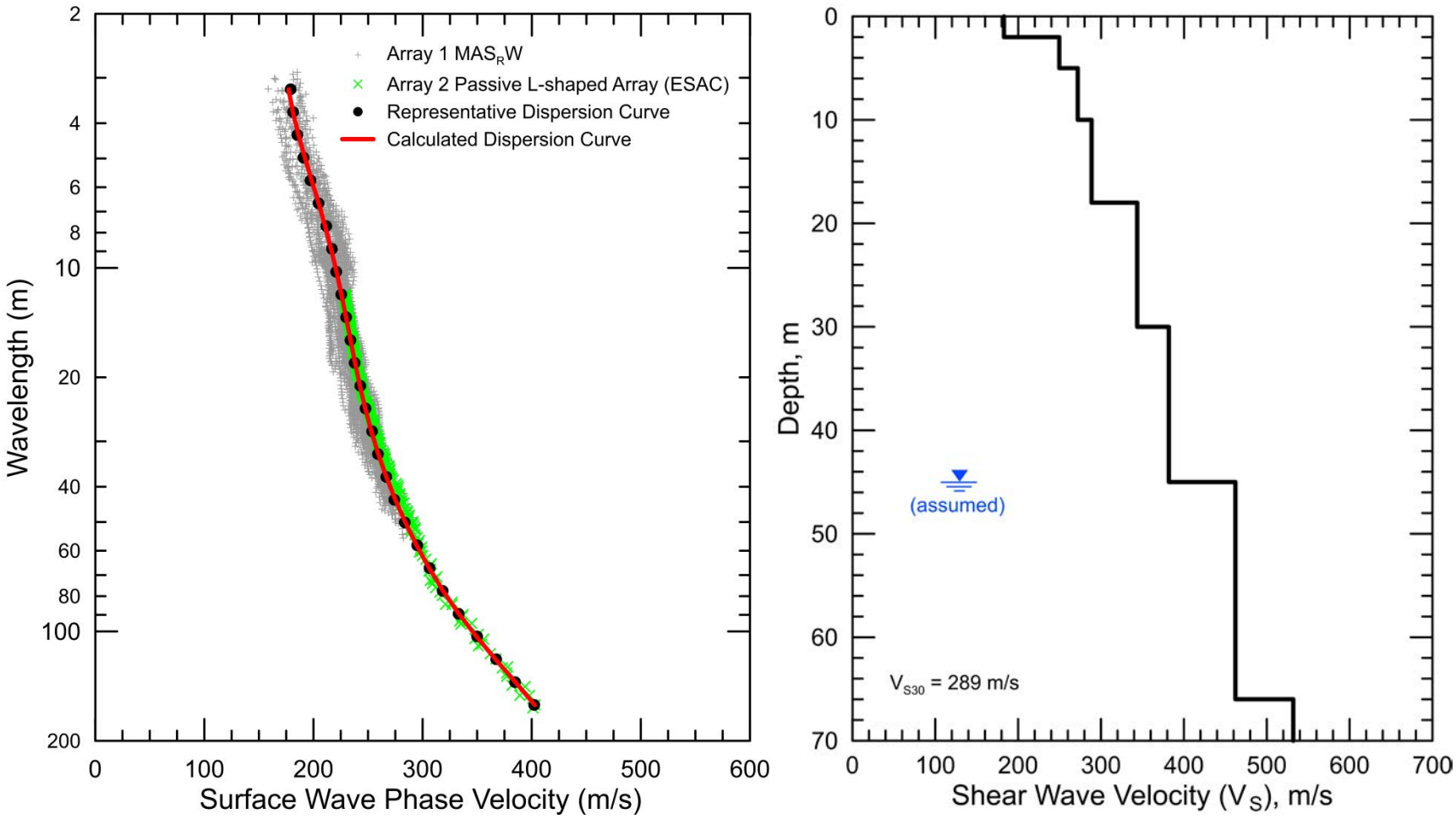

CE.12102 - Field, representative and calculated surface wave dispersion data (left) and associated V_S models (right). V_S increases gradually with depth and, therefore, multiple V_S models are not presented to demonstrate non-uniqueness because all models would show the same general velocity-depth trend.

Site CE.12331

Station Name: Hemet - Stetson Ave Fire Station

Location: Hemet City Fire Station #2, 895 Stetson Ave., Hemet, CA 92543

Latitude: 33.7289 **Longitude:** -116.9797

V_{S30} (measured): 297 m/s

Estimated error in V_{S30}: ± 25 m/s

NEHRP Site Class: D

Geomatrix Code: AHD/AQD

Geologic Conditions/Observations: Site located in area mapped as Quaternary (Holocene and late Pleistocene) young alluvial fan deposits.

Site Conditions: Suburban site with traffic noise from nearby roads, particularly W Stetson Ave. Relatively flat terrain in site vicinity.

Geophysical Methods Utilized: MAS_RW, array microtremor, HVSR

Geophysical Testing Arrays:

1. Array 1: 48 channel "L" shaped array utilizing 4.5 Hz vertical geophones spaced 6 m apart used to acquire passive surface wave data. The S-N and W-E linear segments of array have lengths of 150 and 132 m, respectively.
2. Array 2: 48 channel MAS_RW array utilizing 4.5 Hz vertical geophones spaced 1.5 m apart for a length of 70.5 m, forward and reverse shot locations with multiple source offsets (1.5 to 16 m at south end of array and 1.5 to 15 m at north end of array) and multiple interior source locations. Accelerated weight drop (north source locations) or 20 lb sledgehammer (south source locations) used at all source locations offset from ends of array and 4 and 12 lb hammers used at near-offset source locations and interior source locations.
3. Four HVSR measurement locations; one near the MAS_RW array, two near the seismic station, and one positioned near the southern end of the microtremor array.

Location of Geophysical Testing Arrays:

Location	Latitude	Longitude
Array 1 Passive, South End of Array	33.72929	-116.97879
Array 1 Passive, Northwest Corner of Array	33.72928	-116.98020
Array 1 Passive, East End of Array	33.72793	-116.98019
Array 1 MASW, Southwest End of Array	33.72853	-116.98018
Array 1 MASW, Northeast End of Array	33.72916	-116.98011
HVSR Location 1	33.72877	-116.97964
HVSR Location 2	33.72815	-116.98013
HVSR Location 3	33.72893	-116.98014
HVSR Location 1T	33.72874	-116.97963

Notes: 1) WGS84 Coordinate System (decimal degrees)

Results:

V_S Model

Depth to Top of Layer (m)	Layer Thickness (m)	S-Wave Velocity (m/s)	Inferred P-Wave Velocity (m/s)	Assumed Poisson's Ratio	Assumed Density (g/cm^3)
0	2	165	308	0.300	1.75
2	4	202	377	0.300	1.80
6	14	328	614	0.300	1.90
20	20	380	711	0.300	1.95
40	30	495	1750	0.457	2.05
70	>20	585	1800	0.441	2.10

Notes: 1) Depth of investigation is about 90 m.
2) Bottom layer is a half space.
3) Bedrock with V_S > 1,000 m/s may be as shallow as 120 m based on V_S model and forward modeling of 1.1 Hz HVSR peak.

Observations/Discussion:

- HVSR data collected at Location 1 using a Nanometrics Trillium Compact 120 s seismograph reveals a 1.1 Hz HVSR peak, which is likely associated with crystalline rock at a depth greater than the active and passive surface wave depth of investigation. HVSR data collected at the adjacent Location 1T using a Tromino ENGR seismograph reveals a lower amplitude 1.4 Hz HVSR peak. The Tromino uses higher frequency sensors and is not generally reliable at frequencies below 1.5 Hz. HVSR data were also collected at Locations 2 and 3 with the Tromino with similar results and are, therefore, not presented.
- Noise conditions at the site (multi-directional noise sources) appeared sufficient for successful application of passive surface wave techniques.

- The ESAC technique was used to extract surface wave dispersion data from the ambient noise data collected on the L-shaped Array 1. The minimum wavelength Rayleigh wave extracted from Array 1 was 17 m. The maximum wavelength Rayleigh wave extracted from this array was 180 m.
- Both the ReMi™ and ESAC techniques used to extract surface wave dispersion data from the S-N and W-E linear legs of Array 1. The minimum wavelength Rayleigh wave that could be extracted from these arrays using the ESAC and ReMi™ techniques was about 13 m. The maximum wavelength Rayleigh waves that could be extracted from these arrays using the ESAC and ReMi™ techniques were in the 100 to 180 m range.
- The dispersion curves derived from the W-E linear leg of the L-array, which is aligned along the high traffic W Stetson Ave., using the ESAC and ReMi™ techniques differ over a wide frequency range and data quality is poor, especially at low frequencies. The dispersion curves derived from the S-N linear leg of the L-array, which is perpendicular to the high traffic W Stetson Ave., using the ESAC and ReMi™ techniques are similar to the dispersion curve from the L-shaped array. However, only the dispersion curve from the more reliable L-shaped array was used for modeling.
- Rayleigh wave dispersion data were interpreted from 16 $MAS_R W$ seismic records collected at 11 different source locations using 4 lb hammer, 12 and 20 lb sledgehammer, and 240 lb accelerated weight drop energy sources. Using variable receiver offset ranges, over 60 dispersion curves were extracted and combined for analysis.
- To minimize near field effects and data degradation due to local traffic, the maximum wavelength Rayleigh wave extracted from the $MAS_R W$ data set was set equal to the lesser of 61 m or 1.3 times the distance between the source and midpoint of the active receiver array.
- There is nominally about 30 to 40 m/s of scatter in $MAS_R W$ dispersion data, which is likely in part due to lateral velocity variation.
- The minimum wavelength Rayleigh wave phase velocity data extracted from a 48-channel $MAS_R W$ receiver gather was 5 to 10 m, depending on source location. Reducing data from smaller hammer sources using a limited offset range receiver gather (i.e. less active geophones) allowed for extraction of surface wave dispersion data to a minimum wavelength of about 2 m.
- Surface wave dispersion data from active and passive surface wave data sets are in good agreement over the approximate 13 to 61 m overlapping wavelength range.
- The phase velocity of a 40 m wavelength Rayleigh wave (V_{R40}) is 286 m/s from ESAC analysis of the ambient noise data collected along L-shaped Array 1. V_{R40} is 293 and 280 m/s (5% difference) from the analysis of the ambient noise data collected along the S-N linear leg of Array 1 using the ESAC and ReMi™ techniques, respectively. V_{R40} is 291 and 267 m/s (9% difference) from the analysis of the ambient noise data collected along the W-E linear leg of Array 1 using the ESAC and ReMi™ techniques, respectively. V_{R40} from the $MAS_R W$ dispersion data ranges from 263 to 295 m/s with a mean of 281 m/s and standard deviation of 8.0 m/s. The similarity in V_{R40} of the various surface wave techniques and arrays indicates that each method would have independently yielded acceptable estimates of V_{S30}, even if the V_S models may not have been reliable.

- The mean V_{R40} from the combined MAS_RW and array microtremor dispersion data is 283 m/s with a standard deviation of 6.1 m/s. During these computations the array microtremor data (L-array only) was given equal weight to the MAS_RW data.
- Representative dispersion curves were generated for each surface wave data set using a moving average, polynomial curve fitting routine. These individual representative dispersion curves were combined and a composite representative dispersion curve generated for the combined data set for data modeling.
- The composite representative dispersion curve was inverted using an iterative non-linear least squares inversion routine and fundamental mode Rayleigh wave assumption to derive V_S models. Realistic estimates of Poisson's ratio and density were used to make models as accurate as possible. Review of seismic refraction first arrival data from the seismic records indicates that there is no evidence of saturated sediments in the upper 20 m. For the purpose of data modeling, the saturated zone is assumed to be located at a depth of 40 m. Model layer thicknesses increased with depth to reflect the reduction in model resolution with depth.
- Only a single V_S model was developed to represent the velocity structure at the site because V_S increases gradually with depth and all V_S models with equivalent theoretical dispersion curves would show a similar velocity-depth trend.
- Interactive forward modeling in the software package *HV-Inv* Release 1.0 Beta, based on the diffuse field assumption, using the V_S model developed for the site indicates that the observed 1.1 Hz HVSR peak could be associated with crystalline bedrock (expected V_S > 1,000 m/s) as shallow as 120 m.
- Surface wave depth of investigation is about 90 m based on the one-half of maximum wavelength criteria.
- V_{S30} is 297 m/s (NEHRP Site Class D).
- The average V_S of the upper 90 m (V_{S90}) is 405 m/s.
- The estimated error in V_{S30}, which includes some effects of the lateral velocity variability beneath the testing arrays, is 25 m/s. This is computed based on the sum of the following rounded up to the nearest 5 m/s: an estimated error of 3% and from the realistic assumed layer Poisson's ratios in the model, 1% error from the realistic assumed layer densities in the model, 2% for the variation in V_{S30} associated with non-uniqueness, and the 6.1 m/s standard deviation in V_{R40} between the combined active and passive surface wave dispersion data.
- Interestingly, V_{S30} estimated from V_{R40} using the Brown et al., 2000 relationship ($V_{S30} \cong 1.045V_{R40}$, assuming V_{R40} represents the fundamental mode Rayleigh wave) is 296 m/s, less than 1% different than that estimated from the V_S model.

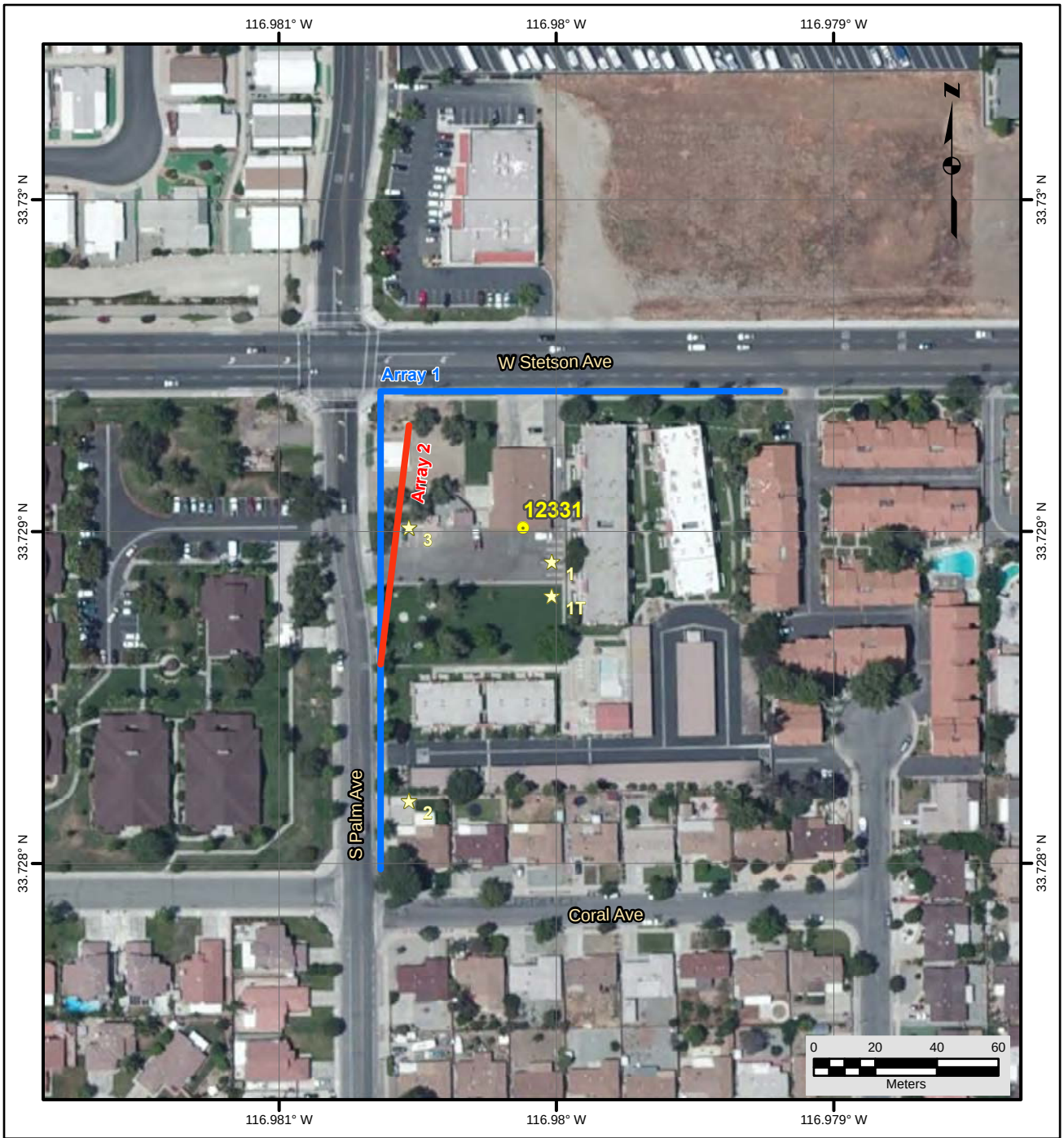

Legend

- CSMIP Station and Number
- H/V Spectral Ratio Measurement Location
- MASW Array
- Passive Surface Wave Array

NOTES:
1. WGS 1984 COORDINATE SYSTEM
2. Image Source: Esri, DigitalGlobe, GeoEye, Earthstar Geographics, CNES/Airbus DS, USDA, USGS, AEX, Getmapping, Aerogrid, IGN, IGP, swisstopo, and the GIS User Community

File Name: 16192_12331-I

Date: 6/30/2016

GEOVision geophysical services

SITE MAP
CE•12331

CGS CALIFORNIA GEOLOGICAL SURVEY

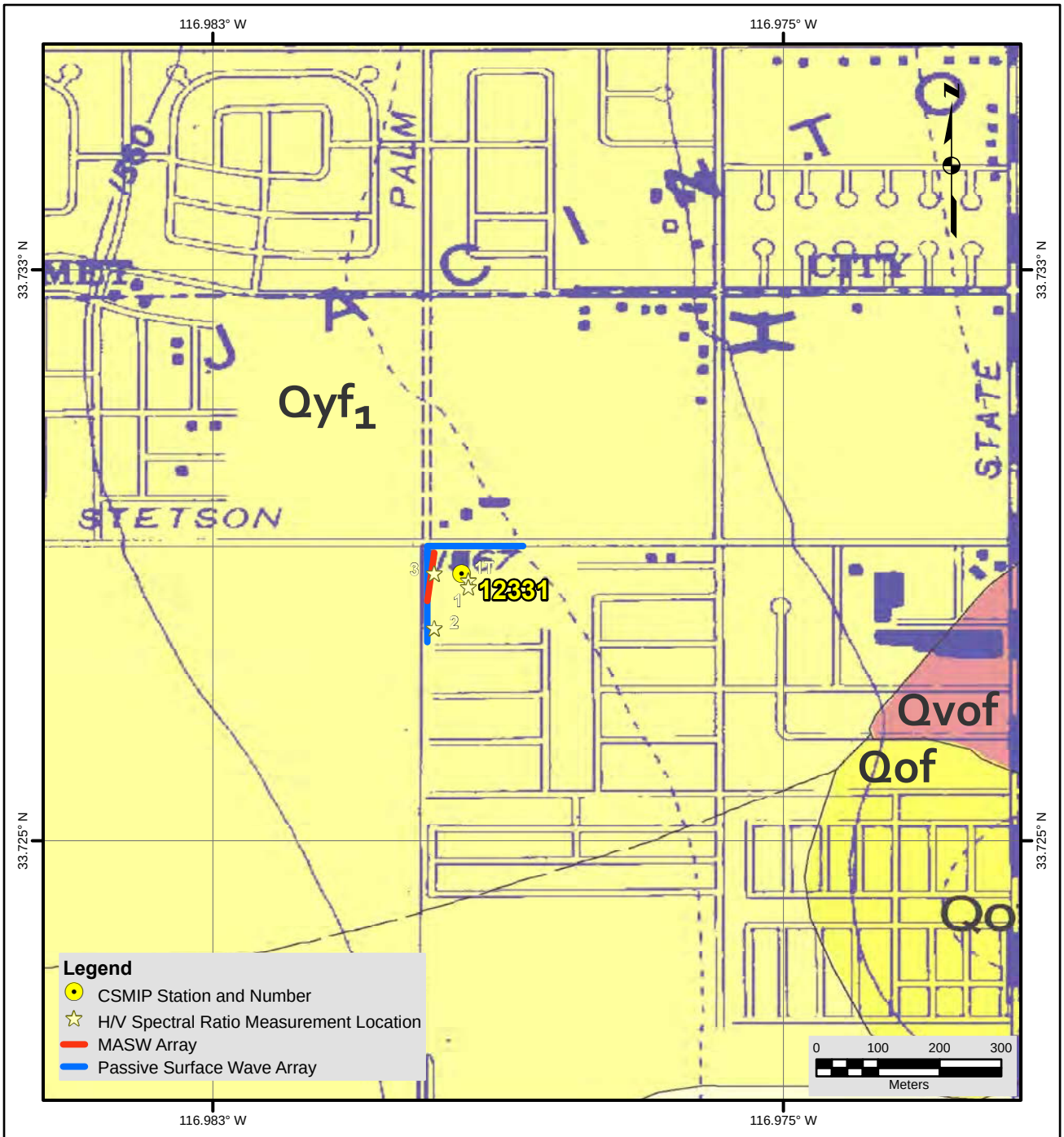

Description of Geologic Map Units

Qyf_1 = Quaternary (Holocene and late Pleistocene) Young alluvial fan deposits, Unit 1.
Qof = Quaternary (late to middle Pleistocene) Old alluvial fan deposits.
Qvof = Quaternary (Pleistocene) Very old alluvial fan deposits.

NOTES:
1. WGS 1984 COORDINATE SYSTEM
2. Geologic Map of the Hemet 7.5' Quadrangle, Riverside County, California by D. M. Morton and J. C. Matti

File Name: 16192_12331

Date: 7/13/2016

GEOVision geophysical services

GEOLOGIC MAP
CE•12331

CGS CALIFORNIA GEOLOGICAL SURVEY

Looking northwest towards CE.12331 seismic station from HVSR Location 1 and 1T

Looking northeast along MASW array 12331-2

Looking west towards HVSR Location 2 from passive surface wave array 12331-1

Data acquisition along MASW array 12331-2

Looking northeast towards fire station from MASW array 12331-2

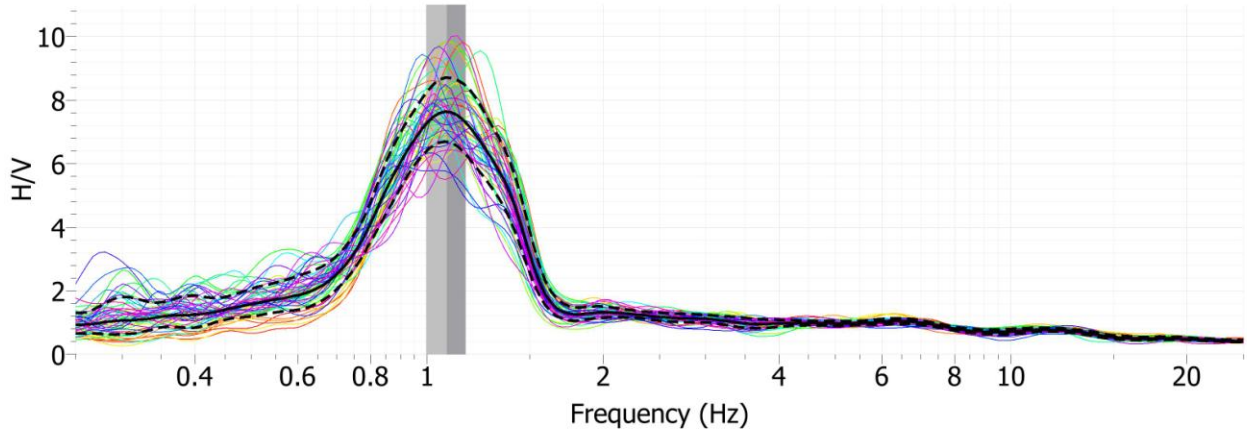

Site CE.12331, HVSR Location 1, Nanometrics Trillium Compact Sensor

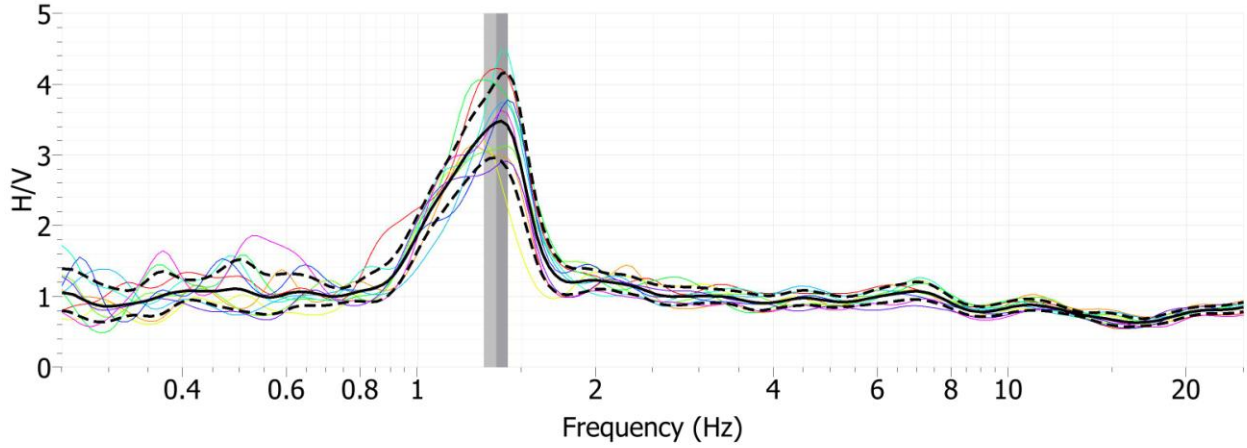

Site CE.12331, HVSR Location 1T, Micromed Tromino ENGR Sensor

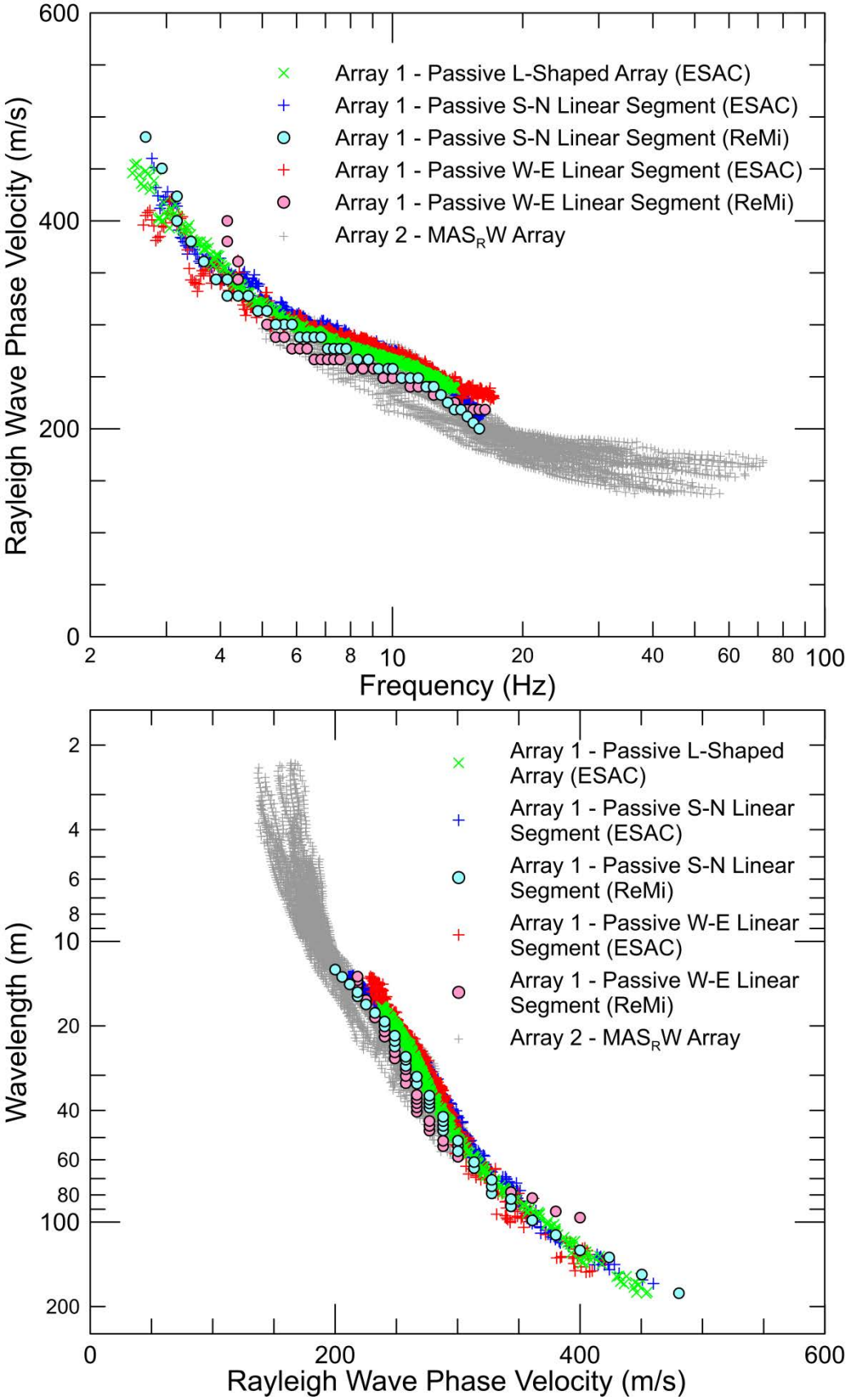

CE.12331 – Dispersion curves derived from active and passive surface wave data. Dispersion curves from ESAC and ReMi™ analysis of the S-N linear leg of the L-array, which is perpendicular to the high traffic Stetson Ave., are similar to the dispersion curve from the L-array. The W-E leg of the L-array does not yield reliable dispersion data. Only the passive surface wave data from the more reliable L-shaped array were used for modeling.

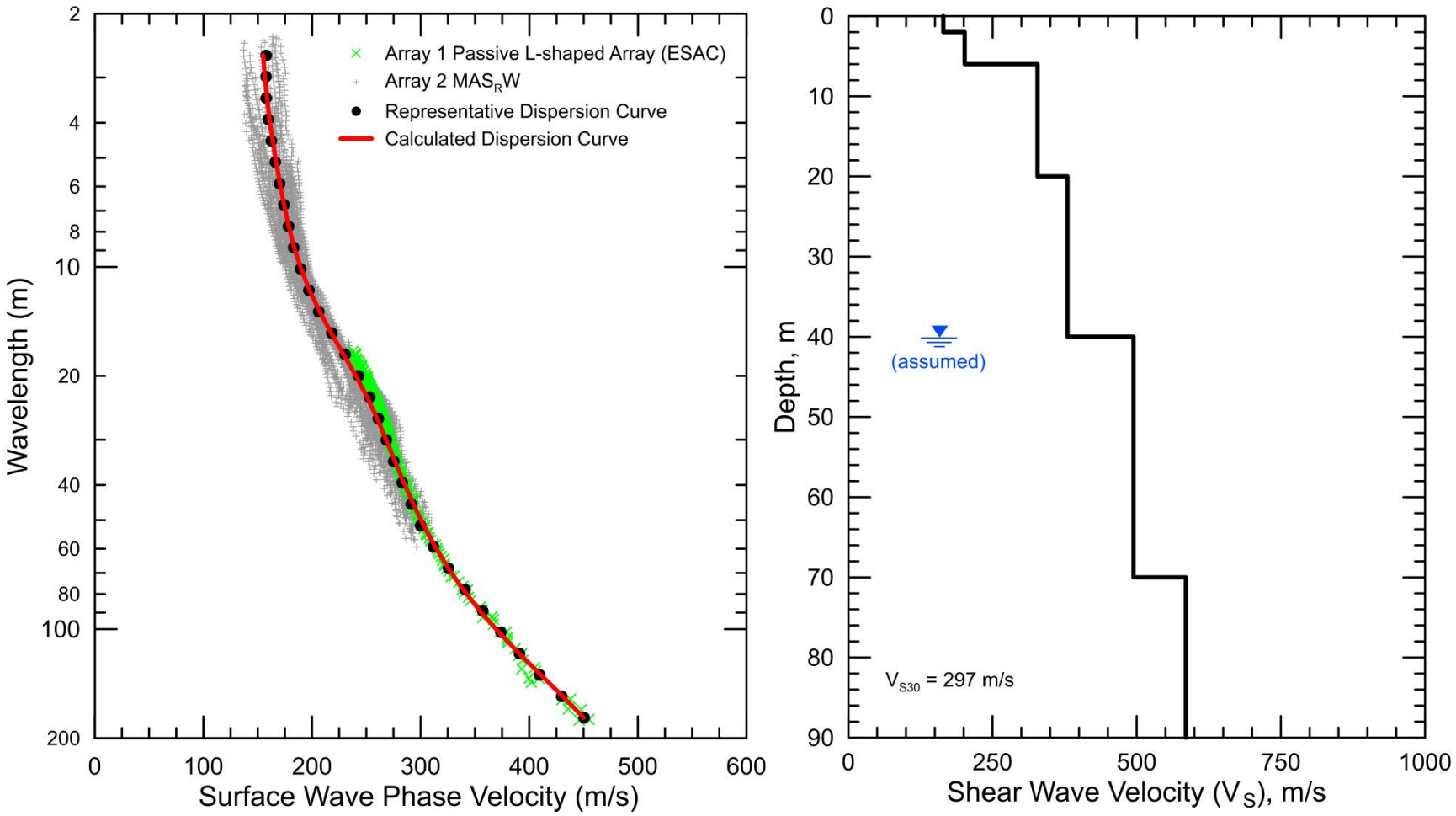

CE.12331 - Field, representative and calculated surface wave dispersion data (left) and associated V_S models (right). V_S increases gradually with depth and, therefore, multiple V_S models are not presented to demonstrate non-uniqueness because all models would show the same general velocity-depth trend.

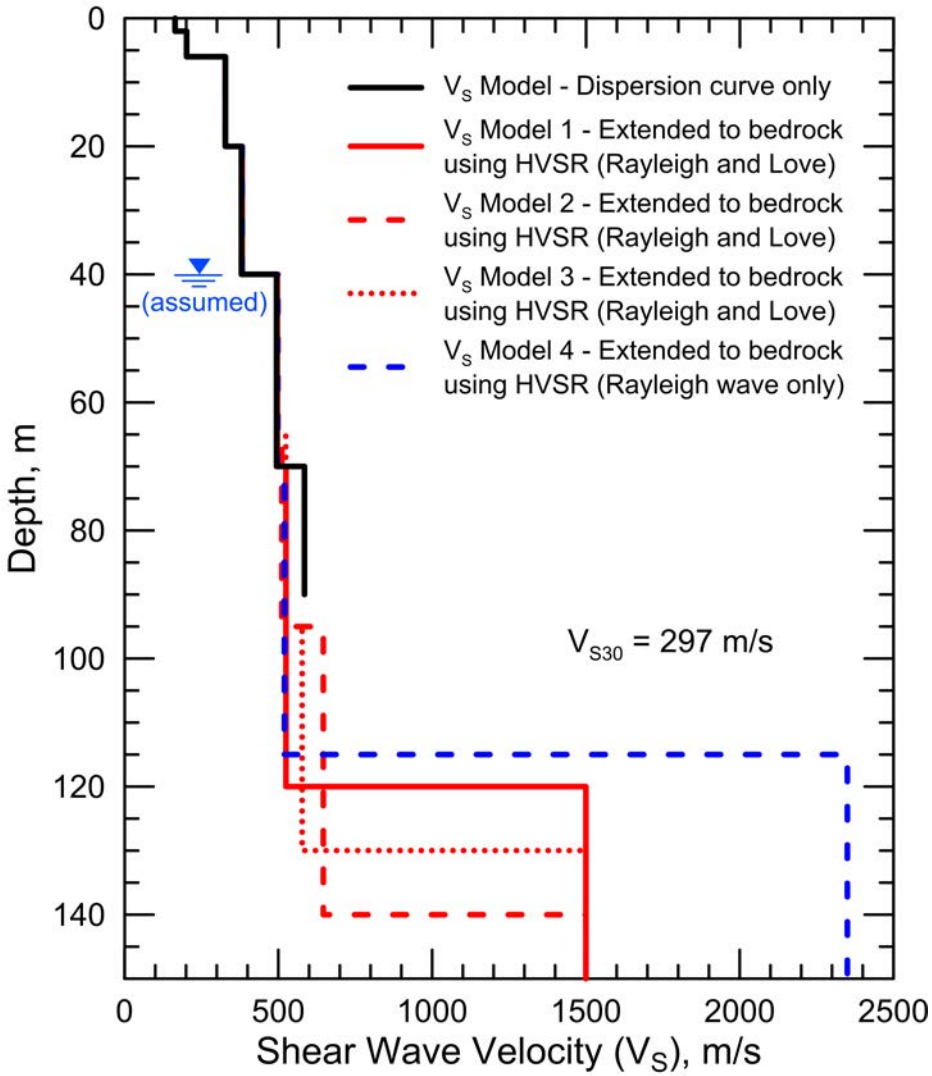

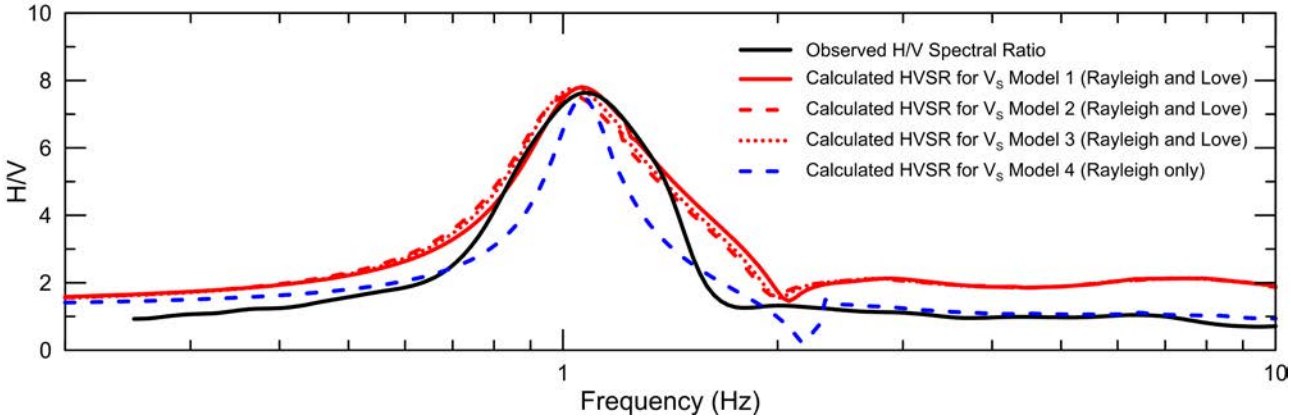

Site CE.12331 – Joint modeling of HVSR and surface wave dispersion data to constrain approximate depth to bedrock.

Site CE.12923

Station Name: Hemet - Acacia & Stanford

Location: Little Lake Fire Station, 25954 Stanford St., Hemet CA 92544

Latitude: 33.7448 **Longitude:** -116.9322

V_{S30} (measured): 273 m/s

Estimated error in V_{S30}: ± 25 m/s

NEHRP Site Class: D

Geomatrix Code: AHD/AQD

Geologic Conditions/Observations: Site located in area mapped as Quaternary (Holocene and late Pleistocene) young alluvial fan deposits. An inferred strand of the San Jacinto Fault in close proximity to the site.

Site Conditions: Suburban site with traffic noise from nearby roads. Relatively flat terrain in site vicinity.

Geophysical Methods Utilized: MAS_RW, array microtremor, HVSR

Geophysical Testing Arrays:

1. Array 1: 48 channel "L" shaped array utilizing 4.5 Hz vertical geophones spaced 6 m apart used to acquire passive surface wave data. The S-N and W-E linear segments of array have lengths of 144 and 138 m, respectively.
2. Array 2: 48 channel MAS_RW array utilizing 4.5 Hz vertical geophones spaced 1.5 m apart for a length of 70.5 m, forward and reverse shot locations with multiple source offsets (1.5 to 11 m at south end of array and 1.5 to 12.5 m at north end of array) and multiple interior source locations. A 20 lb sledgehammer was used at all source locations offset from ends of array and 4 and 12 lb hammers were used at near-offset source locations and interior source locations.
3. One HVSR measurement location in the vicinity of the seismic station.

Location of Geophysical Testing Arrays:

Location	Latitude	Longitude
Array 1 Passive, West End of Array	33.74414	-116.93418
Array 1 Passive, Southeast Corner of Array	33.74414	-116.93269
Array 1 Passive, North End of Array	33.74544	-116.93269
Array 2 MASW, South End of Array	33.74424	-116.93269
Array 2 MASW, North End of Array	33.74487	-116.93269
HVSR Location 1	33.74489	-116.93197

Notes: 1) WGS84 Coordinate System (decimal degrees)

Results:

V_S Model

Depth to Top of Layer (m)	Layer Thickness (m)	S-Wave Velocity (m/s)	Inferred P-Wave Velocity (m/s)	Assumed Poisson's Ratio	Assumed Density (g/cm^3)
0	1	215	403	0.300	1.80
1	2.5	258	482	0.300	1.85
3.5	3.5	226	422	0.300	1.80
7	8	259	485	0.300	1.85
15	12	298	558	0.300	1.85
27	18	330	617	0.300	1.90
45	24	385	1750	0.475	1.95
69	>11	447	1800	0.467	2.00

Notes: 1) Depth of investigation is about 80 m.
2) Bottom layer is a half space.

Observations/Discussion:

- HVSR data collected at Location 1 using a Nanometrics Trillium Compact 120 s seismograph reveals a 0.6 Hz HVSR peak, which is likely associated with crystalline rock at a depth much greater than the active and passive surface wave depth of investigation. HVSR data collected at the same location using a Tromino ENGR seismograph does not reveal the same peak because the instrument does not perform well at low frequencies.
- Noise conditions at the site (multi-directional noise sources) appeared sufficient for successful application of passive surface wave techniques.
- The ESAC technique was used to extract surface wave dispersion data from the ambient noise data collected on the L-shaped Array 1. The minimum wavelength Rayleigh wave

extracted from Array 1 was 9 m. The maximum wavelength Rayleigh wave extracted from the array was 160 m.

- Both the ReMi™ and ESAC techniques used to extract surface wave dispersion data from the S-N and W-E linear legs of Array 1. The minimum wavelength Rayleigh waves that could be extracted from these arrays using the ESAC and ReMi™ techniques were in the 6 to 8 m range. The maximum wavelength Rayleigh waves that could be extracted from these arrays using the ESAC and ReMi™ techniques were in the 135 to 195 m range.
- The dispersion curves derived from the linear legs of the L-array using the ESAC and ReMi™ techniques differ from one another and from the dispersion curve derived from the L-shaped array, especially at long wavelengths. Therefore, only the dispersion curve from the more reliable L-shaped array was used for modeling.
- Rayleigh wave dispersion data were interpreted from 15 MAS_RW seismic records collected at 10 different source locations using 4 lb hammer, and 12 and 20 lb sledgehammers. The array was not accessible for the vehicle mounted, 240 lb accelerated weight drop energy source. Using variable receiver offset ranges, over 55 dispersion curves were extracted and combined for analysis.
- To minimize near field effects and data degradation due to local traffic, the maximum wavelength Rayleigh wave data extracted from the MAS_RW data set was set equal to the lesser of 41 m or 1.3 times the distance between the source and midpoint of the active receiver array. A 20 lb sledgehammer does not typically generate sufficient low frequency energy to extract a 41 m wavelength Rayleigh wave dispersion data at a site such as this and, therefore, there may be increased error in the MAS_RW dispersion data at long wavelengths.
- There is nominally about 20 to 30 m/s of scatter in MAS_RW dispersion data, which is likely in part due to lateral velocity variation.
- The minimum wavelength Rayleigh wave phase velocity data extracted from a 48-channel MAS_RW receiver gather was 4 to 6 m, depending on source location. Reducing data from smaller hammer sources using a limited offset range receiver gather (i.e. less active geophones) allowed for extraction of surface wave dispersion data to a minimum wavelength of about 1.5 m.
- Surface wave dispersion data from MAS_RW and passive L-shaped array are in good agreement over the approximate 9 to 41 m overlapping wavelength range. The surface wave dispersion data from the passive linear arrays diverge from that from the MAS_RW array at higher frequencies/smaller wavelengths.
- The phase velocity of a 40 m wavelength Rayleigh wave (V_{R40}) is 257 m/s from ESAC analysis of the ambient noise data collected along L-shaped Array 1. V_{R40} is 261 and 243 m/s (7% difference) from the analysis of the ambient noise data collected along the S-N linear leg of Array 1 using the ESAC and ReMi™ techniques, respectively. V_{R40} is 247 and 239 m/s (3% difference) from the analysis of the ambient noise data collected along the W-E linear leg of Array 1 using the ESAC and ReMi™ techniques, respectively. V_{R40} from the MAS_RW dispersion data ranges from 242 to 261 m/s with a mean of 252 m/s and standard deviation of 5.2 m/s. The similarity in V_{R40} of the various surface wave techniques and arrays indicates that each method would have independently yielded acceptable estimates of V_{S30}, even if the V_S models may not have been reliable.
- The passive L-shaped array crosses an inferred strand of the San Jacinto Fault. The similarity in V_{R40} between the various arrays indicating that there may not be significant

lateral velocity variability across the fault. Ideally, the passive array would have been located on the northeast side of the inferred fault.

- The mean V_{R40} from the combined MAS_RW and array microtremor dispersion data is 254 m/s with a standard deviation of 4.2 m/s. During these computations the array microtremor data (L-array only) was given equal weight to the MAS_RW data.
- Representative dispersion curves were generated for each surface wave data set using a moving average, polynomial curve fitting routine. These individual representative dispersion curves were combined and a composite representative dispersion curve generated for the combined data set for data modeling.
- The composite representative dispersion curve was inverted using an iterative non-linear least squares inversion routine and fundamental mode Rayleigh wave assumption to derive V_S models. Realistic estimates of Poisson's ratio and density were used to make models as accurate as possible. Review of seismic refraction first arrival data from the seismic records indicates that there is no evidence of saturated sediments in the upper 30 m although there is a possible reflector that could be associated with groundwater at a depth greater than 35 m. For the purpose of data modeling, the saturated zone is assumed to be located at a depth of 45 m. Model layer thicknesses increased with depth to reflect the reduction in model resolution with depth.
- Only a single V_S model was developed to represent the velocity structure at the site because V_S increases gradually with depth and all V_S models with equivalent theoretical dispersion curves would show a similar velocity-depth trend.
- Surface wave depth of investigation is about 80 m based on the one-half of maximum wavelength criteria.
- V_{S30} is 273 m/s (NEHRP Site Class D).
- The average V_S of the upper 80 m (V_{S80}) is 330 m/s.
- The estimated error in V_{S30}, which includes some effects of the lateral velocity variability beneath the testing arrays, is 25 m/s. This is computed based on the sum of the following rounded up to the nearest 5 m/s: an estimated error of 3% and from the realistic assumed layer Poisson's ratios in the model, 1% error from the realistic assumed layer densities in the model, 2% for the variation in V_{S30} associated with non-uniqueness, and the 4.2 m/s standard deviation in V_{R40} between the combined active and passive surface wave dispersion data.
- Interestingly, V_{S30} estimated from V_{R40} using the Brown et al., 2000 relationship ($V_{S30} \cong 1.045V_{R40}$, assuming V_{R40} represents the fundamental mode Rayleigh wave) is 265 m/s, only about 3% different than that estimated from the V_S model.

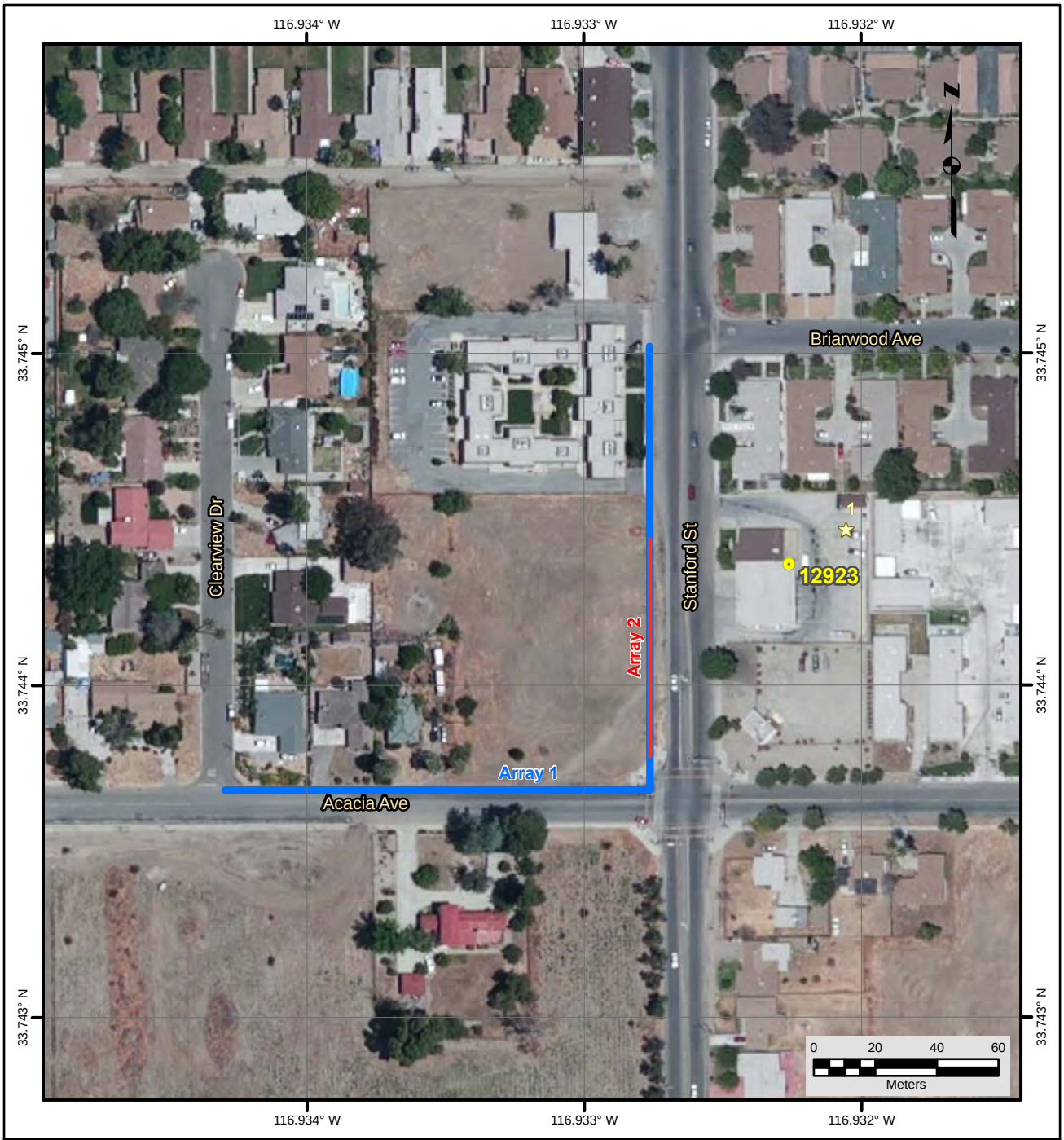

Legend

- H/V Spectral Ratio Measurement Location
- CSMIP Station and Number
- MASW Array
- Passive Surface Wave Array
- Passive Surface Wave Triangle Array

NOTES:
1. WGS 1984 COORDINATE SYSTEM
2. Image Source: Esri, DigitalGlobe, GeoEye, Earthstar Geographics, CNES/Airbus DS, USDA, USGS, AEX, Getmapping, Aerogrid, IGN, IGP, swisstopo, and the GIS User Community

File Name: 16192_12923-I

Date: 6/30/2016

GEOVision geophysical services

SITE MAP
CE•12923

CGS CALIFORNIA GEOLOGICAL SURVEY

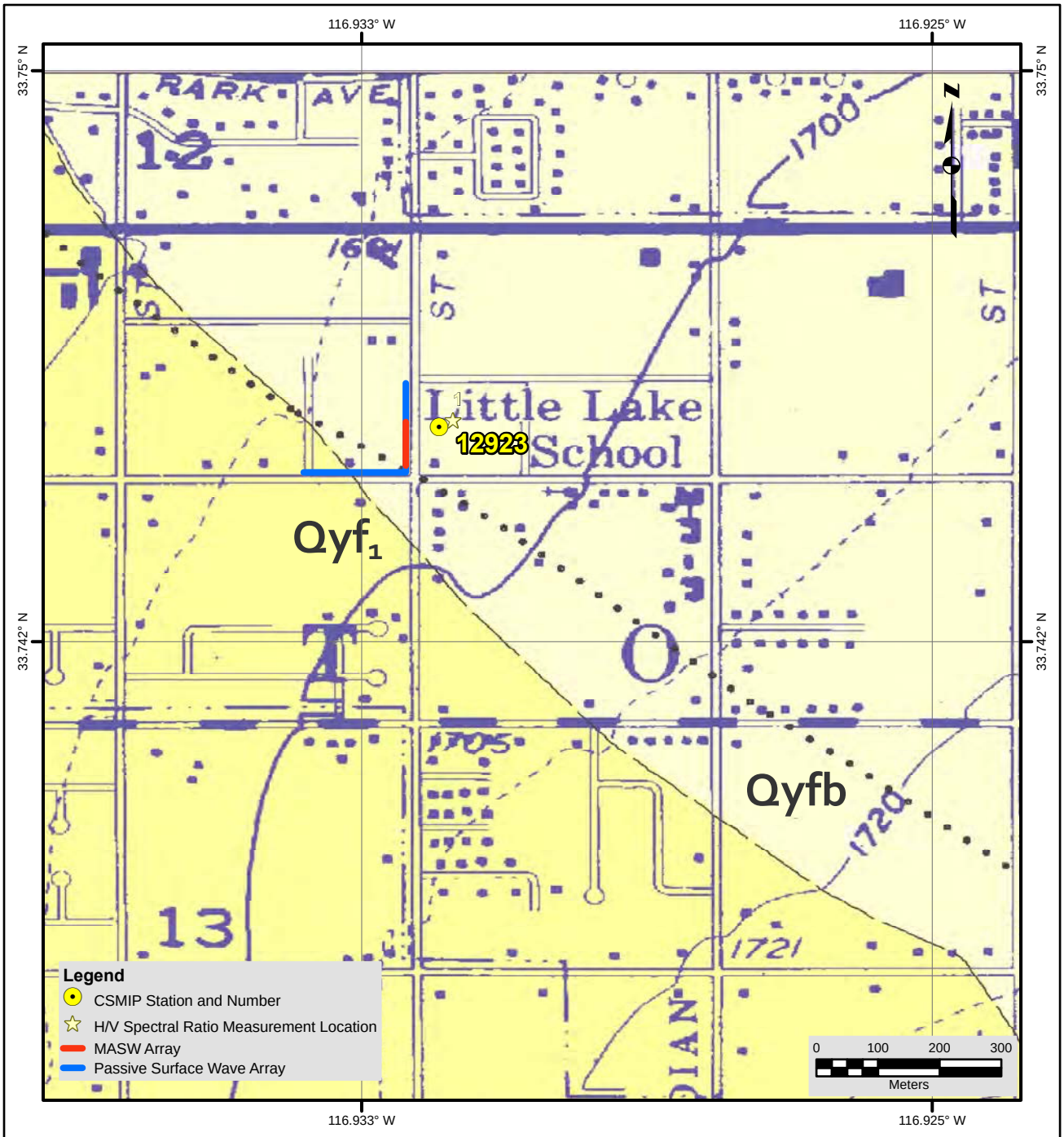

Description of Geologic Map Units

Qyfb = Quaternary (Holocene and late Pleistocene) Young alluvial fan deposits.
Qyf_1 = Quaternary (Holocene and late Pleistocene) Young alluvial fan deposits, Unit 1.

NOTES:
1. WGS 1984 COORDINATE SYSTEM
2. Geologic Map of the Hemet 7.5' Quadrangle, Riverside County, California by D. M. Morton and J. C. Matti

File Name: 16192_12923

Date: 7/13/2016

GEOVision geophysical services

GEOLOGIC MAP
CE•12923

CGS CALIFORNIA GEOLOGICAL SURVEY

Looking southwest towards fire station housing CE.12923 seismic station from HVSR Location 1

Looking west along passive surface wave array 12923-1

Trillium and Tromino sensors used for measurements at HVSR Location 1

Looking north along MASW array 12923-2

Data acquisition along MASW array 12923-2

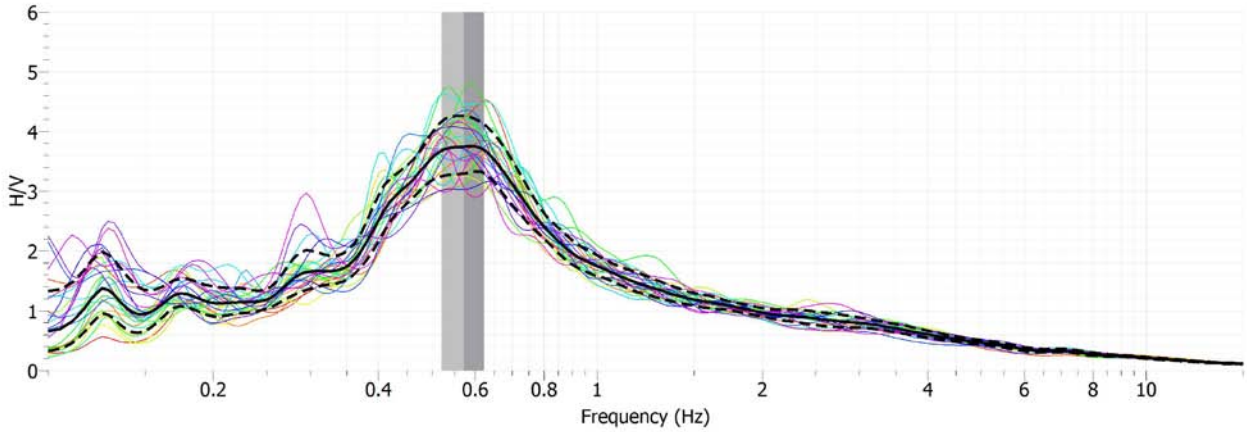

Site CE.12923, HVSR Location 1, Nanometrics Trillium Compact Sensor

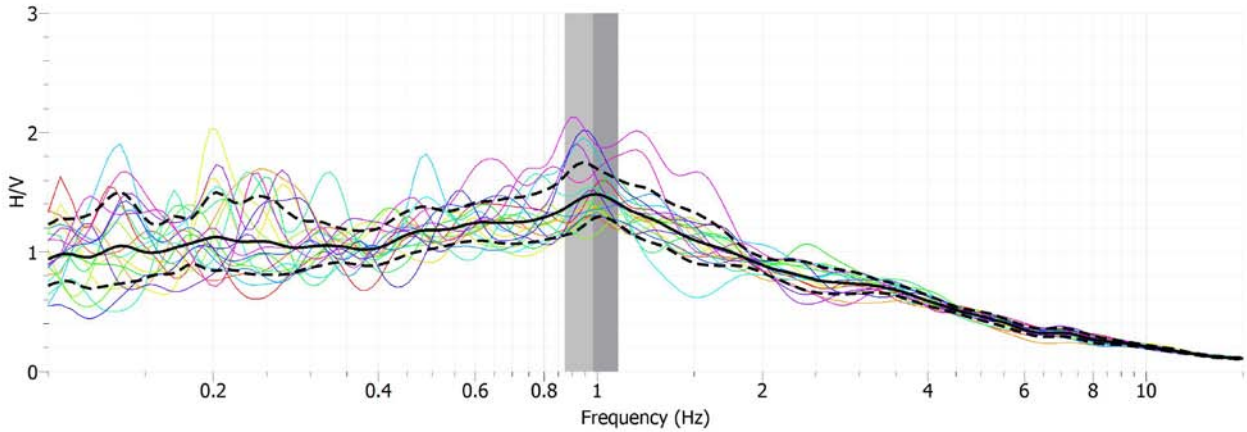

Site CE.12923, HVSR Location 1, Micromed Tromino ENGR Sensor

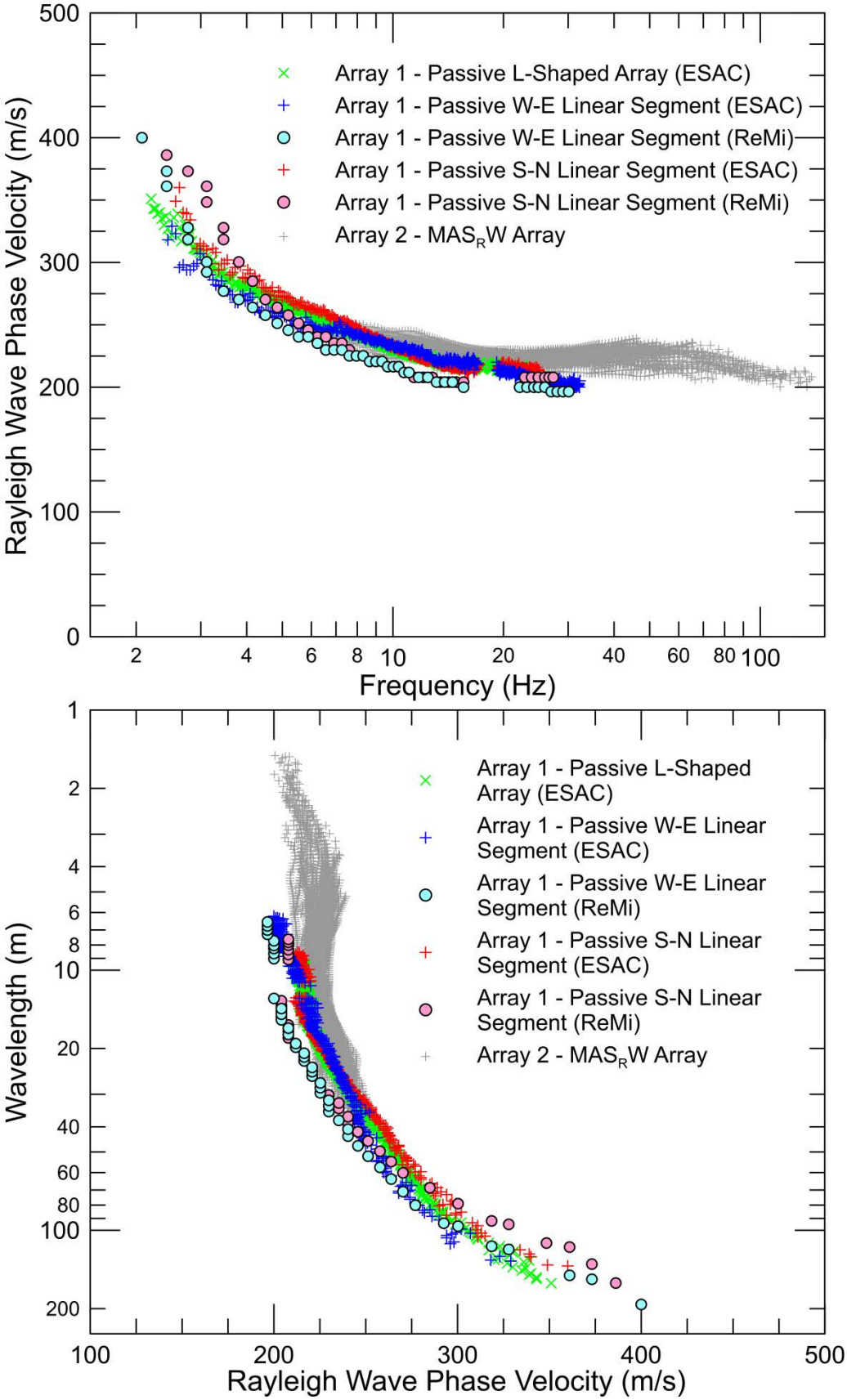

CE.12923 – Dispersion curves derived from active and passive surface wave data. Dispersion curves from ESAC and ReMi™ analysis of the linear legs of the L-array are not in good agreement with one another or the dispersion curve from the L-array, especially at long wavelengths. Therefore, only the passive surface wave data from the more reliable L-shaped array were used for modeling.

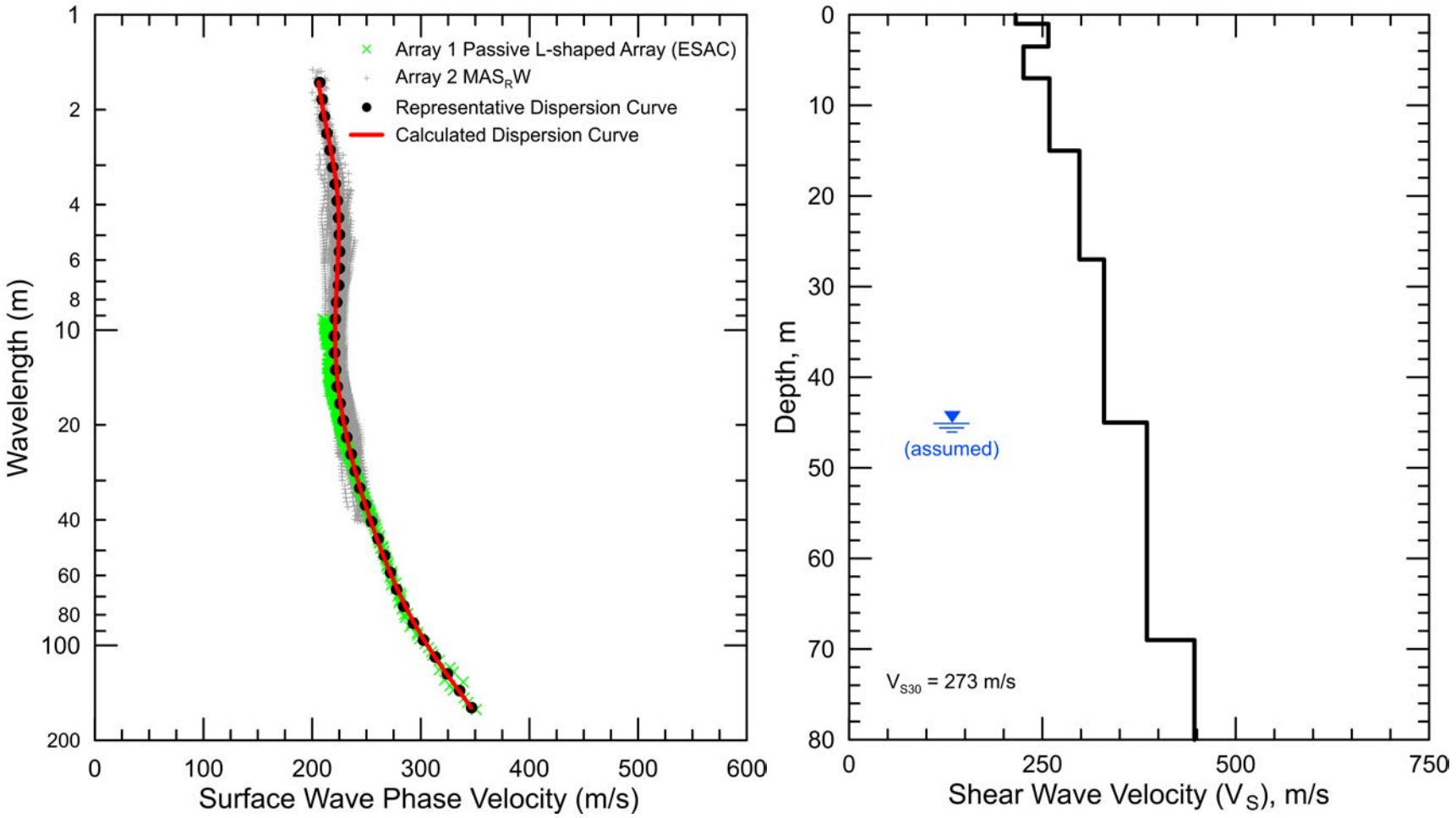

CE.12923 - Field, representative and calculated surface wave dispersion data (left) and associated V_S models (right). V_S increases gradually with depth and, therefore, multiple V_S models are not presented to demonstrate non-uniqueness because all models would show the same general velocity-depth trend.

Site CE.13079

Station Name: Riverside - Hwy 91 & Van Buren

Location: Riverside City Fire Station #2, 9449 Andrew St., Arlington, CA 92503

Latitude: 33.9174 **Longitude:** -117.4430

V_{S30} (measured): 305 m/s

Estimated error in V_{S30}: ± 30 m/s

NEHRP Site Class: D

Geomatrix Code: AHD/AQD

Geologic Conditions/Observations: Site located in area mapped as Quaternary (Holocene and late Pleistocene) young alluvial fan deposits.

Site Conditions: Suburban site with traffic noise from nearby roads, particularly Van Buren Blvd and SR 91. Relatively flat terrain in site vicinity.

Geophysical Methods Utilized: MAS_RW, array microtremor, HVSR

Geophysical Testing Arrays:

1. Array 1: two 10 channel, nested triangle passive surface wave arrays with common center point utilizing 1 Hz geophones and with 45 and 60 m lengths for the outer side of the arrays.
2. Array 2: 24 channel, linear passive surface wave array utilizing 4.5 Hz vertical geophones spaced 6 m apart for a length of 138 m.
3. Array 3: 48 channel MAS_RW array utilizing 4.5 Hz vertical geophones spaced 1.5 m apart for a length of 70.5 m, forward and reverse shot locations with multiple source offsets (1.5 to 30 m at both ends of array) and multiple interior source locations. Accelerated weight drop used at all source locations offset from ends of array and 4 and 12 lb hammers used at near-offset source locations and interior source locations.
4. Three HVSR measurement locations; two in the vicinity of MAS_RW and microtremor arrays and one near the seismic station.

Location of Geophysical Testing Arrays:

Location	Latitude	Longitude
Array 1 Passive, Corner of Array, Sensor Location 1	33.91652	-117.44216
Array 1 Passive, Corner of Array, Sensor Location 3	33.91692	-117.44260
Array 1 Passive, Corner of Array, Sensor Location 5	33.91640	-117.44279
Array 1 Passive, Center of Array, Sensor Location 10	33.91661	-117.44251
Array 2 Passive, Southeast End of Array	33.91606	-117.44166
Array 2 Passive, Northwest End of Array	33.91700	-117.44263
Array 3 MASW, Southeast End of Array	33.91631	-117.44192
Array 3 MASW, Northwest End of Array	33.91679	-117.44241
HVSR Location 1	33.91738	-117.44274
HVSR Location 2	33.91661	-117.44251
HVSR Location 3	33.91631	-117.44192

Notes: 1) WGS84 Coordinate System (decimal degrees)

Results:

V_S Model

Depth to Top of Layer (m)	Layer Thickness (m)	S-Wave Velocity (m/s)	Inferred P-Wave Velocity (m/s)	Assumed Poisson's Ratio	Assumed Density (g/cm^3)
0	2	151	282	0.300	1.70
2	3	211	395	0.300	1.80
5	4	296	554	0.300	1.85
9	6	340	636	0.300	1.90
15	10	371	1750	0.476	1.95
25	12	396	1800	0.475	2.00
37	13	534	1850	0.455	2.05
50	>10	1808	3383	0.300	2.30

Notes: 1) Depth of investigation is about 65 m.
2) The saturated zone with V_P > 1,750 m/s was constrained at a depth of about 15 m based on inspection of seismic refraction first arrival data.
3) Bottom layer is a half space and represents crystalline bedrock.
4) Bedrock depth and velocity not well constrained and may vary by 20%, or more.

Observations/Discussion:

- The HVSR plots show a peak in the 2.4 to 2.7 Hz range. This is indicative of a significant impedance contrast, most likely associated with crystalline bedrock, within the expected depth of investigation of the active and passive surface wave sounding.
- The HVSR plots at Locations 1 and 2 are almost identical with a 2.4 Hz peak, indicating that bedrock depth is similar near the seismic station and in the vicinity of passive surface wave Array 1. There is a slightly higher frequency HVSR peak at Location 3 indicating that bedrock may become shallower to the southeast.
- Noise conditions at the site (multi-directional noise sources) appeared sufficient for successful application of passive surface wave techniques.
- The ESAC technique was used to extract surface wave dispersion data from the ambient noise data collected at the nested triangle Array 1. The minimum wavelength Rayleigh wave extracted from Array 1 was 7 m. The maximum wavelength Rayleigh wave extracted from this array was 155 m, about 2.5 times the maximum receiver separation.
- Both the ReMi™ and ESAC techniques were used to extract surface wave dispersion data from the ambient noise data collected at the linear Array 2. The minimum wavelength Rayleigh wave that could be extracted from these arrays using the ESAC and ReMi™ techniques were about 12 and 17 m, respectively. The maximum wavelength Rayleigh wave that could be extracted from these arrays using the ESAC and ReMi™ techniques were about 150 and 160 m, respectively.
- All passive surface wave dispersion data are in good agreement and were combined with the MAS_RW dispersion data for analysis.
- Rayleigh wave dispersion data were interpreted from 21 MAS_RW seismic records collected at 16 different source locations using 4 lb hammer, 12 lb sledgehammer, and 240 lb accelerated weight drop energy sources. Using variable receiver offset ranges, over 75 dispersion curves were extracted and combined for analysis.
- To minimize near field effects and the influence of high noise data at low frequencies associated with heavy traffic in the site vicinity, the maximum wavelength Rayleigh wave extracted from the MAS_RW data set was set equal to the lesser of 75 m or 1.3 times the distance between the source and midpoint of the active receiver array.
- There is nominally about 30 to 40 m/s of scatter in MAS_RW dispersion data, which is likely in part related to lateral velocity variation.
- The minimum wavelength Rayleigh wave phase velocity data extracted from a 48-channel MAS_RW receiver gather was 9 to 20 m, depending on source location. Reducing data from smaller hammer sources using a limited offset range receiver gather (i.e. less active geophones) allowed for extraction of surface wave dispersion data to a minimum wavelength of about 4 m.
- Surface wave dispersion data from active and passive surface wave data sets are in excellent agreement over the approximate 15 to75 m overlapping wavelength range.
- The phase velocity of a 40 m wavelength Rayleigh wave (V_{R40}) is 308 m/s from ESAC analysis of the ambient noise data collected along Array 1 and 310 and 289 m/s (7% variation) from the analysis of the ambient noise data collected along Array 2 using the ESAC and ReMi™ techniques, respectively. V_{R40} from the MAS_RW dispersion data ranges from 269 to 300 m/s with a mean of 287 m/s and standard deviation of 8.1 m/s.

The similarity in V_{R40} of the various surface wave techniques and arrays indicates that each method alone would have independently yielded acceptable estimates of V_{S30}.

- The mean V_{R40} from the combined MAS_RW and array microtremor dispersion data is 295 m/s with a standard deviation of 12.0 m/s. During these computations, the combined array microtremor data were given equal weight to the MAS_RW data and the combined dispersion data from the passive linear arrays had equal to or lesser weight than that of the 2-D array.
- Representative dispersion curves were generated for each surface wave data set using a moving average, polynomial curve fitting routine. These individual representative dispersion curves were combined and a composite representative dispersion curve generated for the combined data set for data modeling.
- The composite representative dispersion curve was inverted using an iterative non-linear least squares inversion routine and fundamental mode Rayleigh wave assumption to derive V_S models. Realistic estimates of Poisson's ratio and density were used to make models as accurate as possible. High Poisson's ratio, saturated sediments were constrained at a depth of about 15 m with $V_P > 1{,}750$ m/s based on interactive layer-based analysis of seismic refraction first arrival data. Poisson's ratio of the saturated sediments was allowed to gradually decrease with depth as the sediments became stiffer, a common observation in borehole V_P and V_S logs. Model layer thicknesses increased with depth to reflect the reduction in model resolution with depth.
- Surface wave depth of investigation is about 65 m based on the one-half to one-third of the maximum wavelength criteria. A maximum depth of one-half the maximum wavelength is generally appropriate for a site with a gradual increase in velocity with depth; whereas, one-third the maximum wavelength is often more appropriate for a site with an abrupt increase in velocity at depth.
- Several V_S models were developed with almost identical calculated dispersion curves to demonstrate the non-uniqueness inherent in the inversion of surface wave dispersion data; especially at layer boundaries where an abrupt change in seismic velocity occurs. These equivalent V_S models have an abrupt increase in velocity, likely associated with the top of competent crystalline rock, between depths of about 45 and 65 m. These bedrock depths are close to the expected depth of investigation and, therefore, the velocity of the bedrock unit is very poorly constrained and can be allowed to vary by a significant amount in the V_S models.
- The predicted HVSR peak based on the diffuse field assumption, as computed using the software package *HV-Inv* Release 1.0 Beta, is about 2.1 to 2.2 Hz for all of the equivalent V_S models which is slightly lower than the 2.4 Hz peak observed in the vicinity of the seismic station and Array 1.
- The V_S model presented for the purpose of site characterization has the inferred top of the competent rock at a depth of 50 m and the V_S model has a predicted HVSR peak of 2.2 Hz. The HVSR peak seems to be heavily influenced by the depth and velocity of the V_S model layer immediately above the half space. As the depth to the half space increases, the V_S of this layer appears to be more indicative of weathered rock than sediments.
- V_{S30} is 305 m/s for the V_S model presented for the purpose of site characterization (NEHRP Site Class D).
- The estimated error in V_{S30}, which includes some effects of the lateral velocity variability beneath the testing arrays, is 30 m/s. This is computed based on the sum of the following

rounded up to the nearest 5 m/s: an estimated error of 3% from the realistic assumed layer Poisson's ratios in the model, 1% error from the realistic assumed layer densities in the model, 2% for the variation in V_{S30} associated with non-uniqueness, and the 12.0 m/s standard deviation in V_{R40} between the combined active and passive surface wave dispersion data.

- Interestingly, V_{S30} estimated from V_{R40} using the Brown et al., 2000 relationship ($V_{S30} \cong 1.045V_{R40}$, assuming V_{R40} represents the fundamental mode Rayleigh wave) is 308 m/s, only 1% different than that estimated from the V_S model.

Legend

- CSMIP Station and Number
- H/V Spectral Ratio Measurement Location
- MASW Array
- Passive Surface Wave Array
- Passive Surface Wave Triangle Array

NOTES:
1. WGS 1984 COORDINATE SYSTEM
2. Image Source: Esri, DigitalGlobe, GeoEye, Earthstar Geographics, CNES/Airbus DS, USDA, USGS, AEX, Getmapping, Aerogrid, IGN, IGP, swisstopo, and the GIS User Community

File Name: 16192_13079-I

Date: 8/1/2016

GEOVision geophysical services

SITE MAP
CE•13079

CGS CALIFORNIA GEOLOGICAL SURVEY

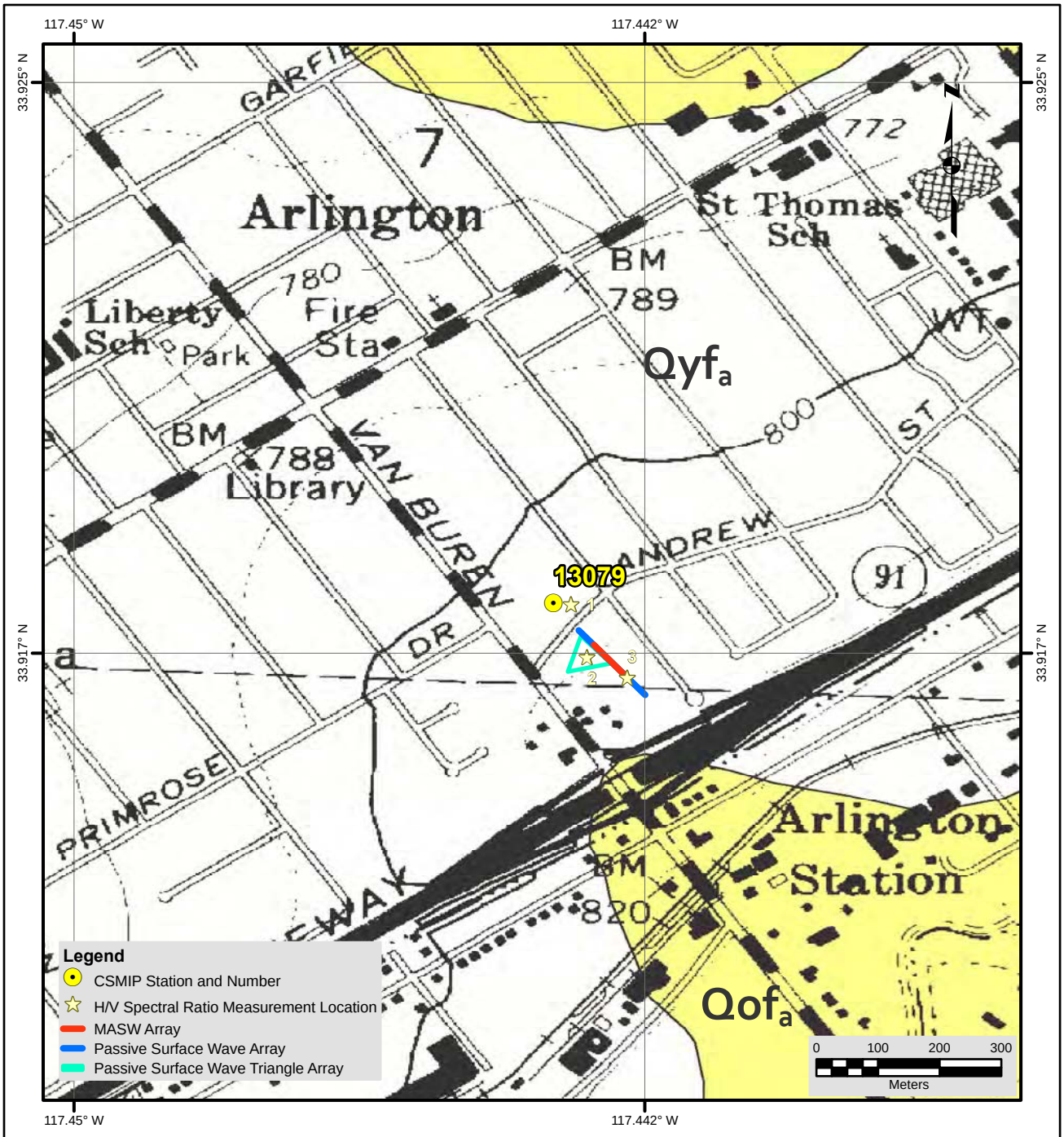

Description of Geologic Map Units

Qyf$_a$ = Quaternary (Holocene and late Pleistocene) young alluvial fan deposits.
Qof$_a$ = Quaternary (late to middle Pleistocene) Old alluvial fan deposits. Fluvial deposits along valley floors.

NOTES:
1. WGS 1984 COORDINATE SYSTEM
2. Geologic Map of the Riverside West 7.5' Quadrangle, Riverside County, California by Douglas M. Morton and Brett F. Cox

File Name: 16192_13079

Date: 8/1/2016

GEOVision geophysical services

GEOLOGIC MAP
CE•13079

CGS CALIFORNIA GEOLOGICAL SURVEY

Looking northwest towards fire station housing CE.13079 seismic station from passive surface wave array 13079-1

Looking northwest towards fire station along passive surface wave array 13079-2

Looking northwest towards HVSR Location 1

Data acquisition using 4 lb hammer on MASW array 13079-3

Looking southeast along MASW array 13079-3

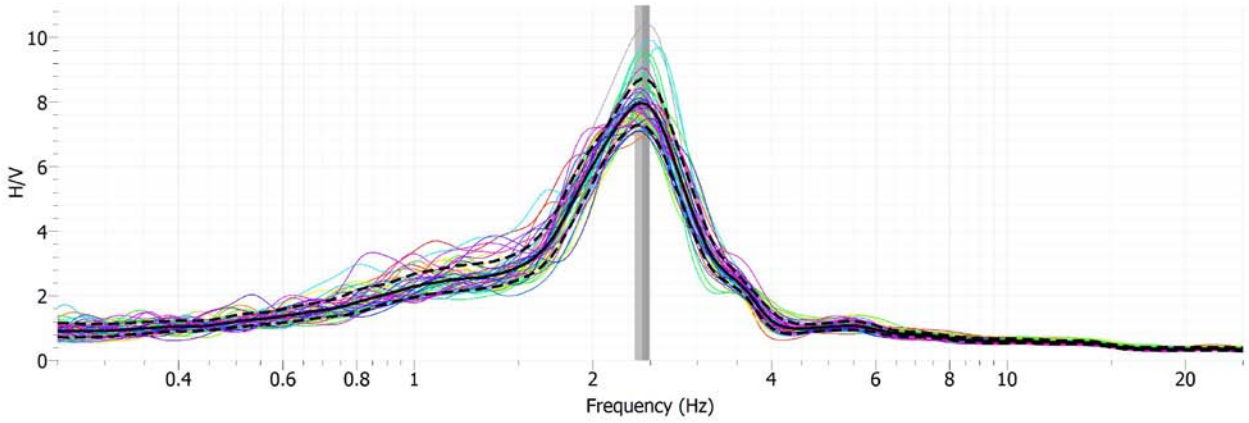

Site CE.13079, HVSR Location 1, Nanometrics Trillium Compact Sensor

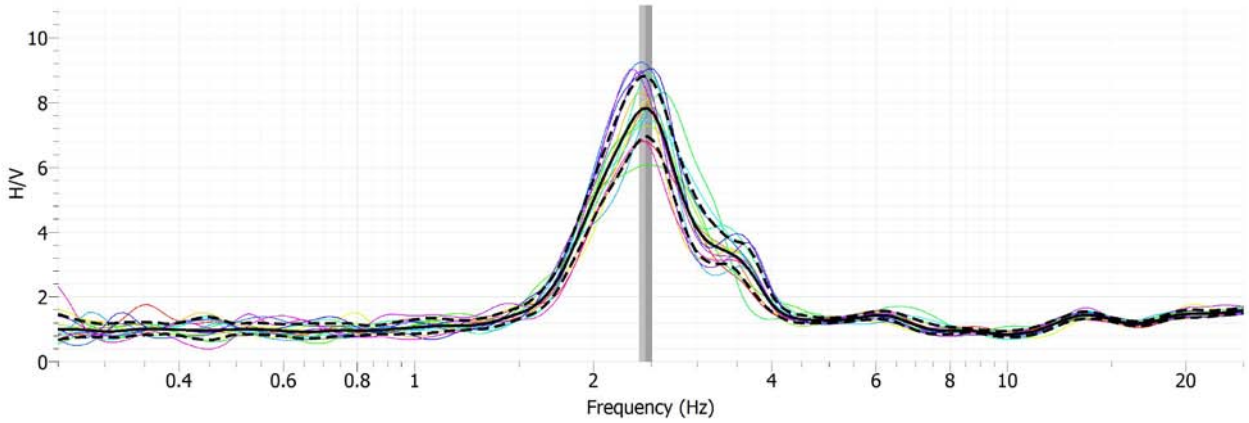

Site CE.13079, HVSR Location 2, Micromed Tromino ENGR Sensor

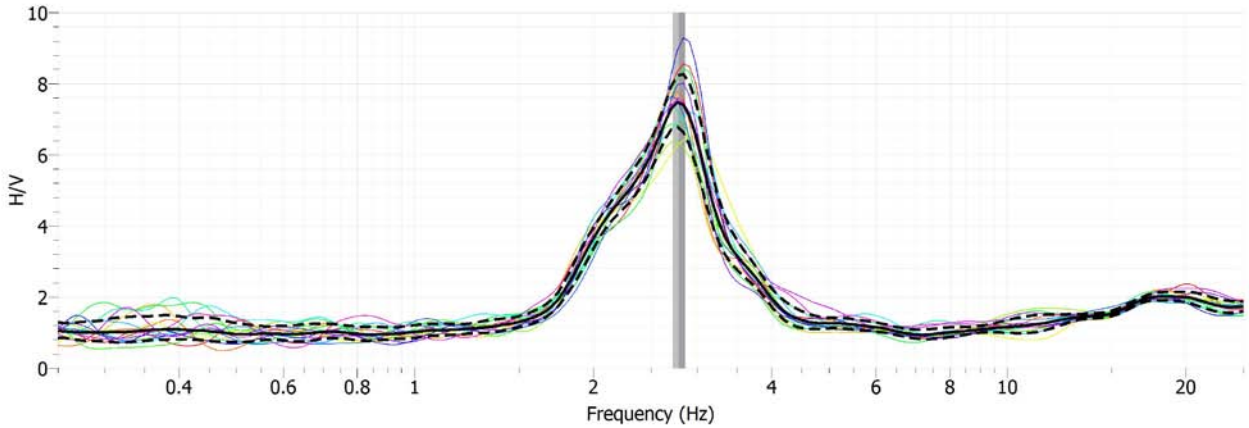

Site CE.13079, HVSR Location 3, Micromed Tromino ENGR Sensor

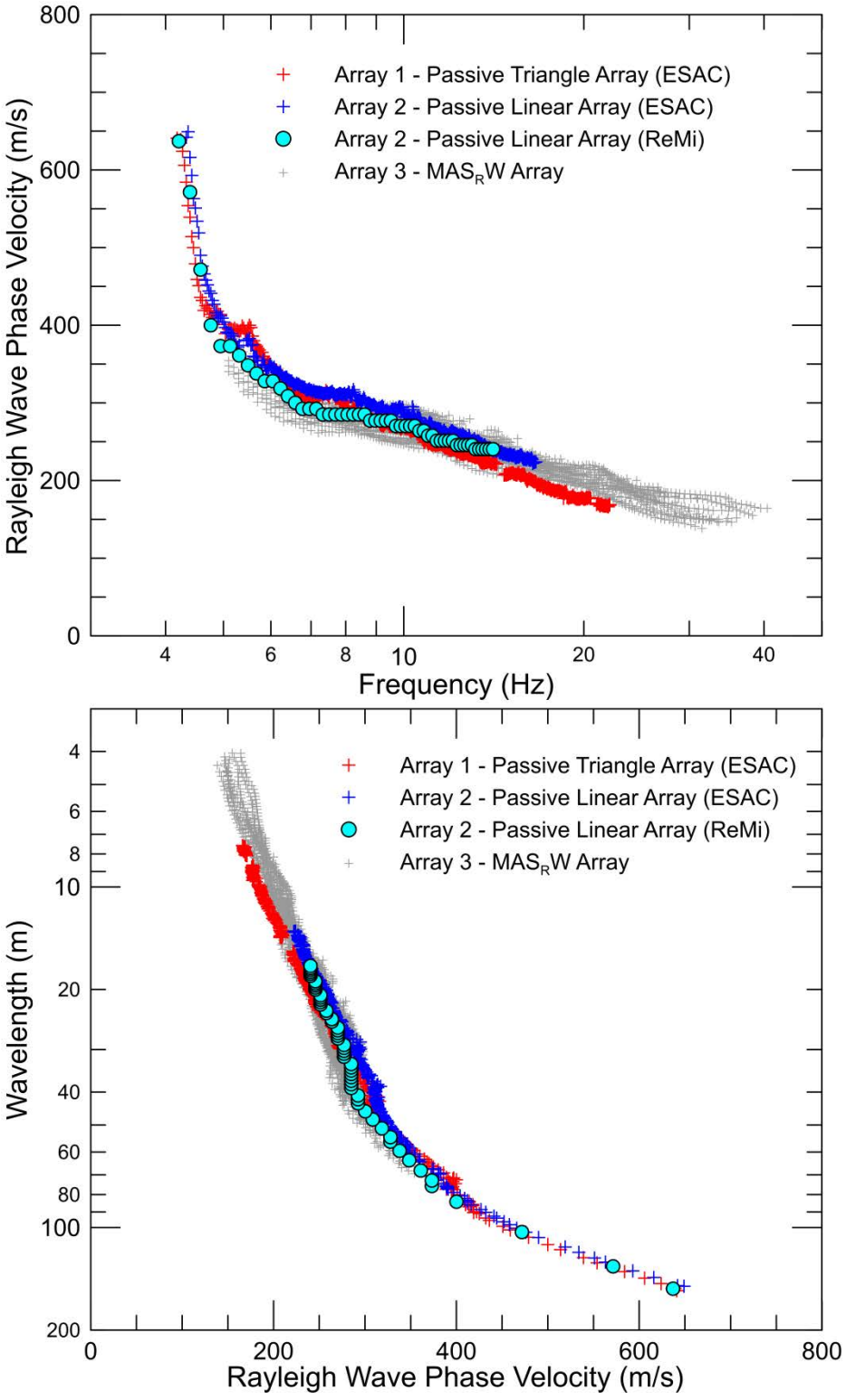

CE.13079 – Dispersion curves derived from active and passive surface wave data. Passive surface wave data from the linear array were reduced using both ESAC and ReMi™ techniques. There is good agreement in the dispersion curves between all active and passive surface wave data sets and, therefore, all of the dispersion curves were used for site characterization.

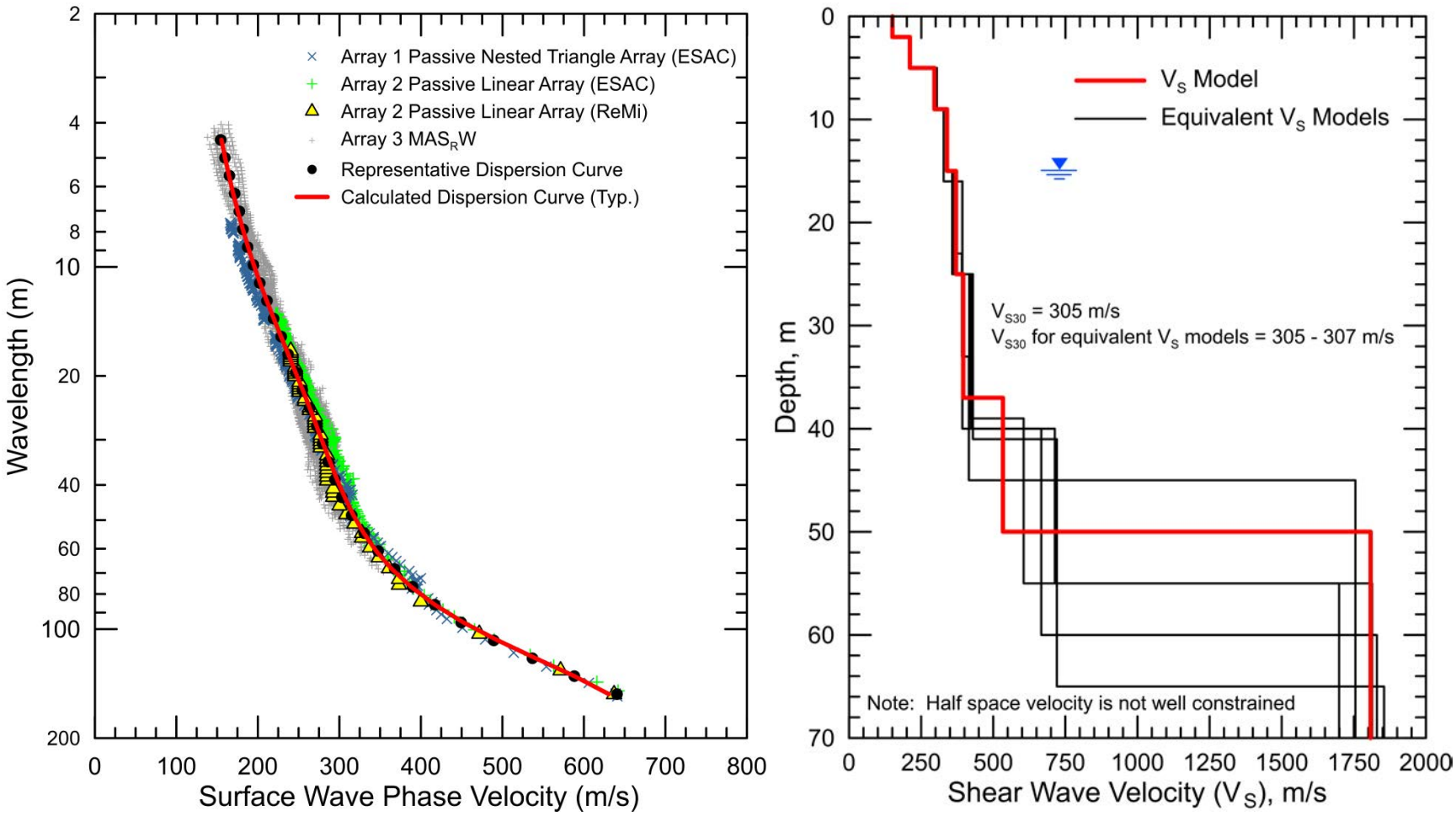

CE.13079 - Field, representative and calculated surface wave dispersion data (left) and associated V_S models (right)

Site CE.13080

Station Name: Moreno Valley - Sunnymead & Village

Location: Sunnymead Ranch Fire Station, 10511 Village Rd., Moreno Valley, CA 92557

Latitude: 33.9677 **Longitude:** -117.2519

V_{S30} (measured): 420 m/s

Estimated error in V_{S30}: ± 40 m/s

NEHRP Site Class: C

Geomatrix Code: AHC/AQC

Geologic Conditions/Observations: Site located in area mapped as Quaternary (early Pleistocene) very old alluvial fan deposits. Quaternary (Holocene and late Pleistocene) young axial channel deposits located approximately 250 m north of the site.

Site Conditions: Suburban site with traffic noise from nearby roads. Relatively flat terrain in site vicinity.

Geophysical Methods Utilized: MAS_RW, array microtremor, HVSR

Geophysical Testing Arrays:

1. Array 1: 10 channel, nested triangle passive surface wave array utilizing 1 Hz geophones and a 60 m length for outer side of array.
2. Array 2: 24 channel, linear passive surface wave array utilizing 4.5 Hz vertical geophones spaced 4.5 m apart for a length of 103.5 m.
3. Array 3: 48 channel MAS_RW array utilizing 4.5 Hz vertical geophones spaced 1 m apart for a length of 47 m, forward and reverse shot locations with multiple source offsets (1 to 20 m at both ends of array) and multiple interior source locations. Accelerated weight drop used at all source locations offset from ends of array and 4 and 12 lb hammers used at near-offset source locations and interior source locations.
4. Array 4: 10 channel, nested triangle passive surface wave array utilizing 1 Hz geophones and a 45 m length for outer side of array and a common array center with Array 1.
5. Array 5: 24 channel, linear passive surface wave array utilizing 4.5 Hz vertical geophones spaced 4 m apart for a length of 92 m.
6. Three HVSR measurement locations; two in the vicinity of MAS_RW and microtremor arrays and one near the seismic station.

Location of Geophysical Testing Arrays:

Location	Latitude	Longitude
Array 1 Passive, Corner of Array, Sensor Location 1	33.96732	-117.25251
Array 1 Passive, Corner of Array, Sensor Location 3	33.96759	-117.25265
Array 1 Passive, Corner of Array, Sensor Location 5	33.96707	-117.25272
Array 1 Passive, Center of Array, Sensor Location 10	33.96729	-117.25213
Array 2 Passive, Southwest End of Array	33.96700	-117.25290
Array 2 Passive, Northeast End of Array	33.96782	-117.25237
Array 3 MASW, Southwest End of Array	33.96728	-117.25272
Array 3 MASW, Northeast End of Array	33.96764	-117.25248
Array 4 Passive, Corner of Array, Sensor Location 1	33.96750	-117.25268
Array 4 Passive, Corner of Array, Sensor Location 3	33.96710	-117.25262
Array 4 Passive, Corner of Array, Sensor Location 5	33.96734	-117.25223
Array 5 Passive, Southwest End of Array	33.96703	-117.25299
Array 5 Passive, Northeast End of Array	33.96750	-117.25218
HVSR Location 1	33.96789	-117.25191
HVSR Location 2	33.96756	-117.25221
HVSR Location 3	33.96732	-117.25251

Notes: 1) WGS84 Coordinate System (decimal degrees)

Results:

V_S Model

Depth to Top of Layer (m)	Layer Thickness (m)	S-Wave Velocity (m/s)	Inferred P-Wave Velocity (m/s)	Assumed Poisson's Ratio	Assumed Density (g/cm^3)
0	1	213	398	0.300	1.80
1	2	271	508	0.300	1.85
3	3	362	677	0.300	1.95
6	12	451	844	0.300	2.00
18	17	492	920	0.300	2.05
35	30	582	1800	0.442	2.10
65	>10	1136	2126	0.300	2.30

Notes: 1) Effective depth of investigation is about 75 m.
2) The saturated zone with assumed V_P > 1,800 m/s was constrained at a depth of about 35 m based on possible reflector from top of saturated zone.
3) Bottom layer is a half space and represents crystalline bedrock.
4) Bedrock depth and velocity not well constrained and may vary by 20%, or more.

Observations/Discussion:

- The HVSR plots show a peak in the 2.2 to 2.4 Hz range. This is indicative of significant impedance contrast, most likely associated with crystalline bedrock, within the expected depth of investigation of the active and passive surface wave sounding.
- Noise conditions at the site (multi-directional noise sources) appeared sufficient for successful application of passive surface wave techniques.
- The ESAC technique was used to extract surface wave dispersion data from the ambient noise data collected on the nested triangle Arrays 1 and 4. The minimum wavelength Rayleigh wave extracted from Array 1 and the combined Arrays 1 and 4 were 17 and 14.5 m, respectively. The maximum wavelength Rayleigh wave extracted from these arrays was 180 m, about 3 times the maximum receiver separation.
- Both the ReMi™ and ESAC techniques were used to extract surface wave dispersion data from the ambient noise data collected at the linear Arrays 2 and 5. The minimum wavelength Rayleigh wave that could be extracted from these arrays is in the 11 to 18 m range. The maximum wavelength Rayleigh wave that could be extracted from these arrays is in the 170 to 200 m range.
- The passive surface wave dispersion data from the linear arrays are generally in acceptable agreement with that from the triangular arrays. However, only the more accurate dispersion data from the triangular arrays were combined with the MAS_RW dispersion data for analysis.
- Rayleigh wave dispersion data were interpreted from 18 MAS_RW seismic records collected at 13 different source locations using 4 lb hammer, 12 lb sledgehammer, and 240 lb accelerated weight drop energy sources. Using variable receiver offset ranges, over 85 dispersion curves were extracted and combined for analysis.
- To minimize near field effects and the influence of high noise data at low frequencies associated with traffic in the site vicinity, the maximum wavelength Rayleigh wave extracted from the MAS_RW data set was set equal to the lesser of 50 m or one times the distance between the source and midpoint of the active receiver array.
- There is nominally about 25 to 75 m/s of scatter in MAS_RW dispersion data, which is likely in part related to lateral velocity variation. At this site near field effects, which often result in underestimated Rayleigh wave phase velocity appear to be more significant that typically observed and contribute significantly to the 75 m/s scatter in dispersion data at long wavelengths.
- The minimum wavelength Rayleigh wave phase velocity data extracted from a 48-channel MAS_RW receiver array was 8 to 20 m, depending on source location. Reducing data from smaller hammer sources using a limited offset range receiver gather (i.e. less active geophones) allowed for extraction of surface wave dispersion data to a minimum wavelength of about 1.7 m.
- Surface wave dispersion data from active and passive surface wave data sets are in excellent agreement over the approximate 15 to 50 m overlapping wavelength range.
- The phase velocity of a 40 m wavelength Rayleigh wave (V_{R40}) is 405 and 408 m/s from ESAC analysis of the ambient noise data collected along the passive triangular Array 1 and combined Arrays 1 and 4, respectively. The phase velocity of a 40 m wavelength Rayleigh wave (V_{R40}) is 434 and 412 m/s (5% difference) from ESAC and ReMi™ analysis of the ambient noise data collected along the linear Array 2, respectively. The

phase velocity of a 40 m wavelength Rayleigh wave (V_{R40}) is 409 and 424 m/s (4% difference) from ESAC and ReMi™ analysis of the ambient noise data collected along the linear Array 5, respectively. V_{R40} from the MAS_RW dispersion data ranges from 370 to 400 m/s with a mean of 384 m/s and standard deviation of 9.1 m/s. It should be noted that the MAS_RW data may slightly underestimate V_{R40} due to near-field effects that appear more significant than usually observed. The similarity in V_{R40} (12% variation) of the various surface wave techniques and arrays indicates that each method alone would have independently yielded acceptable estimates of V_{S30}.

- The mean V_{R40} from the combined MAS_RW and array microtremor dispersion data used for modeling is 395 m/s with a standard deviation of 13.1m/s. During these computations, the combined array microtremor data were given equal weight to the MAS_RW data and the combined dispersion data from the passive linear arrays had equal to or lesser weight than that of the 2-D array.
- Representative dispersion curves were generated for each surface wave data set using a moving average, polynomial curve fitting routine. These individual representative dispersion curves were combined and a composite representative dispersion curve generated for the combined data set for data modeling.
- The composite representative dispersion curve was inverted using an iterative non-linear least squares inversion routine and fundamental mode Rayleigh wave assumption to derive V_S models. Realistic estimates of Poisson's ratio and density were used to make models as accurate as possible. High Poisson's ratio, saturated sediments were constrained at a depth of about 35 m with inferred V_P > 1,800 m/s based on observation of a possible water table reflector in the seismic records. Poisson's ratio of the saturated sediments was allowed to gradually decrease with depth as the sediments became stiffer, a common observation in borehole V_P and V_S logs. Model layer thicknesses increased with depth to reflect the reduction in model resolution with depth.
- Surface wave depth of investigation is about 75 m based on the one-half to one-third of the maximum wavelength criteria. A maximum depth of one-half the maximum wavelength is generally appropriate for a site with a gradual increase in velocity with depth; whereas, one-third the maximum wavelength is often more appropriate for a site with an abrupt increase in velocity at depth.
- Several V_S models were developed with almost identical calculated dispersion curves to explore the non-uniqueness associated with the abrupt increase in velocity associated with expected crystalline bedrock. These equivalent V_S models have modeled bedrock between depths of about 55 and 80 m. These bedrock depths are close to the expected depth of investigation and, therefore, the velocity of the bedrock unit is very poorly constrained and can be allowed to vary by a significant amount in the V_S models.
- The predicted HVSR peak based on the diffuse field assumption, as computed using the software package *HV-Inv* Release 1.0 Beta, is about 2.0 to 2.3 Hz for all of the equivalent V_S models, the higher frequencies being that same as the 2.2 to 2.4 Hz HVSR peaks observed at this site.
- The V_S model presented for the purpose of site characterization has the inferred top of the competent rock at a depth of 65 m, the intermediate modeled depth to bedrock. This V_S model has a predicted HVSR peak of 2.2 Hz, the same as that observed at Location 1, near the seismic station.

- V_{S30} is 420 m/s for the V_S model presented for the purpose of site characterization (NEHRP Site Class C).
- The estimated error in V_{S30}, which includes some effects of the lateral velocity variability beneath the testing arrays, is 40 m/s. This is computed based on the sum of the following rounded up to the nearest 5 m/s: an estimated error of 3% from the realistic assumed layer Poisson's ratios in the model, 1% error from the realistic assumed layer densities in the model, 2% for the variation in V_{S30} associated with non-uniqueness, and the 13.1 m/s standard deviation in V_{R40} between the combined active and passive surface wave dispersion data.
- Interestingly, V_{S30} estimated from V_{R40} using the Brown et al., 2000 relationship ($V_{S30} \cong 1.045V_{R40}$, assuming V_{R40} represents the fundamental mode Rayleigh wave) is 413 m/s, only 2% different than that estimated from the V_S model.

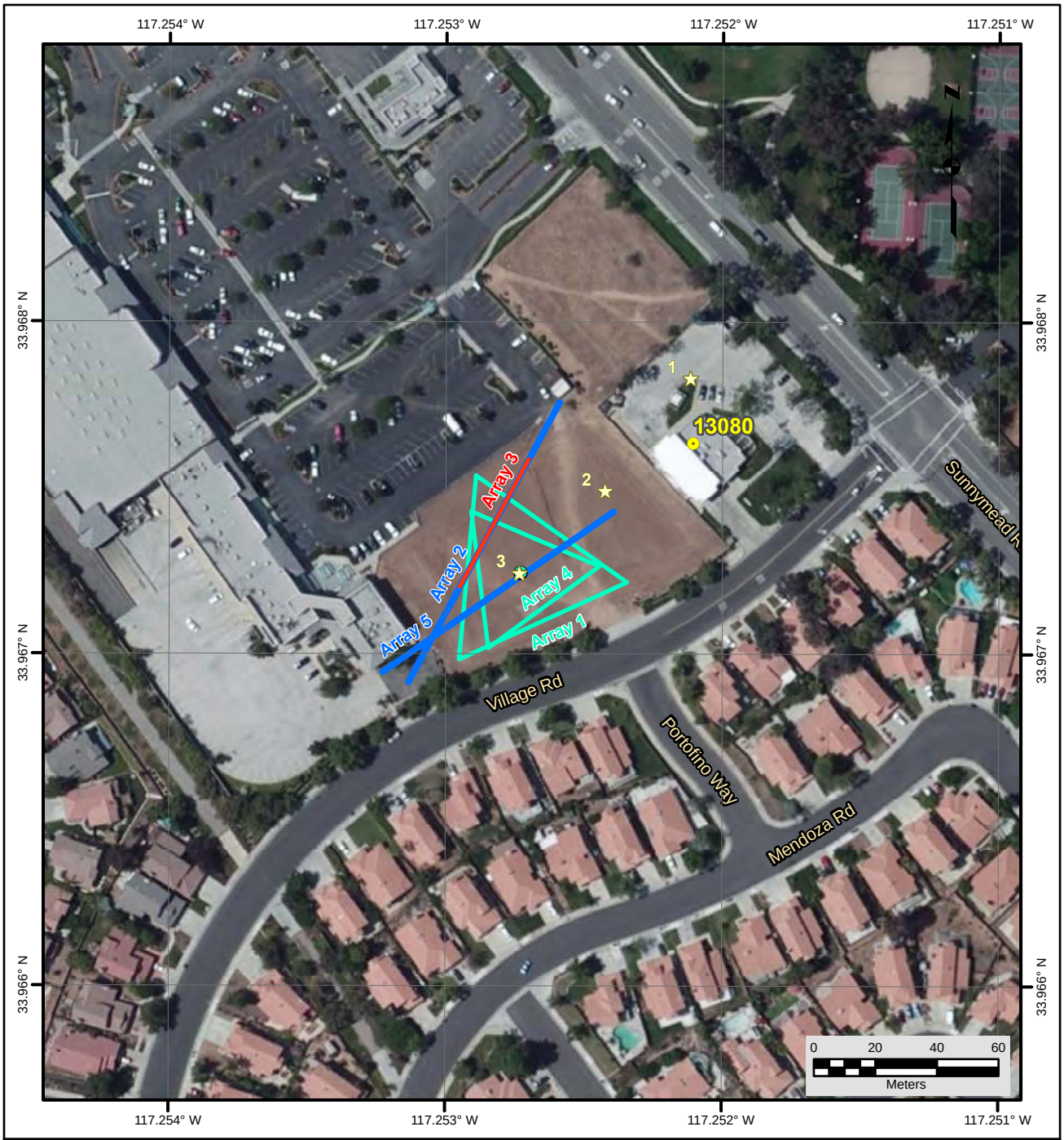

Legend

- CSMIP Station and Number
- H/V Spectral Ratio Measurement Location
- MASW Array
- Passive Surface Wave Array
- Passive Surface Wave Triangle Array

NOTES:
1. WGS 1984 COORDINATE SYSTEM
2. Image Source: Esri, DigitalGlobe, GeoEye, Earthstar Geographics, CNES/Airbus DS, USDA, USGS, AEX, Getmapping, Aerogrid, IGN, IGP, swisstopo, and the GIS User Community

File Name: 16192_13080-I

Date: 7/28/2016

GEOVision geophysical services

SITE MAP
CE•13080

CGS CALIFORNIA GEOLOGICAL SURVEY

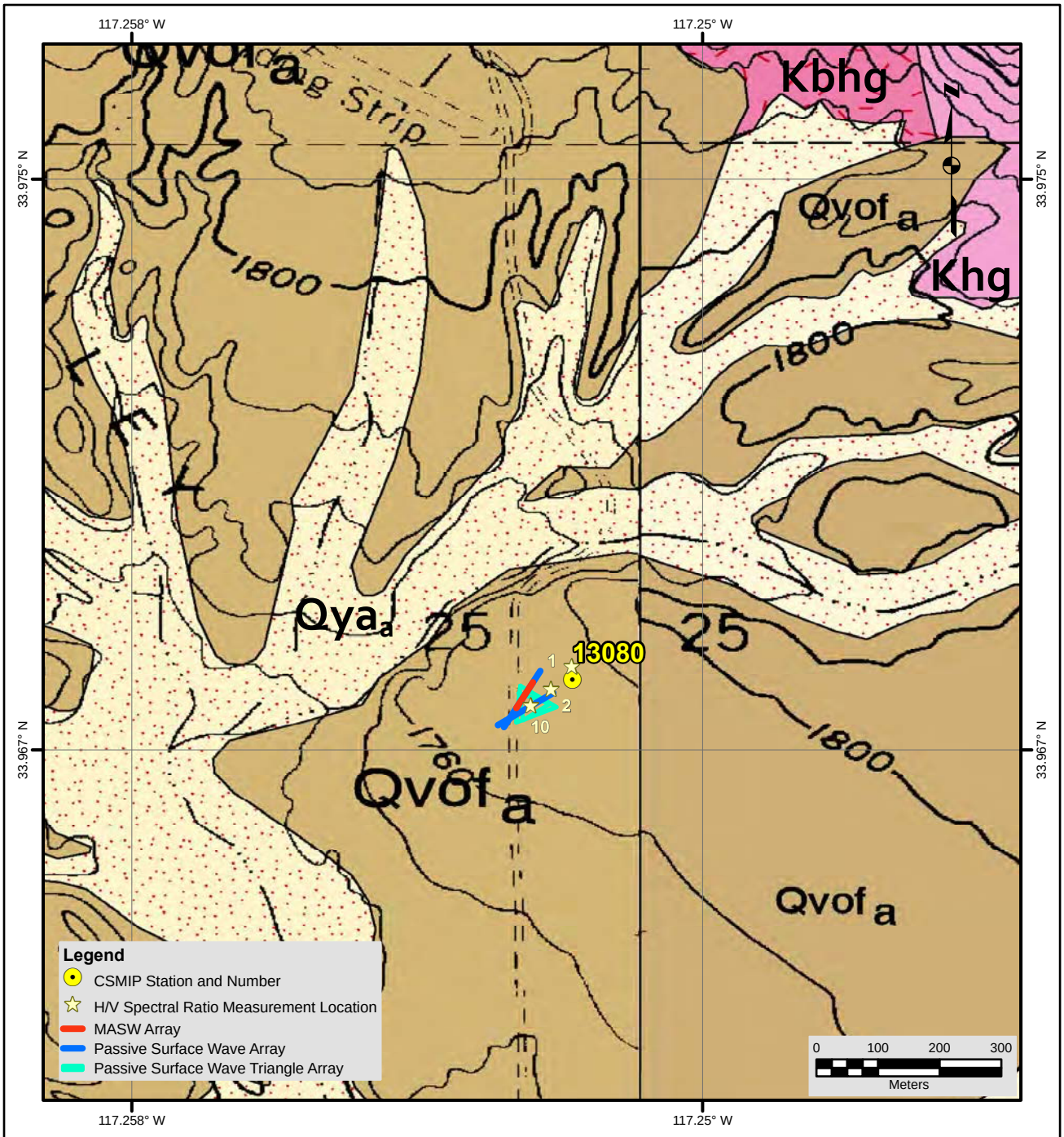

Description of Geologic Map Units

Qya_a = Quaternary (Holocene and late Pleistocene) Young axial channel deposits.
$Qvof_a$ = Quaternary (early Pleistocene) Very old alluvial fan deposits.
Kbhg = Cretaceous Heterogeneous porphyritic granodiorite.
Khg = Cretaceous Heterogeneous granitic rocks.

NOTES:
1. WGS 1984 COORDINATE SYSTEM
2. Geologic Map of the Riverside East and Sunnymead 7.5' Quadrangles, Riverside County, California by Douglas M. Morton, Brett F. Cox and Jonathan C. Matti

File Name: 16192_13080

Date: 7/13/2016

GEOVision geophysical services

GEOLOGIC MAP
CE•13080

CGS CALIFORNIA GEOLOGICAL SURVEY

Looking south towards fire station housing CE.13080 seismic station from HVSR Location 1

Looking northeast towards fire station along passive surface wave array 13080-5

Looking northeast towards fire station from passive surface wave arrav 13080-1

Looking southwest along MASW array 13080-3

Looking northeast along passive surface wave array 13080-2

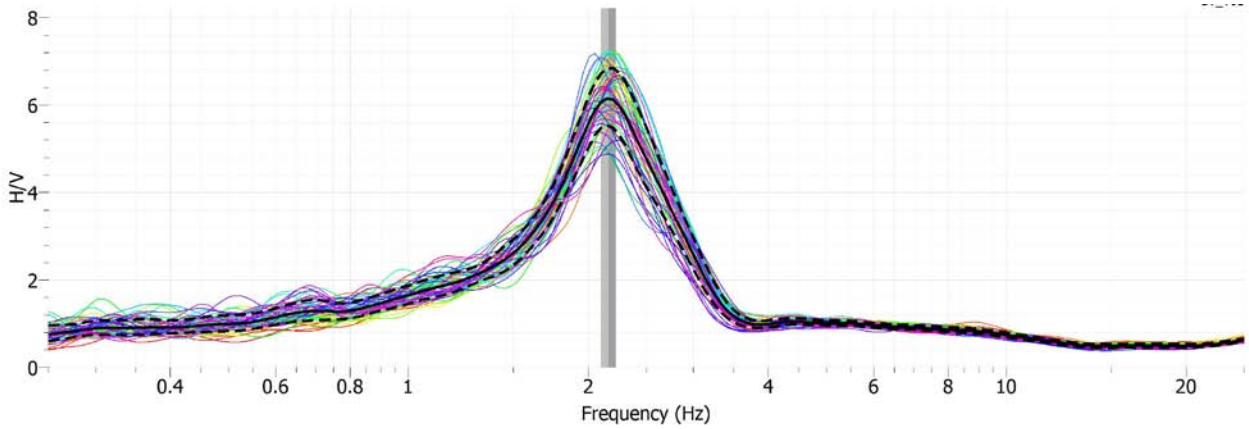

Site CE.13080, HVSR Location 1, Nanometrics Trillium Compact Sensor

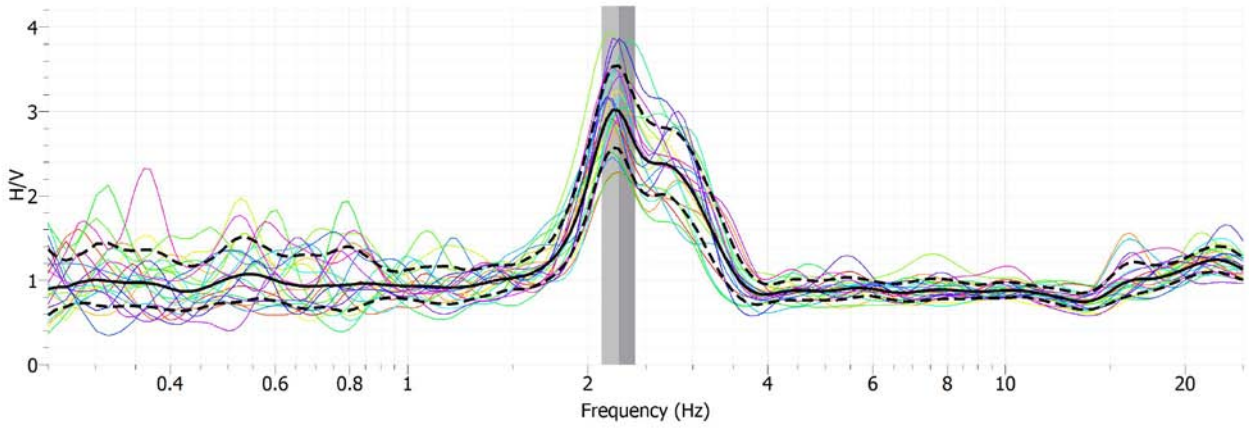

Site CE.13080, HVSR Location 2, Micromed Tromino ENGR Sensor

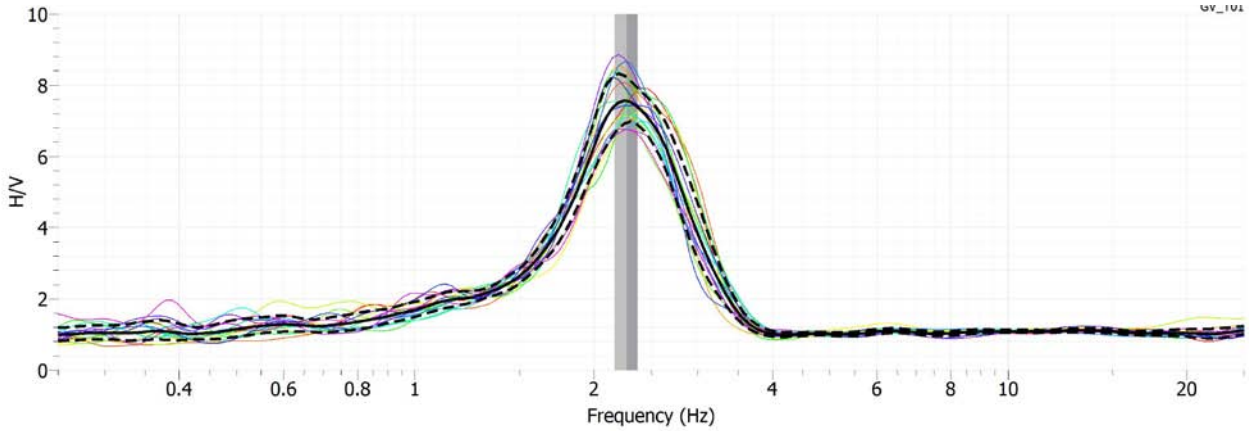

Site CE.13080, HVSR Location 3, Nanometrics Trillium Compact Sensor

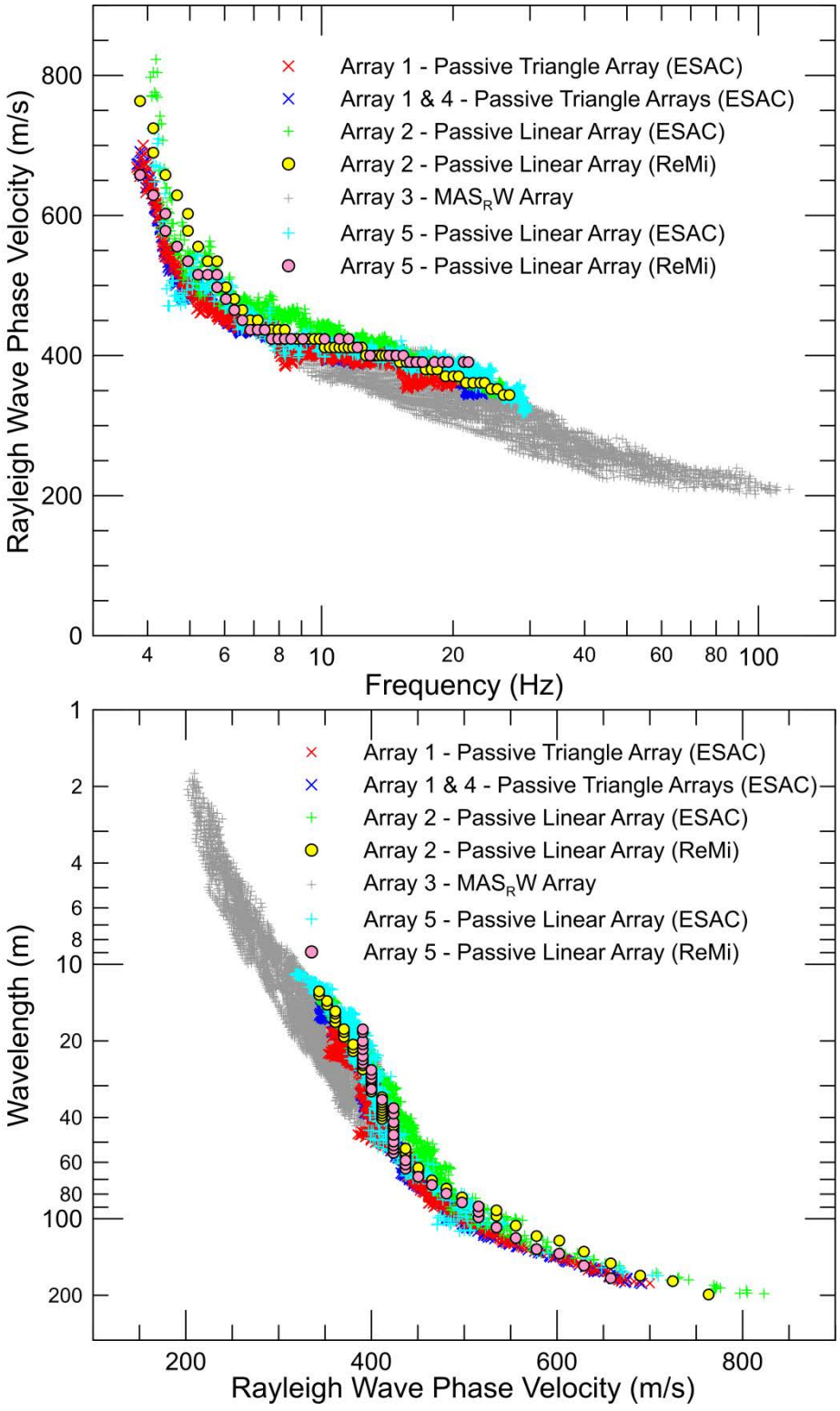

CE.13080 – Dispersion curves derived from active and passive surface wave data. Passive surface wave data from the linear array were reduced using both ESAC and ReMi™ techniques. There is generally acceptable agreement in the dispersion curves between all active and passive surface wave data sets. However, only the more accurate dispersion curves from the passive triangular arrays were combined with the MAS_RW for site characterization.

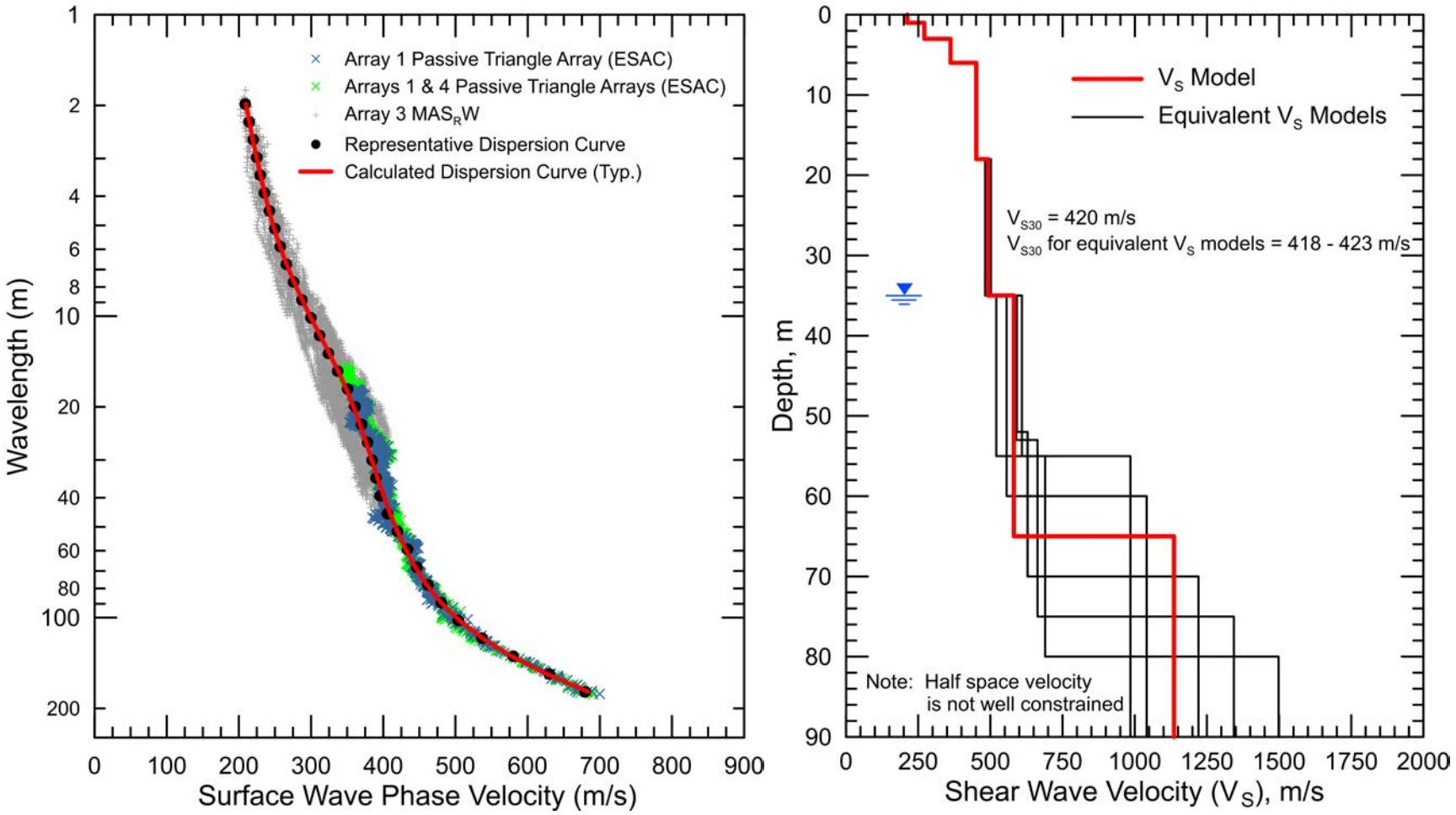

CE.13080 - Field, representative and calculated surface wave dispersion data (left) and associated V_S models (right)

Site CE.13123

Station Name: Riverside - Airport

Location: Riverside Airport, 6905 Airport Dr., Riverside, CA 92504

Latitude: 33.9506 **Longitude:** -117.4453

V_{S30} (measured): 547 m/s

Estimated error in V_{S30}: ± 55 m/s

NEHRP Site Class: C

Geomatrix Code: AQB

Geologic Conditions/Observations: Site located in area mapped as Quaternary (late to middle Pleistocene) old alluvial fan deposits. Quartz diorite mapped approximately 300 m east and north of site. Smooth topography is the site vicinity indicates that the quartz diorite is intensely weathered

Site Conditions: Suburban site. Flat terrain in site vicinity.

Geophysical Methods Utilized: MAS_RW (Rayleigh wave - vertical and horizontal geophones), MAS_LW (Love wave), array microtremor, HVSR

Geophysical Testing Arrays:

1. Array 1: 48 channel MAS_RW array utilizing 4.5 Hz vertical and 4.5 Hz horizontal (radial orientation) geophones spaced 1.5 m apart for a length of 70.5 m, forward and reverse shot locations with multiple source offsets (1.5 to 30 m at both ends of array) and multiple interior source locations. Accelerated weight drop used at all source locations offset from ends of array and 4 and 12 lb hammers used at near-offset source locations and interior source locations. MAS_LW data also acquired along this array using 4.5 Hz horizontal transverse geophones and hammer and traction plank energy source.
2. Array 2: 10 channel, nested triangle passive surface wave array utilizing 1 Hz geophones and a 45 m length for outer side of array.
3. Array 3: 24 channel, linear passive surface wave array utilizing 4.5 Hz vertical geophones spaced 6 m apart for a length of 138 m.
4. Three HVSR measurement locations; two in the vicinity of MAS_RW and microtremor arrays and one near the seismic station.

Location of Geophysical Testing Arrays:

Location	Latitude	Longitude
Array 1 MASW, Northwest End of Array	33.94997	-117.44620
Array 1 MASW, Center of Array	33.94989	-117.44583
Array 1 MASW, Southeast End of Array	33.94983	-117.44545
Array 2 Passive, Corner of Array, Sensor Location 1	33.94987	-117.44572
Array 2 Passive, Corner of Array, Sensor Location 3	33.94979	-117.44524
Array 2 Passive, Corner of Array, Sensor Location 5	33.95017	-117.44538
Array 2 Passive, Center of Array, Sensor Location 10	33.94995	-117.44544
Array 3 Passive, Northwest End of Array	33.95004	-117.44659
Array 3 Passive, Southeast End of Array	33.94977	-117.44514
HVSR Location 1	33.95045	-117.44531
HVSR Location 2	33.94995	-117.44544
HVSR Location 3	33.94989	-117.44583

Notes: 1) WGS84 Coordinate System (decimal degrees)

Results:

V_S Model

Depth to Top of Layer (m)	Layer Thickness (m)	S-Wave Velocity (m/s)	Inferred P-Wave Velocity (m/s)	Assumed Poisson's Ratio	Assumed Density (g/cm^3)
0	1.5	209	391	0.30	1.80
1.5	2.5	331	619	0.30	1.90
4	8	429	803	0.30	1.95
12	16	792	1482	0.30	2.10
28	>12	1576	2950	0.30	2.20

Notes: 1) Depth of investigation is about 40 m.
2) Bottom layer is a half space.

Observations/Discussion:

- HVSR measurements were made at the site on 6/17/16 and 7/6/16. On 6/17/16, a monochromatic noise source (e.g. rotating machinery) with an approximate 6.5 Hz HVSR peak appeared to interfere with the HVSR measurement at Location 1, near the seismic station. This noise source was not present when the measurements were repeated on 7/6/16 and a 4.9 Hz HVSR peak was recovered. HVSR measurements at Locations 2 and 3 were unsuccessful on 6/17/16 as the asphalt surface was too hot to provide a stable

platform for the seismic sensor. These measurements were repeated on 7/6/16, but HVSR data was still very noisy relative to that collected at Location 1. HVSR data did appear to be recovered at Location 2 with a possible HVSR peak at 6.2 Hz. Additional, measurements are necessary to understand the variation in HVSR data in the site vicinity; however, it is possible that geologic conditions beneath the test area do not accurately represent those beneath the seismic station based on HVSR data collected to date.

- Noise conditions in the site vicinity (multi-directional or omni-directional noise sources) appeared sufficient for successful application of passive surface wave techniques. However, geologic maps indicate that probable weathered crystalline rock may be located at relatively shallow depths. High frequency passive surface wave energy does not appear to propagate very efficiently at the site and there was only very light traffic in close proximity to the site during data acquisition. Passive surface wave data was only recovered from passive triangle Array 2 by driving around the site on Flight Road, which circles the parking lot where the array was located, during data acquisition. Passive surface wave data was not acquired into the linear Array 3 during this time; however, it was possible to selectively interpret seismic records showing evidence of vehicular traffic in the site vicinity.
- The ESAC technique was used to extract surface wave dispersion data from the ambient noise data collected on the triangular shaped Array 2. The minimum and maximum wavelength Rayleigh waves extracted from Array 2 are 18 and 110 m, respectively.
- Both the ReMi™ and ESAC techniques were used to extract surface wave dispersion data from the ambient noise data collected along the linear Array 3. The minimum wavelength Rayleigh waves extracted from this array using the two analytical techniques are between 13 and 14 m. The maximum wavelength Rayleigh waves extracted from this array using the two analytical techniques are between 95 and 120 m.
- Inspection of MAS_RW dispersion data indicated that the low frequency/long wavelength component of the dispersion curve associated with probable bedrock was not recovered. It was also noted that the passive surface wave arrays were not yielding very long wavelength dispersion data. Therefore, MAS_LW (Love wave) data were acquired along the same array using 4.5 Hz horizontal (transverse orientation) geophones and a hammer and horizontal traction plank seismic source. Additionally, the MAS_RW survey was repeated using 4.5 Hz horizontal (radial orientation) geophones. The acquisition of MAS_RW data at this site using the horizontal radial geophones allowed Rayleigh wave dispersion data to be recovered to slightly longer wavelengths than the data acquired using the vertical geophones. However, high frequency/small wavelength fundamental mode dispersion data were not recovered from the MAS_RW seismic data collected with horizontal geophones due to a dominant higher mode at high frequencies.
- Rayleigh wave dispersion data were interpreted from 22 MAS_RW (vertical and horizontal radial component) seismic records collected at 17 different source locations using 4 lb hammer, 12 lb sledgehammer, and 240 lb accelerated weight drop energy sources. Using variable receiver offset ranges, over 120 dispersion curves were extracted and combined for analysis.
- To minimize near field effects, the maximum wavelength Rayleigh wave extracted from the MAS_RW data set was set equal to 1.3 times the distance between the source and midpoint of the active receiver array. The maximum wavelength Rayleigh wave

dispersion data extracted from the vertical and horizontal component $MAS_R W$ data were 45 and 56 m, respectively.

- There is nominally about 30 to 75 m/s of scatter in $MAS_R W$ dispersion data, which is likely in part related to lateral velocity variation.
- The minimum wavelength Rayleigh wave phase velocity data extracted from the 48-channel $MAS_R W$ array was 10 to 33 m, depending on source location. Reducing data from smaller hammer sources using a limited offset range receiver gather (i.e. less active geophones) allowed for extraction of surface wave dispersion data to a minimum wavelength of about 1.5 m from the vertical component data. No attempt was made to recover dispersion data at wavelengths less than 11 m from the horizontal component data due to a dominant higher mode at high frequencies.
- $MAS_L W$ data was also acquired at this site along the same array used to acquire $MAS_R W$ data but is not used for site characterization at this time. In theory, Love waves do not exist where there is a high velocity layer at the surface. More research is needed into the impact of a paved surface on Love wave acquisition. It appears that Love wave data was successfully recovered at the site; however, review of the Love wave data indicates that near surface S_H-velocity may be much higher than the S_V-velocity recovered from the Rayleigh wave dispersion data. Similar observations have been made at two other weathered crystalline rock sites in Southern California. At both of these sites the difference is S_V- and S_H-velocity occurred over a narrow depth range and appears to be too large to associate with anisotropy without further study.
- The passive surface wave dispersion data from the triangular shaped Array 2, reduced using the ESAC technique, is in excellent agreement with the $MAS_R W$ dispersion data over the overlapping 18 to 56 m wavelength range. The passive surface wave dispersion data from the linear Array 3 reduced using the ESAC and ReMi™ techniques are also in good agreement with the $MAS_R W$ data and passive dispersion data from the 2-D array. Therefore, all passive surface wave dispersion data were combined with the $MAS_R W$ dispersion data for purpose of site characterization
- The phase velocity of a 40 m wavelength Rayleigh wave (V_{R40}) is 521 m/s from ESAC analysis of the ambient noise data collected along Array 2. V_{R40} is 579 and 566 m/s (2% difference) from ESAC and ReMi™ analysis of the ambient noise data collected along the linear Array 3. V_{R40} from the $MAS_R W$ dispersion data ranges from 509 to 567 m/s with a mean of 535 m/s and standard deviation of 13.5 m/s. V_{R40} is relatively similar for all of the arrays and, therefore, each array would have independently yielded a reasonably accurate estimate of V_{S30}.
- The mean V_{R40} from the combined $MAS_R W$ and array microtremor dispersion data used for modeling is 542 m/s with a standard deviation of 22.0 m/s. During these computations, the combined array microtremor data were given equal weight to the $MAS_R W$ data and the combined dispersion data from the passive linear arrays had equal to or lesser weight than that of the 2-D array.
- Representative dispersion curves were generated for each surface wave data set using a moving average, polynomial curve fitting routine. These individual representative dispersion curves were combined and a composite representative dispersion curve generated for the combined data set for data modeling.
- The composite representative dispersion curve was inverted using an iterative non-linear least squares inversion routine and the effective mode Rayleigh wave assumption to

derive V_S models. The effective mode was used for data modeling because the velocity structure indicated that Rayleigh wave dispersion curve may jump from fundamental to 1st higher mode at low frequencies. Realistic estimates of Poisson's ratio and density were used to make models as accurate as possible. Review of seismic refraction first arrival data provided no evidence of the saturated zone above bedrock at the site. Model layer thicknesses were constrained to increase with depth to reflect the reduction in model resolution with depth.

- Surface wave depth of investigation is about 40 m based on the one-third of the maximum wavelength criteria, which is appropriate for a site with a sharp increase in velocity at depth.
- Several V_S models were developed with almost identical calculated dispersion curves to explore the non-uniqueness associated with the abrupt increase in velocity associated with expected weathered crystalline bedrock. These equivalent V_S models have modeled weathered bedrock between depths of about 10 and 14 m.
- The predicted HVSR peak based on the diffuse field assumption, as computed using the software package *HV-Inv* Release 1.0 Beta, is 6.5 to 6.9 Hz for all of the equivalent V_S models, which are slightly higher than the observed 6.2 Hz HVSR peak at Location 2 and much higher than the observed 4.9 Hz HVSR peak at Location 1. The possibility cannot be discounted that weathered rock is slightly deeper in the vicinity of the seismic station than beneath the testing arrays.
- The V_S model presented for the purpose of site characterization has the inferred top of the weathered rock at a depth of 12 m, one of the intermediate modeled depths to bedrock. This V_S model has a predicted HVSR peak of 6.7 Hz.
- V_{S30} is 547 m/s for the presented V_S model (NEHRP Site Class C).
- It is possible that both the depth to weathered rock and weathering profile within rock is highly variable across the site. Based on HVSR data, the possibility cannot be discounted that the V_S profile developed for the site is not representative of geologic conditions beneath the seismic station. It was, however, difficult to acquire useful HVSR data at this site. Additionally, inspection of the MAS_LW data indicates that the Love wave dispersion data, assuming the fundamental mode was recovered, may yield much higher near surface V_S than the Rayleigh wave data, which needs further study.
- The estimated error in V_{S30}, which includes some effects of the lateral velocity variability beneath the testing arrays, is 55 m/s. This is computed based on the sum of the following rounded up to the nearest 5 m/s: an estimated error of 3% from the realistic assumed layer Poisson's ratios in the model, 1% error from the realistic assumed layer densities in the model, 2% for the variation in V_{S30} associated with non-uniqueness, and the 22.0 m/s standard deviation in V_{R40} between the combined active and passive surface wave dispersion data.
- Interestingly, V_{S30} estimated from V_{R40} using the Brown et al., 2000 relationship ($V_{S30} \cong 1.045V_{R40}$, assuming V_{R40} represents the fundamental mode Rayleigh wave) is 566 m/s, less than 4% different to that that estimated from the V_S model. Although the dispersion data was modeled using an effective mode routine, the estimate of V_{S30} from V_{R40} is still accurate because the fundamental mode Rayleigh wave was recovered at 40 m wavelength.

Legend

- H/V Spectral Ratio Measurement Location
- CSMIP Station and Number
- MASW Array
- Passive Surface Wave Array
- Passive Surface Wave Triangle Array

NOTES:
1. WGS 1984 COORDINATE SYSTEM
2. Image Source: Esri, DigitalGlobe, GeoEye, Earthstar Geographics, CNES/Airbus DS, USDA, USGS, AEX, Getmapping, Aerogrid, IGN, IGP, swisstopo, and the GIS User Community

File Name: 16192_13123-I

Date: 7/28/2016

GEOVision geophysical services

SITE MAP
CE•13123

CGS CALIFORNIA GEOLOGICAL SURVEY

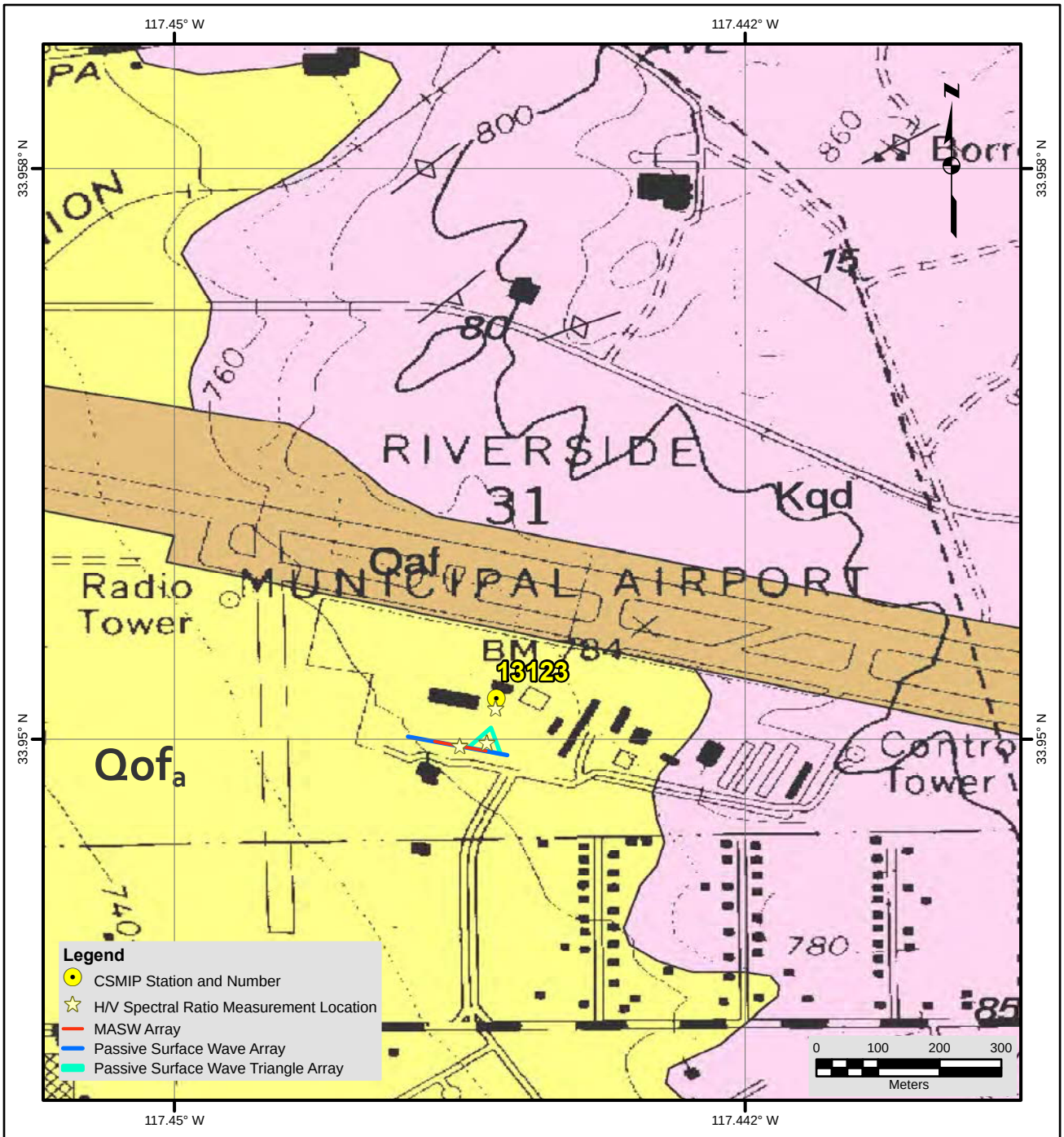

Description of Geologic Map Units

Qaf = Quaternary (late Holocene) Artificial fill deposits resulting from human activities.
Qof$_a$ = Quaternary (late to middle Pleistocene) Old alluvial fan deposits.
Kqd = (Cretaceous) Quartz diorite.

NOTES:
1. WGS 1984 COORDINATE SYSTEM
2. Geologic Map of the Riverside West 7.5' Quadrangle, Riverside County, California by Douglas M. Morton and Brett F. Cox

File Name: 16192_13123

Date: 7/28/2016

GEOVision geophysical services

GEOLOGIC MAP
CE•13123

CGS CALIFORNIA GEOLOGICAL SURVEY

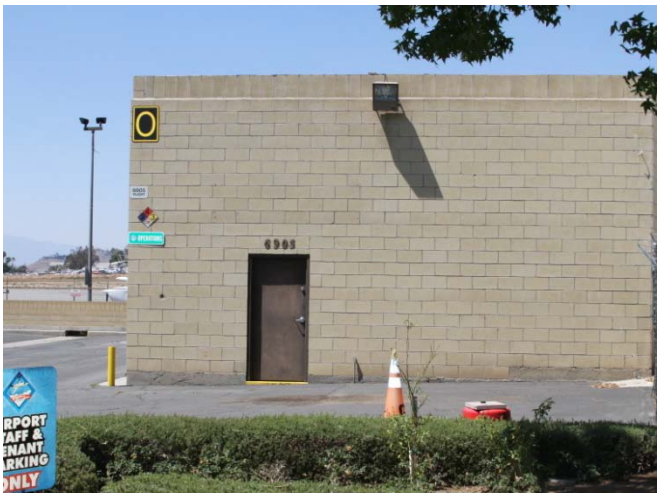

Looking north towards building housing CE.13123 seismic station from HVSR Location 1

Looking west along passive surface wave array 13123-3

Looking north towards seismic station from passive surface wave arrav 13123-2

Looking west along $MAS_R W$ (Rayleigh wave) array 13123-1

Looking east along $MAS_L W$ (Love wave) array 13123-1

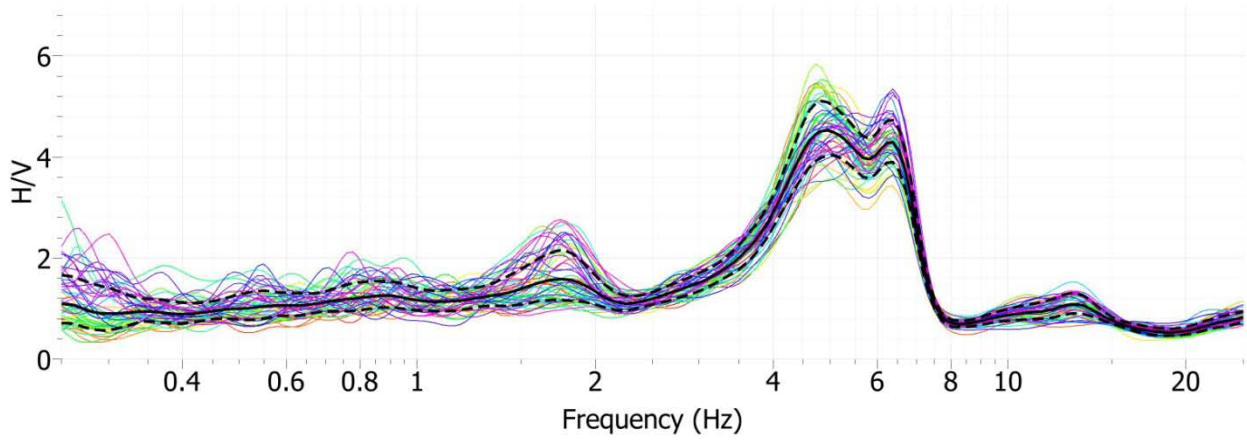

Site CE.13123, HVSR Location 1, Nanometrics Trillium Compact Sensor (6/17/16). Secondary HVSR peak at 6.4 Hz results from a monochromatic noise source (e.g. rotating machinery) and is not related to subsurface geologic conditions.

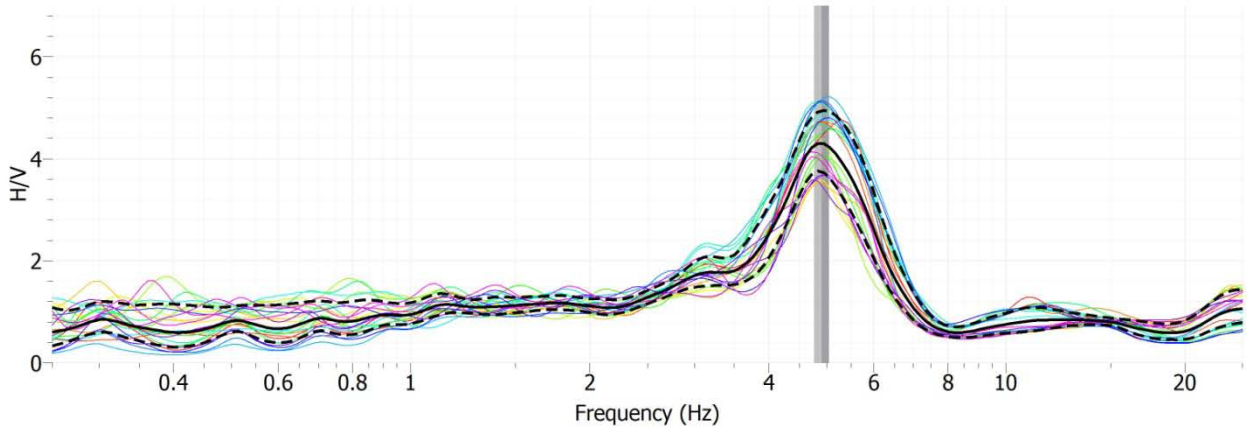

Site CE.13123, HVSR Location 1, Nanometrics Trillium Compact Sensor (7/6/16). There is no monochromatic noise source during data recording.

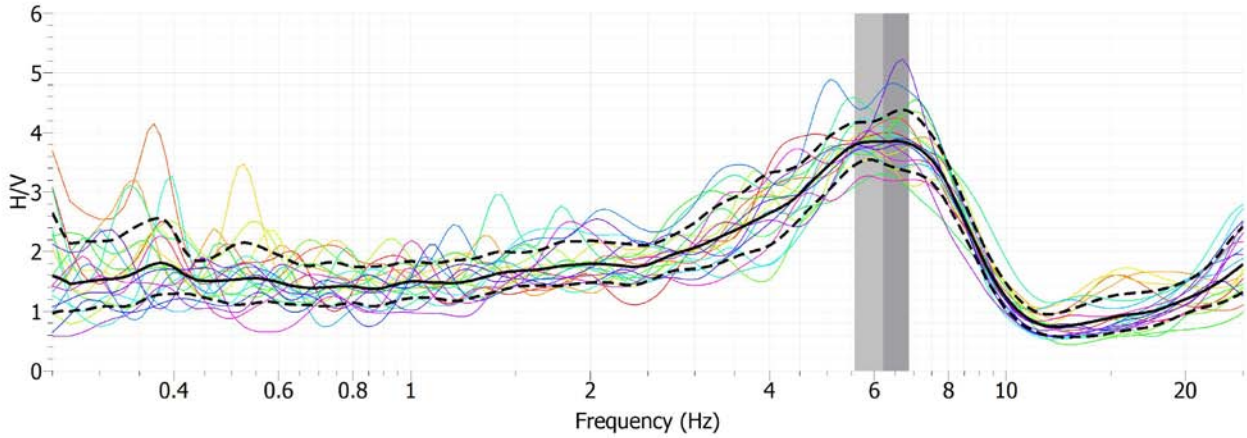

Site CE.13123, HVSR Location 2, Micromed Tromino ENGR (7/6/16).

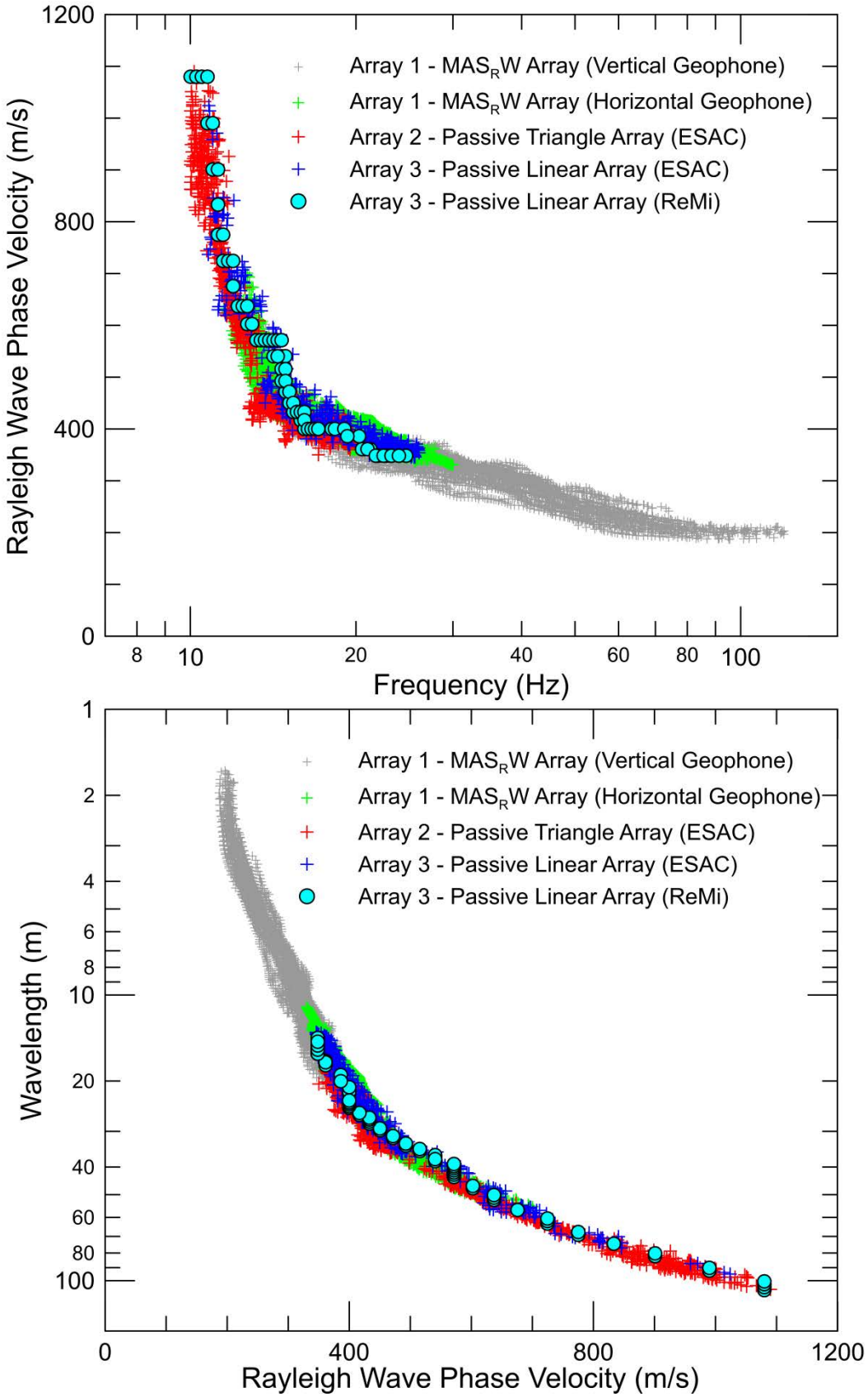

CE.13123 – Dispersion curves derived from active and passive surface wave data. Passive surface wave data from the triangular-shaped Array 2 and linear Array 3 are in good agreement with MAS_RW data and were used for data modeling. It should be noted that usable dispersion data was only obtained from passive arrays when vehicles were driving on Flight Road around the perimeter of the parking lot where surface wave testing was conducted.

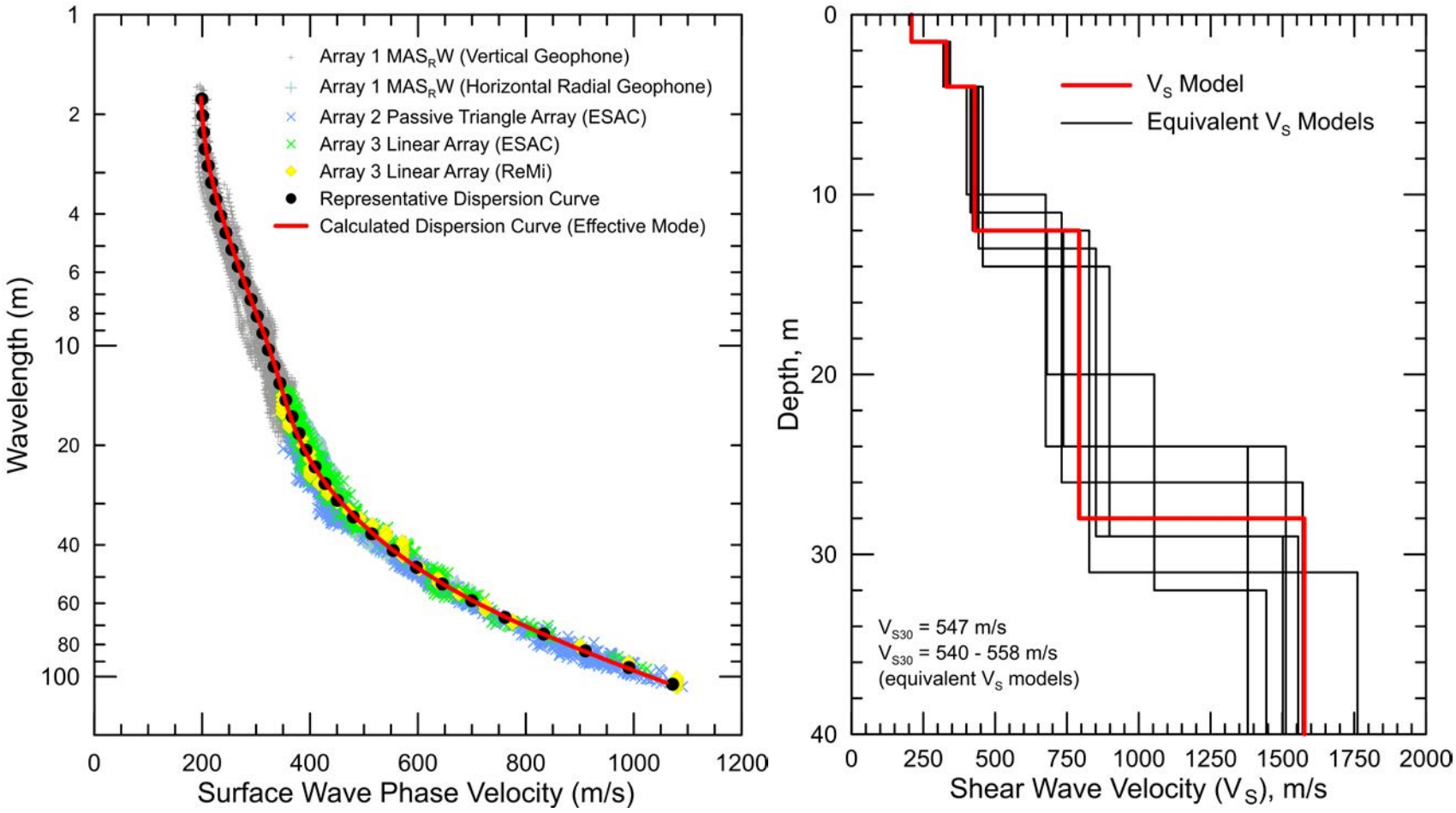

CE.13123 - Field, representative and calculated effective mode surface wave dispersion data (left) and associated V_S models (right). Surface wave dispersion data is plotted as phase velocity versus wavelength.

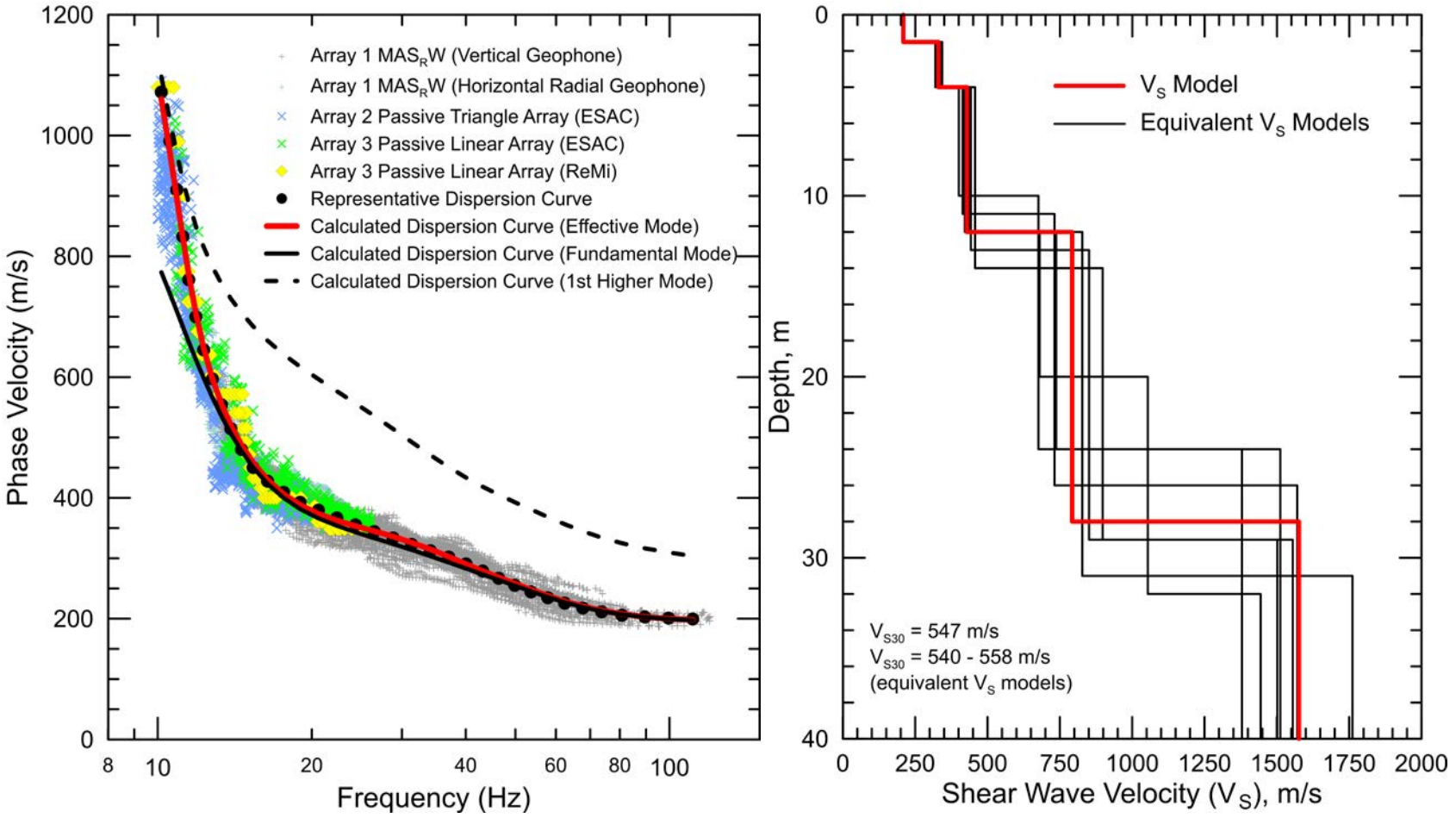

CE.13123 - Field, representative and calculated effective, fundamental and 1st higher mode surface wave dispersion data (left) and associated V_S models (right). Surface wave dispersion data is plotted as frequency versus phase velocity. Note that the fundamental mode and 1st higher mode Rayleigh wave fits the field observations at frequencies above and below about 12 Hz, respectively.

Site CE.13172

Station Name: Temecula - 6th & Mercedes

Location: Temecula Fire Station, 28330 Mercedes St., Temecula, CA 92590

Latitude: 33.4971 **Longitude:** -117.1507

V_{S30} (measured): 350 m/s

Estimated error in V_{S30}: ± 35 m/s

NEHRP Site Class: D/C

Geomatrix Code: AQD/AQC

Geologic Conditions/Observations: Site located in area mapped Quaternary (Pleistocene) old alluvial flood plain deposits. Survey lines cross into area mapped Quaternary (Pleistocene) Pauba Formation sandstone.

Site Conditions: Suburban site with traffic noise from nearby roads, particularly heavy traffic on Temecula Valley Freeway (I15). Relatively flat terrain in site vicinity.

Geophysical Methods Utilized: MAS_RW, array microtremor, HVSR

Geophysical Testing Arrays:

1. Array 1: 48 channel "L" shaped array utilizing 4.5 Hz vertical geophones spaced 4 m apart used to acquire passive surface wave data. The SE-NW and SW-NE linear segments of array have lengths of 96 and 92 m, respectively.
2. Array 2: 48 channel MAS_RW array utilizing 4.5 Hz vertical geophones spaced 1 m apart for a length of 47 m, forward and reverse shot locations with multiple source offsets (1 to 15 m at northwest end of array and 1 to 20 m at southeast end of array) and multiple interior source locations. Accelerated weight drop used at all source locations offset from ends of array and 4 and 12 lb hammers used at near-offset source locations and interior source locations.
3. One HVSR measurement located in the vicinity of MAS_RW, microtremor arrays and seismic station.

Location of Geophysical Testing Arrays:

Location	Latitude	Longitude
Array 1 Passive, Southeast End of Array	33.49652	-117.15034
Array 1 Passive, West Corner of Array	33.49714	-117.15107
Array 1 Passive, Northeast End of Array	33.49773	-117.15036
Array 2 MASW, Northwest End of Array	33.49726	-117.15061
Array 2 MASW, Southeast End of Array	33.49708	-117.15015
HVSR Location 1	33.49724	-117.15060

Notes: 1) WGS84 Coordinate System (decimal degrees)

Results:

V_S Model

Depth to Top of Layer (m)	Layer Thickness (m)	S-Wave Velocity (m/s)	Inferred P-Wave Velocity (m/s)	Assumed Poisson's Ratio	Assumed Density (g/cm^3)
0	2	271	507	0.300	1.85
2	4	297	555	0.300	1.90
6	5	322	602	0.300	1.90
11	7	359	672	0.300	1.95
18	12	402	752	0.300	1.95
30	15	436	1750	0.467	2.00
45	20	476	1800	0.462	2.00
65	25	561	1850	0.449	2.05
90	>10	643	1900	0.435	2.10

Notes: 1) Depth of investigation is about 100 m.
2) Bottom layer is a half space.

Observations/Discussion:

- HVSR data collected at Location 1 using a Nanometrics Trillium Compact 120 s seismograph does not have clear distinct peak. There is a slight maxima at about 0.7 Hz likely associated with geologic structure at significant depth below the expected depth of investigation of the active and passive surface wave sounding. HVSR data also collected at this location using a Tromino ENGR seismograph but does not yield reliable HVSR data. The Tromino uses higher frequency sensors and is not generally reliable at frequencies below 1.5 Hz.
- Noise conditions at the site (multi-directional noise sources) appeared sufficient for successful application of passive surface wave techniques.

- The ESAC technique was used to extract surface wave dispersion data from the ambient noise data collected on the L-shaped Array 1. The minimum wavelength Rayleigh wave extracted from Array 1 was 23 m. The maximum wavelength Rayleigh wave extracted from the array was 225 m.
- Both the ReMi™ and ESAC techniques used to extract surface wave dispersion data from the SE-NW and SW-NE linear legs of Array 1. It was not possible to extract surface wave dispersion data from the SE-NW leg of Array 1, oriented parallel to Interstate 15, using the ESAC method. The minimum wavelength Rayleigh waves that could be extracted from these arrays were in the 9 to 15 m range. The maximum wavelength Rayleigh waves that could be extracted from these arrays were in the 150 to 180 m range.
- The dispersion curve derived from the passive L-shaped array is in good agreement with that derived from the $MAS_R W$ data. The dispersion curves derived from the linear legs of the L-array using the ESAC and ReMi™ techniques are significantly different from those derived from the $MAS_R W$ and L-array data and, therefore, only the passive dispersion curve from the more reliable L-shaped array was used for site characterization.
- Rayleigh wave dispersion data were interpreted from 17 $MAS_R W$ seismic records collected at 12 different source locations using 4 lb hammer, 12 lb sledgehammer, and 240 lb accelerated weight drop energy sources. Using variable receiver offset ranges, over 65 dispersion curves were extracted and combined for analysis.
- To minimize near field effects and data degradation due to heavy traffic on the adjacent freeway, the maximum wavelength Rayleigh wave data extracted from the $MAS_R W$ data set was set equal to the lesser of 55 m or 1.3 times the distance between the source and midpoint of the active receiver array. Due to the proximity of the $MAS_R W$ array to the freeway there may be increased error in the $MAS_R W$ dispersion data at long wavelengths.
- There is nominally about 20 to 40 m/s of scatter in $MAS_R W$ dispersion data, which is likely in part due to lateral velocity variation.
- The minimum wavelength Rayleigh wave phase velocity data extracted from a 48-channel $MAS_R W$ receiver gather was 4 to 11 m, depending on source location. Reducing data from smaller hammer sources using a limited offset range receiver gather (i.e. less active geophones) allowed for extraction of surface wave dispersion data to a minimum wavelength of about 3 m.
- Surface wave dispersion data from $MAS_R W$ and L-shaped passive surface wave data sets are in good agreement over the approximate 23 to 55 m overlapping wavelength range. The surface wave dispersion data from the passive linear arrays are not in good agreement with that from the $MAS_R W$ data.
- The phase velocity of a 40 m wavelength Rayleigh wave (V_{R40}) is 325 m/s from ESAC analysis of the ambient noise data collected along L-shaped Array 1. V_{R40} is 351 m/s from the analysis of the ambient noise data collected along the SE-NW linear leg of Array 1 using the ReMi™ technique. V_{R40} is 360 and 334 m/s (7% difference) from the analysis of the ambient noise data collected along the SW-NE linear leg of Array 1 using the ESAC and ReMi™ techniques, respectively. V_{R40} from the $MAS_R W$ dispersion data ranges from 299 to 349 m/s with a mean of 325 m/s and standard deviation of 15.7 m/s. The similarity in V_{R40} of the various surface wave techniques and arrays indicates that each method would have independently yielded acceptable estimates of V_{S30}, even though there are significant differences in the dispersion curves between the linear

passive arrays and the MAS_RW and L-shaped passive arrays. Any V_S models derived from the linear passive arrays, however, would have been very unreliable.

- The mean V_{R40} from the combined MAS_RW and array microtremor dispersion data is 325 m/s with a standard deviation of 11.0 m/s. During these computations the array microtremor data (L-array only) was given equal weight to the MAS_RW data.
- Representative dispersion curves were generated for each utilized surface wave data set using a moving average, polynomial curve fitting routine. These individual representative dispersion curves were combined and a composite representative dispersion curve generated for the combined data set for data modeling.
- The composite representative dispersion curve was inverted using an iterative non-linear least squares inversion routine and fundamental mode Rayleigh wave assumption to derive V_S models. Realistic estimates of Poisson's ratio and density were used to make models as accurate as possible. Review of seismic refraction first arrival data from the seismic records indicates that there is no evidence of saturated sediments in the upper 20 m. For the purpose of data modeling, the saturated zone is assumed to be located at a depth of 30 m. Model layer thicknesses increased with depth to reflect the reduction in model resolution with depth.
- Only a single V_S model was developed to represent the velocity structure at the site because V_S increases gradually with depth and all V_S models with equivalent theoretical dispersion curves would show a similar velocity-depth trend.
- Surface wave depth of investigation is about 100 m based on the one-half of maximum wavelength criteria.
- V_{S30} is 350 m/s (NEHRP Site Class D/C).
- The average V_S of the upper 100 m (V_{S100}) is 450 m/s.
- The estimated error in V_{S30}, which includes some effects of the lateral velocity variability beneath the testing arrays, is 35 m/s. This is computed based on the sum of the following rounded up to the nearest 5 m/s: an estimated error of 3% and from the realistic assumed layer Poisson's ratios in the model, 1% error from the realistic assumed layer densities in the model, 2% for the variation in V_{S30} associated with non-uniqueness, and the 11 m/s standard deviation in V_{R40} between the combined active and passive surface wave dispersion data.
- Interestingly, V_{S30} estimated from V_{R40} using the Brown et al., 2000 relationship ($V_{S30} \cong 1.045V_{R40}$, assuming V_{R40} represents the fundamental mode Rayleigh wave) is 340 m/s, only about 3% different than that estimated from the V_S model.

Legend

- CSMIP Station and Number
- H/V Spectral Ratio Measurement Location
- MASW Array
- Passive Surface Wave Array
- Passive Surface Wave Triangle Array

NOTES:
1. WGS 1984 COORDINATE SYSTEM
2. Image Source: Esri, DigitalGlobe, GeoEye, Earthstar Geographics, CNES/Airbus DS, USDA, USGS, AEX, Getmapping, Aerogrid, IGN, IGP, swisstopo, and the GIS User Community

File Name: 16192_13172-I

Date: 7/13/2016

GEOVision geophysical services

SITE MAP
CE•13172

CGS CALIFORNIA GEOLOGICAL SURVEY

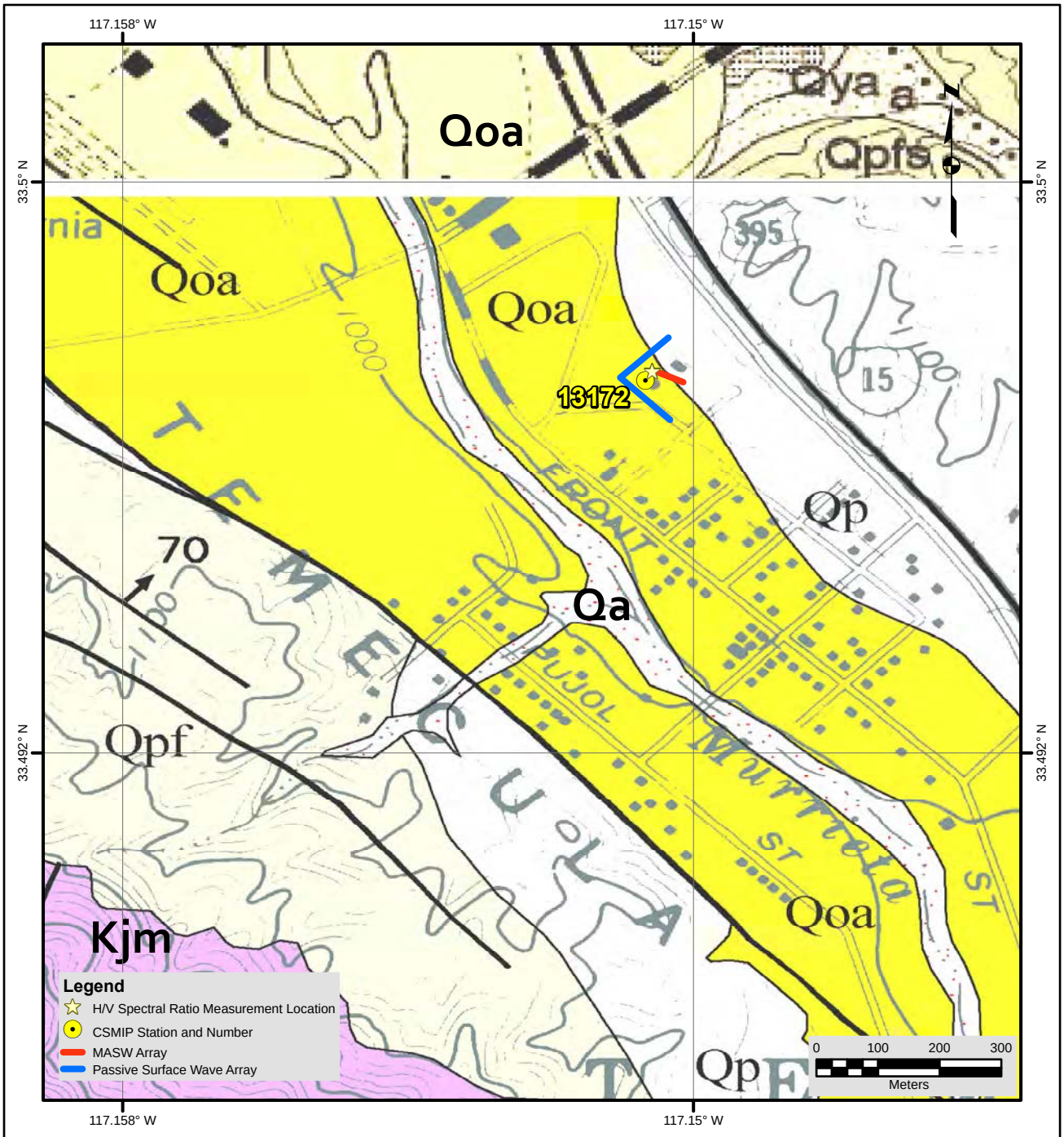

Description of Geologic Map Units

Qa = Quaternary (late Holocene) Alluvial flood plain deposits.
Qya_a = Quaternary (Holocene and late Pleistocene) Young alluvial channel deposits.
Qyv_a = Quaternary (Holocene and late Pleistocene) Young alluvial valleyl deposits.
Qoa = Quaternary (Pleistocene) Older alluvial flood plain deposits.
Qp/Qpfs = Quaternary (Pleistocene) Pauba Formation sandstone facies.
Qpf = Quaternary (Pleistocene) Pauba Formation fanglomerate facies.
KJm = Tertiary (Cretaceous and Jurassic) Metavolcanic and metasedimentary rocks.

NOTES:
1. WGS 1984 COORDINATE SYSTEM
2. Geologic Map of the Temecula and Murrieta 7.5' Quadrangles, San Diego and Riverside Counties, California by Siang S. Tan, Michael P. Kennedy, and D. M. Morton

File Name: 16192_13172

Date: 7/13/2016

GEOVision geophysical services

GEOLOGIC MAP
CE•13172

CGS CALIFORNIA GEOLOGICAL SURVEY

Looking southwest towards fire station housing CE.13172 seismic station from HVSR Location 1

Looking northwest along MASW array 13172-2

Looking east towards seismic station from corner of passive surface wave array 13172-1

4.5 Hz vertical geophone used during MASW data acquisition

Trillium sensor used for measurements at HVSR Location 1

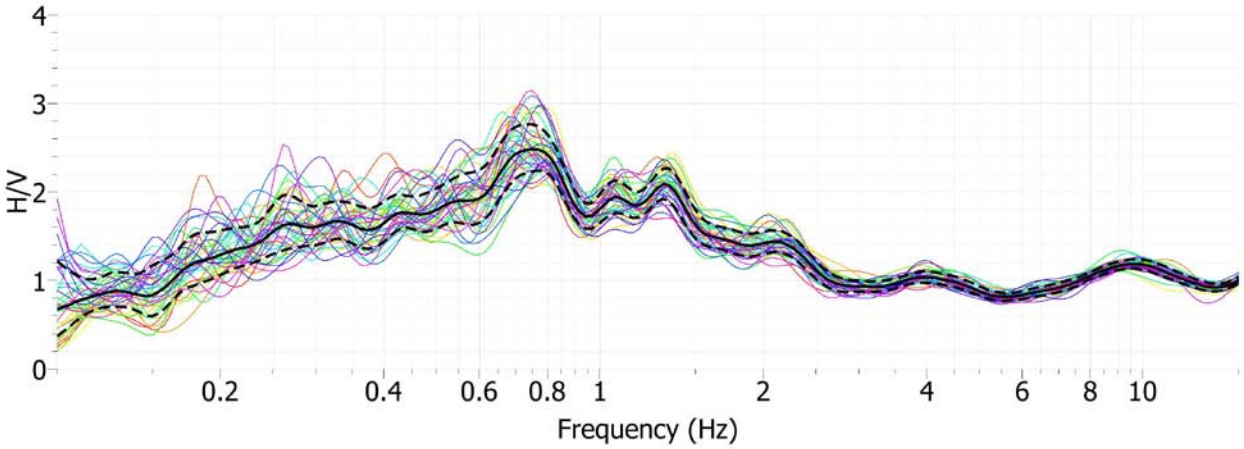

Site CE.13172, HVSR Location 1, Nanometrics Trillium Compact Sensor

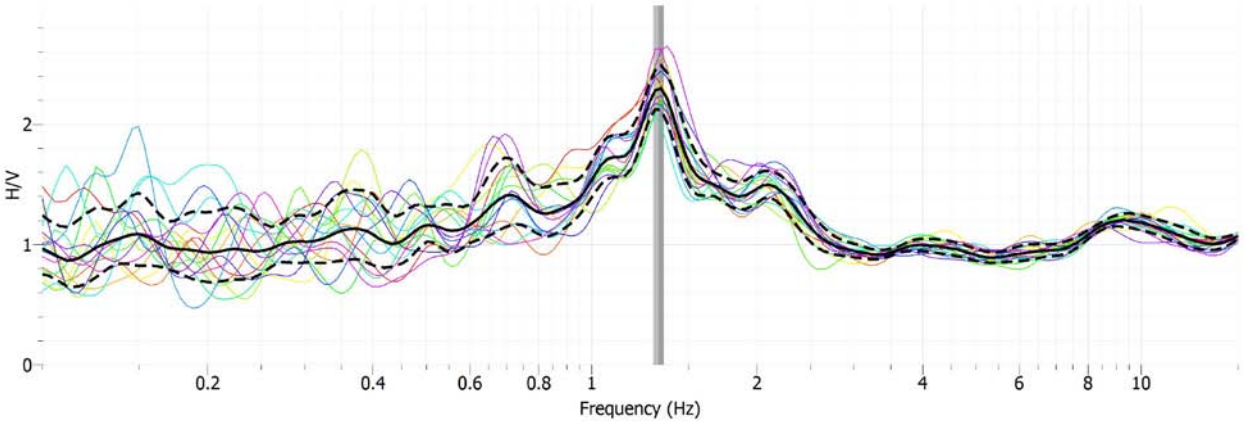

Site CE.13172, HVSR Location 1, Micromed Tromino ENGR Sensor

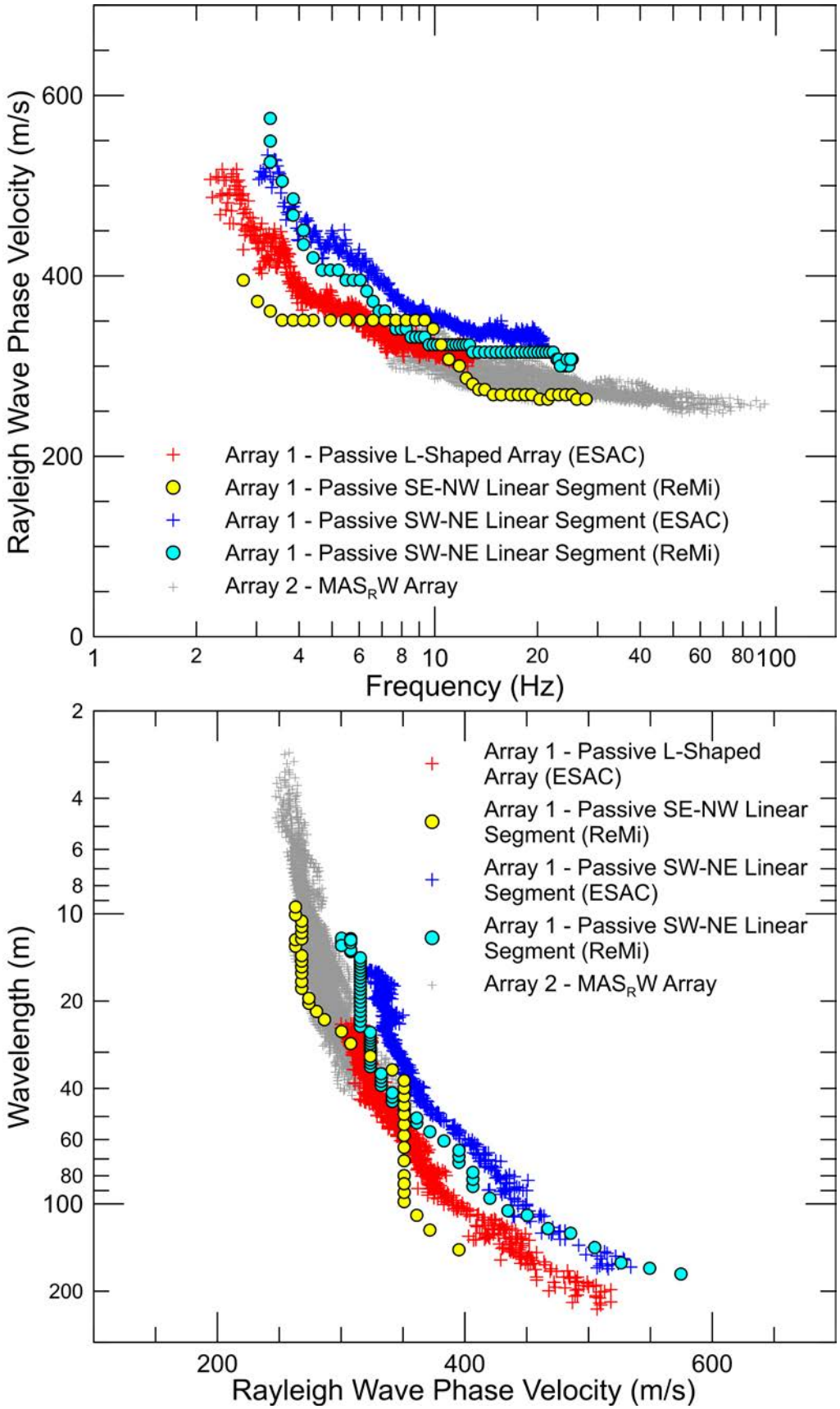

CE.13172 – Dispersion curves derived from active and passive surface wave data. The dispersion curve from ESAC analysis of the array microtremor data collected along the L-shaped Array 1 is in excellent agreement with the MAS_RW dispersion data collected along Array 2. The linear legs of the L-shaped array do not yield accurate dispersion data at this site and were not used for modeling.

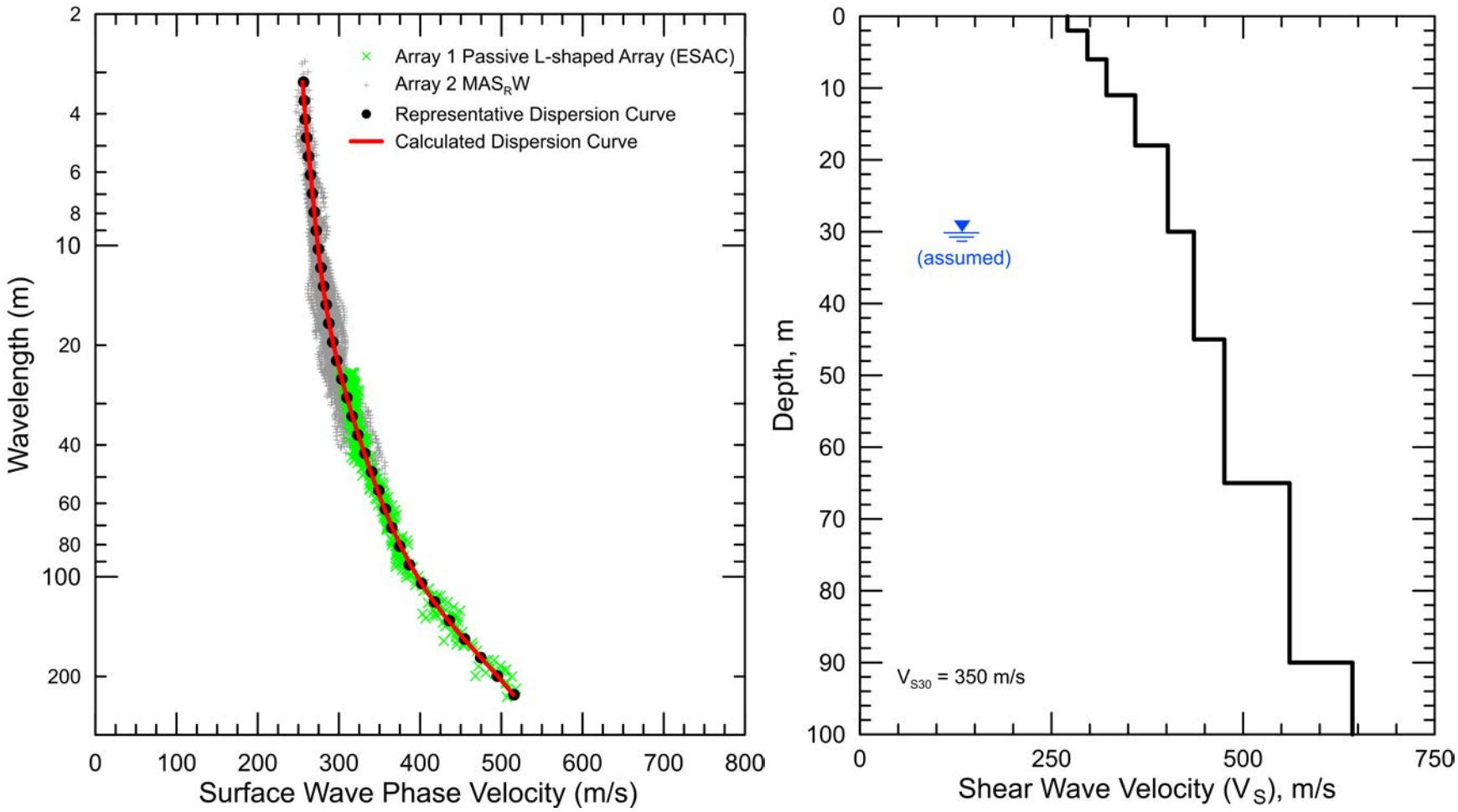

CE.13172 - Field, representative and calculated surface wave dispersion data (left) and associated V_S models (right). V_S increases gradually with depth and, therefore, multiple V_S models are not presented to demonstrate non-uniqueness because all models would show the same general velocity-depth trend.

Site CE.13921

Station Name: Riverside - Limonite & Downey

Location: Pedley Fire Station, 9270 Limonite Ave., Riverside, CA 92509

Latitude: 33.9753 **Longitude:** -117.4865

V_{S30} (measured): 427 m/s

Estimated error in V_{S30}: ± 35 m/s

NEHRP Site Class: C

Geomatrix Code: AQD

Geologic Conditions/Observations: Site located in area mapped as Quaternary (late to middle Pleistocene) old alluvial fan deposits. Crystalline rock outcrop about 425 m north of the site.

Site Conditions: Suburban site with traffic noise from nearby roads, particularly Limonite Ave. Relatively flat terrain in site vicinity.

Geophysical Methods Utilized: MAS_RW, array microtremor, HVSR

Geophysical Testing Arrays:

1. Array 1: 48 channel "L" shaped array utilizing 4.5 Hz vertical geophones spaced 6 m apart used to acquire passive surface wave data. The S-N and W-E linear segments of array have lengths of 144 and 138 m, respectively.
2. Array 2: 10 channel, nested triangle passive surface wave array utilizing 1 Hz geophones and a 60 m length for outer side of array.
3. Array 3: 48 channel MAS_RW array utilizing 4.5 Hz vertical geophones spaced 1.5 m apart for a length of 70.5 m, forward and reverse shot locations with multiple source offsets (1.5 to 10 m at both ends of array) and multiple interior source locations. Accelerated weight drop used at all source locations offset from ends of array and 4 and 12 lb hammers used at near-offset source locations and interior source locations.
4. Three HVSR measurement locations; two in the vicinity of the microtremor arrays and one near the seismic station and MAS_RW array.

Location of Geophysical Testing Arrays:

Location	Latitude	Longitude
Array 1 Passive, South End of Array	33.97412	-117.48530
Array 1 Passive, Northeast Corner of Array	33.97541	-117.48532
Array 1 Passive, West End of Array	33.97542	-117.48679
Array 2 Passive, Corner of Array, Sensor Location 1	33.97482	-117.48606
Array 2 Passive, Corner of Array, Sensor Location 3	33.97489	-117.48542
Array 2 Passive, Corner of Array, Sensor Location 5	33.97531	-117.48583
Array 2 Passive, Center of Array, Sensor Location 10	33.97503	-117.48577
Array 3 MASW, South End of Array	33.97468	-117.48620
Array 3 MASW, North End of Array	33.97532	-117.48620
HVSR Location 1	33.97508	-117.48624
HVSR Location 2	33.97503	-117.48577
HVSR Location 3	33.97492	-117.48542

Notes: 1) WGS84 Coordinate System (decimal degrees)

Results:

V_S Model

Depth to Top of Layer (m)	Layer Thickness (m)	S-Wave Velocity (m/s)	Inferred P-Wave Velocity (m/s)	Assumed Poisson's Ratio	Assumed Density (g/cm^3)
0	1	243	455	0.300	1.85
1	1.5	300	562	0.300	1.85
2.5	2.5	337	630	0.300	1.90
5	4	398	744	0.300	1.95
9	10	436	1600	0.460	2.00
19	16	531	1650	0.442	2.05
35	>15	1168	2185	0.300	2.25

Notes: 1) Depth of investigation is about 50 m.
2) The saturated zone with V_P > 1,600 m/s was constrained at a depth of about 9 m based on inspection of seismic refraction first arrival data.
3) Bottom layer is a half space and represents weathered crystalline bedrock.
4) Bedrock depth and velocity not well constrained and may vary by 20%, or more.

Observations/Discussion:

- The HVSR plots show a peak in the 3.0 to 3.5 Hz range. This is indicative of significant impedance contrast, most likely associated with crystalline bedrock based on rock outcrops in the site vicinity, within the expected depth of investigation of the active and passive surface wave sounding.
- Noise conditions at the site (multi-directional noise sources) appeared sufficient for successful application of passive surface wave techniques. Significant traffic on E-W trending Limonite Ave., which bounds the northern edge of the test area.
- The ESAC technique was used to extract surface wave dispersion data from the ambient noise data collected on the L-shaped Array 1 and triangular shaped Array 2. The minimum wavelength Rayleigh wave extracted from Arrays 1 and 2 are 31 and 26 m, respectively. The maximum wavelength Rayleigh wave extracted from these arrays is about 120 m.
- Both the ReMi™ and ESAC techniques were used to extract surface wave dispersion data from the ambient noise data collected along the linear S-N and E-W linear legs of Array 1. The minimum wavelength Rayleigh wave that could be extracted from these arrays is in the 13 to 21 m range. The maximum wavelength Rayleigh wave that could be extracted from these arrays is in the 120 to 165 m range.
- Rayleigh wave dispersion data were interpreted from 16 MAS_RW seismic records collected at 11 different source locations using 4 lb hammer, 12 lb sledgehammer, and 240 lb accelerated weight drop energy sources. Using variable receiver offset ranges, over 65 dispersion curves were extracted and combined for analysis.
- To minimize near field effects and the influence of high noise data at low frequencies associated with traffic in the site vicinity, the maximum wavelength Rayleigh wave extracted from the MAS_RW data set was set equal to the lesser of 65 m or 1.3 times the distance between the source and midpoint of the active receiver array.
- There is nominally about 25 to 50 m/s of scatter in MAS_RW dispersion data, which is likely in part related to lateral velocity variation.
- The minimum wavelength Rayleigh wave phase velocity data extracted from a 48-channel MAS_RW receiver gather was 9 to 23 m, depending on source location. Reducing data from smaller hammer sources using a limited offset range receiver gather (i.e. less active geophones) allowed for extraction of surface wave dispersion data to a minimum wavelength of about 2 m.
- The passive surface wave dispersion data from the L-shaped and triangular arrays are in excellent agreement with the MAS_RW dispersion data over the overlapping 26 to 65 m wavelength range. The passive surface wave dispersion data from the linear legs of the L-shaped array are not in as good an agreement with the MAS_RW dispersion data and, therefore, were not used for analysis. Of the two passive linear arrays, the S-N oriented array, which is perpendicular to the busy Limonite Ave., has the best quality data.
- The phase velocity of a 40 m wavelength Rayleigh wave (V_{R40}) is 407 and 412 m/s from ESAC analysis of the ambient noise data collected along the passive L-shaped Array 1 and nested triangle Array 2, respectively. The phase velocity of a 40 m wavelength Rayleigh wave (V_{R40}) is 442 and 420 m/s (5% difference) from ESAC and ReMi™ analysis of the ambient noise data collected along the S-N linear leg of Array 1, respectively. The phase velocity of a 40 m wavelength Rayleigh wave (V_{R40}) is 404 and

379 m/s (6% difference) from ESAC and ReMi™ analysis of the ambient noise data collected along the W-E linear leg of Array 1, respectively. V_{R40} from the MAS_RW dispersion data ranges from 387 to 423 m/s with a mean of 408 m/s and standard deviation of 8.2 m/s. With the exception of the ReMi™ analysis of the W-E leg of Array 1 and the ESAC analysis of the S-N leg of Array 1, there is less than a 10% difference in V_{R40} of the various arrays.

- The mean V_{R40} from the combined MAS_RW and array microtremor dispersion data used for modeling is 409 m/s with a standard deviation of 6.0 m/s. During these computations, the combined array microtremor data were given equal weight to the MAS_RW data.
- Representative dispersion curves were generated for each surface wave data set using a moving average, polynomial curve fitting routine. These individual representative dispersion curves were combined and a composite representative dispersion curve generated for the combined data set for data modeling.
- The composite representative dispersion curve was inverted using an iterative non-linear least squares inversion routine and fundamental mode Rayleigh wave assumption to derive V_S models. Realistic estimates of Poisson's ratio and density were used to make models as accurate as possible. High Poisson's ratio, saturated sediments were constrained at a depth of about 9 m with $V_P > 1{,}600$ m/s based on interactive interpretation of seismic refraction first arrival data. Poisson's ratio of the saturated sediments was allowed to gradually decrease with depth as the sediments became stiffer, a common observation in borehole V_P and V_S logs. Model layer thicknesses increased with depth to reflect the reduction in model resolution with depth.
- Surface wave depth of investigation is about 50 m based on the one-half to one-third of the maximum wavelength criteria. A maximum depth of one-half the maximum wavelength is generally appropriate for a site with a gradual increase in velocity with depth; whereas, one-third the maximum wavelength is often more appropriate for a site with an abrupt increase in velocity at depth.
- Several V_S models were developed with almost identical calculated dispersion curves to explore the non-uniqueness associated with the abrupt increase in velocity associated with expected crystalline bedrock. These equivalent V_S models have modeled bedrock between depths of about 25 and 45 m. It should be noted that not all of the equivalent models yield geologically feasible models. V_S models with a shallower bedrock unit may have unrealistically low bedrock velocity and V_S models with deeper bedrock may have velocities of the overlying layer that are too high for sediments and more indicative of weathered rock.
- The predicted HVSR peak based on the diffuse field assumption, as computed using the software package *HV-Inv* Release 1.0 Beta, is about 3.3 to 3.8 Hz for all of the equivalent V_S models, which are relatively close to the observed 3 to 3.5 Hz HVSR peaks at the site.
- The V_S model presented for the purpose of site characterization has the inferred top of the competent rock at a depth of 35 m, one of the intermediate modeled depths to bedrock. This V_S model has a predicted HVSR peak of 3.6 Hz. The predicted HVSR peak for the presented V_S model based on the quarter wavelength approximation is 3.1 Hz, also similar to that observed at the site.
- V_{S30} is 427 m/s for the presented V_S model (NEHRP Site Class C).
- The estimated error in V_{S30}, which includes some effects of the lateral velocity variability beneath the testing arrays, is 35 m/s. This is computed based on the sum of the following

rounded up to the nearest 5 m/s: an estimated error of 3% from the realistic assumed layer Poisson's ratios in the model, 1% error from the realistic assumed layer densities in the model, 2% for the variation in V_{S30} associated with non-uniqueness, and the 6.0 m/s standard deviation in V_{R40} between the combined active and passive surface wave dispersion data.

- Interestingly, V_{S30} estimated from V_{R40} using the Brown et al., 2000 relationship ($V_{S30} \cong 1.045V_{R40}$, assuming V_{R40} represents the fundamental mode Rayleigh wave) is 427 m/s, equal to that that estimated from the V_S model.

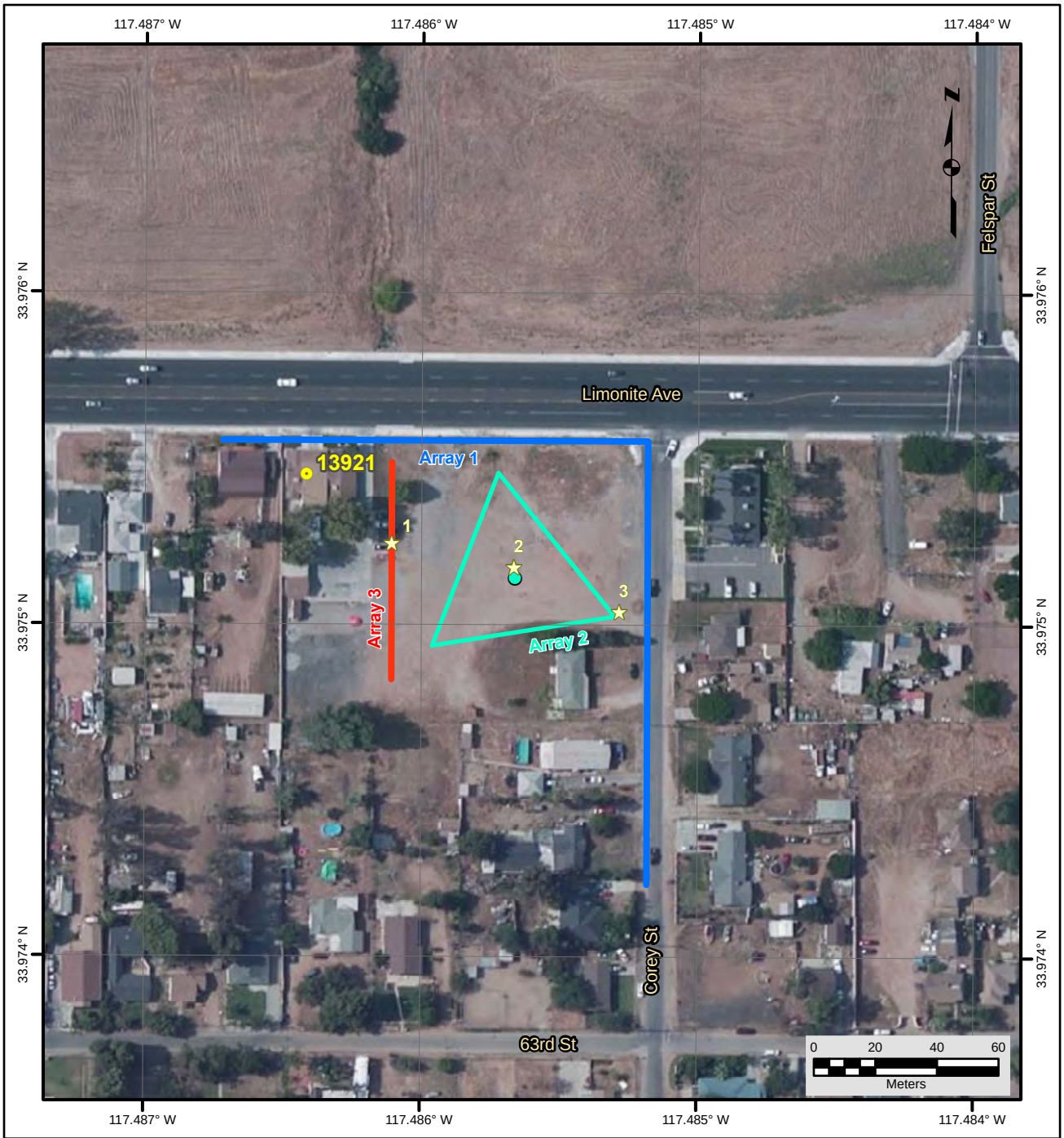

Legend

- CSMIP Station and Number
- H/V Spectral Ratio Measurement Location
- MASW Array
- Passive Surface Wave Array
- Passive Surface Wave Triangle Array

NOTES:
1. WGS 1984 COORDINATE SYSTEM
2. Image Source: Esri, DigitalGlobe, GeoEye, Earthstar Geographics, CNES/Airbus DS, USDA, USGS, AEX, Getmapping, Aerogrid, IGN, IGP, swisstopo, and the GIS User Community

File Name: 16192_13921-I

Date: 6/30/2016

GEOVision geophysical services

SITE MAP
CE•13921

CGS CALIFORNIA GEOLOGICAL SURVEY

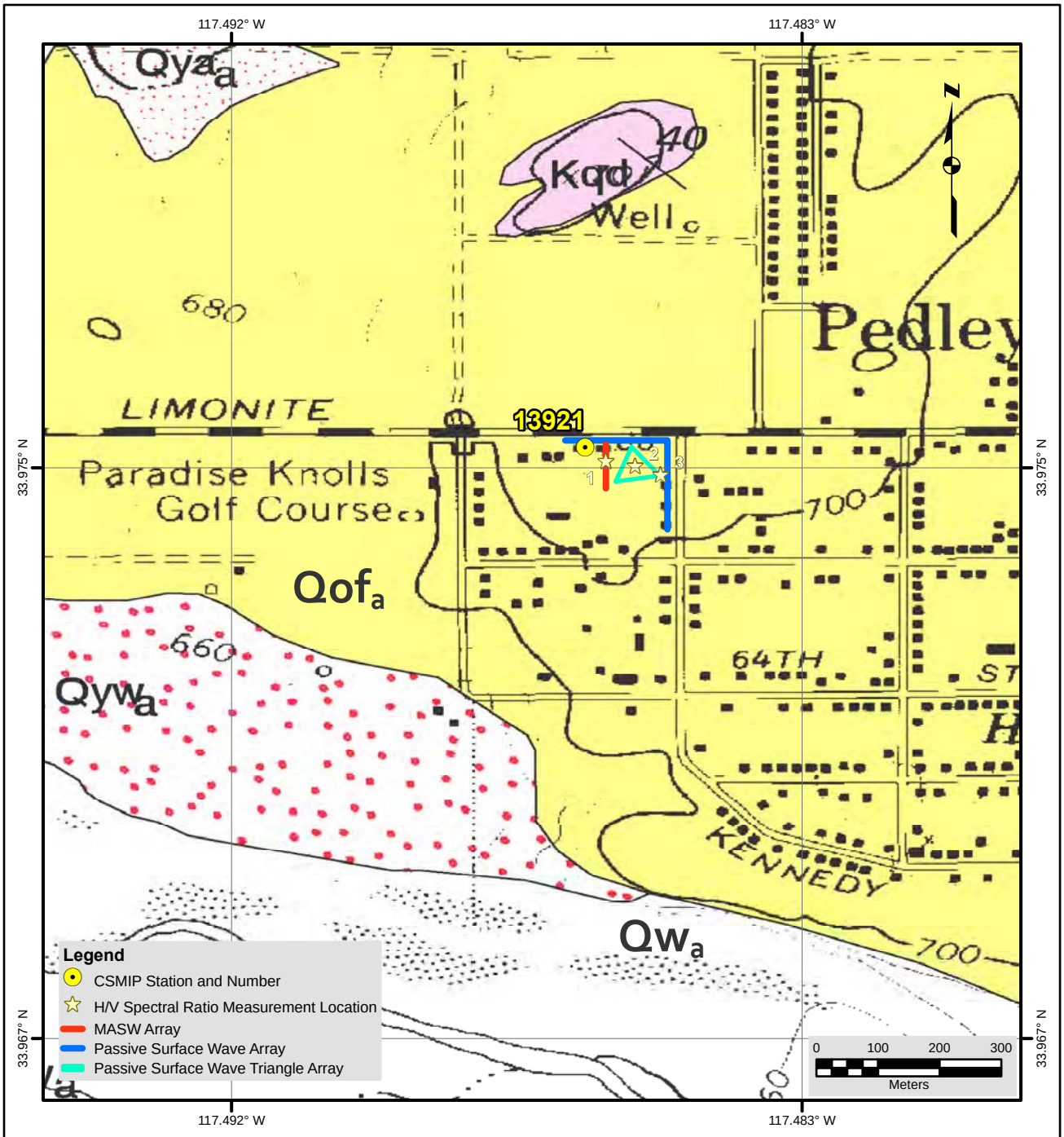

Description of Geologic Map Units

Qw_a = Quaternary (late Holocene) Very young wash deposits.
Qyw_a = Quaternary (Holocene and latest Pleistocene) young wash deposits.
Qya_a = Quaternary (Holocene and late Pleistocene) young axial channel deposits.
Qof_a = Quaternary (late to middle Pleistocene) Old alluvial fan deposits.
Kqd = (Cretaceous) Quartz diorite.

NOTES:
1. WGS 1984 COORDINATE SYSTEM
2. Geologic Map of the Riverside West 7.5' Quadrangle, Riverside County, California by Douglas M. Morton and Brett F. Cox

File Name: 16192_13921

Date: 7/13/2016

GEOVision geophysical services

GEOLOGIC MAP
CE•13921

CGS CALIFORNIA GEOLOGICAL SURVEY

Looking northwest towards CE.13921 seismic station from passive surface wave array 13921-2

Looking south along MASW array 13921-3

Looking north towards fire station from MASW array 13921-3

Data acquisition along MASW array 13921-3

1 Hz geophone used during data acquisition along passive surface wave array 13921-2

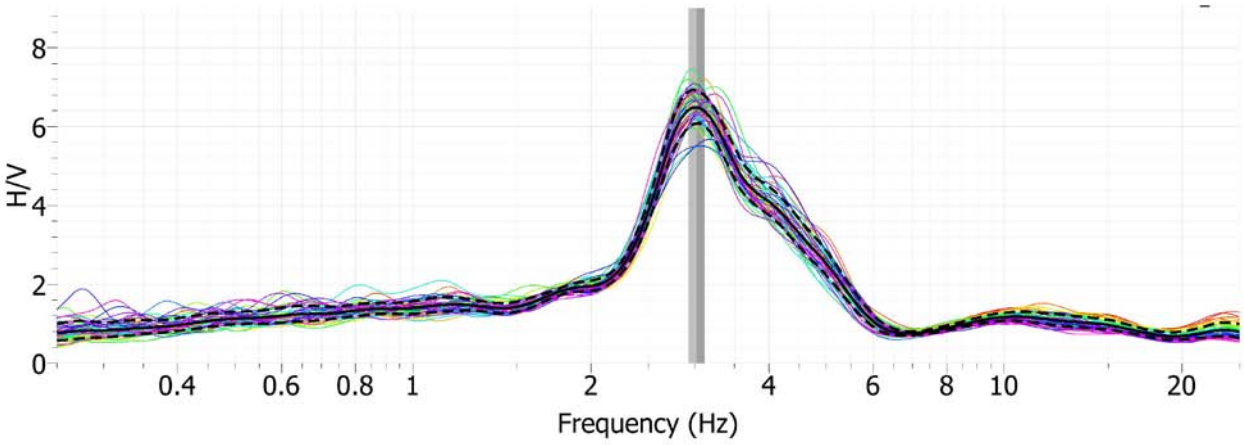

Site CE.13921, HVSR Location 1, Nanometrics Trillium Compact Sensor

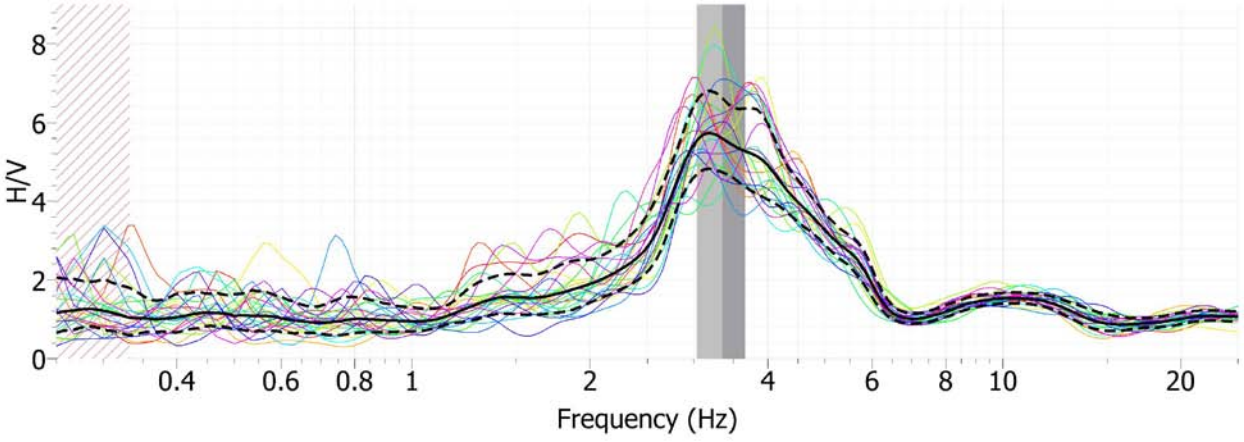

Site CE.13921, HVSR Location 2, Micromed Tromino ENGR Sensor

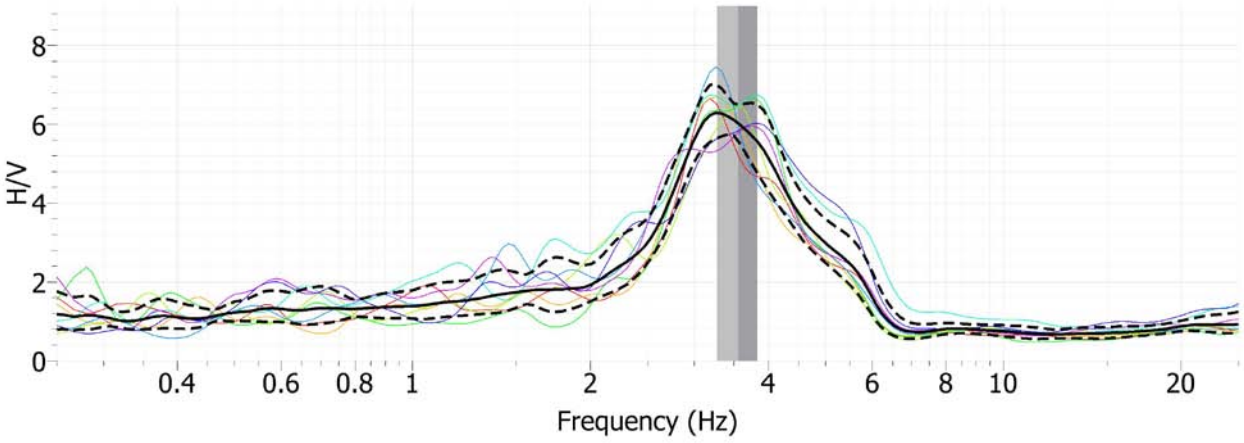

Site CE.13921, HVSR Location 3, Micromed Tromino ENGR Sensor

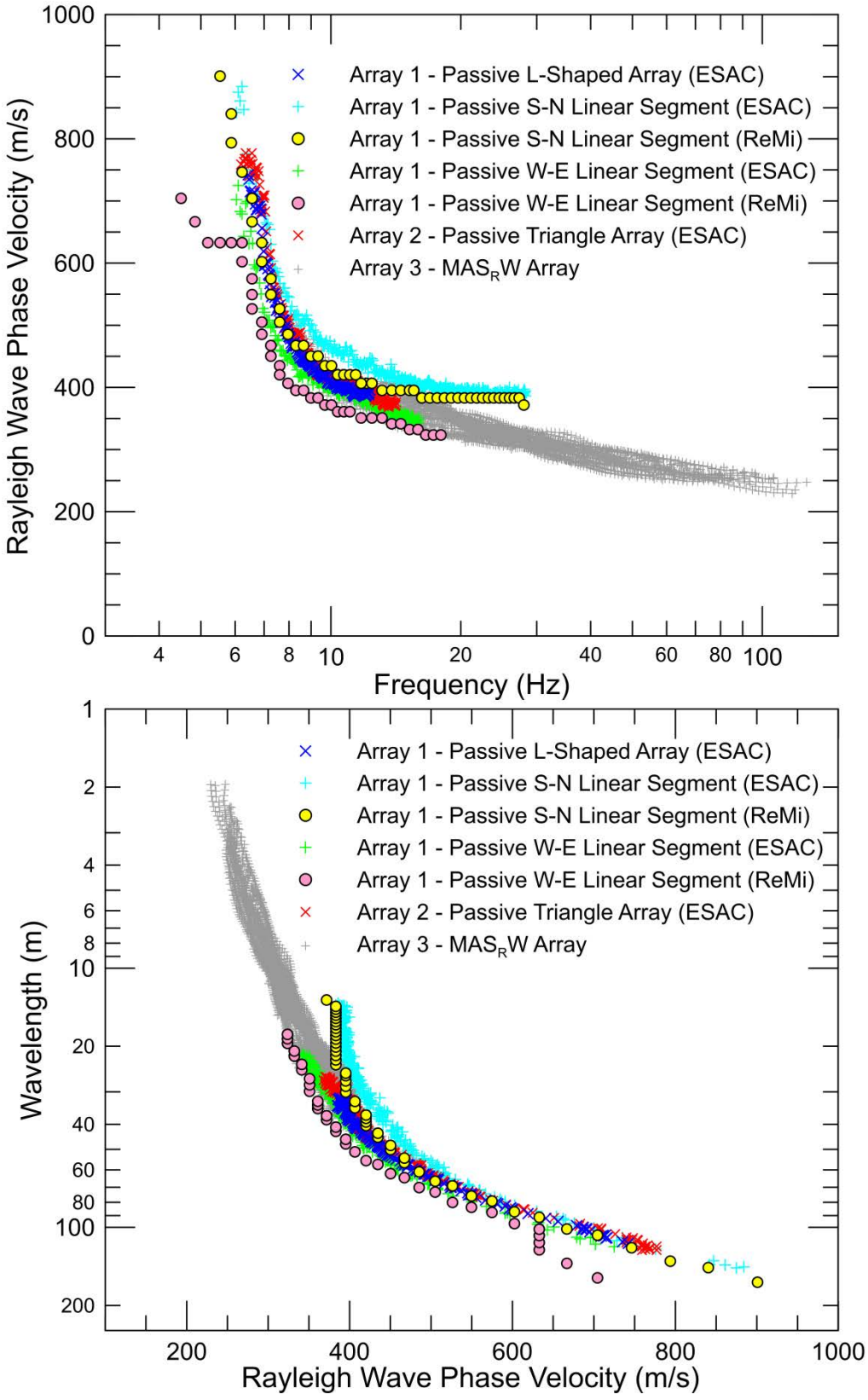

CE.13921 – Dispersion curves derived from active and passive surface wave data. Passive surface wave data from L-shaped Array 1 and triangular shaped Array 2 are in excellent agreement with MAS_RW data. Dispersion curves from the passive linear arrays deviate from the MAS_RW dispersion data and, therefore, were not used for site characterization.

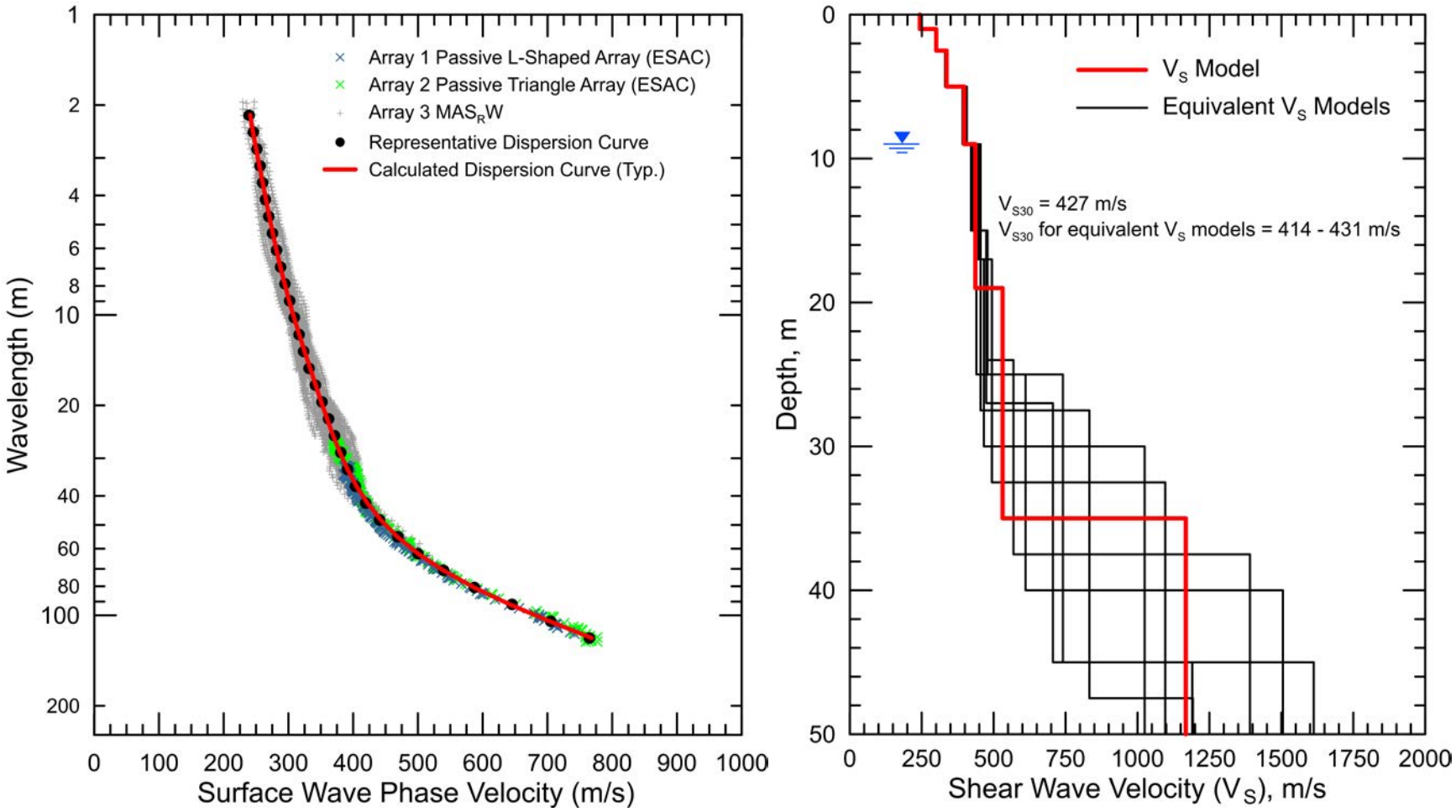

CE.13921 - Field, representative and calculated surface wave dispersion data (left) and associated V_S models (right)

Site CE.13924

Station Name: Homeland - Hwy 74 & Sultanas

Location: Homeland Fire Station, 25730 Sultanas Rd., Homeland, CA 92548

Latitude: 33.7475 **Longitude:** -117.1274

V_{S30} (measured): 475 m/s

Estimated error in V_{S30}: ± 40 m/s

NEHRP Site Class: C

Geomatrix Code: AQD

Geologic Conditions/Observations: Quaternary (late to middle Pleistocene) old alluvial fan deposits. Site located in close proximity to channel of Quaternary (Holocene and late Pleistocene) young alluvial fan deposits. There is an outcrop of crystalline rock about 600 m northeast of the seismic station.

Site Conditions: Rural site with traffic noise from nearby roads, particularly the W-E trending Hwy 74, located 500 m south of the survey area. Relatively flat terrain in site vicinity.

Geophysical Methods Utilized: MAS_RW (Rayleigh wave - vertical and horizontal geophones), MAS_LW (Love wave), array microtremor, HVSR

Geophysical Testing Arrays:

1. Array 1: 48 channel "L" shaped array utilizing 4.5 Hz vertical geophones spaced 6 m apart used to acquire passive surface wave data. The S-N and W-E linear segments of array have lengths of 144 and 138 m, respectively.
2. Array 2: 48 channel MAS_RW array utilizing 4.5 Hz vertical and 4.5 Hz horizontal (radial orientation) geophones spaced 1.5 m apart for a length of 70.5 m, forward and reverse shot locations with multiple source offsets (1.5 to 30 m at both ends of array) and multiple interior source locations. Accelerated weight drop used at all source locations offset from ends of array and 4 and 12 lb hammers used at near-offset source locations and interior source locations. MAS_LW data also acquired along array using 4.5 Hz horizontal transverse geophones and hammer and traction plank or aluminum S-wave energy sources.
3. Three HVSR measurement locations; two in the vicinity of MAS_RW and microtremor arrays and one near the seismic station.

Location of Geophysical Testing Arrays:

Location	Latitude	Longitude
Array 1 Passive, South End of Array	33.74561	-117.12776
Array 1 Passive, Northwest Corner of Array	33.74690	-117.12776
Array 1 Passive, East End of Array	33.74691	-117.12626
Array 2 MASW, South End of Array	33.74627	-117.12776
Array 2 MASW, North End of Array	33.74691	-117.12776
HVSR Location 1	33.74723	-117.12750
HVSR Location 2	33.74690	-117.12757
HVSR Location 3	33.74627	-117.12761

Notes: 1) WGS84 Coordinate System (decimal degrees)

Results:

V_S Model (Rayleigh Wave)

Depth to Top of Layer (m)	Layer Thickness (m)	S-Wave Velocity (m/s)	Inferred P-Wave Velocity (m/s)	Assumed Poisson's Ratio	Assumed Density (g/cm^3)
0	2	277	519	0.300	1.85
2	3	349	652	0.300	1.90
5	4	384	719	0.300	1.90
9	16	494	925	0.300	1.95
25	>15	1091	2040	0.300	2.20

Notes: 1) Depth of investigation is about 40 m.
2) Bottom layer is a half space.
3) Bedrock depth and velocity not well constrained and may vary by 20%, or more.

V_S Model (Love Wave)

Depth to Top of Layer (m)	Layer Thickness (m)	S-Wave Velocity (m/s)	Inferred P-Wave Velocity (m/s)	Assumed Poisson's Ratio	Assumed Density (g/cm^3)
0	1	241	451	0.300	1.85
1	1	336	628	0.300	1.90
2	7	396	741	0.300	1.95
9	16	530	991	0.300	2.00
25	>15	1207	2258	0.300	2.20

Notes: 1) Depth of investigation is about 40 m.
2) Bottom layer is a half space.
3) Bedrock depth and velocity not well constrained and may vary by 20%, or more.

Observations/Discussion:

- The HVSR plots show a peak in the 4.4 to 4.9 Hz range. This is indicative of significant impedance contrast, most likely associated with crystalline bedrock based on the proximity of the site to bedrock outcrops, within the expected depth of investigation of the active and passive surface wave sounding.
- The primary noise source near the site is the W-E trending Hwy 74, 500 m south of the survey area, which provided ambient noise from vehicle traffic over almost a 180 degree azimuth. There was also light traffic on the S-N trending Sultanas Road, located adjacent to the test area, and other nearby roads during geophysical testing.
- The ESAC technique was used to extract surface wave dispersion data from the ambient noise data collected on the L-shaped Array. The minimum and maximum wavelength Rayleigh waves extracted from Array 1 were 17 and 72 m, respectively. It was not possible to extract long wavelength Rayleigh wave dispersion data from this array. A passive triangular-shaped array was not attempted at this site.
- Both the ReMi™ and ESAC techniques were used to extract surface wave dispersion data from the ambient noise data collected along the S-N and W-E linear legs of Array 1. Rayleigh wave dispersion data were extracted over the 13 to 105 m and 13 to 140 m wavelength range from the S-N leg of Array 1 using the ESAC and ReMi™ techniques, respectively. Rayleigh wave dispersion data were extracted over the 13 to 55 m and 13 to 130 m wavelength range from the W-E leg of Array 1 using the ESAC and ReMi™ techniques, respectively. As expected, the S-N leg of Array 1, which is orientated perpendicular to Hwy 74, yielded the most reliable dispersion data from the linear arrays. The dispersion curve from this array extracted using the ESAC technique is in the best agreement with that from the L-array and $MAS_R W$ data.
- Field inspection of $MAS_R W$ dispersion data in the field indicated that the low frequency/long wavelength component of the dispersion curve associated with probable bedrock was not being recovered. It was also noted that the passive surface wave arrays were not yielding long wavelength dispersion data. Therefore, $MAS_L W$ (Love wave) data were acquired along the same array using 4.5 Hz horizontal (transverse orientation) geophones and a hammer and horizontal traction plank or hammer-impact aluminum shear-wave seismic source. Additionally, the $MAS_R W$ survey was repeated using 4.5 Hz horizontal (radial orientation) geophones. The acquisition of $MAS_R W$ data at this site using the horizontal radial geophones allowed Rayleigh wave dispersion data to be recovered at long enough wavelengths to image to 30 m depth.
- Rayleigh wave dispersion data were interpreted from 20 $MAS_R W$ (horizontal radial component) seismic records collected at 15 different source locations using 4 lb hammer, 12 lb sledgehammer, and 240 lb accelerated weight drop energy sources. Using variable receiver offset ranges, over 70 dispersion curves were extracted and combined for analysis.
- To minimize near field effects and the influence of high noise data at low frequencies associated with traffic in the site vicinity, the maximum wavelength Rayleigh wave extracted from the $MAS_R W$ data set was set equal to the lesser of 80 m or 1.3 times the distance between the source and midpoint of the active receiver array.
- There is nominally about 30 to 50 m/s of scatter in $MAS_R W$ dispersion data, which is likely in part related to lateral velocity variation.

- The minimum wavelength Rayleigh wave phase velocity data extracted from a 48-channel $MAS_R W$ receiver gather was 7 to 25 m, depending on source location. Reducing data from smaller hammer sources using a limited offset range receiver gather (i.e. less active geophones) allowed for extraction of surface wave dispersion data to a minimum wavelength of about 3.5 m.
- The passive surface wave dispersion data from the L-shaped array and S-N leg of the L—shaped array reduced using the ESAC technique are in the best agreement with the $MAS_R W$ data over the 13 to 80 m overlapping wavelength range. These combined data sets were used for developing a V_S model.
- Love wave dispersion data were interpreted from 14 $MAS_L W$ seismic records. Using variable receiver offset ranges, over 85 dispersion curves were extracted and combined for analysis.
- To minimize near field effects and the influence of high noise data at low frequencies associated with traffic in the site vicinity, the maximum wavelength Love wave extracted from the $MAS_L W$ data set was set equal to the lesser of 120 m or 1.5 times the distance between the source and midpoint of the active receiver array.
- There is nominally about 50 to 75 m/s of scatter in $MAS_L W$ dispersion data, which is likely in part related to lateral velocity variation. There is more scatter in the Love wave dispersion data than the Rayleigh wave dispersion data, partially due to increased noise in the data as only hammer energy sources were available.
- Love wave data acquisition would have benefited from a longer array and larger energy source.
- The phase velocity of a 40 m wavelength Rayleigh wave (V_{R40}) is 438 m/s from ESAC analysis of the ambient noise data collected along the passive L-shaped Array 1. V_{R40} is 443 and 441 m/s (< 1% difference) from ESAC and ReMi™ analysis of the ambient noise data collected along the S-N linear leg of Array 1, respectively. V_{R40} is 431 and 419 m/s (3% difference) from ESAC and ReMi™ analysis of the ambient noise data collected along the W-E linear leg of Array 1, respectively. V_{R40} from the $MAS_R W$ dispersion data ranges from 434 to 477 m/s with a mean of 452 m/s and standard deviation of 9.3 m/s. The similarity in V_{R40} (13% variation) of the various surface wave techniques and arrays indicates that each method alone would have independently yielded acceptable estimates of V_{S30}, even though some of the dispersion curves would not have yielded reliable V_S models.
- The mean V_{R40} from the combined $MAS_R W$ and array microtremor dispersion data used for modeling is 446 m/s with a standard deviation of 9.2m/s. During these computations, the combined array microtremor data were given equal weight to the $MAS_R W$ data and the combined dispersion data from the passive linear arrays had equal to or lesser weight than that of the 2-D array.
- At this time, no empirical relationship has been developed between Love wave phase velocity and V_{S30}.
- Representative dispersion curves were generated for each surface wave data set using a moving average, polynomial curve fitting routine. These individual representative dispersion curves were combined and a composite representative dispersion curve generated for the combined data set for data modeling.
- The composite representative dispersion curve was inverted using an iterative non-linear least squares inversion routine and fundamental mode Rayleigh or Love wave assumption

to derive V_S models. Realistic estimates of Poisson's ratio and density were used to make V_S models derived from Rayleigh wave dispersion data as accurate as possible. Poisson's ratio has no impact on the inversion of Love wave dispersion data. Seismic refraction first arrival data yields no evidence of saturated sediments overlying bedrock at the site. Review of P- and S- wave seismic refraction data indicates that bedrock is located at a depth on the order of 25 m at the site. Model layer thicknesses in the V_S models increase with depth to reflect the reduction in model resolution with depth.

- Surface wave depth of investigation is about 40 m based on the one-half to one-third of the maximum wavelength criteria for the Rayleigh wave data and one-third of the maximum wavelength of the Love wave dispersion data.
- Several V_S models were developed with almost identical calculated dispersion curves to explore the non-uniqueness associated with the abrupt increase in velocity associated with expected crystalline bedrock. The equivalent V_S models developed from the Rayleigh and Love wave dispersion data have modeled bedrock between depths of about 20 and 32.5 m and 22.5 and 27.5 m, respectively. The velocity of the bedrock unit is not well resolved in the V_S models.
- The predicted HVSR peak, based on the diffuse field assumption, as computed using the software package *HV-Inv* Release 1.0 Beta, is about 4.5 to 4.9 Hz for all of the equivalent V_S models developed from the Rayleigh wave dispersion data, which is within the 4.4 to 4.9 Hz HVSR peak range observed at this site. The V_S models developed from the Love wave dispersion data yield slightly higher predicted HVSR peaks in the 5.1 to 5.4 Hz range.
- The V_S model presented for the purpose of site characterization has the inferred top of the competent rock at a depth of 25 m, the intermediate modeled depth to bedrock. The V_S models with bedrock at 25 m depth, developed from the Rayleigh and Love wave dispersion data, have predicted HVSR peaks of 4.9 and 5.2 Hz, respectively.
- V_{S30} is 475 and 507 m/s for the V_S models developed from the Rayleigh and Love wave dispersion data, respectively (NEHRP Site Class C).
- Small differences in V_{S30} between V_S models developed using Rayleigh and Love wave dispersion data are not unusual for a number of reasons that primarily include error in the models and anisotropy. If the average Poisson's ratio of the sediments was slightly lower than that assumed during modeling of the Rayleigh wave dispersion data, then V_{S30} would be slightly higher than that modeled. Anisotropy, if present in subsurface geologic units, results in the S_V-wave velocity derived from Rayleigh wave data being different from the S_H-wave velocity derived from the Love wave dispersion data.
- At this time, we recommend using the V_S model developed from the Rayleigh wave dispersion data because the model is slightly more consistent with the observed HVSR data and there is less scatter in the Rayleigh wave dispersion data. Additionally, all other sites during this investigation have been characterized using only Rayleigh wave dispersion data.
- The estimated error in V_{S30}, which includes some effects of the lateral velocity variability beneath the testing arrays, is 40 m/s. This is computed based on the sum of the following rounded up to the nearest 5 m/s: an estimated error of 3% from the realistic assumed layer Poisson's ratios in the model, 1% error from the realistic assumed layer densities in the model, 2% for the variation in V_{S30} associated with non-uniqueness, and the 9.2 m/s

standard deviation in V_{R40} between the combined active and passive surface wave dispersion data.

- Interestingly, V_{S30} estimated from V_{R40} using the Brown et al., 2000 relationship ($V_{S30} \cong 1.045V_{R40}$, assuming V_{R40} represents the fundamental mode Rayleigh wave) is 466 m/s, only 2% different than that estimated from the V_S model.

Legend

- H/V Spectral Ratio Measurement Location
- CSMIP Station and Number
- MASW Array
- Passive Surface Wave Array

NOTES:
1. WGS 1984 COORDINATE SYSTEM
2. Image Source: Esri, DigitalGlobe, GeoEye, Earthstar Geographics, CNES/Airbus DS, USDA, USGS, AEX, Getmapping, Aerogrid, IGN, IGP, swisstopo, and the GIS User Community

File Name: 16192_13924-I

Date: 7/15/2016

GEOVision geophysical services

SITE MAP
CE•13924

CGS CALIFORNIA GEOLOGICAL SURVEY

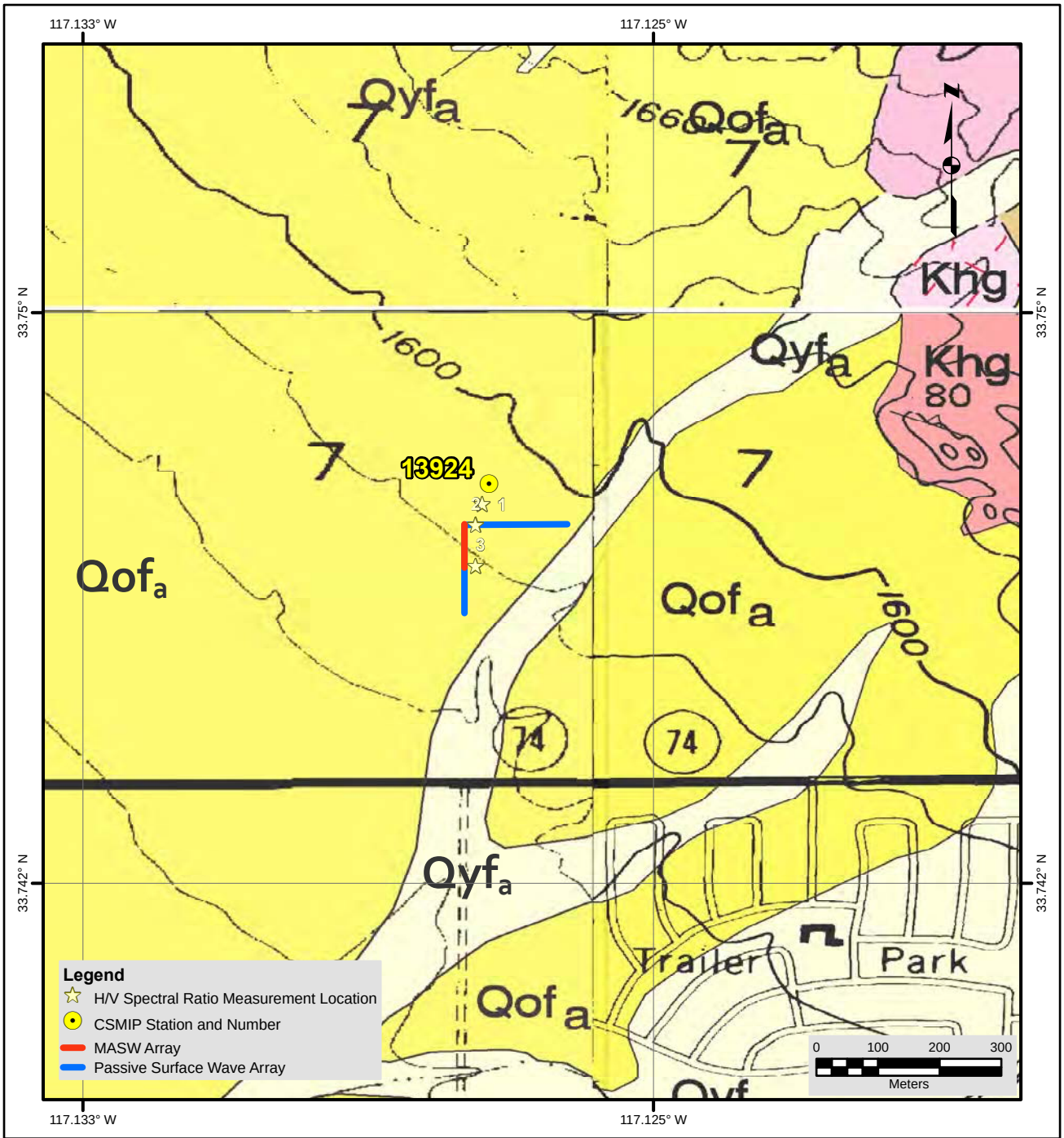

Description of Geologic Map Units

Qyf_a = Quaternary (Holocene and late Pleistocene) young alluvial fan deposits.
Qof_a = Quaternary (late to middle Pleistocene) Old alluvial fan deposits.
Khg = Cretaceous Heterogeneous granitic rocks.

NOTES:
1. WGS 1984 COORDINATE SYSTEM
2. Geologic Map of the Perris, Lakeview, Romoland, and Winchester 7.5', Quadrangles, Riverside County, California by Douglas M. Morton and Jonathan C. Matti (Lakeview)

File Name: 16192_13924

Date: 7/15/2016

GEOVision geophysical services

GEOLOGIC MAP
CE•13924

CGS CALIFORNIA GEOLOGICAL SURVEY

Looking north towards fire station housing CE.13924 seismic station from passive surface wave array 13924-1

Looking north towards fire station from HVSR Location 1

Looking east from corner of passive surface wave arrav 13924-1

4 lb and 12 lb hammers used during data acquisition along MASW array 13924-2

Looking north along MASW array 13924-2

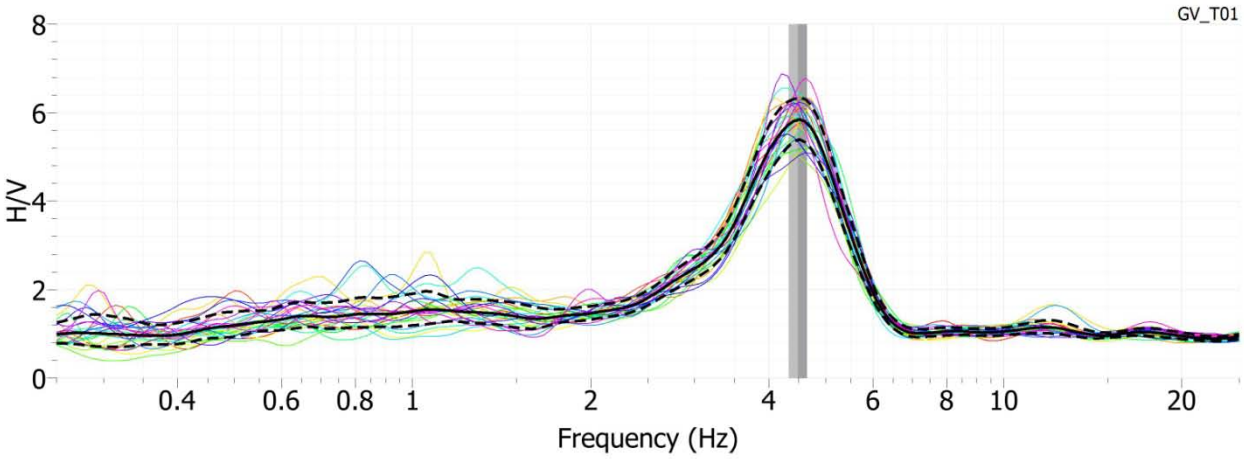

Site CE.13924, HVSR Location 1, Nanometrics Trillium Compact Sensor

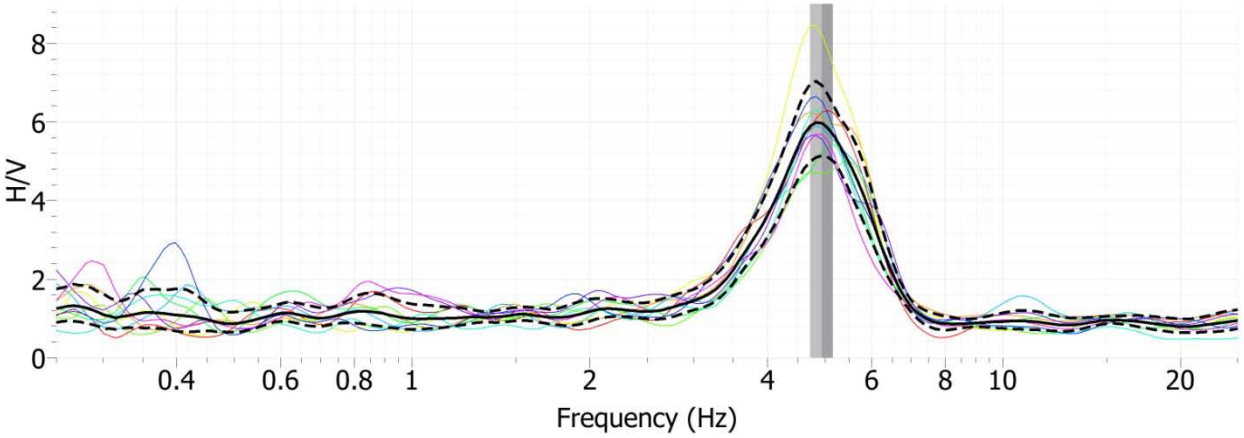

Site CE.13924, HVSR Location 2, Micromed Tromino ENGR Sensor

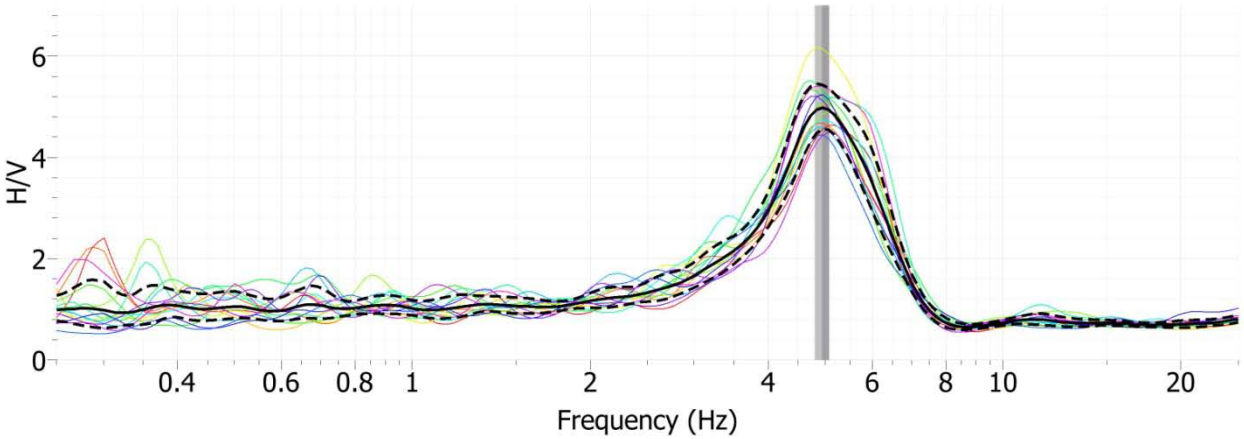

Site CE.13924, HVSR Location 3, Micromed Tromino ENGR Sensor

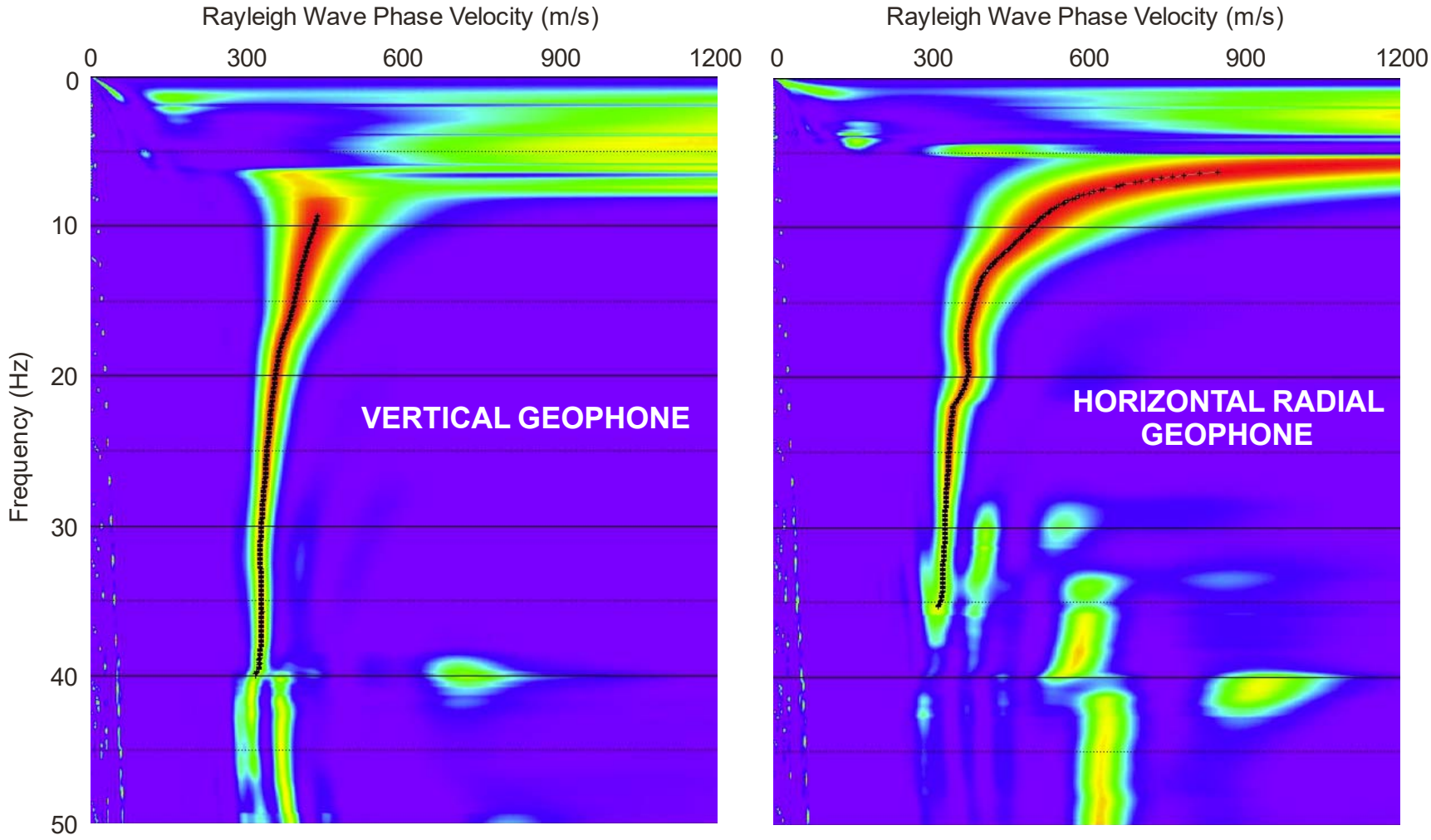

CE.13924 – Frequency-velocity transform of a seismic record collected using an accelerated weight drop source offset 21 m from the near geophone and recorded using both vertical and horizontal (radial orientation) 4.5 Hz geophones. At this site, the vertical geophones do not allow recovery of the fundamental mode Rayleigh wave at frequencies below 9 Hz, whereas the low frequency dispersion data is recovered using the horizontal geophones.

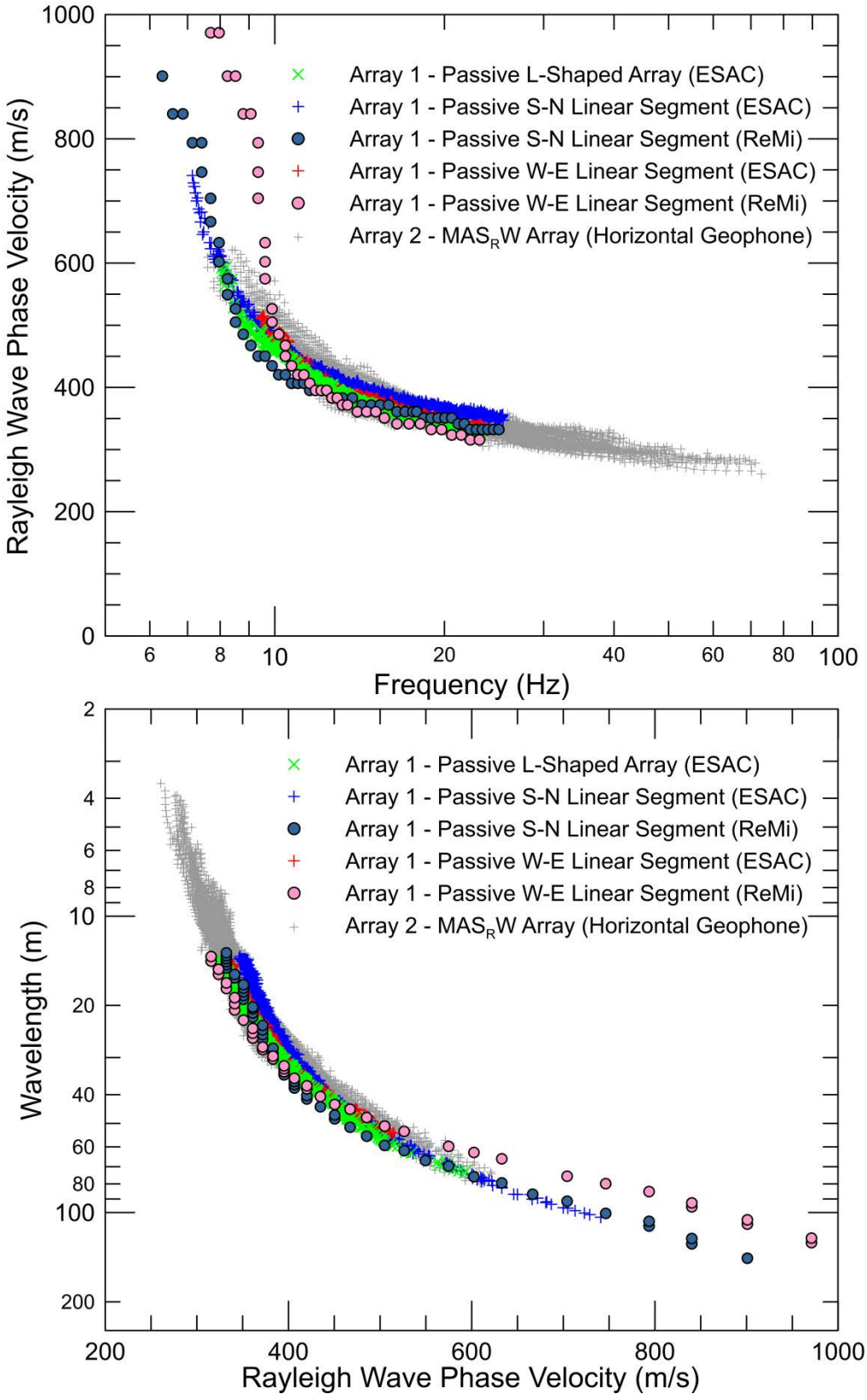

CE.13924 – Dispersion curves derived from active and passive surface wave data. Passive surface wave data from L-shaped Array 1 and S-N linear segment of Array 1 (perpendicular to Hwy 74) analyzed using the ESAC technique are in the best agreement with MAS_RW data and were used for modeling. The W-E linear segment of Array 1 does not yield accurate dispersion data at low frequencies/long wavelengths. Additionally, the L-shaped array did not yield dispersion data at lower frequencies than the MAS_RW data acquired using a horizontal radial geophone.

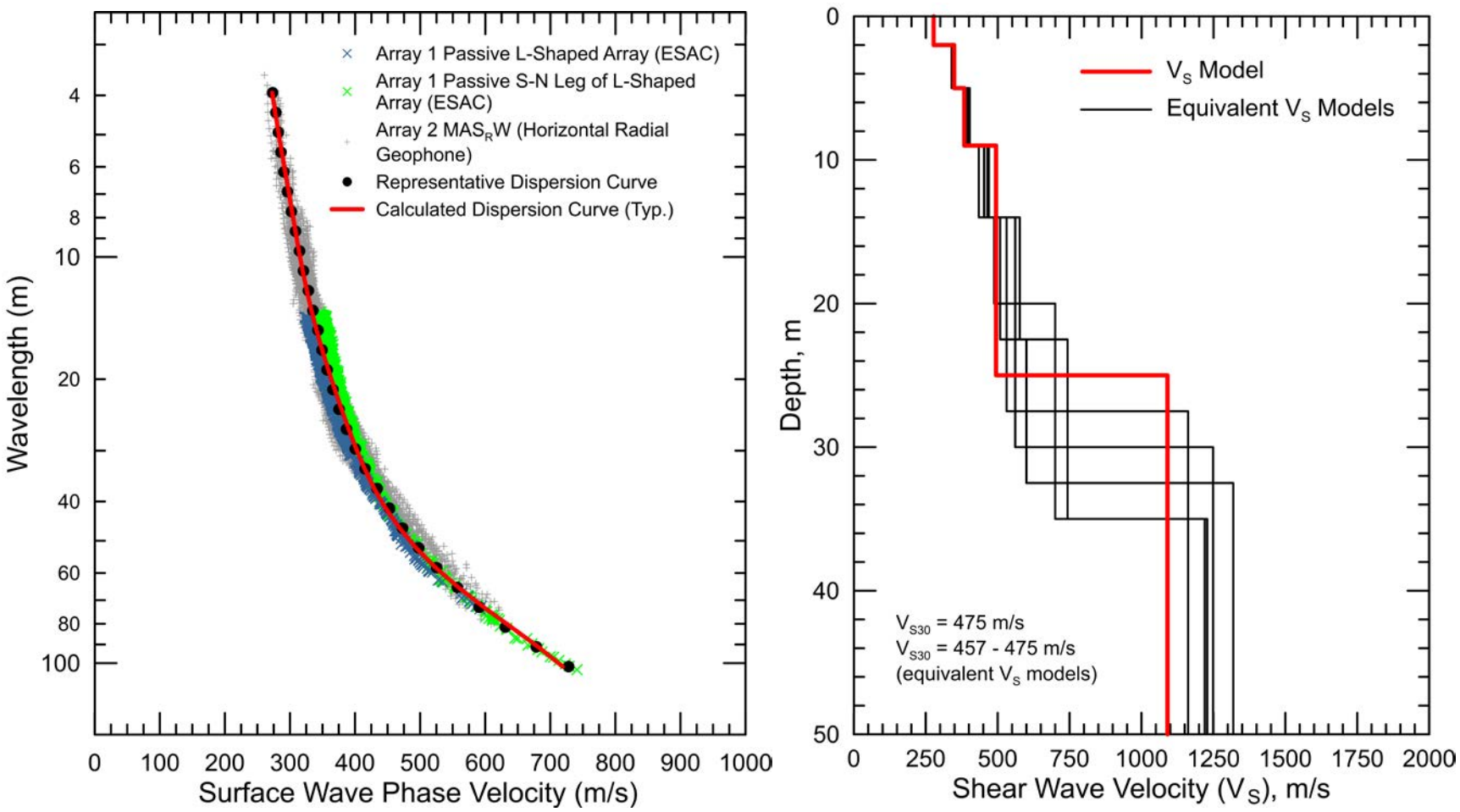

CE.13924 - Field, representative and calculated Rayleigh wave dispersion data (left) and associated V_S models (right)

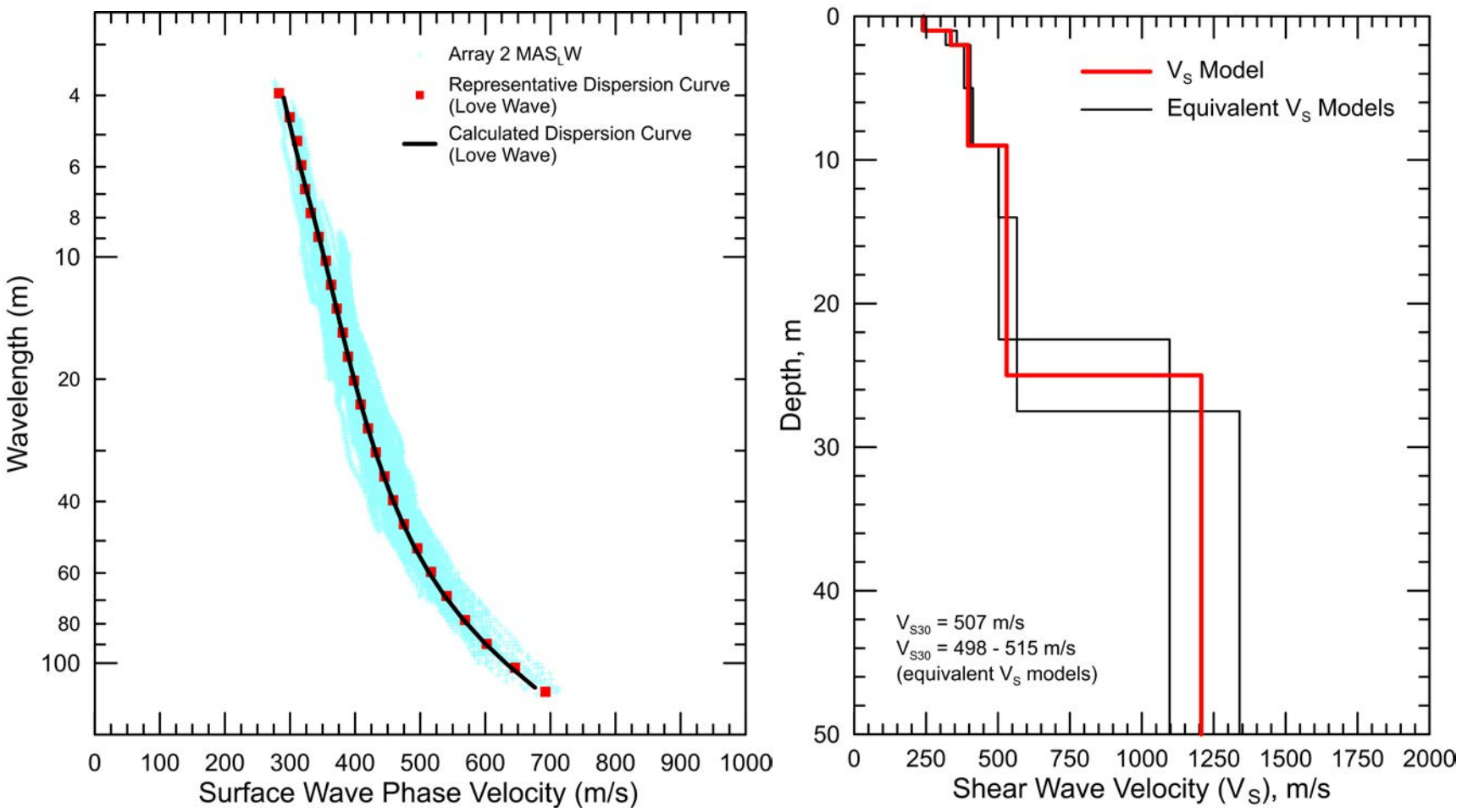

CE.13924 - Field, representative and calculated Love wave dispersion data (left) and associated V_S models (right)

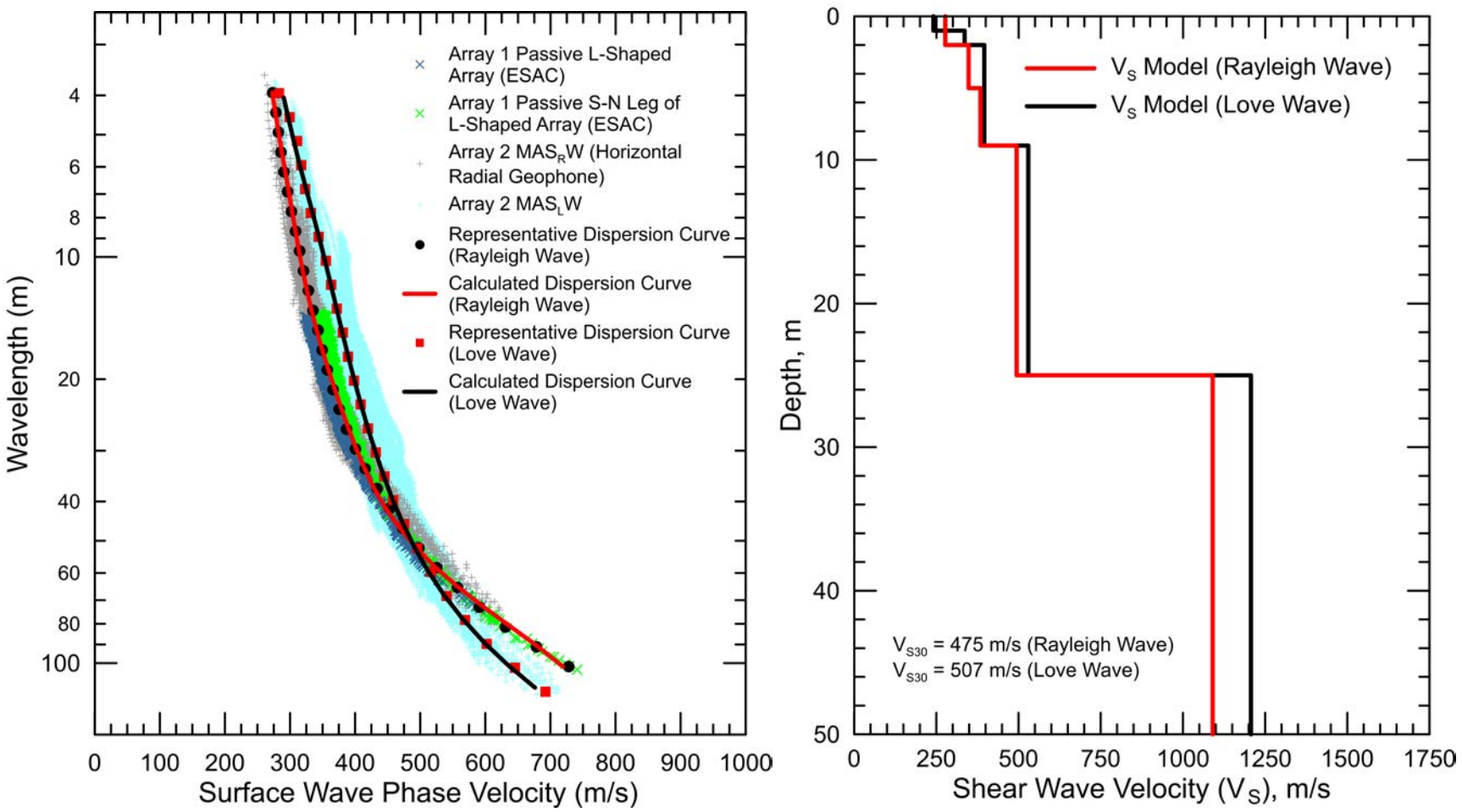

CE.13924 - Field, representative and calculated Rayleigh and Love wave dispersion data (left) and associated V_S models (right)

Site CE.13925

Station Name: Moreno Valley - Indian & Kennedy

Location: Kennedy Park Fire Station, 15111 Indian Ave., Moreno Valley, CA 92551

Latitude: 33.9019 **Longitude:** -117.2355

V_{S30} (measured): 380 m/s

Estimated error in V_{S30}: ±30 m/s

NEHRP Site Class: C

Geomatrix Code: AHD/AQD

Geologic Conditions/Observations: Site located in area mapped as Quaternary (Holocene and late Pleistocene) sand and cobble-sand and gravel-sand deposits.

Site Conditions: Suburban site with traffic noise from nearby roads. Relatively flat terrain in site vicinity.

Geophysical Methods Utilized: MAS_RW, array microtremor, HVSR

Geophysical Testing Arrays:

1. Array 1: 10 channel, nested triangle passive surface wave array utilizing 1 Hz geophones and a 60 m length for outer side of array.
2. Array 2: 24 channel, linear passive surface wave array utilizing 4.5 Hz vertical geophones spaced 5.5 m apart for a length of 126.5 m.
3. Array 3: 48 channel MAS_RW array utilizing 4.5 Hz vertical geophones spaced 1.5 m apart for a length of 70.5 m, forward and reverse shot locations with multiple source offsets (1.5 to 30 m at both ends of array) and multiple interior source locations. A 20 lb sledgehammer was used at all source locations offset from ends of array and 4 and 12 lb hammers were used at near-offset source locations and interior source locations.
4. Three HVSR measurement locations; two in the vicinity of MAS_RW and microtremor arrays and one near the seismic station.

Location of Geophysical Testing Arrays:

Location	Latitude	Longitude
Array 1 Passive, Corner of Array, Sensor Location 1	33.90136	-117.23589
Array 1 Passive, Corner of Array, Sensor Location 3	33.90081	-117.23588
Array 1 Passive, Corner of Array, Sensor Location 5	33.90109	-117.23532
Array 1 Passive, Center of Array, Sensor Location 10	33.90108	-117.23564
Array 2 Passive, West End of Array	33.90086	-117.23655
Array 2 Passive, East End of Array	33.90087	-117.23522
Array 3 MASW, Southeast End of Array	33.90109	-117.23570
Array 3 MASW, Northwest End of Array	33.90170	-117.23590
HVSR Location 1	33.90082	-117.23585
HVSR Location 2	33.90108	-117.23564
HVSR Location 3	33.90201	-117.23571

Notes: 1) WGS84 Coordinate System (decimal degrees)

Results:

V_S Model

Depth to Top of Layer (m)	Layer Thickness (m)	S-Wave Velocity (m/s)	Inferred P-Wave Velocity (m/s)	Assumed Poisson's Ratio	Assumed Density (g/cm^3)
0	3	230	431	0.301	1.80
3	4	305	570	0.299	1.85
7	5	317	594	0.302	1.90
12	6	429	802	0.300	2.00
18	17	521	1621	0.442	2.10
35	>15	1208	2309	0.312	2.25

Notes: 1) Depth of investigation is about 50 m.
2) Saturated zone constrained at a depth of about 18 m, based on review of seismic refraction first arrival data.
3) Bottom layer is a half space.
4) Bedrock depth and velocity not well constrained and may vary by 20%, or more.

Observations/Discussion:

- The HVSR plots show a peak in the 3.4 to 3.5 Hz range. This is indicative of significant impedance contrast, most likely associated with crystalline bedrock, within the expected depth of investigation of the active and passive surface wave sounding.
- Noise conditions at the site (multi-directional noise sources) appeared sufficient for successful application of passive surface wave techniques.
- The ESAC technique was used to extract surface wave dispersion data from the ambient noise data collected on the triangle-shaped Array 1. The minimum and maximum wavelength Rayleigh waves extracted from Array 1 are 19 and 160 m, respectively.
- Both the ReMi™ and ESAC techniques were used to extract surface wave dispersion data from the ambient noise data collected along the linear Array 2. The minimum and maximum wavelength Rayleigh waves extracted from Array 2 are 12 and 140 m, respectively.
- Rayleigh wave dispersion data were interpreted from 20 MAS_RW seismic records collected at 15 different source locations using 4 lb hammer, and 12 and 20 lb sledgehammer energy sources. Using variable receiver offset ranges, over 70 dispersion curves were extracted and combined for analysis.
- To minimize near field effects and the influence of high noise data at low frequencies associated with traffic in the site vicinity, the maximum wavelength Rayleigh wave extracted from the MAS_RW data set was set equal to the lesser of 80 m or 1.3 times the distance between the source and midpoint of the active receiver array.
- There is nominally about 30 to 40 m/s of scatter in MAS_RW dispersion data, which is likely in part related to lateral velocity variation.
- The minimum wavelength Rayleigh wave phase velocity data extracted from a 48-channel MAS_RW receiver gather was 3 to 11 m, depending on source location. Reducing data from smaller hammer sources using a limited offset range receiver gather (i.e. less active geophones) allowed for extraction of surface wave dispersion data to a minimum wavelength of about 2 m.
- The passive surface wave dispersion data from the triangle Array 1 and linear Array 2, reduced using the ESAC technique, are in excellent agreement with the MAS_RW dispersion data over the overlapping 12 to 80 m wavelength range. The passive surface wave dispersion data from the linear Array 2 reduced using the ReMi™ technique diverge from the other dispersion curves at low frequencies/long wavelengths and, therefore, was not used during data modeling.
- The phase velocity of a 40 m wavelength Rayleigh wave (V_{R40}) is 358 m/s from ESAC analysis of the ambient noise data collected along the passive triangle Array 1. V_{R40} is 364 and 356 m/s (2% difference) from ESAC and ReMi™ analysis of the ambient noise data collected along the linear Array 2, respectively. V_{R40} from the MAS_RW dispersion data ranges from 353 to 369 m/s with a mean of 362 m/s and standard deviation of 4.6 m/s. V_{R40} is very similar for all of the arrays and, therefore, each array would have independently yielded an accurate estimate of V_{S30}.
- The mean V_{R40} from the combined MAS_RW and array microtremor dispersion data used for modeling is 361 m/s with a standard deviation of 4.1 m/s. During these computations, the combined array microtremor data were given equal weight to the MAS_RW data and

the combined dispersion data from the passive linear arrays had equal to or lesser weight than that of the 2-D array.

- Representative dispersion curves were generated for each surface wave data set using a moving average, polynomial curve fitting routine. These individual representative dispersion curves were combined and a composite representative dispersion curve generated for the combined data set for data modeling.
- The composite representative dispersion curve was inverted using an iterative non-linear least squares inversion routine and the effective mode Rayleigh wave assumption to derive V_S models. The effective mode was used for data modeling because the velocity structure indicated that Rayleigh wave dispersion curve may jump from fundamental to 1st higher mode at low frequencies. Realistic estimates of Poisson's ratio and density were used to make models as accurate as possible. High Poisson's ratio, saturated sediments were constrained at a depth of about 18 m with V_P > 1,600 m/s based on interactive interpretation of seismic refraction first arrival data. Model layer thicknesses were constrained to increase with depth to reflect the reduction in model resolution with depth.
- Surface wave depth of investigation is about 50 m based on the one-third of the maximum wavelength criteria, which is appropriate for a site with a sharp increase in velocity at depth.
- Several V_S models were developed with almost identical calculated dispersion curves to explore the non-uniqueness associated with the abrupt increase in velocity associated with expected crystalline bedrock. These equivalent V_S models have modeled bedrock between depths of about 31 and 38 m.
- The predicted HVSR peak based on the diffuse field assumption, as computed using the software package *HV-Inv* Release 1.0 Beta, is 3.6 to 3.7 Hz for all of the equivalent V_S models, which are relatively close to the observed 3.4 to 3.5 Hz HVSR peak at the site.
- The V_S model presented for the purpose of site characterization has the inferred top of the competent rock at a depth of 35 m, one of the intermediate modeled depths to bedrock. This V_S model has a predicted HVSR peak of 3.6 Hz. The predicted HVSR peak for the presented V_S model based on the quarter wavelength approximation is 2.8 Hz, lower than that observed at the site.
- V_{S30} is 380 m/s for the presented V_S model (NEHRP Site Class C).
- The estimated error in V_{S30}, which includes some effects of the lateral velocity variability beneath the testing arrays, is 30 m/s. This is computed based on the sum of the following rounded up to the nearest 5 m/s: an estimated error of 3% from the realistic assumed layer Poisson's ratios in the model, 1% error from the realistic assumed layer densities in the model, 2% for the variation in V_{S30} associated with non-uniqueness, and the 6.0 m/s standard deviation in V_{R40} between the combined active and passive surface wave dispersion data.
- Interestingly, V_{S30} estimated from V_{R40} using the Brown et al., 2000 relationship ($V_{S30} \cong 1.045V_{R40}$, assuming V_{R40} represents the fundamental mode Rayleigh wave) is 377 m/s, less than 1% different to that that estimated from the V_S model. Although the dispersion data was modeled using an effective mode routine, the estimate of V_{S30} from V_{R40} is still accurate because the fundamental mode Rayleigh wave was recovered at 40 m wavelength.

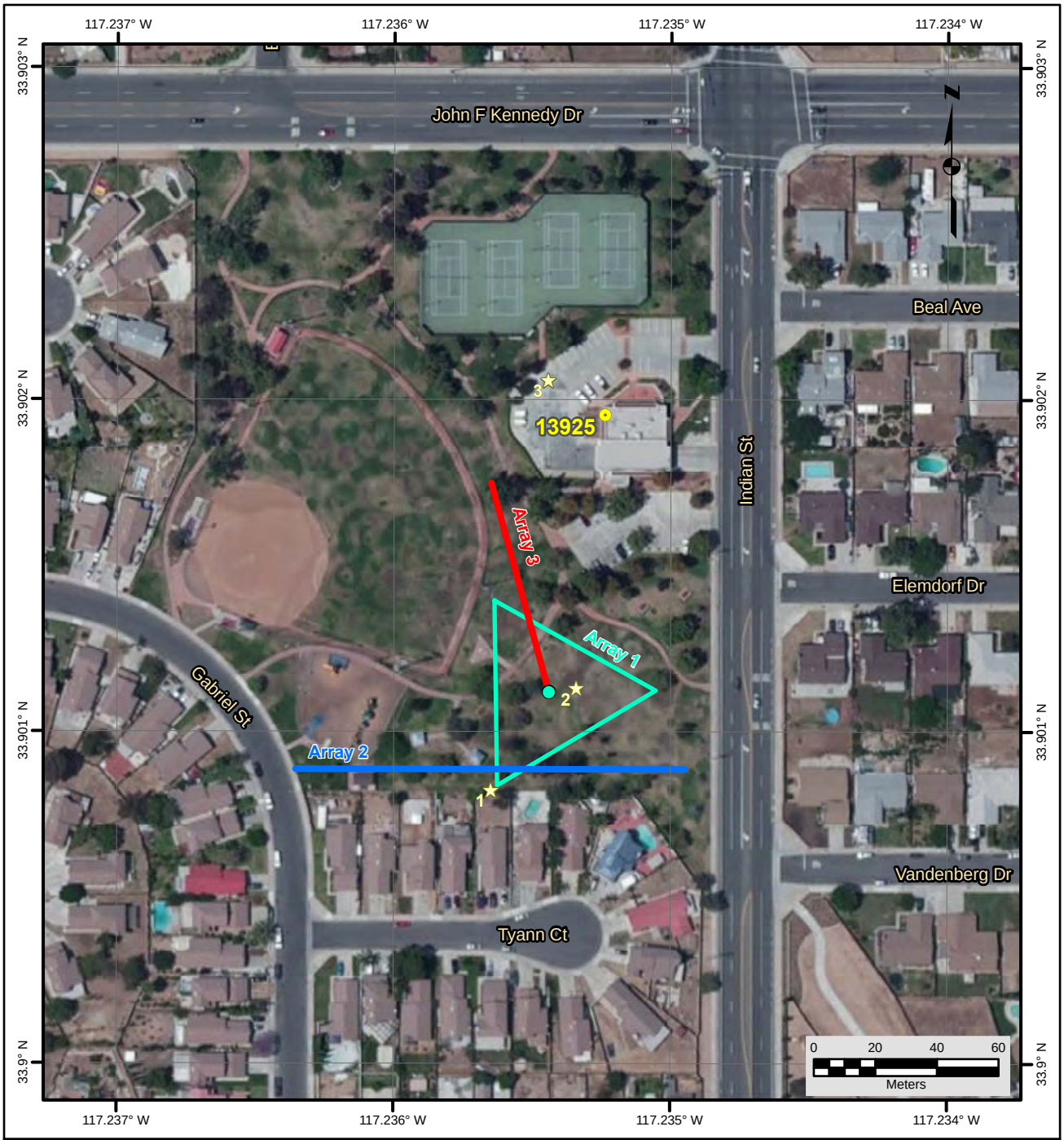

Legend

- CSMIP Station and Number
- H/V Spectral Ratio Measurement Location
- MASW Array
- Passive Surface Wave Array
- Passive Surface Wave Triangle Array

NOTES:
1. WGS 1984 COORDINATE SYSTEM
2. Image Source: Esri, DigitalGlobe, GeoEye, Earthstar Geographics, CNES/Airbus DS, USDA, USGS, AEX, Getmapping, Aerogrid, IGN, IGP, swisstopo, and the GIS User Community

File Name: 16192_13925-I

Date: 6/30/2016

GEOVision geophysical services

SITE MAP
CE•13925

CGS CALIFORNIA GEOLOGICAL SURVEY

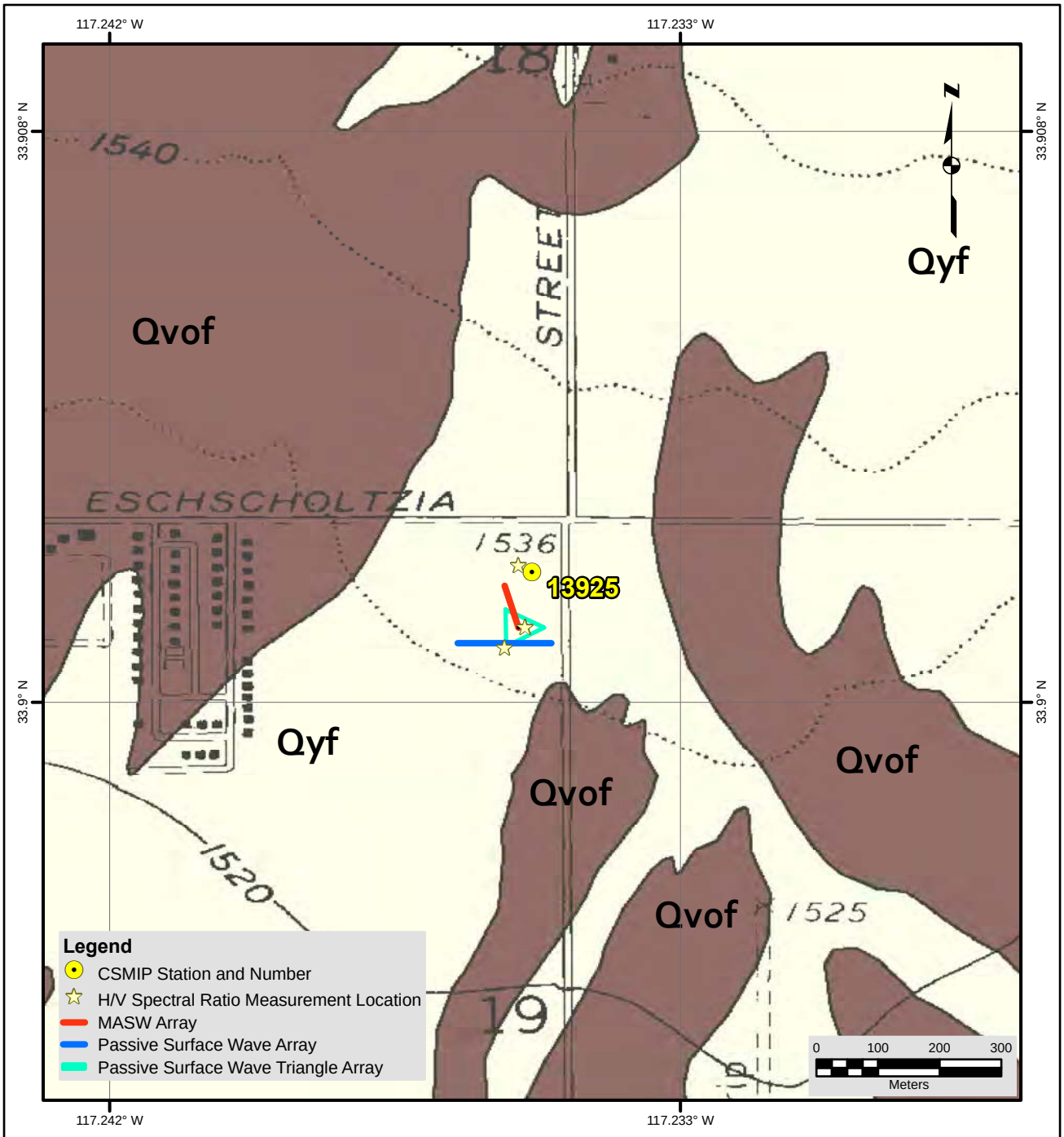

Description of Geologic Map Units

Qyf = Quaternary (Holocene and late Pleistocene) Sand and cobble-sand and gravel-sand deposits.
Qvof = Quaternary (early Pleistocene) Sand deposits, containing minor gravel.

NOTES:
1. WGS 1984 COORDINATE SYSTEM
2. Geologic Map of the Sunnymead 7.5' Quadrangle, Riverside County, California by Douglas M. Morton (1978, 1996-7) and Jonathan C. Matti (1996-7)

File Name: 16192_13925

Date: 7/13/2016

GEOVision geophysical services

GEOLOGIC MAP
CE•13925

CGS CALIFORNIA GEOLOGICAL SURVEY

Looking north towards fire station housing CE.13925 seismic station from passive surface wave array 13925-1

Trillium and Tromino sensors used for measurements at HVSR Location 1

Looking southeast along MASW array 13925-3

Looking east along passive surface wave array 13925-2

1 Hz geophone used on passive surface wave array 13925-1 and Tromino sensor used for measurements at HVSR Location 2

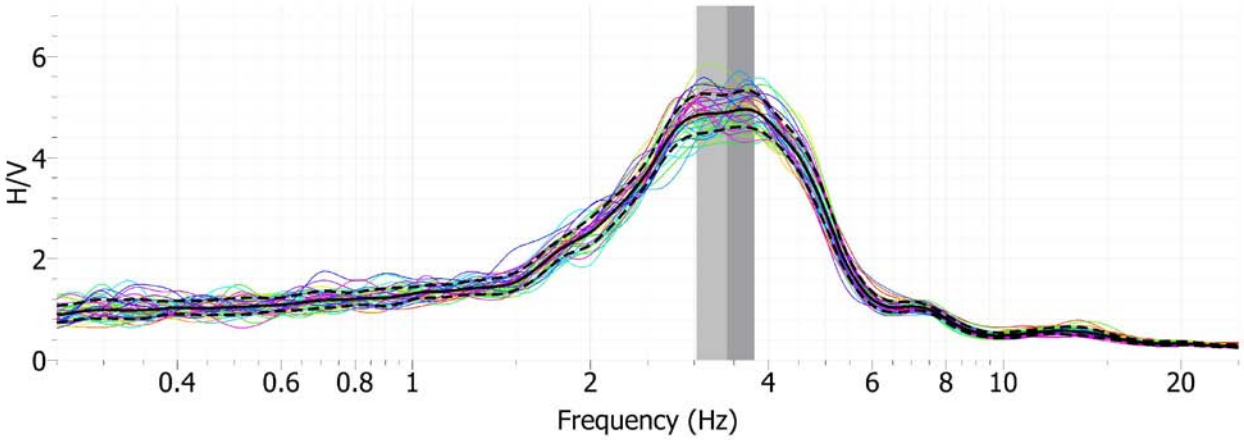

Site CE.13925, HVSR Location 1, Nanometrics Trillium Compact Sensor

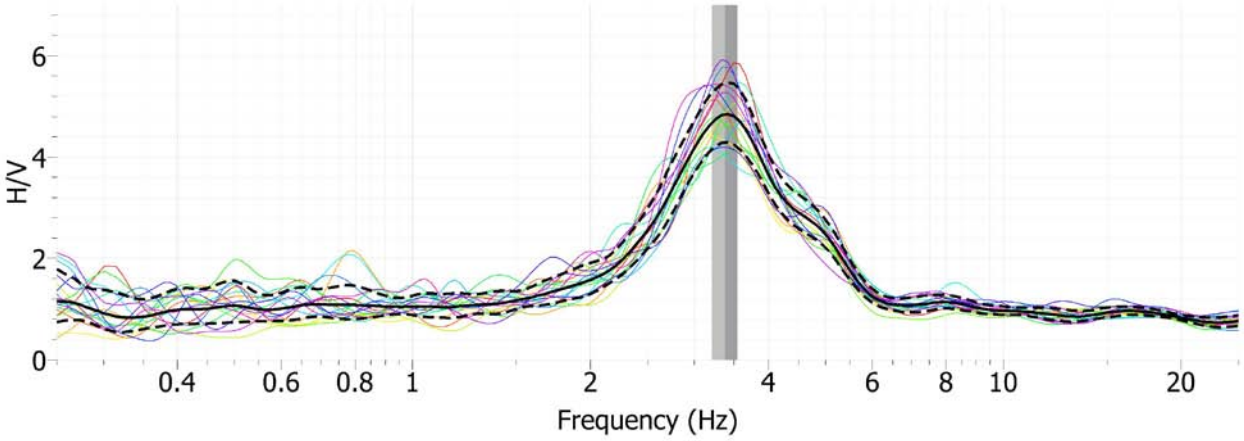

Site CE.13925, HVSR Location 2, Micromed Tromino ENGR Sensor

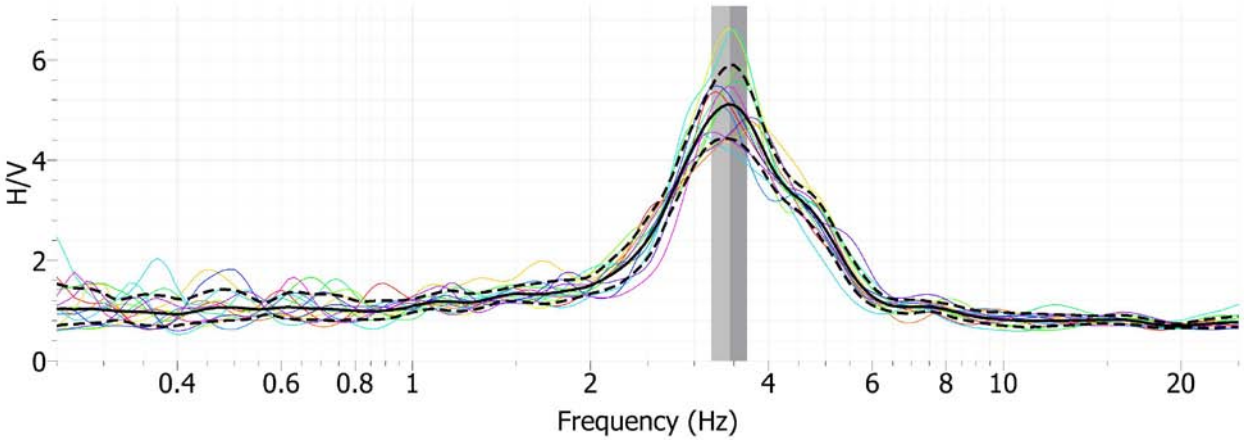

Site CE.13925, HVSR Location 3, Micromed Tromino ENGR Sensor

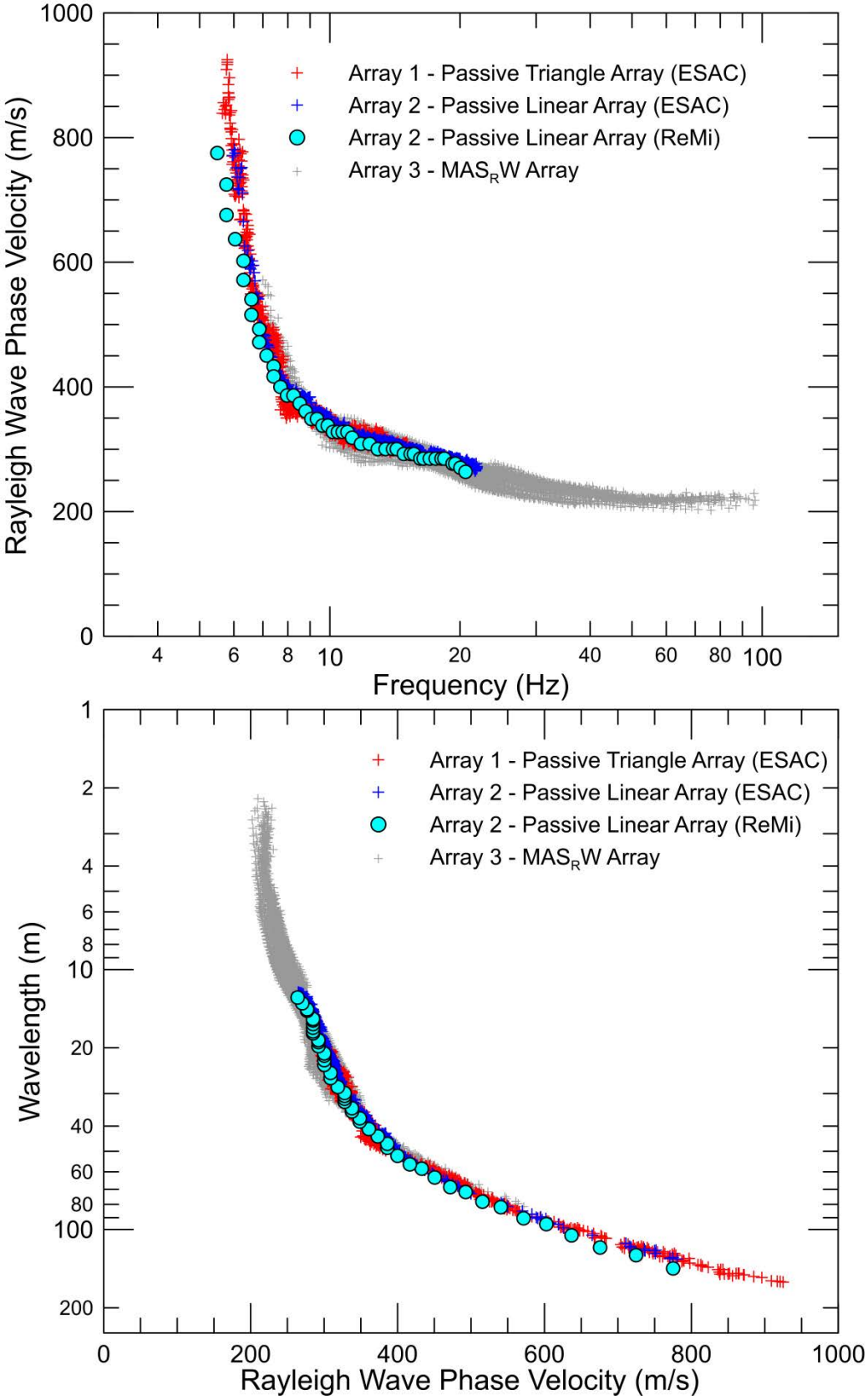

CE.13925 – Dispersion curves derived from active and passive surface wave data. Passive surface wave data from the triangular shaped Array 1 and linear Array 2 analyzed using the ESAC method are in excellent agreement with MAS_RW data. The dispersion curve from the passive linear Array 2 analyzed using the ReMi™ technique diverges from the other dispersion curves at low frequencies/long wavelengths and, therefore, was not used for data modeling.

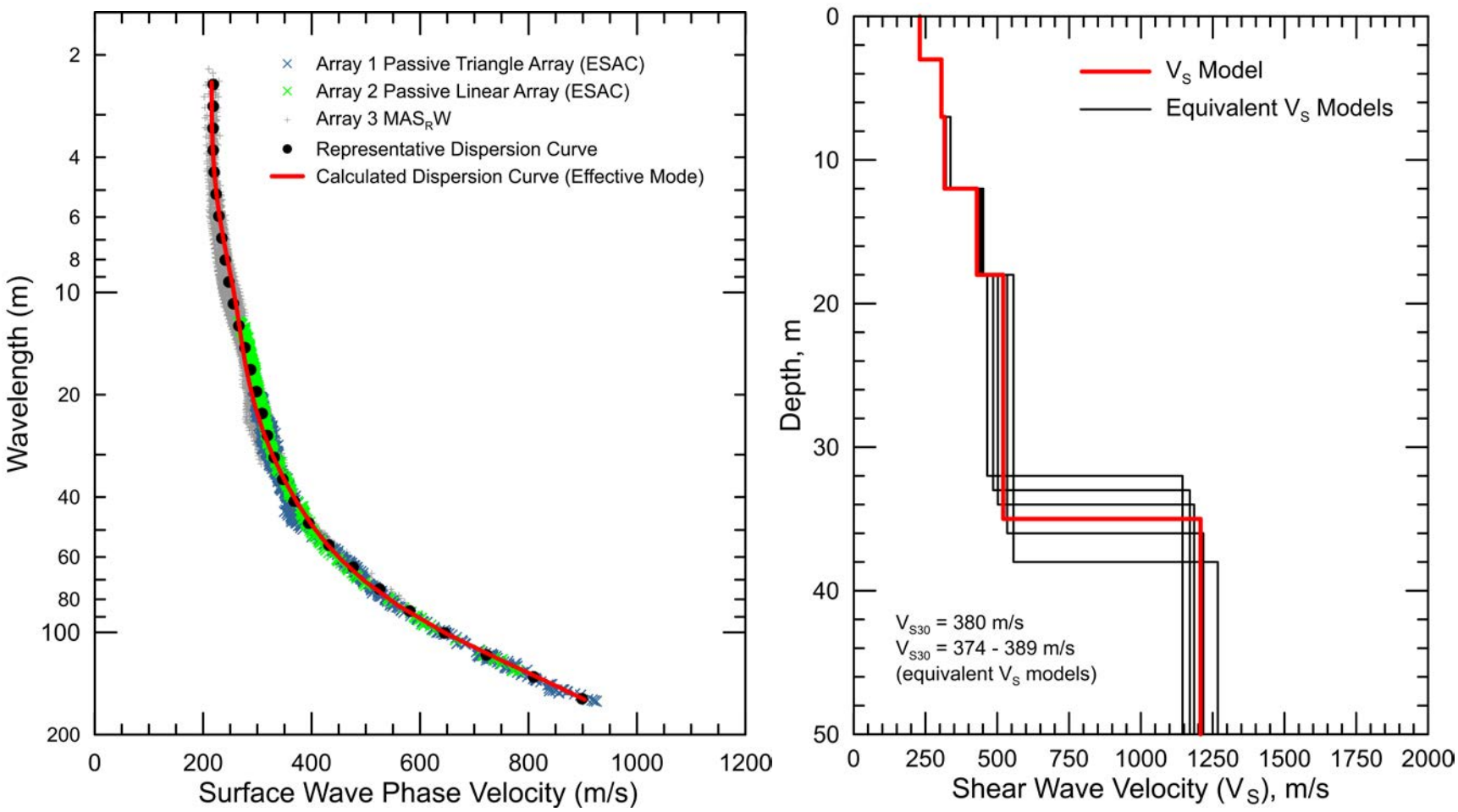

CE.13925 - Field, representative and calculated effective mode surface wave dispersion data (left) and associated V_S models (right). Surface wave dispersion data is plotted as phase velocity versus wavelength.

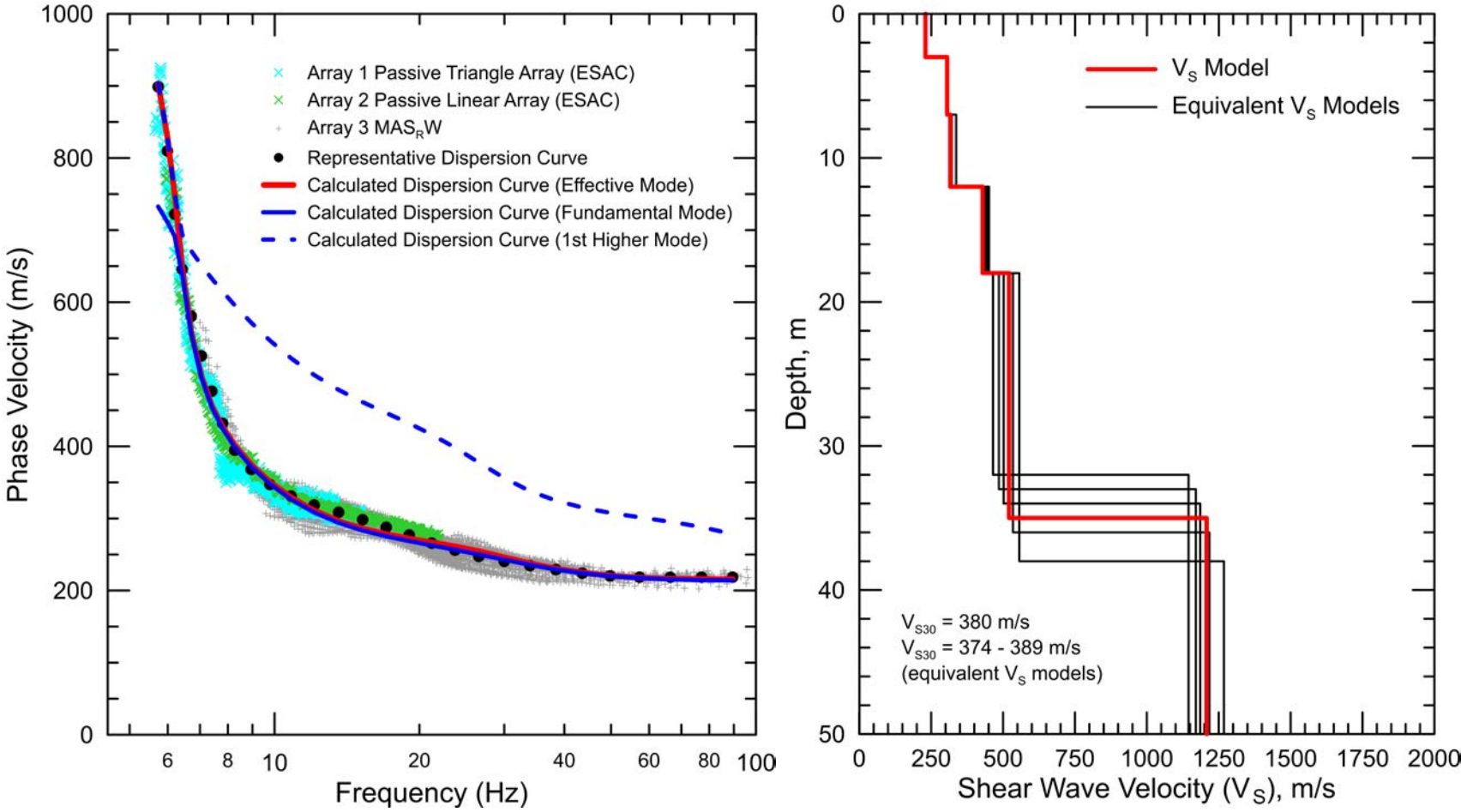

CE.13925 - Field, representative and calculated effective, fundamental and 1st higher mode surface wave dispersion data (left) and associated V_S models (right). Surface wave dispersion data is plotted as frequency versus phase velocity. Note that the fundamental mode and 1st higher mode Rayleigh wave fits the field observations at frequencies above and below 6.5 Hz, respectively.

Site CE.13927

Station Name: Moreno Valley - Alessandro & Moreno Bch

Location: Former Moreno Valley Fire Station, 28020 Bay Ave., Moreno Valley, CA 92555

Latitude: 33.9212 **Longitude:** -117.1731

V_{S30} (measured): 325 m/s

NEHRP Site Class: D

Estimated error in V_{S30}: ± 35 m/s

Geomatrix Code: AHD/AQD

Geologic Conditions/Observations: Site located in area mapped as Quaternary (Holocene and late Pleistocene) alluvium. Outcrop of Cretaceous tonalite about 500 m north of site.

Site Conditions: Suburban site with traffic noise from nearby roads, particularly Moreno Beach Drive. Relatively flat terrain in site vicinity.

Geophysical Methods Utilized: MAS_RW, array microtremor, HVSR

Geophysical Testing Arrays:

1. Array 1: 48 channel MAS_RW array utilizing 4.5 Hz vertical geophones spaced 1.5 m apart for a length of 70.5 m, forward and reverse shot locations with multiple source offsets (1.5 to 24 m at southwest end of array and 1.5 to 21 m at northeast end of array) and multiple interior source locations. Accelerated weight drop used at all source locations offset from ends of array and 4 and 12 lb hammers used at near-offset source locations and interior source locations.
2. Array 2: 48 channel "L" shaped array utilizing 4.5 Hz vertical geophones spaced 4 m apart used to acquire passive surface wave data. The S-N and W-E linear segments of array have lengths of 84 and 104 m, respectively.
3. Array 3: 10 channel, nested triangle passive surface wave array utilizing 1 Hz geophones and a 48 m length for outer side of array.
4. Three HVSR measurement locations; two in the vicinity of MAS_RW and microtremor arrays and one near the seismic station.

Location of Geophysical Testing Arrays:

Location	Latitude	Longitude
Array 1 MASW, Southwest End of Array	33.92150	-117.17370
Array 1 MASW, Northeast End of Array	33.92180	-117.17300
Array 2 Passive, South End of Array	33.92114	-117.17280
Array 2 Passive, Northeast Corner of Array	33.92190	-117.17280
Array 2 Passive, West End of Array	33.92190	-117.17393
Array 3 Passive, Corner of Array, Sensor Location 1	33.92150	-117.17348
Array 3 Passive, Corner of Array, Sensor Location 3	33.92151	-117.17296
Array 3 Passive, Corner of Array, Sensor Location 5	33.92188	-117.17322
Array 3 Passive, Center of Array, Sensor Location 10	33.92163	-117.17323
HVSR Location 1	33.92121	-117.17323
HVSR Location 2	33.92188	-117.17281
HVSR Location 3	33.92166	-117.17337

Notes: 1) WGS84 Coordinate System (decimal degrees)

Results:

V_S Model

Depth to Top of Layer (m)	Layer Thickness (m)	S-Wave Velocity (m/s)	Inferred P-Wave Velocity (m/s)	Assumed Poisson's Ratio	Assumed Density (g/cm^3)
0	2	178	334	0.30	1.80
2	4	212	396	0.30	1.80
6	6	336	630	0.30	1.90
12	10	374	697	0.30	1.90
22	22	453	847	0.30	1.95
44	>16	1374	2568	0.30	2.20

Notes: 1) Depth of investigation is about 60 m.
2) Bottom layer is a half space.
3) Bedrock depth and velocity not well constrained and may vary by 20%, or more.

Observations/Discussion:

- The HVSR plots show a peak in the 2.4 to 2.7 Hz range. This is indicative of a significant increase in seismic velocity associated crystalline bedrock (based on outcrop 150 m from site), within the expected depth of investigation of the active and passive surface wave sounding.
- Noise conditions at the site (multi-directional noise sources, particularly from the S-N trending Moreno Beach Drive bounding the site) appeared sufficient for successful application of passive surface wave techniques.

- The ESAC technique was used to extract surface wave dispersion data from the ambient noise data collected on the L-shaped Array 2 and triangular shaped Array 3. The minimum and maximum wavelength Rayleigh waves extracted from Array 2 are 12 and 195 m, respectively. The minimum and maximum wavelength Rayleigh waves extracted from Array 3 are 13 and 155 m, respectively.
- Both the ReMi™ and ESAC techniques were used to extract surface wave dispersion data from the ambient noise data collected along the S-N and W-E linear legs of Array 2. The minimum wavelength Rayleigh waves extracted from these arrays are between 9 and 12 m. The maximum wavelength Rayleigh waves extracted from these arrays are between 130 and 200 m.
- Rayleigh wave dispersion data were interpreted from 20 MAS_RW seismic records collected at 15 different source locations using 4 lb hammer, 2 lb sledgehammer, and 240 lb accelerated weight drop energy sources. Using variable receiver offset ranges, over 85 dispersion curves were extracted and combined for analysis.
- To minimize near field effects and the influence of high noise data at low frequencies associated with traffic in the site vicinity, the maximum wavelength Rayleigh wave extracted from the MAS_RW data set was set equal to the lesser of 80 m or 1.3 times the distance between the source and midpoint of the active receiver array.
- There is nominally about 25 to 50 m/s of scatter in MAS_RW dispersion data, which is likely in part related to lateral velocity variation.
- The minimum wavelength Rayleigh wave phase velocity data extracted from a 48-channel MAS_RW receiver gather was 11 to 17 m, depending on source location. Reducing data from smaller hammer sources using a limited offset range receiver gather (i.e. less active geophones) allowed for extraction of surface wave dispersion data to a minimum wavelength of about 1.5 m.
- The passive surface wave dispersion data from the L-shaped Array 2 and triangular shaped Array 3, reduced using the ESAC technique, are in excellent agreement with the MAS_RW dispersion data over the overlapping 12 to 80 m wavelength range. The passive surface wave dispersion data from the linear W-E leg of Array 2 (perpendicular to Moreno Beach Drive) reduced using the ESAC and ReMi™ techniques are also in good agreement with the MAS_RW data and passive dispersion data from the 2-D arrays. The passive surface wave dispersion data from the linear S-N leg of Array 2 (parallel to Moreno Beach Drive) reduced using the ESAC and ReMi™ techniques are not in good agreement with the other data sets and, therefore, were not used during data modeling.
- The phase velocity of a 40 m wavelength Rayleigh wave (V_{R40}) are 326 and 331 m/s from ESAC analysis of the ambient noise data collected along Arrays 2 and 3, respectively. V_{R40} is 332 and 324 m/s (2% difference) from ESAC and ReMi™ analysis of the ambient noise data collected along the S-N linear leg of Array 2, respectively. V_{R40} is 313 and 319 m/s (2% difference) from ESAC and ReMi™ analysis of the ambient noise data collected along the W-E linear leg of Array 2, respectively. V_{R40} from the MAS_RW dispersion data ranges from 289 to 321m/s with a mean of 307 m/s and standard deviation of 7.9 m/s. V_{R40} is very similar for all of the arrays and, therefore, each array would have independently yielded an accurate estimate of V_{S30}, although several of the arrays may have not yielded reliable V_S models.
- The mean V_{R40} from the combined MAS_RW and array microtremor dispersion data used for modeling is 316 m/s with a standard deviation of 11.5 m/s. During these

computations, the combined array microtremor data were given equal weight to the MAS_RW data and the combined dispersion data from the passive linear arrays had equal to or lesser weight than that of the 2-D array.

- Representative dispersion curves were generated for each surface wave data set using a moving average, polynomial curve fitting routine. These individual representative dispersion curves were combined and a composite representative dispersion curve generated for the combined data set for data modeling.
- The composite representative dispersion curve was inverted using an iterative non-linear least squares inversion routine and the effective mode Rayleigh wave assumption to derive V_S models. The effective mode was used for data modeling because the velocity structure indicated that Rayleigh wave dispersion curve may jump from fundamental to 1st higher mode at low frequencies. Realistic estimates of Poisson's ratio and density were used to make models as accurate as possible. Review of seismic refraction first arrival data provided no evidence of the saturated zone in the upper 30 m at the site. Model layer thicknesses were constrained to increase with depth to reflect the reduction in model resolution with depth.
- Surface wave depth of investigation is about 60 m based on the one-third of the maximum wavelength criteria, which is appropriate for a site with a sharp increase in velocity at depth.
- Several V_S models were developed with almost identical calculated dispersion curves to explore the non-uniqueness associated with the abrupt increase in velocity associated with expected crystalline bedrock. These equivalent V_S models have modeled bedrock between depths of about 36 and 52 m. The models with greater depth to rock appear to have unrealistically high V_S for the sediment layer immediately overlying rock.
- The predicted HVSR peak based on the diffuse field assumption, as computed using the software package *HV-Inv* Release 1.0 Beta, is 2.5 to 2.8 Hz for all of the equivalent V_S models, which are very close to the observed 2.4 to 2.7 Hz HVSR peak at the site.
- The V_S model presented for the purpose of site characterization has the inferred top of the competent rock at a depth of 44 m, one of the intermediate modeled depths to bedrock. This V_S model has a predicted HVSR peak of 2.6 Hz. The predicted HVSR peak for the presented V_S model based on the quarter wavelength approximation is 2.0 Hz, lower than that observed at the site.
- V_{S30} is 325 m/s for the presented V_S model (NEHRP Site Class D).
- The estimated error in V_{S30}, which includes some effects of the lateral velocity variability beneath the testing arrays, is 35 m/s. This is computed based on the sum of the following rounded up to the nearest 5 m/s: an estimated error of 3% from the realistic assumed layer Poisson's ratios in the model, 1% error from the realistic assumed layer densities in the model, 2% for the variation in V_{S30} associated with non-uniqueness, and the 11.5 m/s standard deviation in V_{R40} between the combined active and passive surface wave dispersion data.
- Interestingly, V_{S30} estimated from V_{R40} using the Brown et al., 2000 relationship ($V_{S30} \cong 1.045V_{R40}$, assuming V_{R40} represents the fundamental mode Rayleigh wave) is 330 m/s, less than 2% different from that that estimated from the V_S model. Although the dispersion data was modeled using an effective mode routine, the estimate of V_{S30} from V_{R40} is still accurate because the fundamental mode Rayleigh wave was recovered at 40 m wavelength.

Legend

- H/V Spectral Ratio Measurement Location
- MASW Array
- Passive Surface Wave Array
- Passive Surface Wave Triangle Array

NOTES:
1. WGS 1984 COORDINATE SYSTEM
2. Image Source: Esri, DigitalGlobe, GeoEye, Earthstar Geographics, CNES/Airbus DS, USDA, USGS, AEX, Getmapping, Aerogrid, IGN, IGP, swisstopo, and the GIS User Community

File Name: 16192_13927-I

Date: 7/28/2016

GEOVision geophysical services

SITE MAP
CE•13927

CGS CALIFORNIA GEOLOGICAL SURVEY

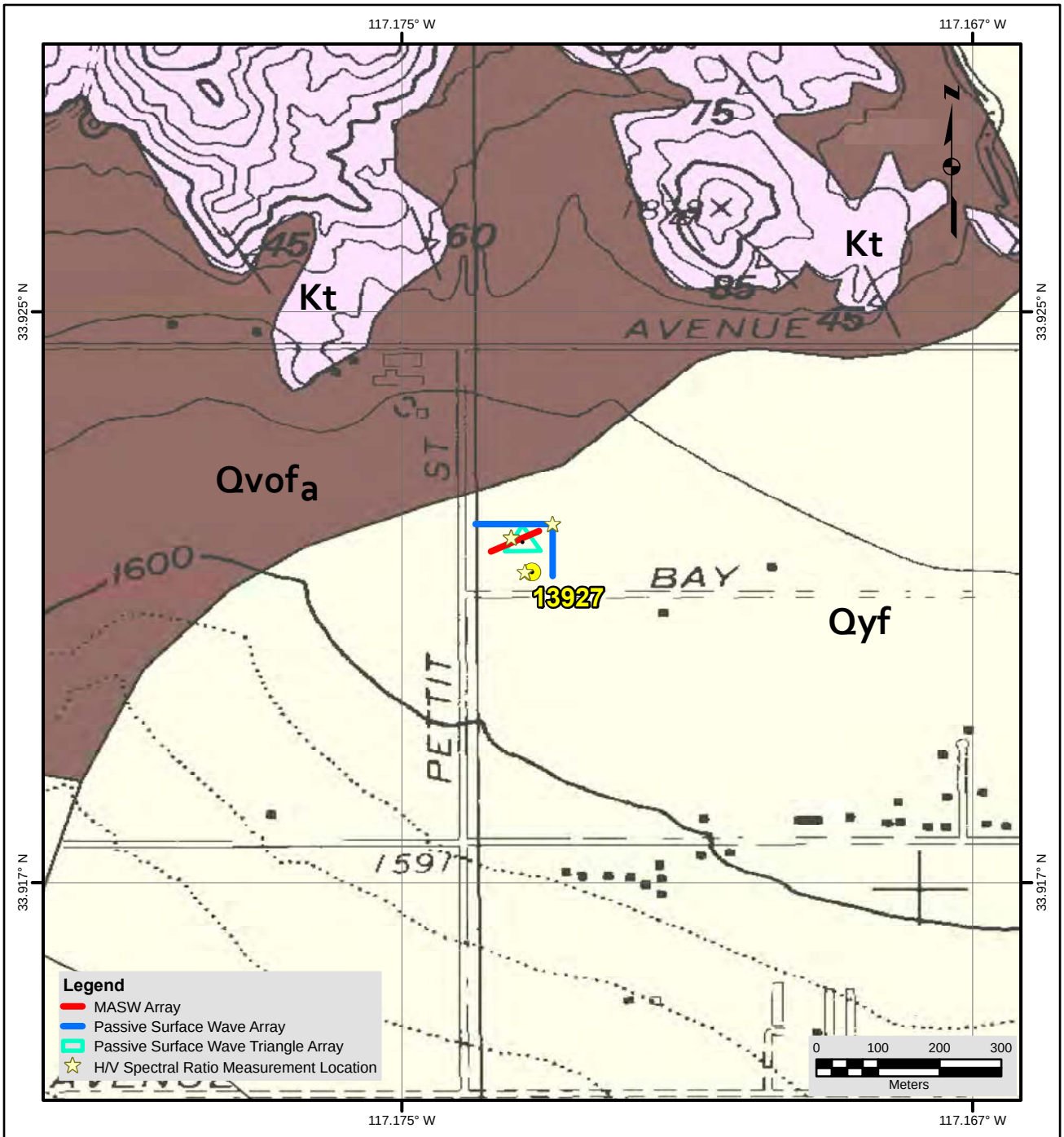

Description of Geologic Map Units

Qyf = Quaternary (Holocene and late Pleistocene) Sand and cobble-sand and gravel-sand deposits.
Qvof = Quaternary (early Pleistocene) Sand deposits, containing minor gravel.
Kt = Cretaceous tonalite.

NOTES:
1. WGS 1984 COORDINATE SYSTEM
2. Geologic Map of the Sunnymead 7.5' Quadrangle, Riverside County, California by Douglas M. Morton (1978, 1996-7) and Jonathan C. Matti (1996-7)

File Name: 16192_13927

Date: 7/13/2016

GEOVision geophysical services

GEOLOGIC MAP
CE•13927

CGS CALIFORNIA GEOLOGICAL SURVEY

Looking southwest towards building housing CE.13927 seismic station from passive surface wave array 13927-2

Looking northeast along MASW array 13927-1

Looking southeast from center of passive surface wave array 13927-3

Looking east towards building housing seismic station from HVSR Location 1

Looking south along passive surface wave array 13927-2

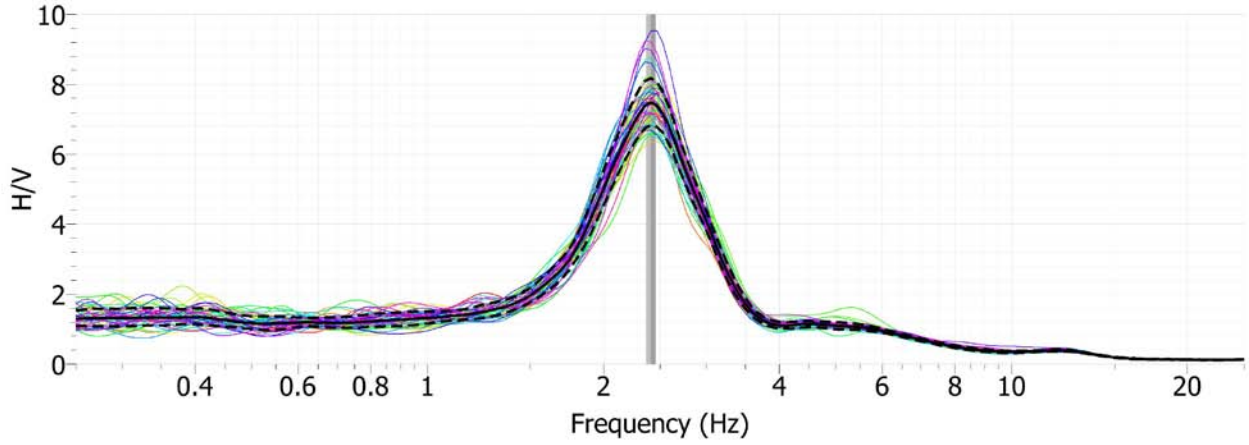

Site CE.13927, HVSR Location 1, Nanometrics Trillium Compact Sensor

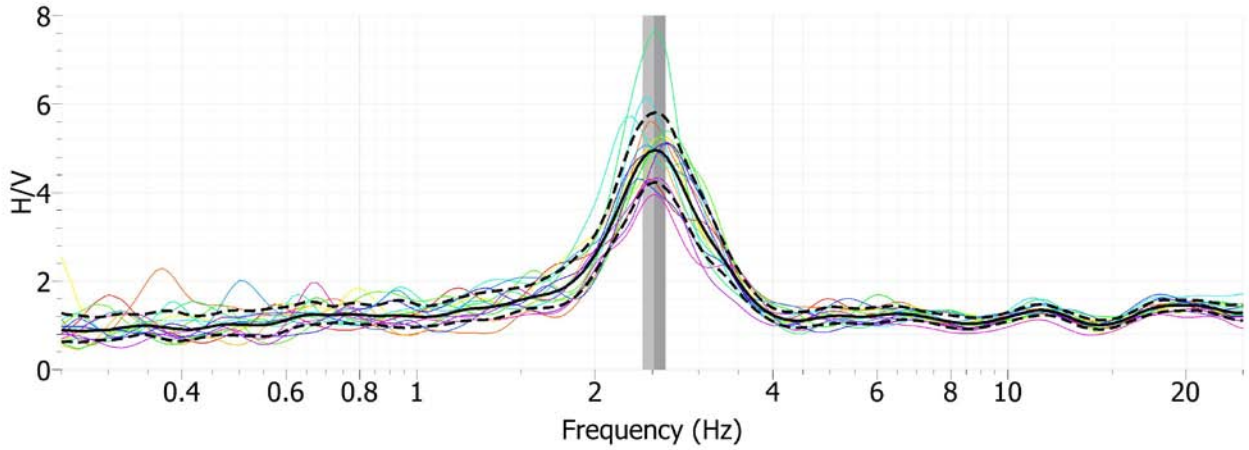

Site CE.13927, HVSR Location 2, Micromed Tromino ENGR Sensor

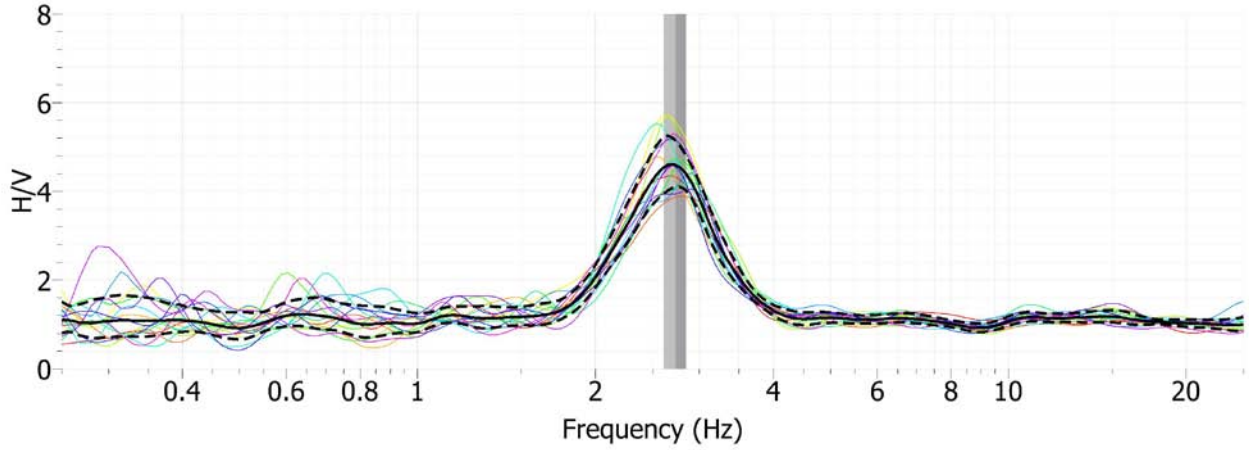

Site CE.13927, HVSR Location 3, Micromed Tromino ENGR Sensor

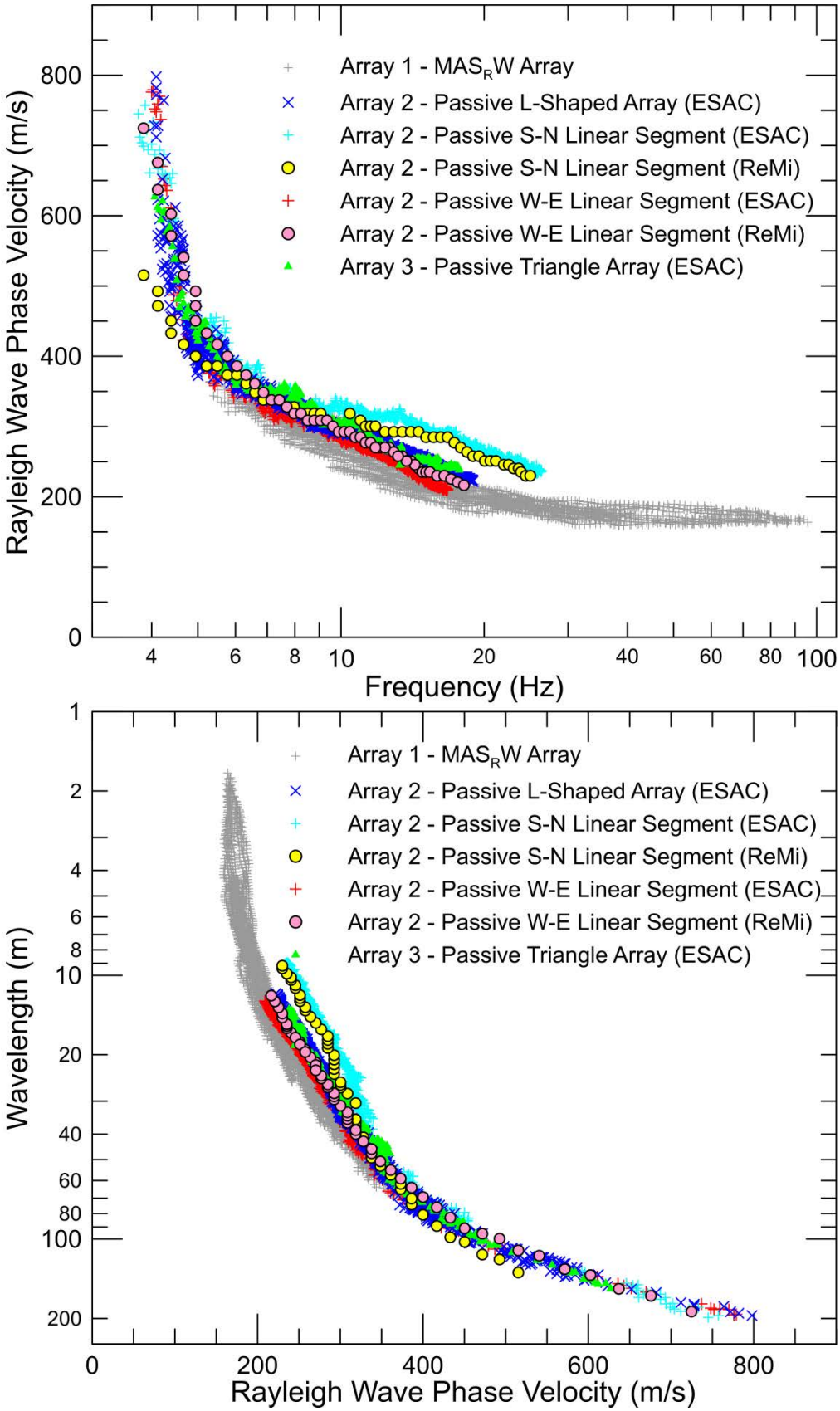

CE.13927 – Dispersion curves derived from active and passive surface wave data. Passive surface wave data from the L-shaped Array 2, triangular shaped Array 3 and W-E linear leg of Array 2 are in excellent agreement with MAS_RW data and were used for data modeling. The dispersion curves from the S-N linear leg of Array 2 are not in good agreement with the other dispersion data and, therefore, were not utilized for data modeling.

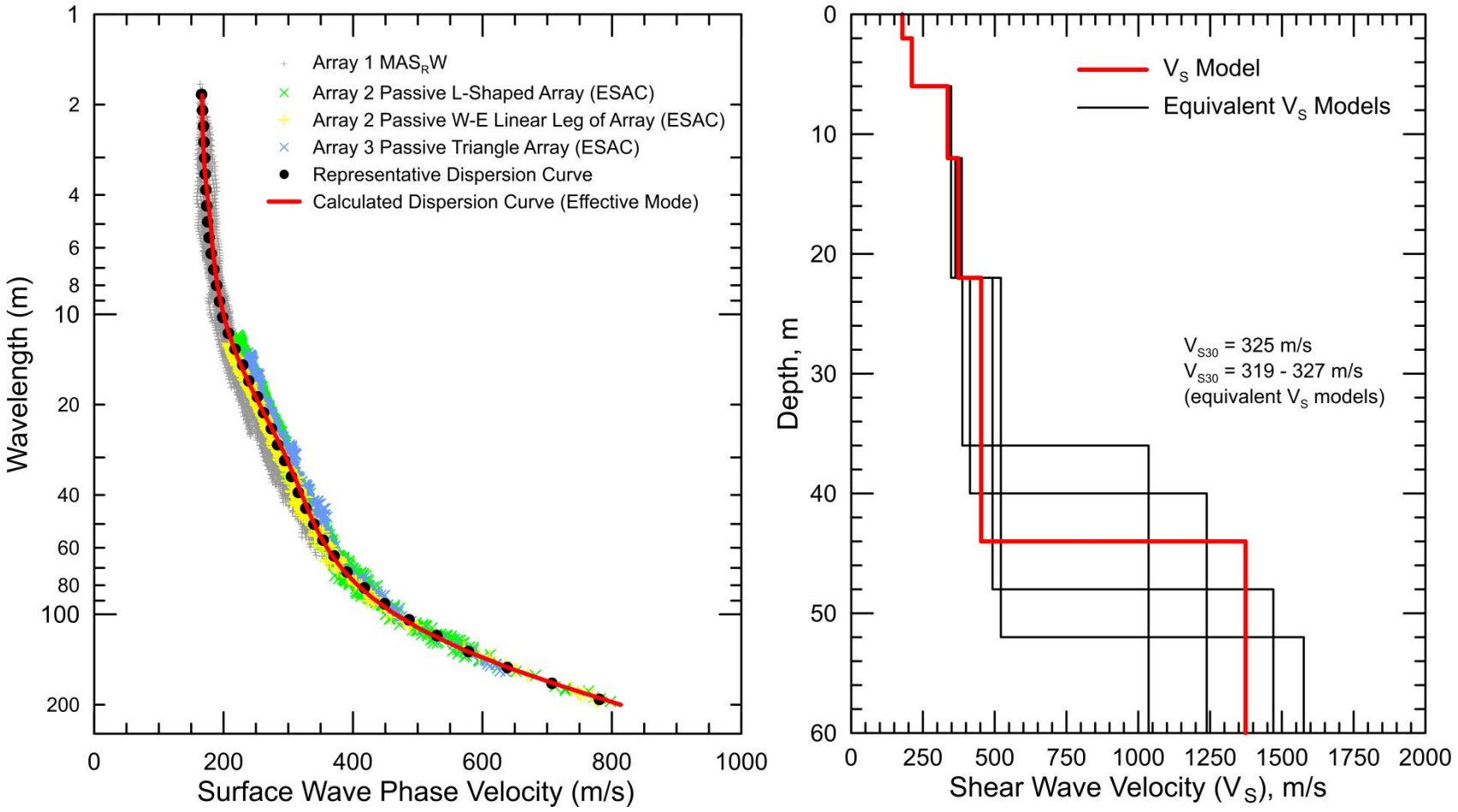

CE.13927 - Field, representative and calculated effective mode surface wave dispersion data (left) and associated V_S models (right). Surface wave dispersion data is plotted as phase velocity versus wavelength.

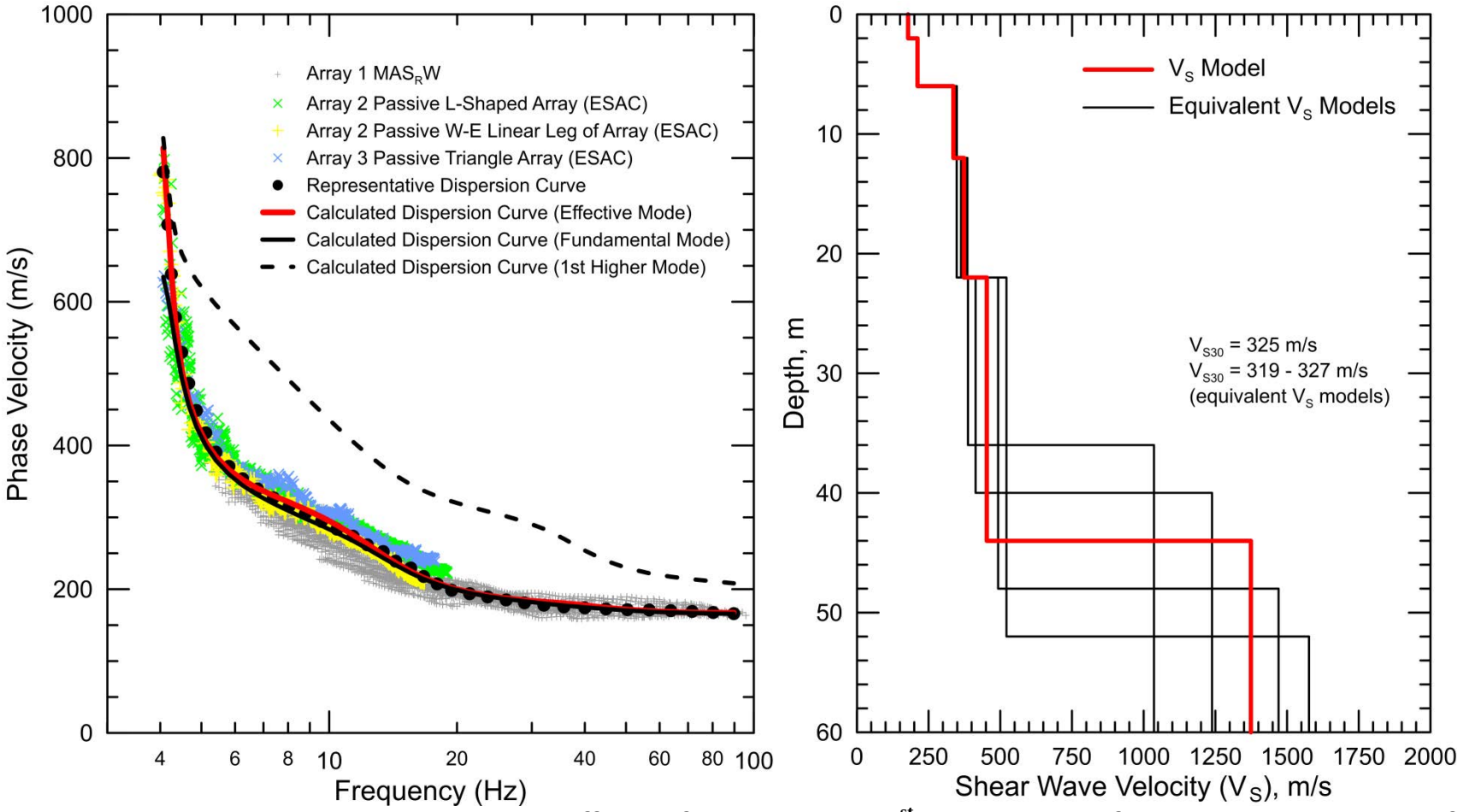

CE.13927 - Field, representative and calculated effective, fundamental and 1st higher mode surface wave dispersion data (left) and associated V_S models (right). Surface wave dispersion data is plotted as frequency versus phase velocity. Note that the fundamental mode and 1st higher mode Rayleigh wave fits the field observations at frequencies above and below about 4.5 Hz, respectively.